



AALBORG UNIVERSITY
STUDENT REPORT

IMPACT OF DIFFUSE CEILING VENTILATION SYSTEMS ON INDOOR ENVIRONMENTAL QUALITY IN CLASSROOMS

A Field Study, Full-Scale Experimental and Numerical Investigation

Martin Heine Kristensen
Jakob Søland Jensen

Master's Thesis
Department of Civil Engineering
Indoor Environmental Engineering

June 2015

Preface

This thesis documents the work carried out in partial fulfilment of the requirements for the degree of *Master of Science in Indoor Environmental and Energy Engineering* at the Department of Civil Engineering at Aalborg University, Denmark. The thesis is carried out in the period between September 2014 and June 2015 corresponding to a total of 50 ECTS points.

During the project period the authors have participated in the ELFORSK PSO-project named *Natural Cooling and Ventilation through Diffuse Ceiling Supply and Thermally Activated Building Constructions* with project number 345-061. The participants include the companies; Aalborg University, Spændcom A/S, WindowMaster A/S and Troldtekt A/S. Parts of the thesis conclusion and experimental findings from Part 1 and Part 2 have been presented on project meetings and discussed with the other participants.

In addition to this thesis report the authors have written and published a technical report for the Department of Civil Engineering at Aalborg University named *Air Temperature Measurements Using Dantec Draught Probes* with ISSN 1901-726X. It comes as DCE Technical Report No. 189.

Overall thesis supervision is given by Professor Per Kvols Heiselberg assisted by Associate Professor Rasmus Lund Jensen in terms of experimental equipment and test facilities.

The authors will like to extend our gratitude to everybody at Solbjergskolen for their hospitality and aid in making the field studies possible. We would also like to thank Asger Nybo Larsen from Bascon A/S for providing technical drawings and answering questions regarding the Diffuse Ceiling Ventilation system at Solbjergskolen.

Department of Civil Engineering, Aalborg University, June 2015.

Jakob Søland Jensen

Martin Heine Kristensen

Abstract

The scope of this thesis is to answer the question: "*What influences the functionality and delivered indoor thermal comfort of a diffuse ceiling ventilation system?*" This endeavour is pursued by means of two overall methodologies;

- through two field study experiments in classrooms during true operating conditions
- through 70 full-scale laboratory experiments quantifying how the supply opening area influences the cooling capacity, thermal comfort and airflow pattern in rooms with DCV

Investigations show how high cooling capacities (above 130 W/m^2) can be achieved while still complying with thermal comfort category B. DCV systems are capable of delivering high ventilation rates (from $6\text{-}16 \text{ h}^{-1}$) with minimal risk of draught due to the application of large supply opening areas compared to conventional ventilation systems. The combination of ventilation rate and inlet air temperature comprising the cooling capacity is given in terms of a design chart for three different supply opening areas (18 %, 50 % and 100 % diffuse ceiling area).

Correlation of important parameters in DCV system design show how the airflow pattern is mainly heat load dominated but also affected by ventilation inlet momentum for all typical ventilation rates, hence airflow patterns are better described by Archimedes number than Reynolds number. Furthermore, it is found that total mixing of room air is effectuated both during true operation conditions and in experiments. This mixing, as well as the preheating capabilities of the inlet air while passing through the plenum volume, is also found to be a function of Archimedes number.

Numerical predictions using CFD is attempted applied for a broad parametric study investigating the robustness of system critical parameters towards changes in the boundary conditions, however, the numerical model proved invalid in describing the fluid mechanical system.

Keywords: Diffuse Ceiling Ventilation, DCV, Cooling Capacity, thermal comfort, Design Chart, Classrooms, Field Experiments, Full-Scale Laboratory Experiments, CFD.

Abstract in Danish

Formålet med dette speciale er at svare på spørgsmålet: *"Hvad påvirker funktionaliteten og leveret termisk komfort for ventilationssystemer med diffus loftindblæsning?"* Dette er undersøgt ved anvendelse af to overordnede metoder:

- gennem to feltforsøg i klasseværelser under faktiske driftsbetingelser
- gennem 70 fuldskala laboratorieforsøg, der kvantificerer, hvordan loftindblæsningsarealet påvirker kølekapaciteten, den termiske komfort samt luftstrømningsmønstret i rum med ventilation ved diffus loftindblæsning

Forsøgene viser, hvordan høje kølekapaciteter (over 130 W/m^2) kan opnås samtidig med, at termisk komfort kategori B overholdes. Denne type ventilationssystemer er i stand til levere høje ventilationsrater (luftsifter fra $6\text{-}16 \text{ h}^{-1}$) med minimal trækrisiko grundet anvendelsen af store indblæsningsarealer sammenlignet med traditionelle ventilationssystemer. Kombinationen af ventilationsmængde og temperaturforskelle, der udgør kølekapaciteten, er givet i form af en design-kurve for tre forskellige diffuse loftindblæsningsarealer (18 %, 50 % og 100 % diffust loftindblæsningsareal).

En korrelationsundersøgelse af vigtige designparametre viser, hvordan luftstrømningsmønstret hovedsageligt er domineret af varmekilderne (opdriftskrafter) men også påvirket af indblæsningsimpulsen for alle normale ventilationsmængder. Således beskrives strømningsmønstret bedre af Arkimedes tal end af Reynolds tal. Der er ikke fundet nogen signifikant sammenhæng mellem strømningsmønstret og loftindblæsningsarealet. Herudover er der observeret total opblanding af rumluft i såvel feltforsøg som i laboratorieforsøg. Denne opblanding samt forvarmningen af friskluftindtaget, der sker over det nedhængte loft, er fundet at være en funktion af Arkimedes tal samt loftsindblæsningsarealet.

Numeriske analyser med CFD er forsøgt anvendt til et bredt parametervariationsstudie af robustheden i designet af diffuse loftsindblæsningssystemer, men den numeriske model viste sig ugyldig i forhold til at beskrive fluidbevægelsen.

Nøgleord: ventilation ved diffus loftindblæsning, kølekapacitet, termisk komfort, design-kurve, klasseværelser, feltforsøg, fuldskala laboratorieforsøg, CFD.

Table of Contents

1	Introduction	1
1.1	Background	1
1.2	Literature Study	3
1.3	Thesis Statement	5
1.4	Research Design	6
1.5	Analysis Tools and Theoretical Offset	8
1.6	Report Structure	20
 Part 1 Field Study Investigations in a Danish Classroom		23
2	Pilot Study	25
2.1	Planned Investigations	25
2.2	Field Study: Solbjergskolen, 6th grade classroom	26
2.3	Test Procedure and Instrumentation	32
2.4	Measurement Results	37
2.5	Analysis of Plenum	39
2.6	Analysis of Classroom	41
2.7	Findings	46
3	Main Study	47
3.1	Planned Investigations	47
3.2	Field Study: Solbjergskolen, 9th grade classroom	48
3.3	Test Procedure and Instrumentation	49
3.4	Measurement Results	51
3.5	Analysis of Plenum	53
3.6	Analysis of Classroom	57
3.7	Findings	63
 Part 2 Experimental and Numerical Investigations		65
4	Influence of Supply Opening Area	67
4.1	Planned Investigations	67
4.2	Hotbox as Test Facility	69
4.3	Test Procedure and Instrumentation	76
4.4	Measurement Results	88

4.5	Analysis of Thermal Comfort Limited Cooling Capacity	93
4.6	Analysis of Air Permeability and Plenum Effects	99
4.7	Analysis of Airflow Elements and Patterns	105
4.8	Findings	117
5	Robustness of DCV System Design by Numerical Analysis	119
5.1	Planned Investigations	119
5.2	Setup of CFD model	123
5.3	Validation	131
5.4	Findings	141
Part 3	Recapitulation	143
6	Discussion	145
6.1	Field Study Investigations	145
6.2	Experimental Investigations	147
6.3	Numerical Investigations	149
6.4	Comparison of Field and Experimental Findings	151
6.5	Future Work	152
7	Conclusion	153
Part 4	References and Nomenclature	157
	Bibliography	159
	Nomenclature	163
	List of Figures	167
	List of Tables	171
Part 5	Appendix Report	1
A	Field Investigations	
B	Experimental Investigations	

Chapter 1

Introduction

In this initial chapter the foundation of this thesis is outlined. This is done by introducing the background for the problem behind this thesis followed by a literature study in the area. Based on these preliminary studies an overall thesis statement and supporting project objectives are formulated. Hereafter it is described how the objectives are solved and a presentation of fundamental analysis tools and theory is made. The final section of this chapter describes the report structure and referencing method.

1.1 Background

Ventilation is a requirement in buildings. We need fresh air to breath and feel in comfort. The Indoor Air Quality (IAQ) highly affects our performance of work and learning capability. Moreover, it is often combined with some sort of mechanical heating or cooling system making the ventilation application the most essential part of any HVAC-system. In consequence ventilation accounts for a major part of HVAC operation and maintenance costs in buildings and is therefore an important area where current practice should be constantly challenged and new ideas investigated.

For long, mechanical ventilation, mainly in terms of Mixing Ventilation and Displacement Ventilation, has dominated the marked. In some cases the use of ventilation driven by natural forces (Natural Ventilation) has proven applicable, but difficulties in proper control and sufficient driving forces has always been an issue. A "new" ventilation principle has in recent years entered the marked and is in these days subjected to intensive studies at several scientific institutions in Denmark alone (Aalborg University, Technical University of Denmark and Aarhus University). The system is called Diffuse Ceiling Ventilation (DCV) and utilizes a suspended ceiling as a single big air terminal device (see figure 1.1D). This may happen because air is supplied to the plenum above the suspended ceiling through ducts, openings in the walls or the like thus creating an overpressure where the plenum acts as a pressure chamber. With a relatively larger pressure drop across the suspended ceiling than inside the plenum itself, the inlet air can be evenly distributed across the entire ceiling area. This leads to one of the biggest advantages of DCV; because air is supplied across a large inlet area, high ventilation rates may be delivered at a low momentum and thus low velocities creating a diffuse 'carpet' of inlet air on top of the thermally driven flows in the room. In this way DCV may potentially ensure a better indoor climate, where draught

risks are minimized.

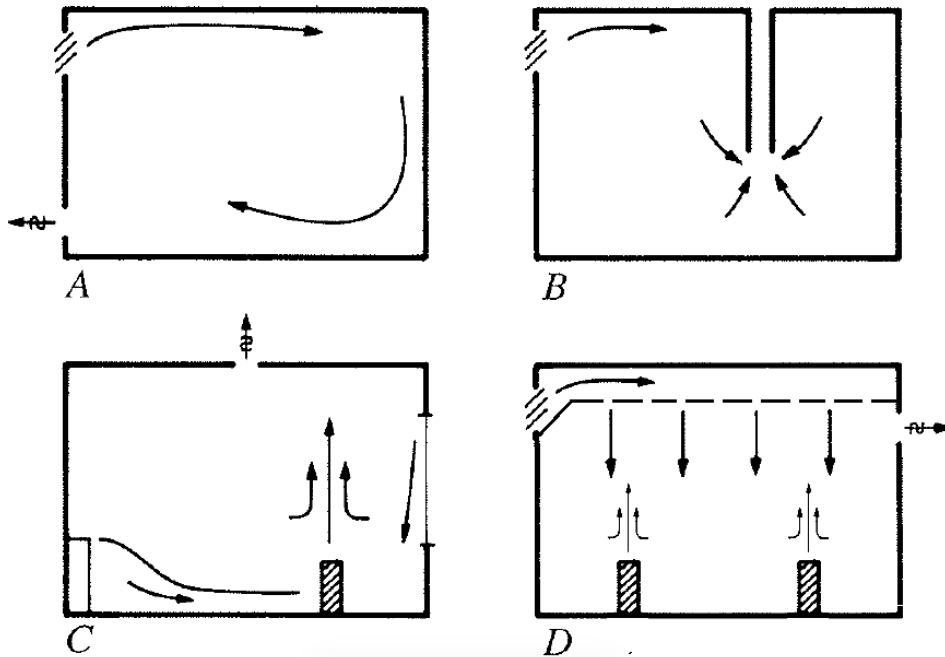


Figure 1.1: Four different types of air distribution systems. A: Mixing ventilation, B: Local exhaust ventilation, C: Displacement ventilation, and D: Diffuse ceiling ventilation. Sketches are reproduced from Nielsen, P. V. (1995) and slightly changed.

Apart from the above described indoor environmental benefits DCV also shows promising potential in relation to energy savings. The fact that a lot of ductwork may be eliminated, combined with a very low inlet pressure drop means that the total pressure loss the ventilation unit has to overcome can be greatly reduced compared to conventional mechanical ventilation systems.

In DCV some preheating of the inlet air should theoretically take place in the plenum above the suspended ceiling due to excess heat from the room underneath, hereby minimizing, or maybe even removing, the need for additional mechanical preheating during the heating season. Furthermore, as many new buildings have significant cooling loads it may prove very efficient that DCV allows relatively high ventilation rates at low inlet velocities, potentially limiting the energy use for cooling, which often is a necessity during working hours in the majority of the year.

Several controlled experiments, numerical simulations and some preliminary pilot test has already provided good results in regards to the applicability of DCV, however, more studies of the performance of the system during actual and realistic operating conditions are needed. Moreover, the combination of DCV and natural driving forces is still a relatively unexplored area, which may prove ideal due to the very low pressure losses in the system.

1.2 Literature Study

In order to identify the current state-of-the-art knowledge concerning DCV a literature study is conducted. This serves as the starting point in defining the thesis statement and specific projects objectives.

Publications

Zhang, C. et al. has summarized the conclusions of a large literature review on DCV and reached the following overall conclusions (reproduced in shortened form):

- The flow pattern generated by DCV can be either buoyancy controlled or momentum controlled, depending on the ventilation rate. However, buoyancy controlled patterns has great potential to apply for non-industrial purpose, because it is possible to handle high heat loads without generating draught.
- Based on air path, diffuse ceiling inlets can be divided into three types: air supply through connection slots, air supply through both connection slots and perforated ceiling tiles, air supply through perforated ceiling.
- Small vertical temperature gradients ranging from 0.3 to 1 K/m is observed in the case of cooling, while it rises to 2 K/m in the heating case. Heat loads in the occupied zone could increase mixing level, which is beneficial to thermal comfort. It should be recommended to use DCV systems together with convectors in the heating mode.
- Using diffuse ceilings as air terminal devices can provide a low draught risk. The highest risk of draught is found at the ankle level. The draught level is independent of flow rate, but it is influenced by heat sources. CFD simulations indicated that the thermal plumes force the supply air to regions with no heat sources, leading to cold downdraft and risk of draught in those regions. In addition, discomfort caused by radiant asymmetry of cool ceiling can be negligible.
- Heat sources layout has significant impact in the buoyancy driving air distribution. The highest cooling capacity can be obtain for equally distributed heat sources. Heat loads placed at the floor level give the highest risk of draught. Heat loads placed at the upper zone (e.g. lighting) generate the lowest risk of draught.
- The air change efficiency is comparable to perfect mixing ventilation. There is not any stagnant zone or short-circuiting ventilation in the room with DCV.
- The pressure drop is dependent on the design of the diffuse ceiling inlet, such as shape, material, porosity of the ceiling, connection profile, etc. Generally, DCV has a significantly lower pressure drop than conventional ventilation systems.
- The critical issues regarding the proper design of plenum to uniform the air distribution and surface temperature, as well as design of the suspended ceiling to optimize the radiant cooling potential by thermal mass, should be addressed in the future research.

As listed above the review by Zhang, C. et al. finds that the airflow pattern (either buoyancy controlled or momentum controlled) is governed by the ventilation rate. This conclusion is to some extent supported in a new study by Petersen, S. et al. (2014). Petersen, S. et al. (2014) finds that DCV can result in a resemblance of displacement ventilation, however, that this tendency is more dependent on the temperature difference between inlet air and room air than the ventilation rate itself. Moreover, it is found that the displacement effects happen at low internal heat loads

(air falls to the floor near external walls and rise towards the ceiling at point heat sources thus creating a vortex on room level) and develops towards fully mixing with increased internal heat loads. Finally, Petersen, S. et al. (2014) conclude that vertical air velocity profiles, temperature distribution and ventilation efficiency in DCV systems are independent of Archimedes number. The study do, however, argue that further investigations of proper ceiling design and heat load influence should be done.

The documentation available on DCV deals with many different efforts in describing such systems and their applicability. However, almost all of the research conducted in the area has been from a controlled experimental point of view or in the form of numerical CFD-simulations. Only few studies document how DCV work in buildings under true daily conditions thus making the conclusions less valid. Only Jacobs, P. et al. (2008), Jacobs, P. and Knoll (2009) and Hviid, C. A. and Terkildsen (2012) seem to have done this. In their studies the main focus have been on ceiling design and draught risk in the occupied zone.

The conclusion that more studies of DCV during true operating conditions has to be performed is to some extend supported by Iqbal, A. et al. (2013), who has investigated how the use of Computational Fluid Dynamics (CFD) may be used as a tool to simulate the pressure drop across porous acoustic ceiling panels. Their findings show how it is possible to perform CFD predictions of the pressure drop with a predefined permeability at high-velocity isothermal airflows with an error less than 15 % and an error as low as 1% when simulating low-velocity isothermal flows. An uncertainty of 15 % may in some cases be satisfactory, however, as it may be reasonable to expect higher errors when performing more complex simulations like whole rooms and especially during dynamic conditions, 15 % is a high uncertainty. However, the conclusions by Iqbal, A. et al. (2013) is found based on the assumption that the permeability of the porous membrane (diffuse ceiling panel) is predefined and modelled using Darcy's formula. Moreover, only isothermal flow is assessed and it is assumed that the flow direction is unchanged as it passes through the membrane (uniform flow direction). This assumption could potentially cause unrealistic results, as room heat loads in some case will force air up though the suspended ceiling.

What Remains to be Done

Research in the following areas have not yet been documented thoroughly and should be investigated further in order to raise the reliability in the results:

- Performance of DCV during true operating conditions
- Influence of DCV characteristic elements (plenum, suspended ceiling, geometry etc.) on ventilation effectiveness and indoor environmental quality
- Combination of DCV with radiant cooling technologies
- Combination of DCV with natural or hybrid ventilation principles
- Construction of a reliable numerical model for predicting airflows in rooms with DCV.

1.3 Thesis Statement

On the basis of the initial literature study a main working question, or objective, is formulated to frame the scope of the thesis and enclose the project work. In order to answer the main question in both a valid and reliable way two supporting objectives are stated and should serve as milestones or working tasks. These create the premises and conditions necessary to conclude on the main objective as a logical consequence of the work with the supporting objectives.

Main Working Question

What influences the functionality and delivered indoor thermal comfort of a diffuse ceiling ventilation system?

By "influences" is meant an effect or system parameter, which in terms of its presence or value cause significant changes to either, or both;

- the technical functionality of the ventilation system consisting of e.g. airflow distribution, ventilation effectiveness etc.
- the indoor environmental quality.

The exploratory nature of the main working question calls for a wide range of additional questions, hypotheses and potential conclusions, which is why it is delimited to the following two supporting objectives that serve as the tasks to be addressed in this thesis. Both objectives relate to the main working question in terms of their contribution to the answering of it.

Supporting Objective 1

How does diffuse ceiling ventilation systems perform during true operating conditions?

This question is important because only few previous studies have thoroughly investigated the performance of DCV during true conditions, and no one in a way that the conclusions are unambiguously valid. By investigating the performance during true operating conditions. Moreover, dealing with this question gives a unique insight into some of the implications with DCV.

Supporting Objective 2

To what degree does the supply opening area of a diffuse ceiling ventilation system influence the functionality and delivered indoor thermal comfort of a diffuse ceiling ventilation system?

The supply opening area, in terms of the permeable suspended ceiling area, is assessed to be a major part contributing and affecting the indoor climate and system functionality when using DCV.

The objective is assisted by the following hypothesis:

The supply opening area of a diffuse ceiling system has a significant influence on:

- *airflow patterns and thus thermal comfort in the occupied zone*
- *air and temperature distribution in the plenum volume*

1.4 Research Design

From the following description the overall approach of finding solutions to the thesis statement and the supporting objectives, as well as how the solution is delimited, is given. A general presentation of applied analysis tools and theory used in all parts of the thesis is presented in section 1.5 on page 8. The more detailed methodology and practical implementation is described in the relevant chapters of the report. Thus the descriptions below serve as a preliminary introduction for the reader.

To answer the thesis statement the problem is mainly approached from an overall quantitative-positivistic point of view using a combination of confirmatory and exploratory experimental research. The main focus is on quantitative methods in order to quantify the perspective of DCV in relation to other ventilation systems.

Supporting Objective 1

Supporting Objective 1 deals with the performance of DCV during true operating conditions. To do so a building with DCV currently installed and running actively is applied as test case in a semi-experimental field investigation. The performance is evaluated based on the following analyses; using the analysis tools presented in section 1.5:

- Plenum effects (air distribution and preheating of inlet air)
- Room airflow patterns
- User behaviour and system control

Initially, a pilot study is performed to review the ventilation system, its control strategy and to evaluate any practical challenges. Based on experience gained from the pilot study a more comprehensive measurement setup is later installed and a main study is carried out, from which conclusions are drawn.

By implementing this two-step approach it is secured that all relevant information and parameters are measured correctly and thus the risk of failure and erroneous results are minimized. Moreover, the advantage of the field studies is that outcomes are observed in a natural setting rather than in a contrived laboratory environment. For this reason, it is assessed that the results of the field experiments have a higher external validity, versus had the investigations been carried out using laboratory experiments alone.

Supporting Objective 2

To assess the influence of the suspended ceiling design on system performance, an overall quantitative-positivistic approach is applied. It is done through the use of full-scale experimental investigations in laboratory and also numerical predictions (CFD). The application of a controlled research environment is found necessary in order to account for possible influencing parameters and correlations between them. Moreover, large empirical data sets are a prerequisite for ensuring reliability and validity within the results when seeking to establish correlations between variables. This is hardly obtainable through qualitative research such as case-studies, reviews or other descriptive research methods.

The influence of the suspended diffuse ceiling is assessed through the following investigations using the analysis tools described in section 1.5:

- Cooling capacity
- Plenum effects (air permeability and preheating of inlet air)
- Room airflow patterns

For these parameters correlations are sought, which makes it possible to draw conclusions on proper ceiling design and how it affects system performance. In general, results obtained through the investigations of Supporting Objective 1 and 2 is sought treated in a similar manner making result more comparable.

Procurement of data for the analyses of Supporting Objective 2 involves two sub-methodologies:

Experimental steady-state investigations. A controlled full-scale experimental setup is used for a correlation study using a parametric variation methodology involving the suspended ceiling layout and other selected boundary conditions. By simultaneously measuring important indoor environmental factors, the study is meant to reveal correlations and form the basis of the abovementioned analyses.

Numerical steady-state investigation. The numerical predictions is used for testing the robustness or uncertainty of the suspended ceiling design at different conditions, which otherwise would be too extensive to perform through the use of experimental measurements such as changing room geometry, heat load distribution etc. The CFD model is constructed and calibrated based on findings and measurements from the experimental investigations. This way the experimental measurements serve as validation benchmarking data for the creation of a reliable CFD model.

1.5 Analysis Tools and Theoretical Offset

Equations, definitions and analyses used throughout the thesis are presented in this section. Specific analyses only relevant in some parts of the thesis are presented along with the results of such analyses. To assist the understanding of introduced theory please find lists of applied abbreviations and symbols in the thesis nomenclature on page 163.

Diffuse Ceiling Ventilation System

Diffuse Ceiling Ventilation (DCV) system may be configured in many different ways. In this thesis, a DCV system is defined as a system with a separated pressure chamber - the plenum volume - which is located in between the true ceiling and a false suspended ceiling. The plenum is supplied with fresh air from either dampers in the walls, ducts etc. As such, air supply may be either mechanical driven (balanced ventilation) or alone exhaust driven. The suspended ceiling works as diffuser of inlet air, with the supply opening area being configured with porous panels securing a pressure resistance. This pressure resistance - expressed as the permeability - of these diffuser panels must be high enough to uphold an even pressure distribution throughout the plenum, defined as the pressure chamber effect. By utilizing a large supply opening area, inlet momentum is very low - referred to as *diffuse* - compared to conventional solution e.g. mixing ventilation where high-momentum inlet jets are utilized. This way large ventilation rates may be supplied at low air speed.

A typical system layout with key important parameters are presented in figure 1.2 and elaborated below the figure.

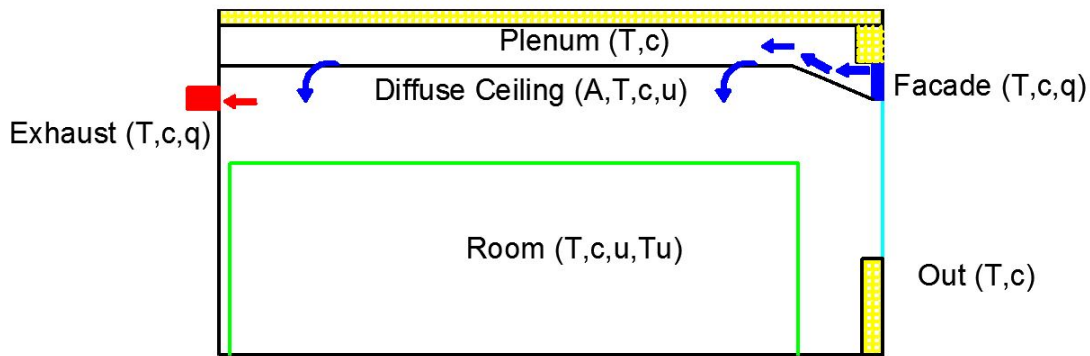


Figure 1.2: Sketch defining DCV parameters.

where:

- T = Temperature [$^{\circ}\text{C}$]
- c = Concentration of air component, e.g. CO_2 [ppm]
- u = air velocity [m/s]
- Tu = turbulence intensity [-]
- q = airflow rate [m^3/s]
- A = area [m^2]

One of the important parameters in DCV, and focus of this thesis, is the area (A) of diffuse ceiling panels (DC), defined as A_{DC} . A dimensionless form of diffuse ceiling area, A_{DC}^+ , is defined as:

$$A_{DC}^+ = \frac{A_{DC}}{A_{ceiling}} \quad (1.1)$$

where:

$$\begin{aligned} A_{DC}^+ &= \text{dimensionless diffuse ceiling area (diffuser area) [-]} \\ A_{DC} &= \text{area of diffuse ceiling [m}^2\text{]} \\ A_{ceiling} &= \text{area of suspended ceiling [m}^2\text{]} \end{aligned}$$

It is worth noticing that the supply air velocity through the diffuse ceiling, u_{DC} , is not a measured parameter but calculated from the ventilation rate, q_v , and diffuse ceiling area, A_{DC} , as presented in equation 1.2.

$$u_{DC} = \frac{q_v}{A_{DC}} \quad (1.2)$$

As the supply air velocity, u_{DC} , is a derived parameter it alone express the average air velocity through the diffuse ceiling panels.

Indoor Environmental Quality

Evaluation of indoor environmental quality (IEQ) is limited to assessment of indoor air quality (IAQ) and thermal comfort.

Indoor Air Quality. Analyses are limited to measurements and evaluation of CO₂-concentrations in the occupied zone. In accordance with Danish building legislation (BR10) ventilation in rooms must be capable of ensuring that CO₂-concentration does not exceed 1000 ppm for an extended time period (BR10, 2010). IAQ analyses are only conducted for the field studies in this thesis.

Thermal Comfort. The static PMV/PPD model developed by P. O. Fanger is used for evaluation of thermal comfort utilizing heat balance equations of the human body (Fanger, P. O., 1970). Thermal comfort assessment is based upon the categorizing of thermal classes as done in ISO-7730 (2006). Of the three comfort categories (A, B and C) category B is chosen as satisfying indoor comfort as this is the standard criterion, which also makes comparison to previous studies easier. The specific criteria of all three thermal comfort classes can be seen from table 1.1. There is no allowance for partial fulfilment of categories so as soon as one criterion is not met in the given category the entire comfort assessment moves down a level.

Table 1.1: Categories of thermal environment. Reproduced from ISO-7730 (2006).

Category	Thermal state of the body as a whole		Local discomfort			
	PPD [%]	PMV [-]	DR [%]	PD [%] caused by		
				Vertical air temperature difference	Warm or cold floor	Radiant asymmetry
A	<6	-0.2<PMV <+0.2	<10	<3	<10	<5
B	<10	-0.5<PMV <+0.5	<20	<5	<10	<5
C	<15	-0.7<PMV <+0.7	<30	<10	<15	<10

As seen from table 1.1 thermal comfort is divided into global comfort for the body as a whole (PMV and PPD) and local discomfort, i.e. unwanted cooling or heating of a single body part. The analyses performed in this thesis are mainly focused on the local discomfort criteria as the resulting local discomfort is what makes one ventilation system differ from another when the same global comfort is sustained by the heating system. All local discomfort criteria are evaluated as Percentage Dissatisfied (PD). The definitions and equations for calculation of local discomfort parameters are presented below and duplicated from ISO-7730 (2006).

Draught Rating expresses the expected percentage of people to be bothered by draught. DR is calculated cf. equation 1.3.

$$DR = (34 - T_{air}) (u_{air} - 0.05)^{0.62} (0.37 \cdot u_{air} \cdot Tu + 3.14) \quad (1.3)$$

where:

- DR = draught rating [%]
- T_{air} = air temperature [°C]
- u_{air} = air speed [m/s]
- Tu = air turbulence intensity [%]

Vertical temperature differences for an upwards increasing temperature difference between ankles and head can cause discomfort. From equation 1.4 the PD due to vertical temperature difference, $\Delta T_{head/ankles}$ is calculated. Temperatures must be measured in 0.1 m and 1.1 m above floor level for sedentary activity.

$$PD_{\Delta T_{head/ankles}} = \frac{100}{1 + \exp(5.76 - 0.856 \cdot \Delta T_{head/ankles})} \quad (1.4)$$

where:

- $PD_{\Delta T}$ = percentage dissatisfied due to vertical air temperature difference [%]
- $\Delta T_{head/ankles}$ = vertical air temperature difference between head and ankles [°C]

The equation is only valid for temperature differences, $\Delta T_{head/ankles} < 8^\circ\text{C}$. For category B the vertical temperature difference must be smaller than 3°C .

Warm or cold floor can cause local discomfort for people wearing light indoor shoes, where it is the temperature of the floor, T_{floor} , rather than the material, which is important for comfort. Too cold or warm floors can cause discomfort for the feet, and so the PD with cold or warm floor can be calculated cf. equation 1.5.

$$PD_{floor} = 100 - 94 \cdot \exp(1.387 + 0.118 \cdot T_{floor} - 0.0025 \cdot T_{floor}^2) \quad (1.5)$$

where:

$$\begin{aligned} PD_{floor} &= \text{percentage dissatisfied due to too warm or cold floors [\%]} \\ T_{floor} &= \text{floor surface temperature [}^\circ\text{C]} \end{aligned}$$

This equation is also valid for people sitting or lying on the floor. To comply with category B temperature range of the floor must be 19°C - 29°C .

Radiant asymmetry is a local discomfort criterion, which estimates the expected PD from uneven surface temperature distribution. Differences are evaluated horizontally and vertically. As cold air is delivered through the diffuse ceiling it is especially the radiant asymmetry between ceiling and body-plane that is of interest. The equation for PD estimation due to cold ceilings is seen from equation 1.6. Although only the equation for cold ceiling is presented here, the evaluation of thermal comfort in the analyses in the thesis will include calculations of PD for all four radiant asymmetries; Warm Ceiling, Cold Ceiling, Cold Wall and Warm wall. The equations for the remaining three radiant asymmetries can be found in ISO-7730 (2006).

$$PD_{\Delta T_{pr}} = \frac{100}{1 + \exp(2.84 - 0.174 \cdot \Delta t_{pr})} - 5.5 \quad (1.6)$$

where:

$$\begin{aligned} PD_{\Delta T_{pr}} &= \text{percentage dissatisfied due to radiant asymmetry [\%]} \\ \Delta T_{pr} &= \text{radiant temperature asymmetry [}^\circ\text{C]} \end{aligned}$$

The calculation provides a conservative estimate of discomfort, i.e. no other position of the body causes higher discomfort. Equation 1.6 is only valid for $\Delta t_{pr} < 23^\circ\text{C}$. For category B radiant asymmetry, Δt_{pr} for cold ceilings must be smaller than 14°C .

Cooling Capacity and Design Chart

The cooling capacity of a DCV system, Φ_{DCV} , is described by the amount of thermal energy removed by ventilation, which is a function of the temperature difference between inlet and outlet, ΔT , and the rate of ventilation, q_v , as given in equation 1.7.

$$\Phi_{cool} = q_v \cdot \rho \cdot c_p \cdot (T_{exhaust} - T_{facade}) \quad (1.7)$$

where:

- Φ_{cool} = cooling capacity of DCV system, Φ_{DCV} [W]
- q_v = ventilation rate [m^3/s]
- ρ = air density ($\approx 1.2 \text{ kg}/\text{m}^3$) [kg/m^3]
- c_p = air specific heat capacity ($\approx 1005 \text{ J}/(\text{kgK})$) [$\text{J}/(\text{kgK})$]
- $T_{exhaust}$ = air temperature in exhaust opening [$^{\circ}\text{C}$]
- T_{facade} = air temperature in facade opening [$^{\circ}\text{C}$]

The main objective for this analysis is to establish a correlation between temperature difference and ventilation rate describing the system cooling capacity when limited by a retention of thermal comfort. This correlation may be presented in terms of a $(q_v, \Delta T)$ -chart also known as a *Design Chart* as illustrated schematically in figure 1.3.

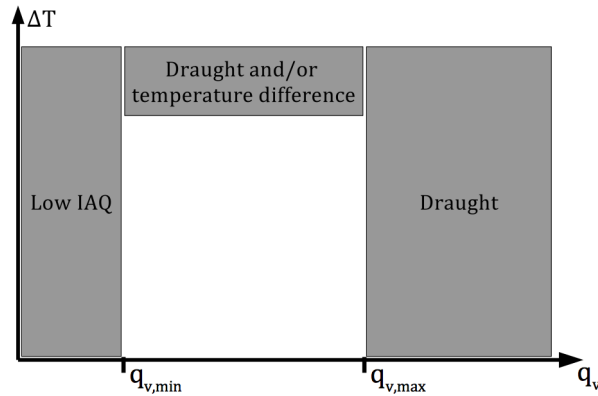


Figure 1.3: Exemplary design chart, showing limiting parameters for temperature differences (y -axis) and ventilation rate (x -axis).

The chart express comfort limiting combinations of ventilation rate and temperature difference for a given ventilation system design.

Airflow patterns

Distribution of the ventilation air is of great importance, both in terms of system efficiency and the indoor environmental quality of the occupied zone. In order to analyse the airflow generated in rooms with DCV a number of airflow analyses must be conducted. A special characteristic, and important part of the analysis of DCV systems, is the plenum above the suspended ceiling. Analysis of airflow is directly quantified from measured values and presented in either absolute values, normalized values or dimensionless model numbers.

Dimensionless analysis. Dimensionless analysis is often a convenient way of assessing fluid properties as it cancels out any physical dimension of the variable making it possible to compare otherwise incomparable quantities. In this thesis it incorporates *normalization* of the measured results with a reference value or other model specific parameters. The normalization of results is helpful in comparisons between different investigations, such as field studies and experimental studies. The normalized dimensionless air speed in the room, u_x^* , is calculated as done in equation 1.8.

$$u_x^* = \frac{u_x}{u_{DC}} \quad (1.8)$$

where:

$$\begin{aligned} u_x^* &= \text{dimensionless local air speed [-]} \\ u_x &= \text{local air speed [m/s]} \\ u_{DC} &= \text{supply air speed through diffuse ceiling (see equation 1.2) [m/s]} \end{aligned}$$

For the normalization of air speeds across different system configurations, e.g. different diffuse ceiling areas, it is often convenient to compare those air speeds to a reference air speed, u_{ref} , for the system. For this purpose equation 1.9 is introduced giving the ventilation rate, q_v , through a reference area, in this case the entire ceiling area, $A_{ceiling}$.

$$u_{ref} = \frac{q_v}{A_{ceiling}} \quad (1.9)$$

where:

$$\begin{aligned} u_{ref} &= \text{reference air speed [m/s]} \\ q_v &= \text{ventilation rate [m}^3\text{/s]} \\ A_{ceiling} &= \text{suspended ceiling area [m}^2\text{]} \end{aligned}$$

The normalized maximum air speed in the occupied zone, $u_{max,OZ}^*$, is defined as presented in equation 1.10. By normalizing with the reference air speed, u_{ref} , defined above, the normalized maximum air speed in the occupied zone is independent of the ventilation rate and thus dimensionless.

$$u_{max,OZ}^* = \frac{u_{max,OZ}}{u_{ref}} = \frac{u_{max,OZ}}{\frac{q_v}{A_{ceiling}}} \quad (1.10)$$

where:

$u_{max,OZ}^*$ = normalised maximum air speed in occupied zone [-]

$u_{max,OZ}$ = maximum air speed in occupied zone [m/s]

u_{ref} = reference air speed (see equation 1.9) [m/s]

q_v = ventilation rate [m³/s]

$A_{ceiling}$ = suspended ceiling area [m²]

Normalized analyses of temperature development or CO₂-concentration from inlet to outlet is calculated as presented in the equations below. They express the ratio between increment from inlet to present point x in relation to the total increment from inlet to outlet. 'Inlet' is typically the facade inlet into the plenum or the supply opening area in the diffuse ceiling. 'Outlet' is typically the exhaust opening, but can also be the diffuse ceiling inlet into the room if the present analysis focus on the plenum effects.

$$T_x^* = \frac{T_x - T_{inlet}}{T_{outlet} - T_{inlet}} \quad (1.11)$$

$$c_x^* = \frac{c_x - c_{inlet}}{c_{outlet} - c_{inlet}} \quad (1.12)$$

where:

T_x^* = dimensionless temperature [-]

T_x = local temperature [°C]

T_{inlet} = temperature in inlet, either T_{facade} or T_{DC} [°C]

T_{outlet} = temperature in outlet, either $T_{exhaust}$ or T_{DC} [°C]

c_x^* = dimensionless CO₂-concentration [-]

c_x = local CO₂-concentration [ppm]

c_{inlet} = CO₂-concentration in inlet [ppm]

c_{outlet} = CO₂-concentration in outlet [ppm]

To express the ventilation effectiveness, ε_v , of the ventilation system, equation 1.13 is used. The ventilation effectiveness characterises the mass transport in the room. The temperature effectiveness, ε_T , is calculated in the same way, and describes the energy transport in the room. The effectiveness is the inverse of the dimensionless quantity or gradient defined in equation 1.11 and 1.12.

$$\varepsilon_v = \frac{c_{exhaust} - c_{facade}}{c_x - c_{facade}} \quad (1.13)$$

$$\varepsilon_T = \frac{T_{exhaust} - T_{facade}}{T_x - T_{facade}} \quad (1.14)$$

where:

ε_v	= ventilation effectiveness [-]
c_x	= local CO ₂ -concentration [ppm]
c_{facade}	= CO ₂ -concentration in facade opening [ppm]
$c_{exhaust}$	= CO ₂ -concentration in exhaust opening [ppm]
ε_T	= temperature effectiveness [-]
T_x	= local temperature [°C]
T_{facade}	= temperature in facade opening [°C]
$T_{exhaust}$	= temperature in exhaust opening [°C]

Reynolds number (Re). Reynolds number describes the relationship between inertial forces and viscous forces, and is defined as shown in equation 1.15. Re is useful in describing inherent turbulence level of the airflow investigated and by correlating Reynolds number and maximum air speed, u_{max} it is easy to e.g. characterise if a fully turbulent flow regime is reached. Reynolds number is calculated using a reference velocity, in this case the supply air speed through the diffuse ceiling area, u_{ref} , which alone is a function of the ventilation rate, q_v .

$$Re = \frac{u_{ref} l}{\nu} \quad (1.15)$$

where:

Re	= Reynolds number [-]
u_{ref}	= reference air speed (see equation 1.9) [m/s]
l	= characteristic length (square root of ceiling area, $\sqrt{A_{ceiling}}$) [m]
ν	= kinematic viscosity of air ($\approx 1.48 \cdot 10^{-5} \text{m}^2/\text{s}$) [m ² /s]

Archimedes number (Ar). Archimedes number describes the relationship between buoyancy forces and inertial forces of the airflow and is defined in the equation below. Especially for DCV systems where flow is expected to be dominated by the room heat sources Ar-analyses can offer important correlations and assist in future design of DCV systems for different rooms.

$$Ar = \frac{g\beta l(T_{final} - T_{initial})}{u_{ref}^2} \quad (1.16)$$

where:

- Ar = Archimedes number [–]
- g = gravitational acceleration [m/s²]
- β = thermal expansion coefficient (= 1/T) [1/K]
- l = characteristic length (square root of ceiling area, $\sqrt{A_{ceiling}}$) [m]
- u_{ref} = reference air speed (see equation 1.9) [m/s]

As it is a goal to establish the main airflow patterns of the ventilated room as function of diffuse ceiling area, and to confirm whether or not the developed airflow patterns are dependent upon the different combinations of temperature difference, ΔT , and ventilation rate, q_v , that make up the cooling capacity, Φ_{vent} , this is investigated by characterising the flow as function of Archimedes number, Ar .

Statistical Analysis

Through analysis of the measured data it is possible to account for correlations using statistical tools. These tools will quantify how parameters affecting a DCV system is correlated, which is helpful in future designing of systems as it is known how a choice of a given parameter affects the rest of the DCV system.

Application of Statistical Analysis. Both regression and correlation analysis is in this thesis used as a quantitative tool for answering especially Supporting Objective 2 in relation to the coherence between the supply opening area as predictor variable and various other system variables defined in the hypothesis. Statistical analysis is performed using Matlab 2014b Curve Fitting Tool, applying the regression method of *least squares*.

Regression Analysis. Regression is used to establish relationships (models) relating the criterion variable (y) to one or more other predictor variables (x_1, x_2, \dots, x_n). The predictor variables are variables for which their variation is believed to cause or agree with variation in the criterion variation.

Correlation Analysis. Correlation analysis provides a means of drawing inferences about *strength* of the relationship between two or more variables. I.e., it is a measure of the degree to which the values of these variables vary in a systematic manner. Thus, it provides a quantitative index of the degree to which one or more variables can be used to predict the values of another variable. It is important to note that correlation analysis does not indicate whether a relationship is causal; it is necessary for the investigator to determine whether there is a cause-and-effect (causal) relationship between the variables. Correlation analysis only indicates whether the degree of common variation is significant (Ayyub, B.M. and McCuen, 2011).

Figure 1.4 shows different samples of data for two variables having different degrees of common variation.

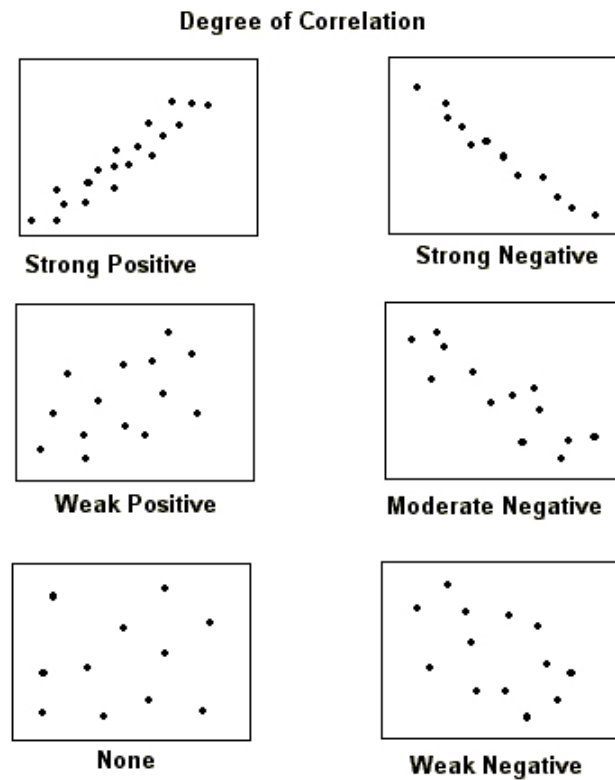


Figure 1.4: Correlation of data. (Cedar Crest College, 2015)

The degree of common variation - their correlation - is quantified by the correlation coefficient, an index of their association. Many different indexes of correlation exist. This thesis only makes use of the Spearman rank correlation coefficient, ρ_s , which is defined as the Pearson correlation coefficient between the ranked variables.

Spearman's rank correlation coefficient assesses how well the relationship between two variables can be described by a monotonic function and not only a linear function. The coefficient is defined from -1 to +1, where 1 is total positive monotonic correlation, 0 is no monotonic correlation, and -1 is total negative monotonic correlation (see figure 1.4). The strength of the correlation is defined in table 1.2.

Table 1.2: Strength of correlations.

Value of correlation coefficient	Strength of the correlation
-1 or +1	Perfect
-0.7 to -0.9 or +0.7 to +0.9	Strong
-0.4 to -0.6 or +0.4 to +0.6	Moderate
-0.1 to -0.3 or +0.1 to +0.3	Weak
0	None

Correlation provides a measure of goodness of fit and is used for assessment of the reliability of a regression.

Statistical Significance. Even though a correlation is found strong based on the correlation coefficient the conclusion that it is strong is not necessarily *statistically significant* or probable. The correlation coefficient only examines the *strength* of the correlation, however, the *significance* of the correlation also needs being addressed. To do that, a two-tailed hypothesis test (t-test) is performed investigating whether or not the sample supports the conclusion at a given significance level, α . The procedure used include formulating a null hypothesis, H_0 , which is sought rejected by testing it against an alternative hypothesis, H_A .

$$H_0 \text{ (null hypothesis)} : \rho_s = 0 \quad (1.17)$$

$$H_A \text{ (alternative hypothesis)} : \rho_s \neq 0 \quad (1.18)$$

The test statistic, t , is calculated for the data sample using equation 1.19.

$$t = \rho \cdot \frac{\sqrt{n-2}}{\sqrt{1-\rho^2}} \quad (1.19)$$

where:

- t = test statistic [-]
- ρ = correlation coefficient [-]
- n = sample size [-]

Using the test statistic, t , the critical value, $t_{\frac{\alpha}{2}, n-2}$, at the given significance level with $n-2$ degrees of freedom, is determined, which is the answer to the question: "*How likely is it that we'd get a test statistic, t , as extreme as we did if the null hypothesis were true?*" The chosen significance level for any hypothesis test in this thesis is:

Significance level, $\alpha = 5\%$

If the test statistic, t , is less than or equal to the critical value, $t_{\frac{\alpha}{2}, n-2}$ (refer to t -distribution tables), it is concluded that the null hypothesis is true or that the analysis fail to reject the null hypothesis at the significance level, meaning that the correlation is insignificant. Otherwise, if the test statistic, t , is larger than the critical value, it is concluded that the alternative hypothesis is true or that the null hypothesis is rejected at the significance level, meaning that the correlation is significant.

1.6 Report Structure

The report is structured around the solution of the supporting objectives. It is divided into five parts:

- Part 1 Field Study Investigations in a Danish Classroom
- Part 2 Experimental and Numerical Investigations
- Part 3 Recapitulation
- Part 4 References and Nomenclature
- Part 5 Appendix Report

Part 1 address the treatment of Supporting Objective 1. It is subdivided into two chapters; the preliminary *Pilot Study* and later *Main Study* comprising the final investigation during true operating conditions.

Part 2 deals with the solution of Supporting Objective 2. It is subdivided into two chapters; *Influence of Supply Opening Area* covering laboratory steady-state experiments and *Robustness of DCV System Design by Numerical Analysis* addressing the robustness of the experimental laboratory findings through numerical predictions.

Part 3 is where findings of the different investigations are subjected to an overall discussion in which results are questioned and put into perspective in relation to the thesis statement. Subsequently a final conclusion summarizes the main results and answers the thesis statement.

Part 4 encompass nomenclature and cited references. Moreover, lists of figures and tables may be found here.

Appendices are found in Part 5 comprising detailed descriptions of measurement equipment, and calibration hereof, used in the investigations throughout the thesis.

References

Source references are done according to the Harvard-method, also known as the Author and date system. In the text a reference will have the form; (Authors Surname, Year). In the reference list the full source is described. Standards and norms are referred to as; (Number, Year) e.g. (EN-12543-4, 1998). Books and Manuals are stated with Author, Title, Edition, Publisher and ISBN no. Internet sites are stated with Author, Title, Year and direct link. References appertaining a whole section are placed after the headline or right aligned after the section. References to a single sentence are placed directly after the sentence. Are there no references the material is made by the authors themselves. Figures and tables are numbered in accordance with chapter number and explanatory text can be found above or below the object.

A newly published technical report from the Department of Civil Engineering at Aalborg University is subjoined, as this report is made by the authors of this thesis and presents content used in present thesis.

Part 1

Field Study Investigations in a Danish Classroom

Answering Supporting Objective 1:

*How does diffuse ceiling ventilation systems perform
during true operating conditions?*

A field study investigation of Diffuse Ceiling Ventilation
system functionality during true operating conditions on
Solbjergskolen south of Aarhus, Denmark.

Chapter 2

Pilot Study

In this first chapter of Part 1 an initial pilot study of the DCV system installed on Solbjergskolen near Aarhus is presented. The reader is introduced to the test facility, a sixth grade classroom, and later guided through the setup of measurement equipment and finally analyses of measured variables. The outcome of the pilot study is a list of findings that serve as starting point for the bigger and more thorough main study presented in chapter 3.

2.1 Planned Investigations

As described above the overall scope of the pilot study is to gain preliminary knowledge about the DCV system installed on the test facility, Solbjergskolen, which is introduced below. The scope is also to review any practical implications on how to perform more extensive studies in the later more in-depth main study.

System Functionality

The functionality and physical mechanisms behind the DCV system is of key importance in understanding the ventilation principle and its applicability. The analyses necessary to review this system functionality includes:

- Air distribution (pressure chamber effect) in plenum and through the diffuse ceiling panels
- Preheating of inlet air in plenum above suspended ceiling
- Air distribution in room
- Practical and actual control of the ventilation system
- User behaviour and its influence on system functionality

Indoor Environmental Quality

Investigations and analyses of the Indoor Environmental Quality (IEQ)-conditions that arise due to the functionality of the DCV system cover: (1) Vertical temperature gradient in room, (2) Radiant temperature asymmetry caused by diffuse ceiling panels, (3) Air velocity in room, (4) Draught rate in room and (5) Air quality in room.

2.2 Field Study: Solbjergskolen, 6th grade classroom

The test facility used in the field study for both this pilot study and the main study is Solbjergskolen located 15 km South-West of Aarhus, Denmark (see figure 2.1). Solbjergskolen is a Danish municipal primary and lower secondary school that houses 620 students and 70 teachers. It was energy-renovated and retrofitted with DCV in 2009. DCV solutions are designed by Danish consulting engineering company Bascon A/S.

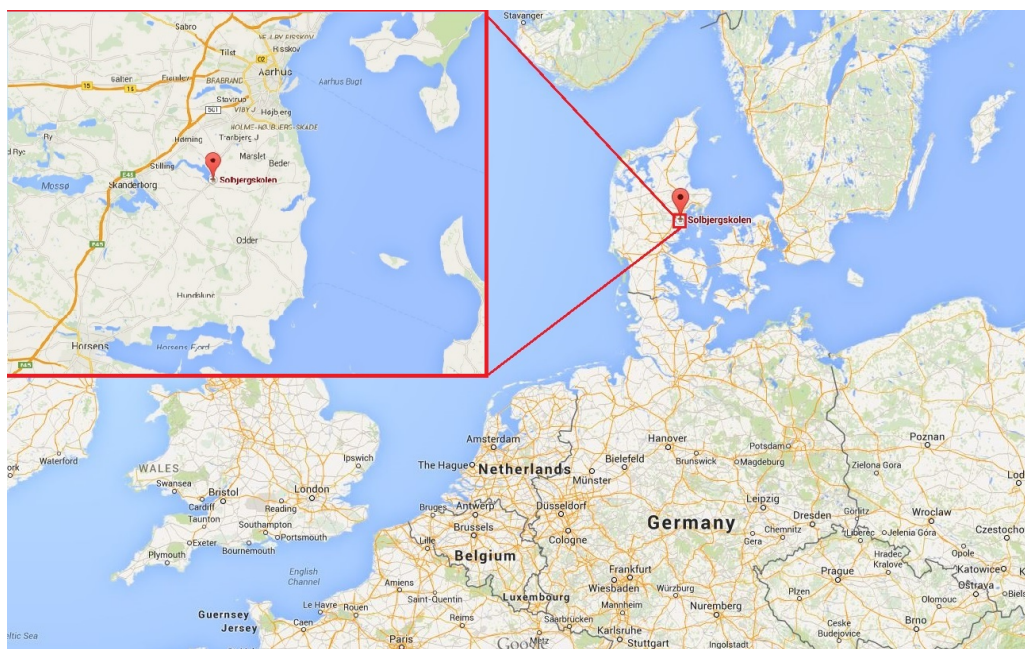


Figure 2.1: Location of case site: Solbjergskolen, Denmark [Google Maps, 2014].

DCV System Layout

The DCV system installed on Solbjergskolen consists of several partially centralised exhaust driven mechanical ventilation systems with no pre-conditioning of intake air.

Each room has individual façade inlets for fresh air, while central exhaust Air Handling Units (AHU) services up to four classrooms each. In figure 2.2 a sketch of the DCV system is shown as a cross-sectional view of a typical classroom, similar to the one where measurements are performed in the pilot and main study.

2. Pilot Study

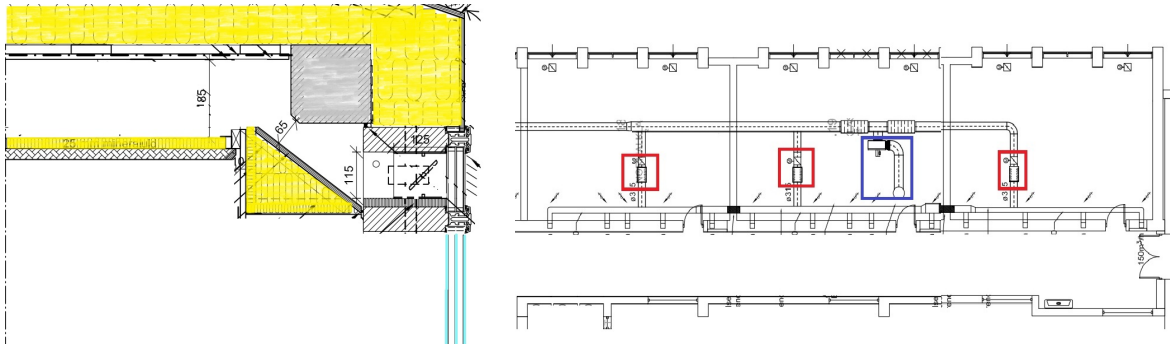


Figure 2.4: Technical drawings of ventilation inlet and exhaust. Left: Fresh air inlet from outdoor to plenum. Right: Exhaust layout showing VAV-dampers (red) for each classroom with central exhaust AHU (blue). Drawings reproduced from Bascon-A/S (N.A.).

In the right drawing of figure 2.4 the exhaust layout is shown. It should be observed how a central exhaust AHU removes air from multiple classrooms. Exhaust airflow from each room is individually controlled through VAV-dampers.

As indicated by figure 2.2 and figure 2.4 intake air enters the plenum through dampers in the façade with no mechanical pre-conditioning. This means that any preheating of inlet air happens in the plenum above the suspended ceiling when fresh, cold, outdoor air is heated by the warm, uprising, room air of the classroom. Negative pressure in the classroom, created by the exhaust fan and natural driving forces, drives outdoor air into the plenum down through the diffuse ceiling inlets to the room. Each classroom has two façade inlet dampers, four ventilation exhausts openings and typically 12 permeable/diffuse ceiling inlets as depicted in figure 2.5. Exhaust openings are placed with equal distances between them and mounted in the back wall of the room (wall opposite the façade).

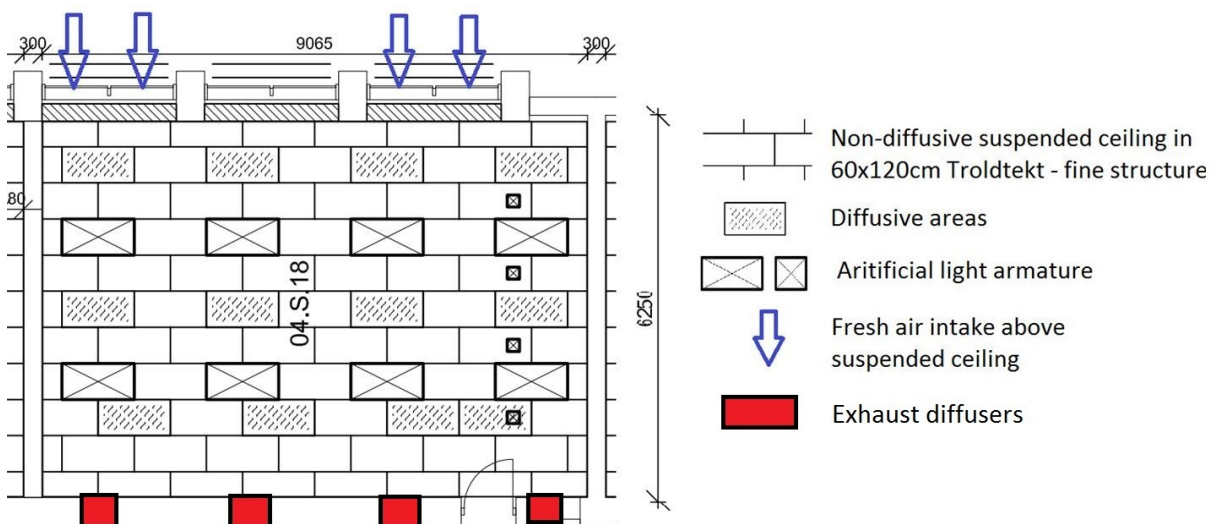


Figure 2.5: Top-view of suspended ceiling layout in test classroom. Drawings reproduced from Bascon-A/S (N.A.).

The diffusive panels shown in figure 2.5 are 35 mm thick 'fine-structured' Trolldtekt acoustic

panels (cement-bonded wood wool). The diffuse ceiling layout consist of 12 diffuse panels corresponding to 15% of the total ceiling area. The non-diffuse panels are only different from the diffuse panels by having a 25 mm air-tight insulation glued on the top side of the panel (see figure 2.6). Hence from the room side of the suspended ceiling it is not possible to see which areas are diffuse and which are not.

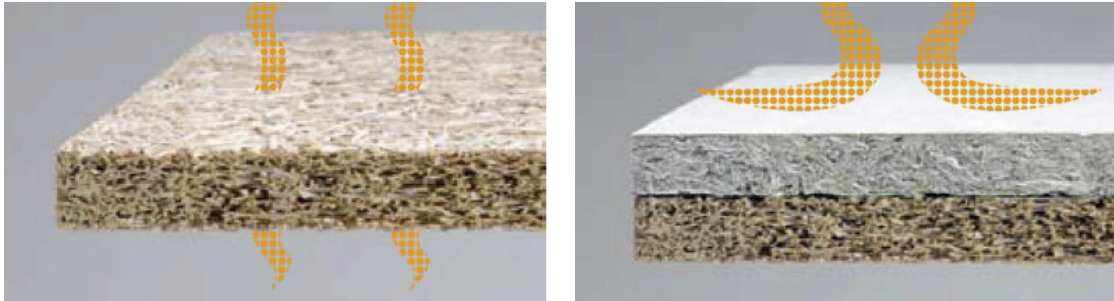


Figure 2.6: Cement-bonded wood wool ceiling panels from Trolldtekt. Left: Diffuse panel. Right: Non-diffuse panel.

The ceiling panels are screw-mounted into a metal framework, which carries the suspended ceiling as seen in figure 2.7. The metal framework rests on beams along the side walls of the classroom and in metal wires mounted in the actual ceiling.



Figure 2.7: Plenum above suspended ceiling.

Figure 2.7 shows a picture of the plenum volume above the suspended ceiling. Plenum height is 18.5 cm, however, as it is packed with light armatures, cables, etc., the effective height is much smaller in some regions, potentially decreasing air movement. Plenum volume make up 6.4% of the total room volume.

The façade inlet openings from where fresh air flows into the plenum make up approximately two-thirds of the total room length as seen on figure 2.5.

People Load

The measurements performed at Solbjergskolen are carried out in a typical 6th grade classroom. The classroom contains up to 26 students plus a teacher. Floor area of the investigated classroom is approximately 57 m^2 resulting in 0.5 pupil/m^2 . With a room height of 2.7 m the room volume is 154 m^3 .

Average school days range from 08:00 to 14:30, however, the daily occupancy of the room is very fluctuating as pupils often work in groups inside and outside the classroom and some classes are taught in dedicated workshop rooms.

BMS control

The school is equipped with a central Building Management System (BMS) that controls several HVAC services, including the DCV system. In figure 2.8 a logic chart of the BMS control of DCV on room level is shown.

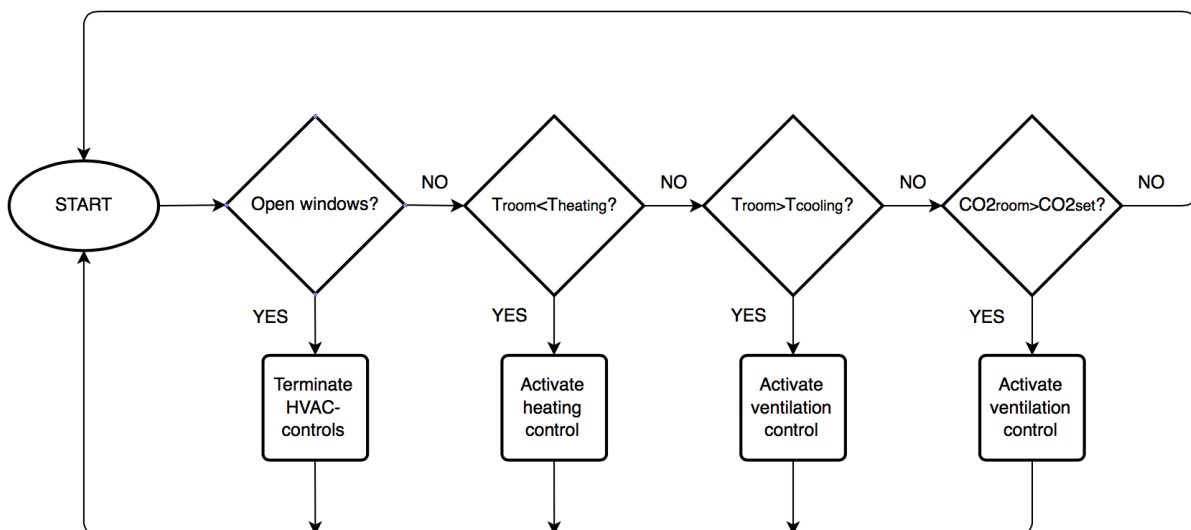


Figure 2.8: Flow diagram of BMS logic control for DCV on room level.

As indicated in the logic chart above the BMS system has a number of overwrite functions on the DCV functionality:

- If windows are opened the system is disabled in terms of both heating and ventilation (radiator valve and VAV-damper shuts down to a minimum).
- Heating/cooling set point has priority compared to CO₂ set point, i.e. ventilation rates can only be increased for IAQ reasons after thermal set points is reached. However, ventilation may be increased for thermal reasons (to comply with cooling set point) even though IAQ is satisfied.
- Temperature set point for heating is 20°C and 25°C for cooling. Temperature set points and time schedules are defined by the technical supervisor.
- CO₂ set point for ventilation increase beyond base ventilation is fixed at 1250 ppm. CO₂ set point for ventilation deactivation is fixed at 1000 ppm.

The BMS manages a number of closed loop control systems such as the operation of VAV dampers and exhaust fan, based on inputs and feedback signals as shown in the PI-diagram in figure 2.9.

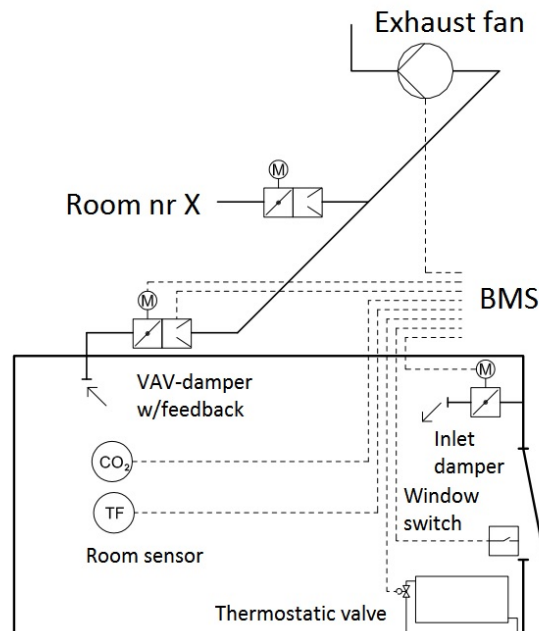


Figure 2.9: PI-diagram of BMS control connections on room level. Drawings reproduced from Bascon-A/S (N.A.).

The central exhaust fan (Exhausto BESB 315-4-1FC) may remove from 570-3590 m³/h making the ventilation a Variable Air Volume (VAV) system providing exhaust for multiple rooms. The room-based exhaust and closed-loop control of the exhaust fan is governed by the position of VAV-dampers, which are located in the exhaust duct of each room. VAV-dampers regulate exhaust airflows in the interval 300-750 m³/h based on both air temperature and CO₂-concentration measurements from two room sensors. Sensors are placed in the corner near the door.

2.3 Test Procedure and Instrumentation

To perform the planned investigations of the DCV system in Solbjergskolen, the following methodology is applied. It describes in detail the approach and necessary equipment in obtaining the required knowledge using the facilities of the classroom. A detailed description of the instrumentation and applied measurement equipment is to be found in Appendix A, which also include calibration formulas.

As the investigations are performed during true operating conditions (actual teaching take place during the measurements), it is not possible to control the environment and compromises must be done. In order to keep track of the environment and system operation, measurements of boundary conditions are essential. As such, the planned investigations of system functionality and indoor environmental quality are performed simultaneously. This way all parameters are measured coherently making it possible to draw conclusions about interconnected relationships and correlations that otherwise would be difficult to deduce due to the non-controlled conditions in the classroom.

The measurements are conducted for three whole school days; Friday 21st, Monday 24th and Tuesday 25th of November 2014.

Measurements of Boundary Conditions and System Functionality Parameters

Parameters related to the DCV system functionality and various boundary conditions are monitored to get a detailed description of how it operates under given conditions. These are in particular the ones related to the plenum of the DCV.

Façade inlet. Air temperature, T_{facade} , and CO₂-concentration, c_{facade} , is measured by a combined wireless temperature and CO₂-sensor (Eltek GD47), which is placed on the inside of each damper in the ramp construction shown in figure 2.4. The recording of temperature and CO₂-concentration in the inlet air is important for evaluation of the potential preheating effects in the plenum and ventilation effectiveness.

Diffuse ceiling inlet. Air temperature, T_{DC} , is measured by a wireless temperature sensor (Eltek GC10), which is screwed on the underside of each of the diffuse panels to measure the inlet air temperature through the panel. The attachments of the sensors can be seen from figure 2.10. These measurements will make it possible to evaluate the air distribution and preheating effect in the plenum above the suspended ceiling. Moreover, it may be used for the quantification of a vertical temperature profile inside the classroom.



Figure 2.10: Eltek GC10 wireless transmitter attached to diffuse ceiling panel measuring air temperature. The build-in temperature sensor is touching the ceiling panel.

Exhaust duct. Air temperature, $T_{exhaust}$, and CO₂-concentration, $c_{exhaust}$, is measured in two of the four exhaust openings in the back wall of the classroom, as shown in figure 2.11. For this a combined wireless temperature and CO₂-sensor (Eltek GD47) is used. These measurements are needed to evaluate the efficiency of the ventilation system.



Figure 2.11: Eltek GD47 wireless transmitter located in exhaust opening measuring air temperature and CO₂-concentration.

Furthermore, the following parameters are manually observed throughout the measurements:

- Number of people in the room
- Activity level and clothing of people
- Opening of windows and doors
- Mechanical heat loads (lighting, laptops, projectors etc.)

Measurements of Indoor Environmental Quality (IEQ)

Inside the classroom the amount of measurement equipment is limited due to the presence of pupils and the teaching that takes place. As a result, investigation of the air distribution and IEQ parameters are evaluated by the use of three moveable measurement columns. They are placed in different locations each lesson to assess local variations and dead zones in the classroom. However, as the experiment is conducted during actual school lessons compromises are necessary e.g. consideration for the view of the children must be shown.

The columns have temperature, CO2 and velocity sensors (anemometers) attached in different heights. The mounting of sensors on these columns are shown in table 2.1 and figure 2.12.

Table 2.1: Setup scheme for measurement of air temperature (Temp.), CO2-concentration (CO2) and air velocity (Vel.) on the three moveable measurement columns.

Measurement Height	Column 1			Column 2			Column 3		
	Temp.	CO2	Vel.	Temp.	CO2	Vel.	Temp.	CO2	Vel.
0.1 m	✓		✓	✓		✓	✓		✓
0.6 m	✓		✓	✓		✓	✓		✓
1.1 m	✓	✓	✓	✓	✓	✓	✓	✓	✓
1.7 m	✓	✓	✓	✓	✓	✓	✓	✓	✓
2.4 m							✓		✓

Measurement heights are selected in accordance with ISO-7726 (1998) and SBI-130 (1983), which advise on the measurement of such parameters for the evaluation of IEQ.

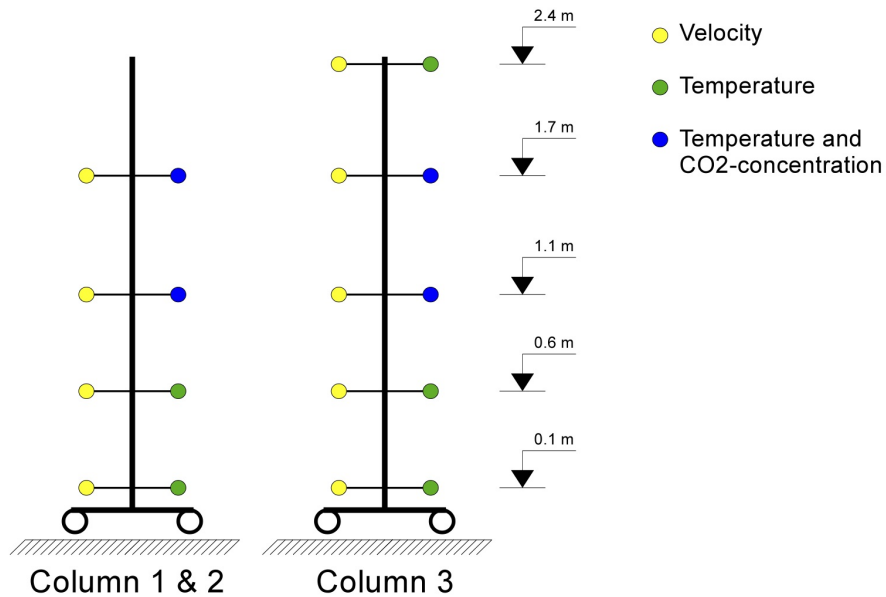


Figure 2.12: Sketch of three moveable measurement columns and the attachment of sensors.

Room air. Temperature, T_{air} , and CO₂-concentration, c_{air} , measurements are done using wireless Eltek GD47 sensors. Velocity, u_{air} , measurements are done using Dantec 54R102 hot sphere anemometers. It should be noted that the data logging equipment used with the anemometers (Dantec Flowmaster 54N10 datalogger) does not fulfil the official requirement of at least 2 Hz for data sampling frequency in order to use the velocity measurements for analysis of turbulence intensity.

The classroom is divided into 9 equally sized cells according to figure 2.13 below. These cells are used as possible locations for the moveable measurement columns during lessons.

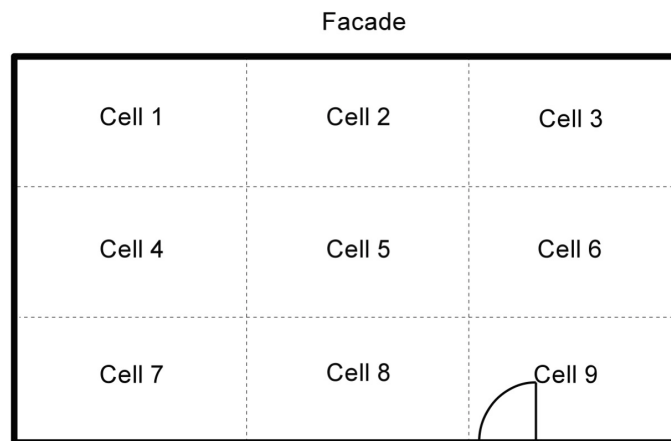


Figure 2.13: Sketch of the classroom divided into 9 possible column locations.

From figure 2.14 below moveable measurement column 1 is seen placed in between the pupils on the border of cells 5 and 8 of figure 2.13.



Figure 2.14: Moveable measurement column 1 located between cell 5 and 8 (see figure 2.13 for explanation).

Data sampling. All sensors - both Eltek wireless sensors and Dantec wired anemometers - are set to sample continuously and while the Eltek-data is logged every 2nd minute the velocity data from anemometers is logged every 4th second. This was chosen as reasonable logging frequencies for the four measured variables (temperature, CO₂-concentration, mean air velocity and peak air velocity).

Smoke visualisation. To investigate the inlet air distribution just below the ceiling panels, smoke visualisations are furthermore used to obtain a more coherent "picture" of the airflow streamlines. Visualisations are performed as spot measurements using air current tubes (see figure 2.15), making the investigations more qualitatively in nature.



Figure 2.15: Air current tube used for visualising air distribution by manually injecting smoke to the inlet air.

2.4 Measurement Results

The presented measurement results are mainly focused on measurements done Friday 21st of November as these showed most representative for the whole measurement period and because they were only interfered by external factors to a minor degree compared to the measurements of Monday and Tuesday.

Operation of Ventilation System

Proper control and operation of any HVAC system is of key importance as bad control can delimit its functionality. In order to understand the measurement results obtained from the classroom the operation of its DCV system is shortly analysed.

From figure 2.16 the influence of occupancy and opening of windows on the DCV functionality is plotted by means of the CO₂-concentration near the inlet damper in the facade and in the exhaust duct. The base load of 2 persons is the observers. The opening of windows and thus the deactivation of the DCV system is illustrated by dark patches.

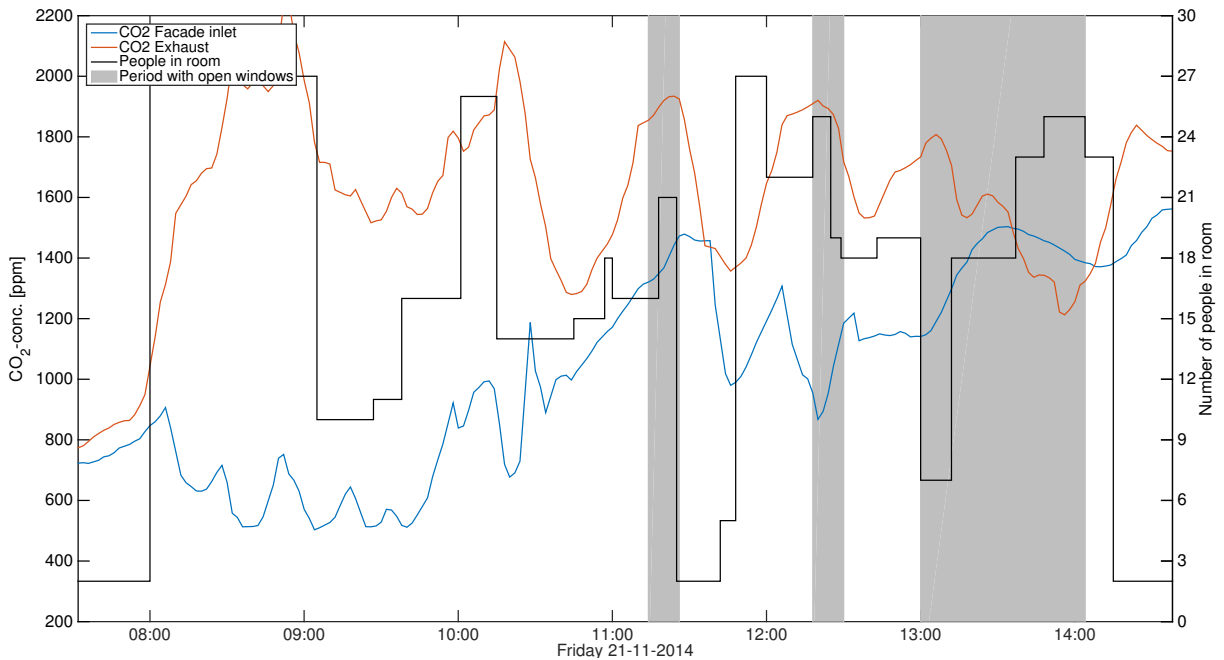


Figure 2.16: Presence of people, CO₂-concentration in facade inlet and exhaust and periods with open windows.

It is obvious how the presence of people in the classroom influences the CO₂-concentration - as expected. In addition to this, it is seen how the opening of windows increase the ventilation and lowers the CO₂-concentration significantly (see figure 2.16 and figure 2.19). It should also be noticed that the absolute CO₂-concentration throughout the entire measurement period is higher than the set point (1250 ppm) thus indicating that the highest achievable ventilation rate is too low to satisfy IAQ demands or that the BMS room sensor measures wrong/unrepresentative.

Looking at the façade inlet air temperature (figure 2.17 on page 39) the picture is more blurred. From the figure it should be noticed that the façade inlet air temperature fluctuate more or

less independently of both the number of people present in the classroom and the opening of windows. Only at around 08:00 in the morning when people enter the room one could explain the sudden drop in temperature as the activation of the ventilation and thus the opening of the inlet damper in the façade letting in cold outdoor air. However, the on-going fluctuation from around 08:15 to 11:45 cannot be explained. Moreover, the inlet temperature continue to increase after around 11:00 indicating that the inlet damper is closed and thus the ventilation is deactivated even though IAQ is not satisfactory and room air temperature is (measured temperature around 23 °C and CO₂-concentration around 1500 ppm - see figure 2.22 and figure 2.19). This clearly proves how the BMS room sensor measure wrong since CO₂-levels are above the set point.

2.5 Analysis of Plenum

Measurements of air temperature obtained in the plenum air inlet above the classroom (and immediately below diffuse panels) are analysed in terms of the distribution of heat transfer across the ceiling.

From figure 2.17 the time rate of change of air temperature underneath each of the ten diffuse ceiling panels is shown together with measurements of temperature after the facade inlet damper and in the exhaust duct.

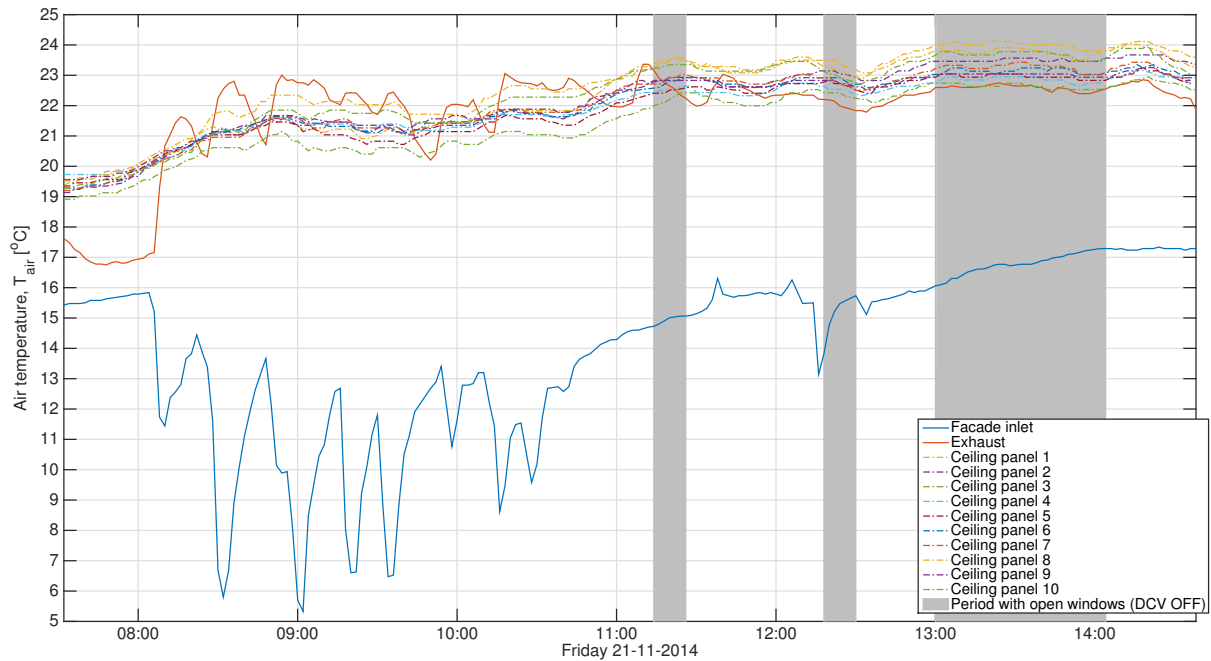


Figure 2.17: Air temperature underneath ten diffuse ceiling panels as well as in facade inlet and exhaust openings.

It is observed how the exhaust temperature changes from being the highest temperature in the first part of the day to being lower than the ceiling inlet temperature in the last part of the day. This indicates either a short circuiting of the inlet air or simply a reduced/deactivated ventilation system.

The plenum air temperature at each of the diffuse ceiling panels is approximated by measurements of the ceiling inlet temperature underneath the diffuse panels. From figure 2.18 the plenum air temperature is plotted as both absolute values, T_{air} , and as normalized values, T_{air}^* , cf. equation 1.11 on page 14 as function of distance from the facade inlet. The normalized values, T_{air}^* , represent the amount of heat-up in a given measurement point in relation to the total supplied heat from facade inlet to exhaust duct.

The two graphs encompass distance-averaged measurements perpendicular to the facade with vertical errorbars indicating the standard deviation of contained values in the given time period.

2. Pilot Study

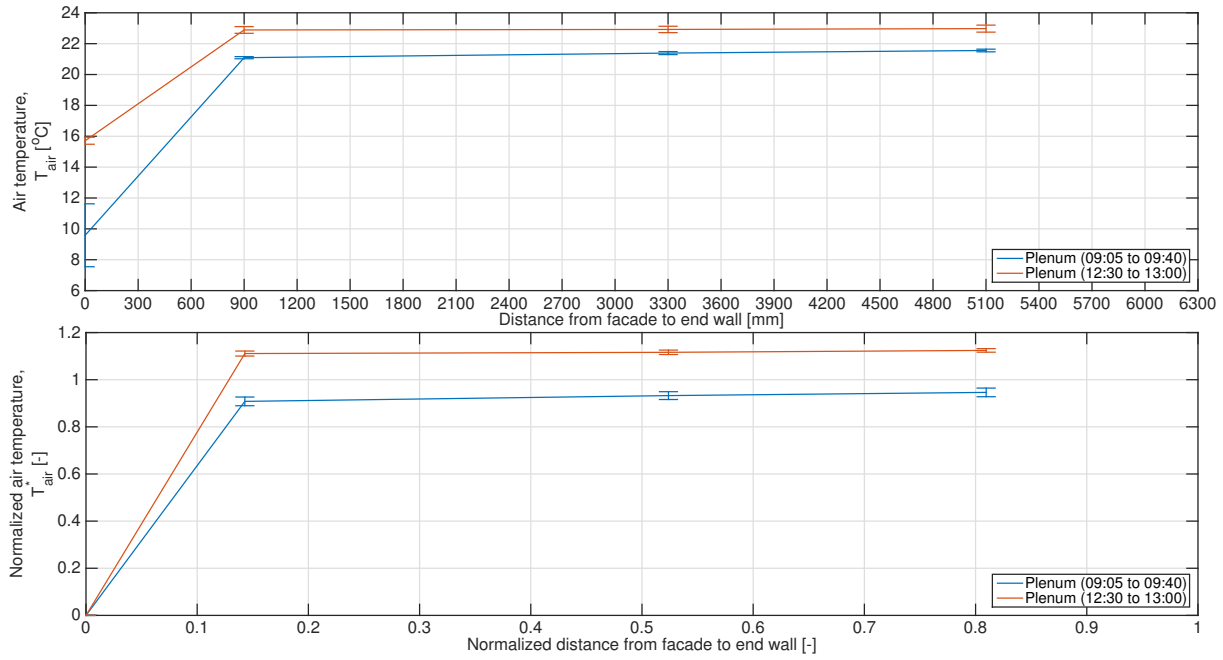


Figure 2.18: Air temperature profiles across plenum. Top: Absolute profile for two time periods. Bottom: Normalized profile for the same two time periods.

As seen, the temperature does not vary much in the plenum volume as soon as the initial heat-up within the 0.9 m has taken place. In fact, the temperature reaches the exhaust temperature almost instantaneously. However, the reliability of such a conclusion is questionable as the measurements are conducted underneath the diffuse panels and thus sensitive to room air mixing. In order to be able to assess the *true* preheating effect inside the plenum one should instead measure the ceiling panel inlet temperature immediately above each panel instead of underneath them to ensure room heat loads does not interfere the measurements in such a high degree. This measurement of *true* plenum air temperature does therefore also require a positive mass flow rate down through the panels to avoid the interference from the room. To evaluate the flow direction a concurrent measurement of the CO₂-contration above the panels could be used, as it would indicate whether or not the façade inlet air concentration is contaminated by the room air below.

2.6 Analysis of Classroom

Measurements obtained by the use of measurement columns in the occupied zone of the classroom are analysed in terms of the distribution of heat and mass transfer.

Measurement Columns

Location of measurement columns during the measurements is given in table 2.2.

Table 2.2: Location of moveable columns in classroom during the measurement period, which all results in this chapter originate from. For cell explanation number see figure 2.13.

Date	Start time	End Time	Column 1	Column 2	Column 3
21/11/2014	07:45	08:55	Cell 7	Cell 1	Cell 4
21/11/2014	08:55	11:25	Cell 5-8	Cell 3	Cell 9
21/11/2014	11:25	14:39	Cell 5-8	Cell 3	Cell 2

As seen in the table columns 1 and 2 are kept in the same position through the majority of the measurement period. This is done as these spots in the classroom are thought to be the most representative for the occupied zone as they are placed close to the desks of the pupils and at the same time in the passageways between the desks, so also interference from pupil movement can be measured in terms of velocity.

Air Distribution

From figure 2.19 the time rate of change of CO₂-concentration for the three measurement columns is shown as averaged values for the two measurement heights; 1.1 m and 1.7 m.

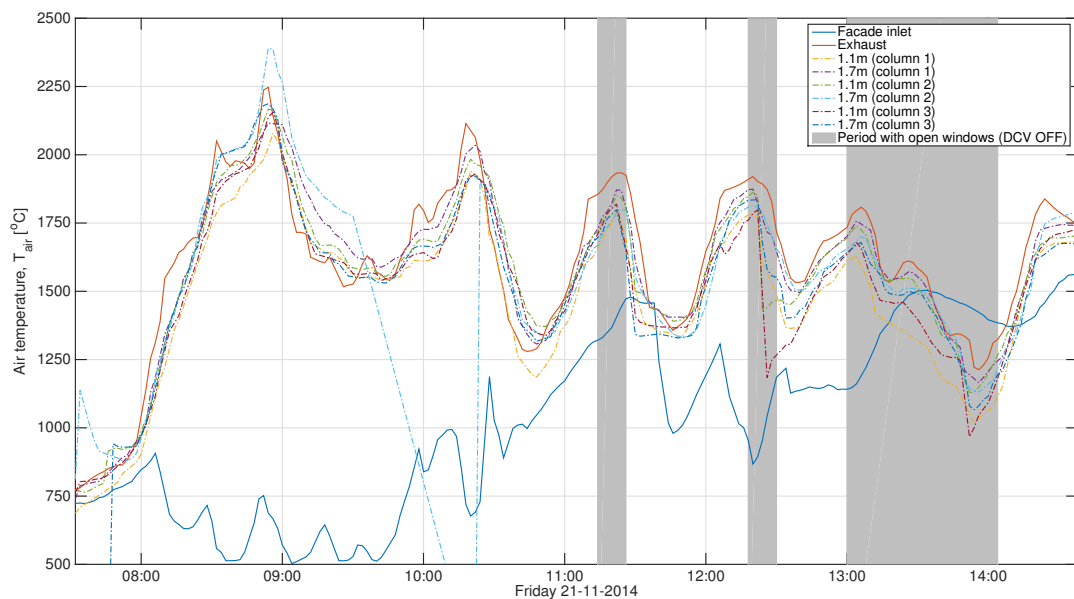


Figure 2.19: Air CO₂-concentration for two heights in the classroom as well as in facade inlets and exhaust openings.

2. Pilot Study

As seen from figure 2.19 the CO₂-concentration seems fully mixed with the entire room air and follows the exhaust concentration. This relationship is plotted below in figure 2.20 showing the ventilation effectiveness, ε_v , as defined in equation 1.13 on page 15.

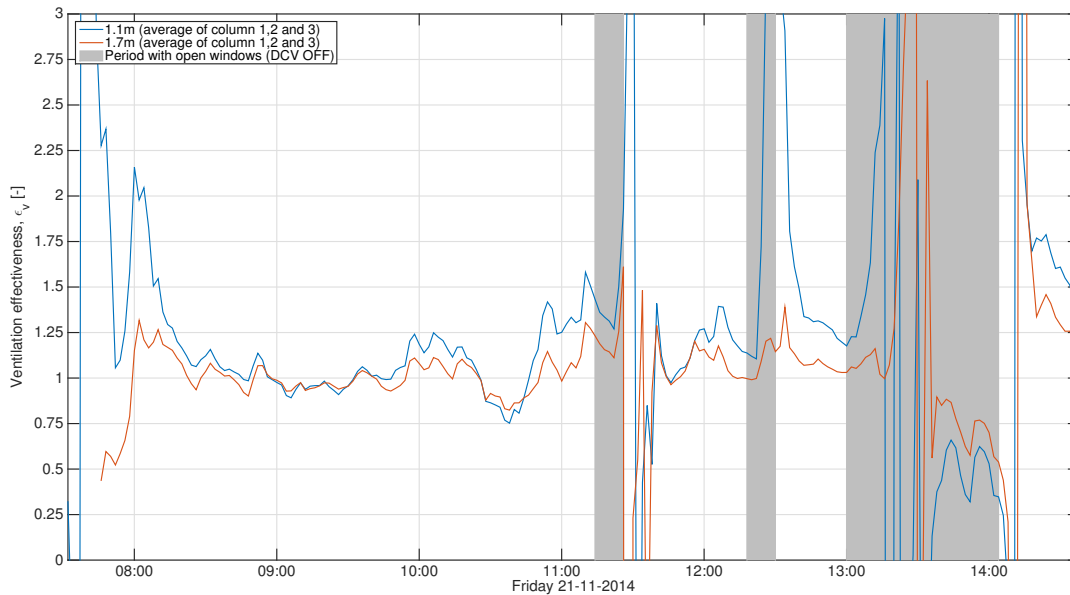


Figure 2.20: Ventilation effectiveness for two heights in the classroom.

If disregarding the chaotic values when windows are opened, and shortly after closing them again, a mean ventilation effectiveness around 1.0 is observed.

Measured air speeds, u_{air} , and their variation in terms of turbulence intensity, Tu_{air} , is given in figure 2.21 below. Both measured speeds and turbulence intensities are 3 minutes mean values in accordance with DS-474 (1995).

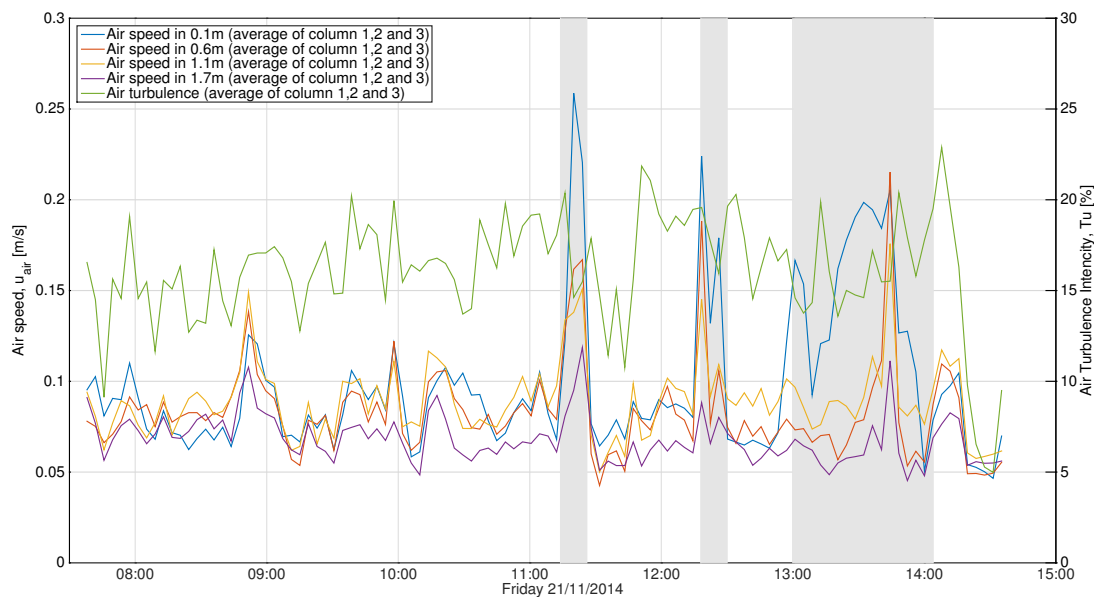


Figure 2.21: Mean air speeds in different heights and locations (left axis) and room mean turbulence intensity (right axis) in the classroom. Values are time-averaged over 3 minutes.

From the figure it is clear how the opening of windows highly affect the air velocities, however, not so much the turbulence intensity. Room day mean velocity magnitude, when windows are closed, is below 1.0 m/s. The turbulence intensity is also rather low with an average of 16 % during the day.

Temperature Distribution

From figure 2.22 the temperature measurements are shown averaged in their respective measurement heights; 0.1 m, 0.6 m, 1.1 m, 1.7 m and 2.4 m above floor level.

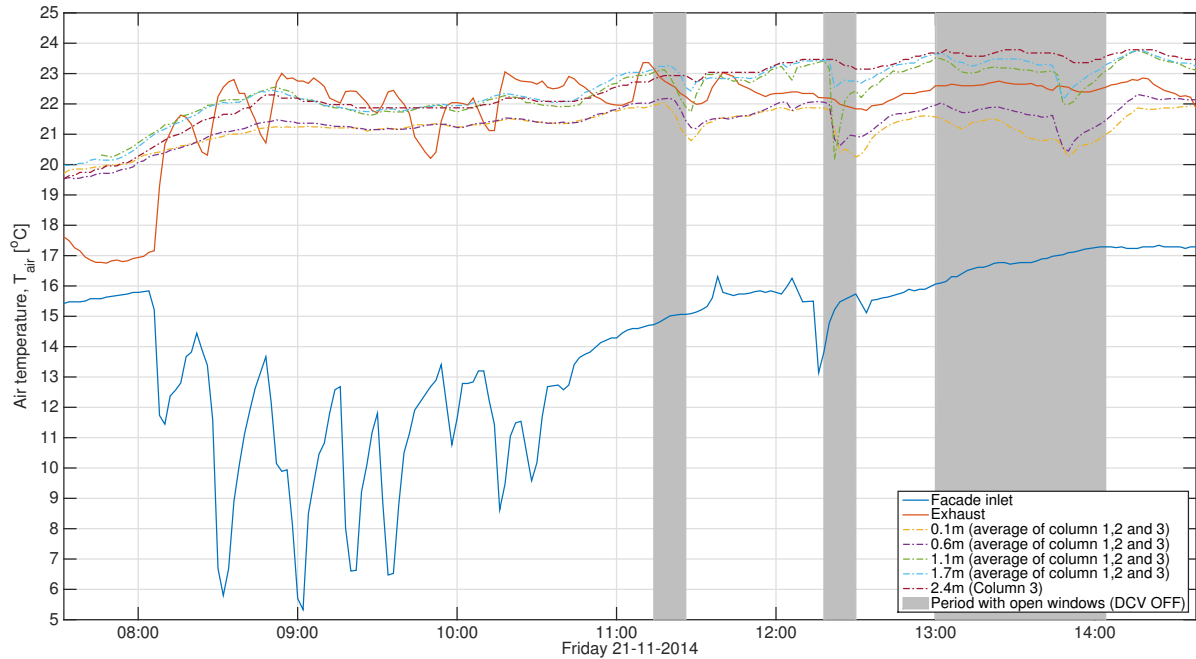


Figure 2.22: Air temperature in different heights in the classroom as well as in facade inlet and exhaust openings.

An upward-positive temperature gradient is observed throughout most of the day. From figure 2.23 the temperature readings are normalized and presented as the temperature effectiveness, ε_T , in the five measurement heights. The effectiveness is calculated cf. equation 1.14 on page 15.

2. Pilot Study

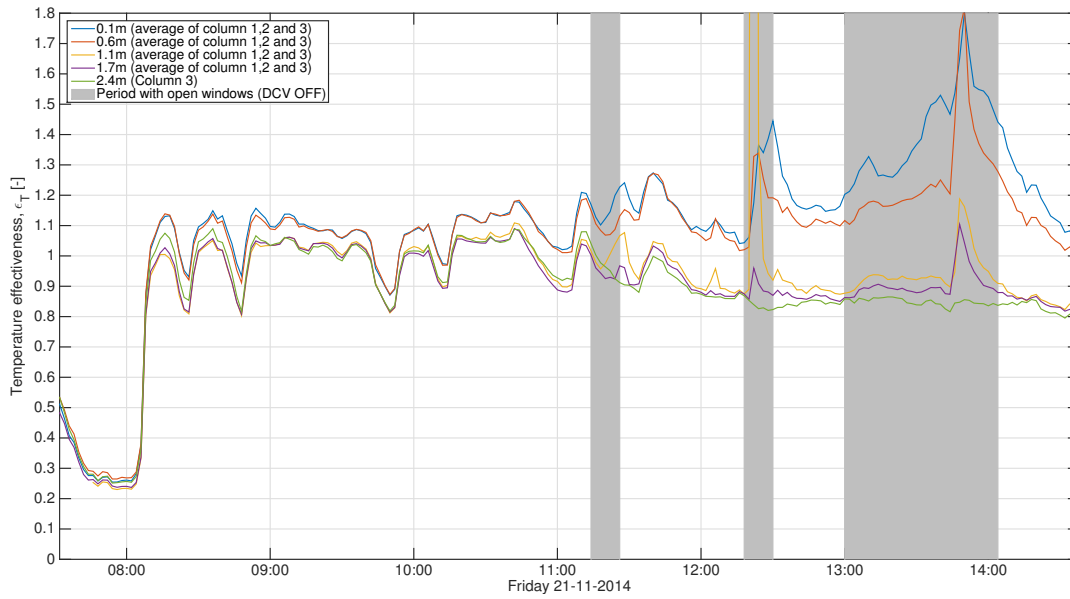


Figure 2.23: Air temperature effectiveness in different heights and locations in the classroom.

As with the ventilation effectiveness, a temperature effectiveness of around 1.0 is observed, however, vertical differences are seen. These differences are plotted in figure 2.24 showing vertical temperature gradients for the three measurement columns, both as absolute values, T_{air} , and as normalized values in terms of the temperature effectiveness, ε_T . Horizontal errorbars indicate the standard deviation of contained values in the averaged time period.

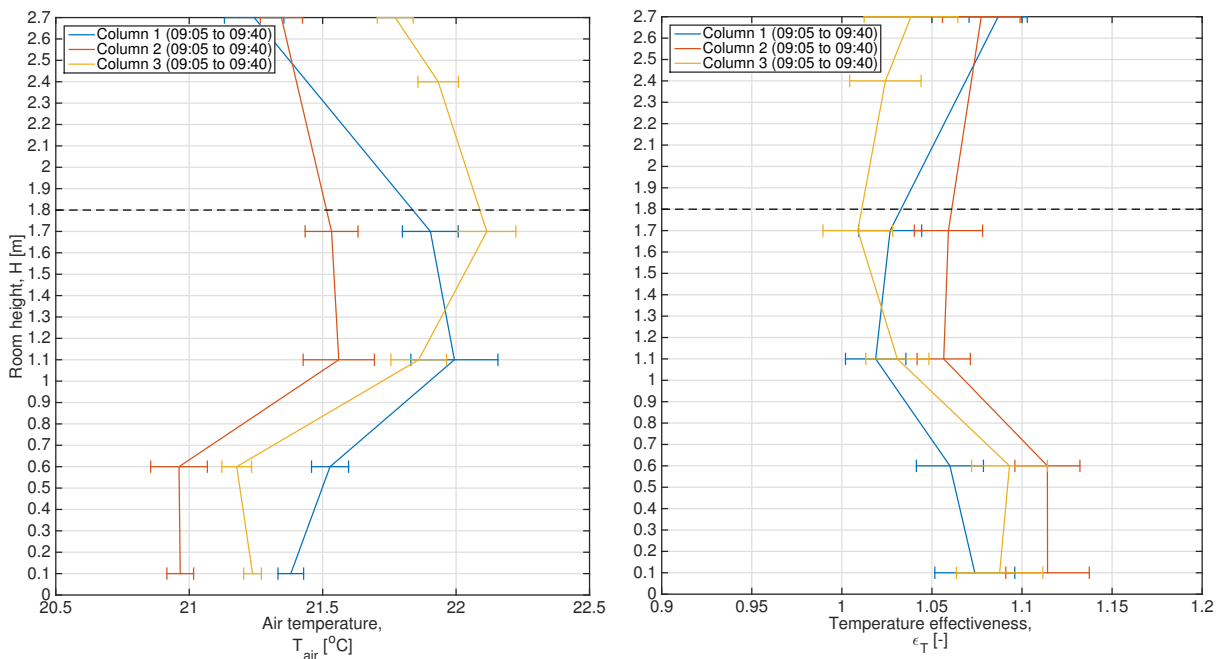


Figure 2.24: Air temperature profiles in classroom. Left: Absolute profile for three columns. Right: Temperature effectiveness for three columns. Dotted black line represent the limitation of the occupied zone.

The exhaust hoods are located right underneath the suspended ceiling in approximately 2.65 m above floor level, which is also where the highest temperatures are observed.

Draught Distribution

From figure 2.25 the draught level is given as 3 minute averaged values for the three measurement columns.

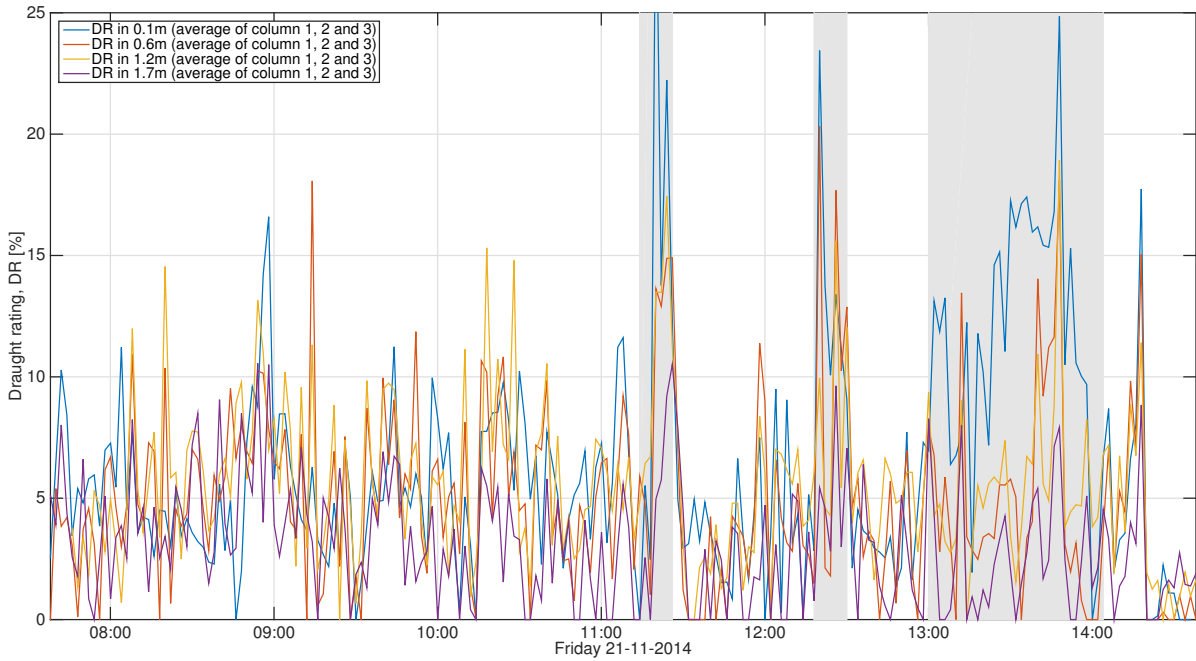


Figure 2.25: Draught rating in different heights and locations in the classroom.

As seen the mean draught level is well below 10% most of the day, indicating indoor environmental category A. Highest draught ratings are observed near the floor level. Only a few times and when windows are opened, is draught increased beyond category A.

2.7 Findings

In conclusion of the pilot study the following findings are highlighted.

Evaluation of the operation of the DCV system was only partly successful. It is found that the operation and control does not work satisfactory due to wrong BMS sensor readings. Moreover, the ventilation rate may be too small to maintain a good IAQ (CO₂-concentration was well above 1250 ppm most of the day, and as high as 2250 ppm). However, in order to unambiguously draw such a conclusion, measurements of the actual ventilation rate needs to be performed. The IEQ is so bad that pupils and teachers open the windows several times a day to increase the ventilation. The opening of windows turns off the ventilation and as such only worsens the comfort as measurements show that it increases air velocities and decreases air temperatures below an acceptable point.

Evaluation of the potential preheating effects in the plenum was not successful. New measurements need to be performed with measurements of temperature and CO₂-concentration immediately above the ceiling panels. Furthermore, measurements of outdoor parameters are necessary.

In future studies the evaluation of the air distribution in the plenum is also recommended. This would be possible with the measurement of pressure difference across the ceiling panels. This analysis is neither performed here or in the main study.

Evaluation of air distribution inside the classroom was successful. Ventilation effectivities and temperature effectivities of around 1.0 were detected in periods without interference from open windows. Measurements of CO₂-concentration in 1.1 m and 1.7 m above floor showed only small variations. Air velocities above 0.15 m/s were only measured in periods with open windows. Spot test of airflow visualisation with air current tubes, however, showed no usable results.

Evaluation of the thermal comfort was successful. Air temperature gradients were measured and showed no problems - temperature differences of around 1.0 °C between head and ankles were detected. The air draught rating was in the range of 0-10 %.

Chapter 3

Main Study

Based on the preliminary pilot study conducted at Solbjergskolen (see Chapter 2) a second study - the main study - is presented in this chapter. It comprises improved measurements based on the findings of the pilot study thus also better analyses and more descriptive and valid conclusions. Where the pilot study is conducted in a 6th grade classroom, the main study is conducted in a 9th grade classroom also at Solbjergskolen.

3.1 Planned Investigations

As it in the pilot study is found that the school has difficulties controlling both heating and DCV system making the maintaining of proper IEQ very difficult, the scope of the main study is largely focused on system effectiveness and functionality. As such, the analyses of measured variables seek to normalize the conditions by making the investigated parameters dimensionless.

With a new and enhanced measurement setup, the following analyses are conducted:

- Air distribution (pressure chamber effect) in plenum and through the diffuse ceiling panels
- Preheating of inlet air in plenum above suspended ceiling
- Air distribution in room

The investigations will focus on describing both transient and steady characteristics of the system.

3.2 Field Study: Solbjergskolen, 9th grade classroom

In the pilot study a 6th grade classroom is investigated in the southern wing of the school, however, as the DCV system in that area of the school was taken out of operation due to defect BMS control when the main study was to be conducted, a 9th grade classroom was selected instead.

The DCV system and BMS control in the 9th grade classroom is the same as the one investigated in the pilot study (see figures 2.2, 2.4, 2.8 and 2.9). The suspended ceiling layout is, however, a bit different. From figure 3.1 a top view of the suspended ceiling layout in the 9th grade classroom is seen.

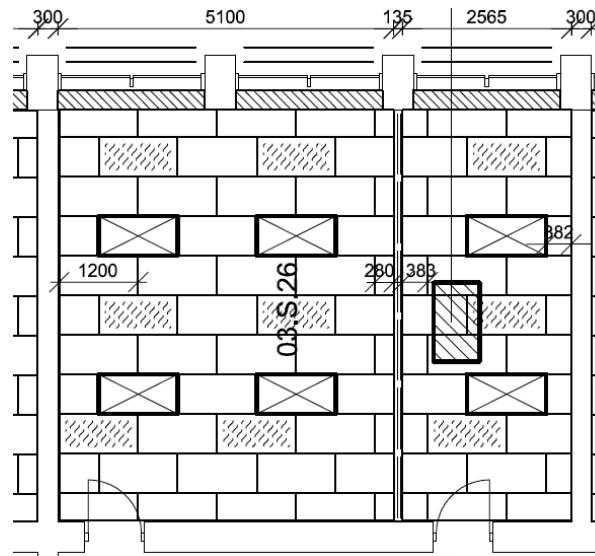


Figure 3.1: Top-view of suspended ceiling layout in 9th grade classroom. Drawings reproduced from Bascon-A/S (N.A.).

People Load

The main study is carried out in a 9th grade classroom. The classroom contains 16 pupils plus a teacher. Floor area of the investigated classroom is approximately 49 m^2 resulting in 0.31 pupil/m^2 . In brakes the number of persons in the room often increase beyond 20. With a room height of 2.7 m the room volume is 132 m^3 .

Average school days range from 08:00 to 14:30, however, the daily occupancy of the room is very fluctuating as pupils often work in groups inside and outside the classroom and some classes are taught in dedicated workshop rooms.

3.3 Test Procedure and Instrumentation

Measurements are conducted for three whole days; Thursday 23rd, Friday 24th and Monday 27th of April 2015.

Measurements of Boundary Conditions and System Functionality Parameters

Boundary condition measurements consists of largely the same as in the pilot study, however, a few alternations and additions are made to the measurement setup used in the pilot study.

Outdoor air. Air temperature, T_{out} , and CO₂-concentration, c_{out} , is measured using a combined wireless temperature and CO₂-sensor (Eltek GD47) in a free hanging steel frame to protect from sun radiation (see figure 3.2). The recording of outdoor air parameters is not essential in performing the intended analyses, but it is helpful in understanding variations of especially the facade inlet air.



Figure 3.2: Protecting steel frame used for outdoor air measurements.

Facade inlet. Air temperature, T_{facade} , and CO₂-concentration, c_{facade} , is measured as done in the pilot study; combined wireless temperature and CO₂-sensors (Eltek GD47) are placed on the inside of the facade inlet damper.

Diffuse ceiling inlet. Air temperature, T_{DC} , and CO₂-concentration, c_{DC} , is measured immediately above each diffuse ceiling panel by combined wireless temperature and CO₂-sensors (Eltek GD47) as seen on figure 3.3. This is done as the measurement of temperature immediately underneath the diffuse ceiling panels in the pilot study showed insufficient in describing the correct plenum air temperature and distribution across the plenum.

Exhaust duct. Air temperature, $T_{exhaust}$, and CO₂-concentration, $c_{exhaust}$, is measured as done in the pilot study (see figure 2.11). For this a combined wireless temperature and CO₂-sensor (Eltek GD47) is used. These measurements are needed to evaluate the effectiveness of the ventilation system.

Ventilation rate. Ventilation rate, q_v , is indirectly measured using a pitot-static tube (prandtl tube) connected to wireless pressure difference sensors (Eltek GD84). The pitot-static tube is

inserted into the upstream airflow of the exhaust duct thus measuring stagnation pressure, which is afterwards converted to airflow velocity. Under the assumption that the flow is fully developed turbulent, the airflow rate is calculated.



Figure 3.3: Eltek GD47 wireless transmitter located above diffuse ceiling panel measuring air temperature and CO₂-concentration.

Furthermore, the following parameters are manually observed throughout the measurements:

- Number of people in the room
- Opening of windows and doors

Measurements of Indoor Environmental Quality

As for the pilot study, three moveable measurement columns are used for measurements of indoor environmental quality and air distribution. See table 2.1 and figure 2.12 on page 34 for information about measurement heights.

Room air temperature, T_{air} , and speed, u_{air} , is measured using upgraded Dantec 54R103 hot-sphere anemometer probes. The probes are calibrated in accordance with Kristensen, M. H. et al. (2015). Combined with a Dantec 54N90 ComfortSense datalogger, the equipment does fulfil the requirements for measurements of turbulence intensity (Sampling rate > 2 Hz), which was not the case with the equipment used for the pilot study.

Room air CO₂-concentration, c_{air} , is measured using wireless Eltek GD47 sensors as in the pilot study.

3.4 Measurement Results

The presented results and analyses are focused on measurements performed Friday 24th of April 2015 as these contain the largest time periods with the DCV system activated. Measurements from Thursday 23rd and Monday 27th have also been analysed but left out of the report as periods of continuous DCV operation is sparse.

Test Conditions

From figure 3.4 below the outdoor air temperature and CO₂-concentration of the analysed day is plotted.

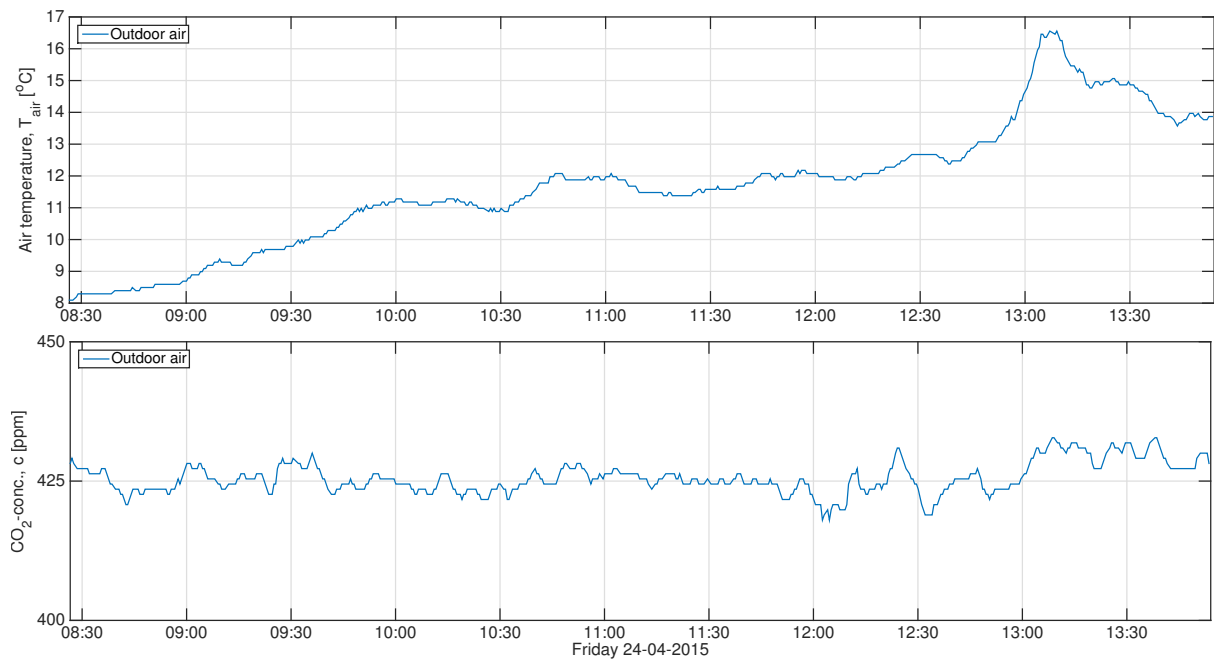


Figure 3.4: Outdoor air temperature and CO₂-concentration during Friday 24th of April 2015.

Although no additional heating was necessary in the classroom, radiators were continuously supplying large amounts of heat. Confronting the technical staff about this problem it was learned that the radiator valves connected to the BMS system was broken. As such, the indoor thermal environment was largely influenced by the high thermal radiation and convection from those radiators.

Presence of People and DCV Activation/Deactivation Periods

From figure 3.5 the influence of occupancy and opening of windows and door on the DCV functionality is plotted by means of the CO₂-concentration near the inlet damper in the facade and in the exhaust duct. The base load of 1 person is the observer. The opening of windows and thus the deactivation of the DCV system is illustrated by dark patches. Opening of the classroom door is illustrated by red patches.

3. Main Study

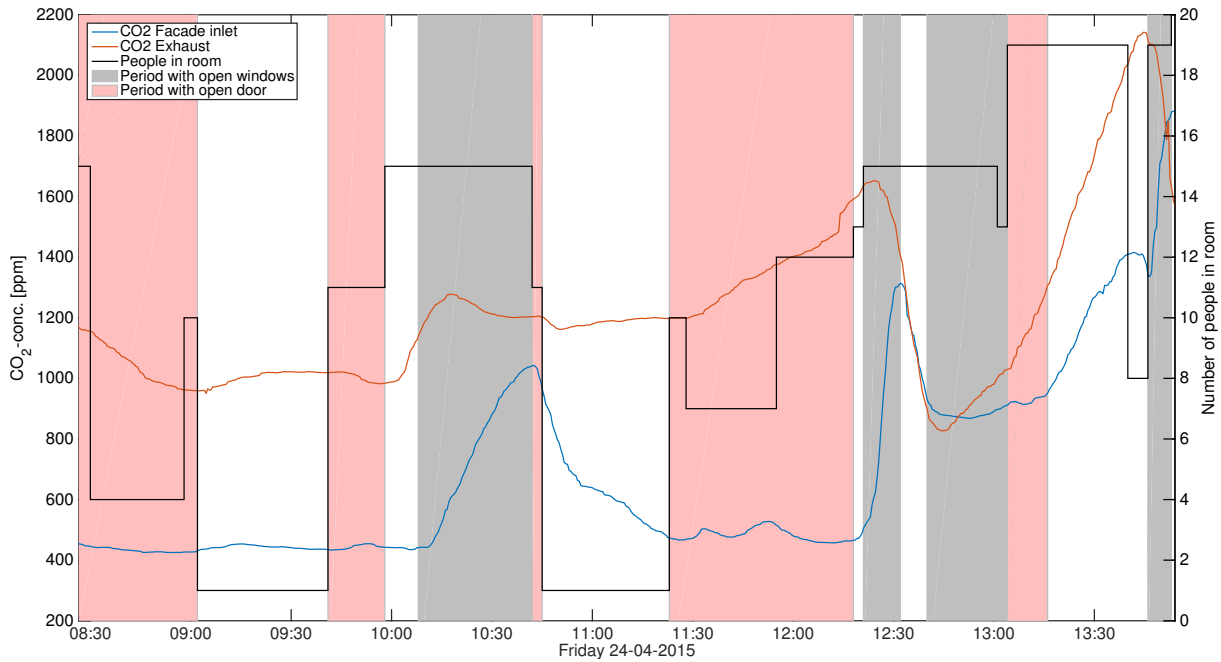


Figure 3.5: Presence of people and periods with open windows and doors.

As seen from figure 3.5 only in a few short periods during the day is the DCV actually running without interferences from either opening of windows or door. Moreover, in the two longest periods where both all windows and the door is closed (from 09:00-09:40 and from 11:25-11:45), the pupils have left the classroom. However, based on the development of the CO₂-concentration variations the influence of an open classroom door (red patches) is deemed negligible and thus it is not taken into account in the forthcoming analyses.

3.5 Analysis of Plenum

Measurements obtained in the plenum volume above the classroom are analysed in terms of the distribution of heat and mass transfer across the ceiling.

Air Distribution

From figure 3.6 the time rate of change of CO₂-concentration above each of the eight diffuse ceiling panels is shown.

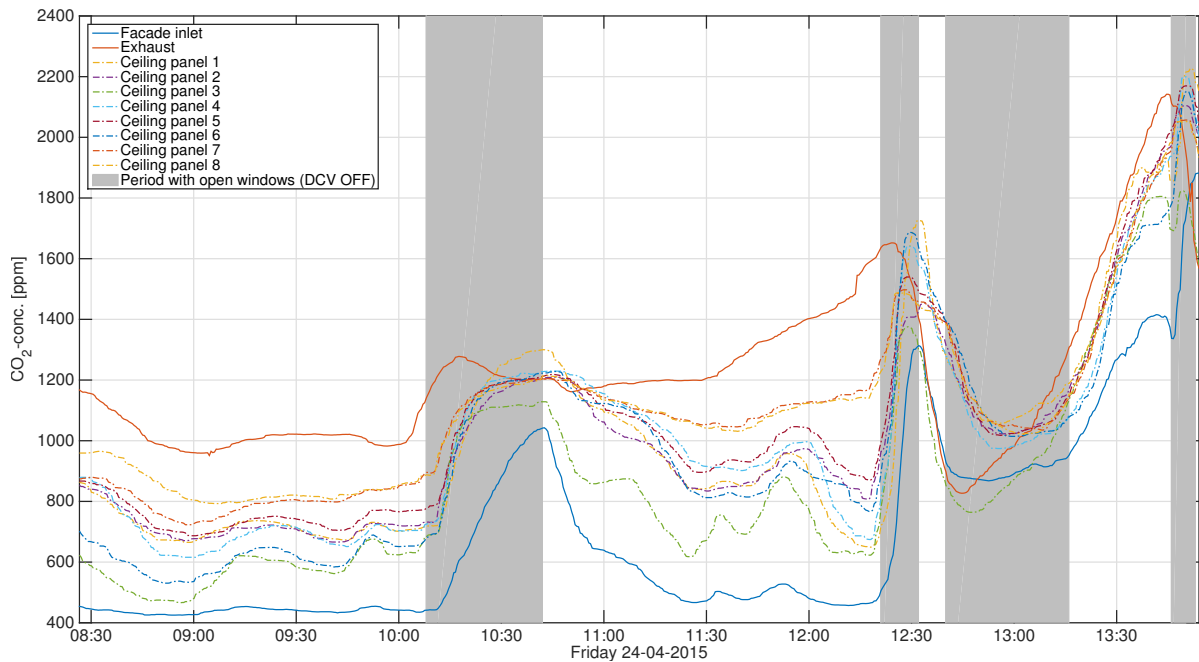


Figure 3.6: CO₂-concentration above eight diffuse ceiling panels as well as in facade inlet and exhaust openings.

It should be noticed how some of the panels show higher CO₂-concentrations than the exhaust duct in some parts of the day. This is a result of open windows, which deactivates the DCV system thus leaving the airflow pattern to be governed by mainly natural convection, i.e. warm, polluted, air enters the plenum from the room.

Moreover, a concentration increment is observed as function of increased distance from the facade inlet. This convection of mass from facade inlet to each diffuse ceiling panel is plotted in figure 3.7 by means of the contained CO₂-concentration, c , both as measured absolute values and as normalized values, c^* , in accordance with equation 1.12 on page 14. The two graphs encompass distance-averaged measurements perpendicular to the facade with vertical errorbars indicating the standard deviation of contained values in the given time period.

3. Main Study

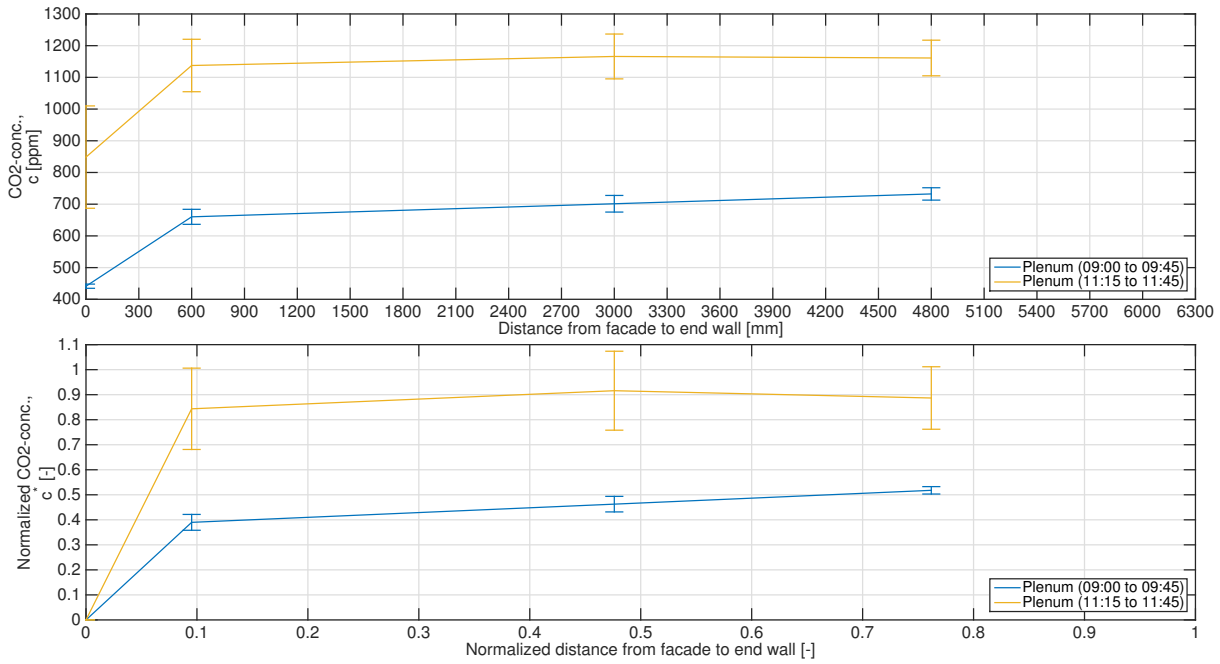


Figure 3.7: CO₂-concentration profiles across plenum. Top: Absolute profile for two time periods. Bottom: Normalized profile for the same two time periods.

Different gradients are seen from figure 3.7 depending on the time period investigated. In the first period (09:00 to 09:45) the plenum CO₂-concentration reaches about 50 % of the final exhaust concentration indicating an overall positive flow direction, however, the plenum concentration remains relatively large compared to the facade concentration meaning that some mixing with room air does indeed take place. This effect is only increased as seen from the second time period investigated (11:15 to 11:45) where the plenum concentration reaches 100 % of the final exhaust concentration.

Temperature Distribution (Preheating)

From figure 3.8 the time rate of change of air temperature above each of the eight diffuse ceiling panels is shown.

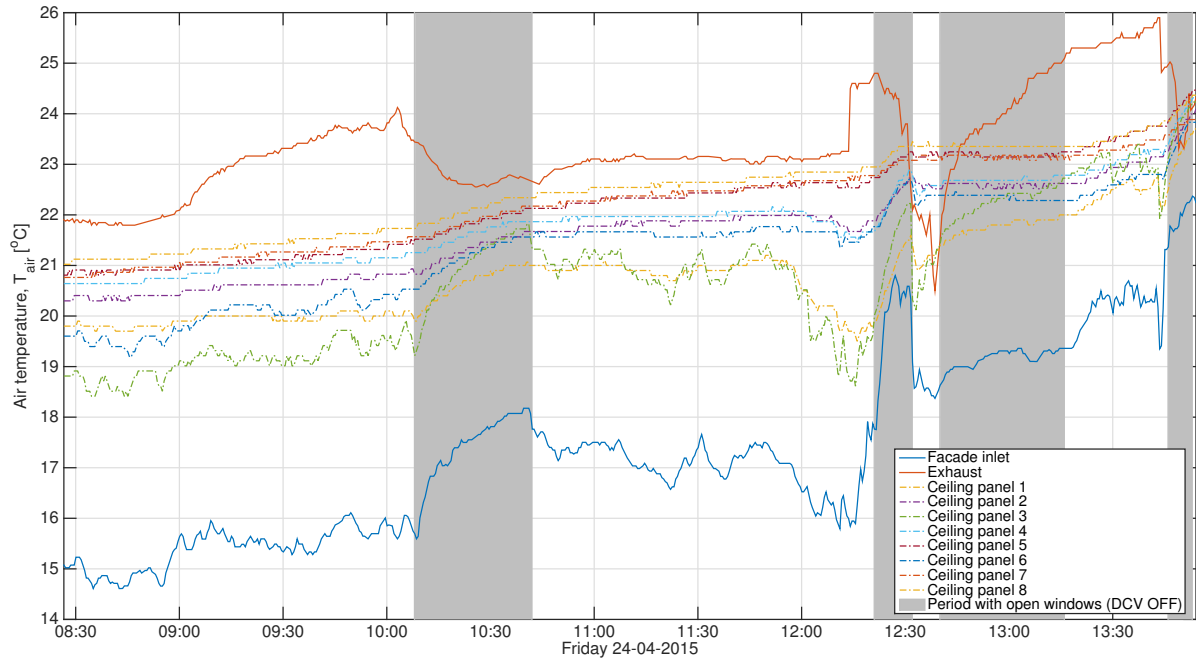


Figure 3.8: Air temperature above eight diffuse ceiling panels as well as in facade inlet and exhaust openings.

It is seen that the air temperature immediately above the ceiling panels is higher than the exhaust temperature through most of the day. This leads to two interpretations, either does the ventilation air enter the classroom near the facade and does not get pulled through the plenum volume, or, the ventilation system is short-circuited by infiltration from e.g. the door.

From the findings of figure 3.6 and figure 3.7 the first argument seem legit, moreover, the first argument is also supported by the parallel development between facade inlet temperature and that of ceiling panel 1 (yellow) and 3 (green), which are located nearest the facade. This parallel development is effectively diminishing as the distance from the facade is increased. However, preheating effects in the plenum caused by light fittings and room heat exchange could easily explain the increasing temperatures.

The convection of heat energy across the diffuse ceiling, from facade inlet to each ceiling panel is plotted in figure 3.9 by means of the air temperature both as measured absolute values, T_{air} , and as normalized values, T_{air}^* , in accordance with equation 1.11 on page 14. The two graphs encompass distance-averaged measurements perpendicular to the facade with vertical errorbars indicating the standard deviation of contained values in the given time period.

3. Main Study

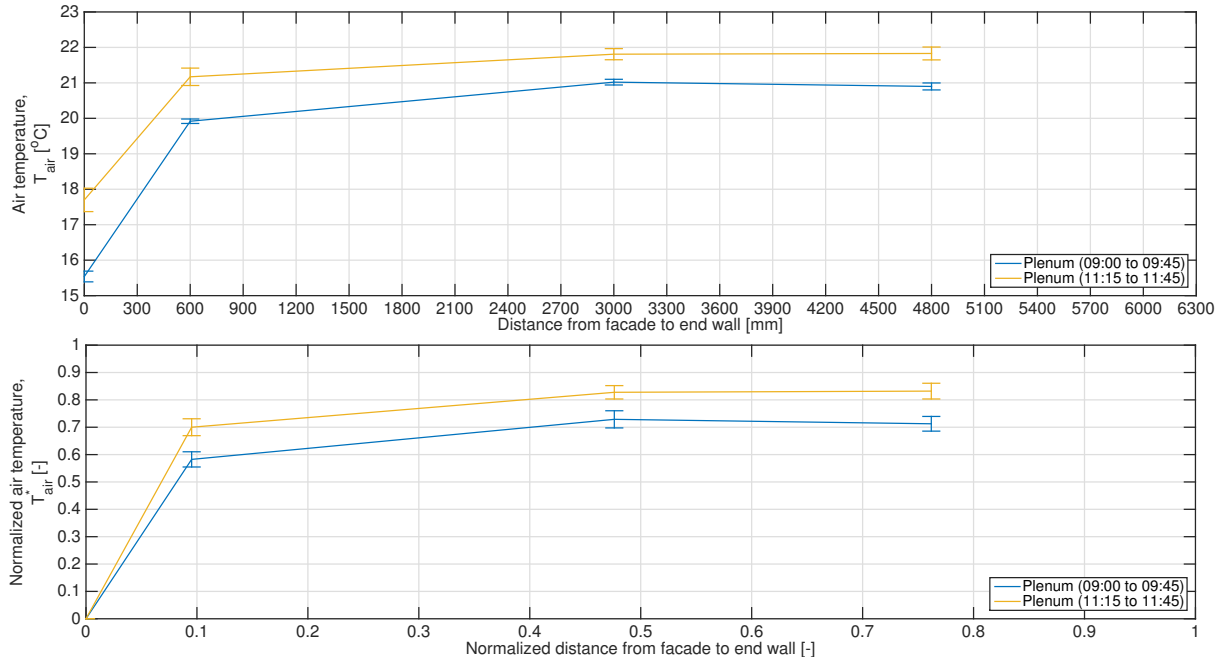


Figure 3.9: Air temperature profiles across plenum. Top: Absolute profile for two time periods. Bottom: Normalized profile for two time periods.

As seen from figure 3.9 the plenum temperature quickly reaches a level just below the exhaust temperature ($T_{air}^* = 0.6-0.9$). This picture is approximately the same as seen in the pilot study, where normalized temperatures around 0.9-1.2 was observed. Compared to the measurement underneath the diffuse panels in the pilot study, the reliability of these measurements above the panels is higher.

3.6 Analysis of Classroom

Measurements obtained by the use of measurement columns in the classroom are analysed in terms of the distribution of heat and mass transfer.

Location of Measurement Columns is chosen as stationary. From figure 3.10 below the location is shown. Stationary placement is chosen in consideration of the pupils. Sensors are placed close to the occupants in pathways between desks so the movement of pupils is present in measured data.

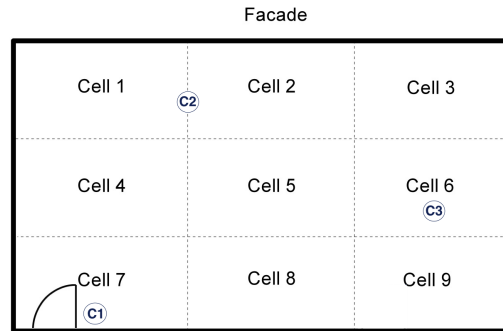


Figure 3.10: Location of measurement columns (C1, C2 and C3).

Air Distribution

From figure 3.11 the time rate of change of CO₂-concentration for the three measurement columns is shown as averaged values in the two measurement heights; 1.1 m and 1.7 m. CO₂-concentrations are generally high and only below 1000 ppm in the first part of the day. In the end of the day it increases beyond 2000 ppm, properly due to open windows and thus too low and ineffective ventilation rates based on natural ventilation.

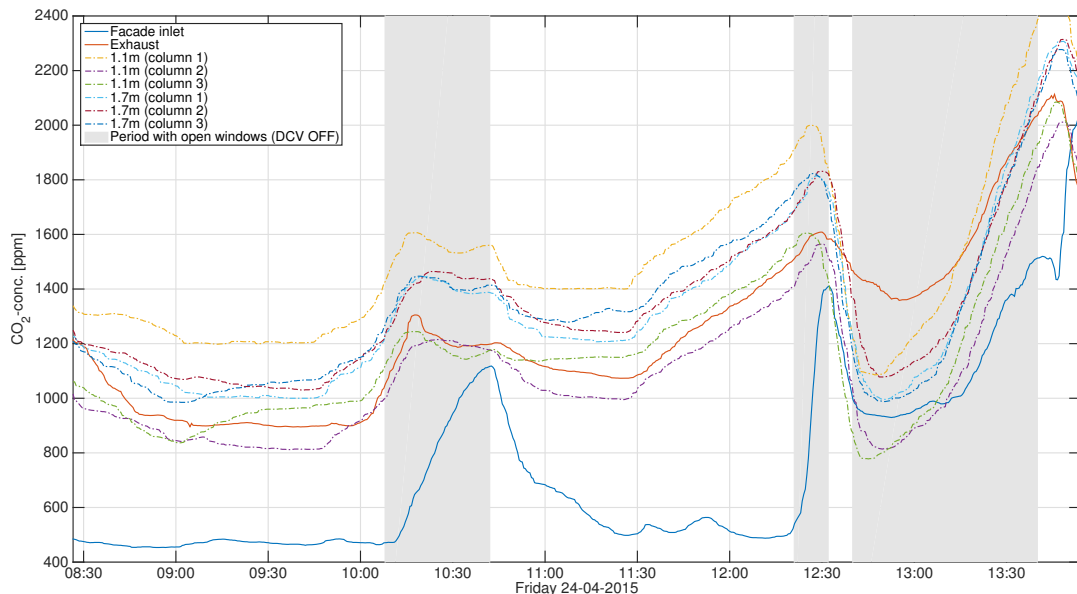


Figure 3.11: CO₂-concentration in different heights and locations in the classroom as well as in facade inlet and exhaust openings.

No clear pattern may be pointed out from figure 3.11 in relation to the CO₂-mixing in the room besides the fact that the internal layering or gradient between the six measurement points seem to be kept intact throughout the day with a maximum variation of approximately 300-400 ppm between the six measurement points.

The mixing of room air is in figure 3.12 represented as the change of ventilation effectiveness, ε_v , with time calculated cf. equation 1.13 on page 15. Ventilation effectiveness is based on CO₂-concentrations. It should be observed how the effectiveness seems reasonable stable around 0.8 to 1.2 when disregarding the most chaotic periods where windows are opened. The variation is much like what was observed in the pilot study where a ventilation effectiveness around 1.0 was found.

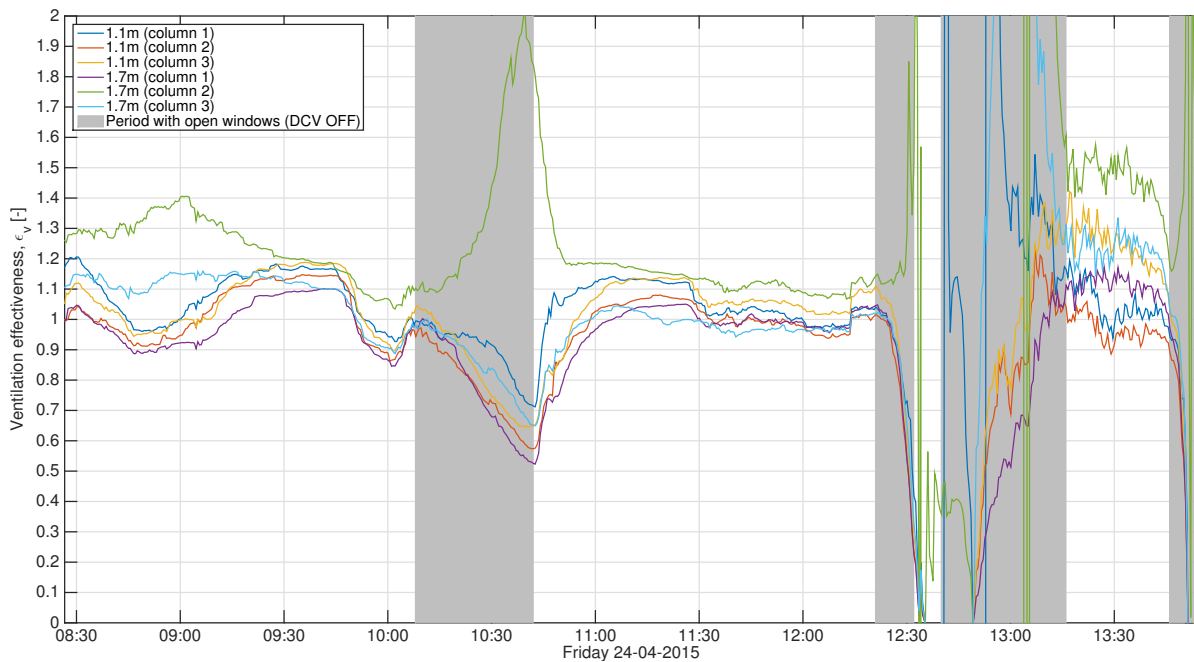


Figure 3.12: Ventilation effectiveness based on CO₂-concentrations in different heights and locations in the classroom.

The ventilation effectiveness variations can be ascribed to the random movement of the pupils and opening of the door. Such movement gives rise to air velocity fluctuations. Measured air speeds, u_{air} , and their variation in terms of turbulence intensity, Tu_{air} , is plotted in figure 3.13. Both measured speeds and turbulence intensities are 3 minutes mean values in accordance with DS-474 (1995).

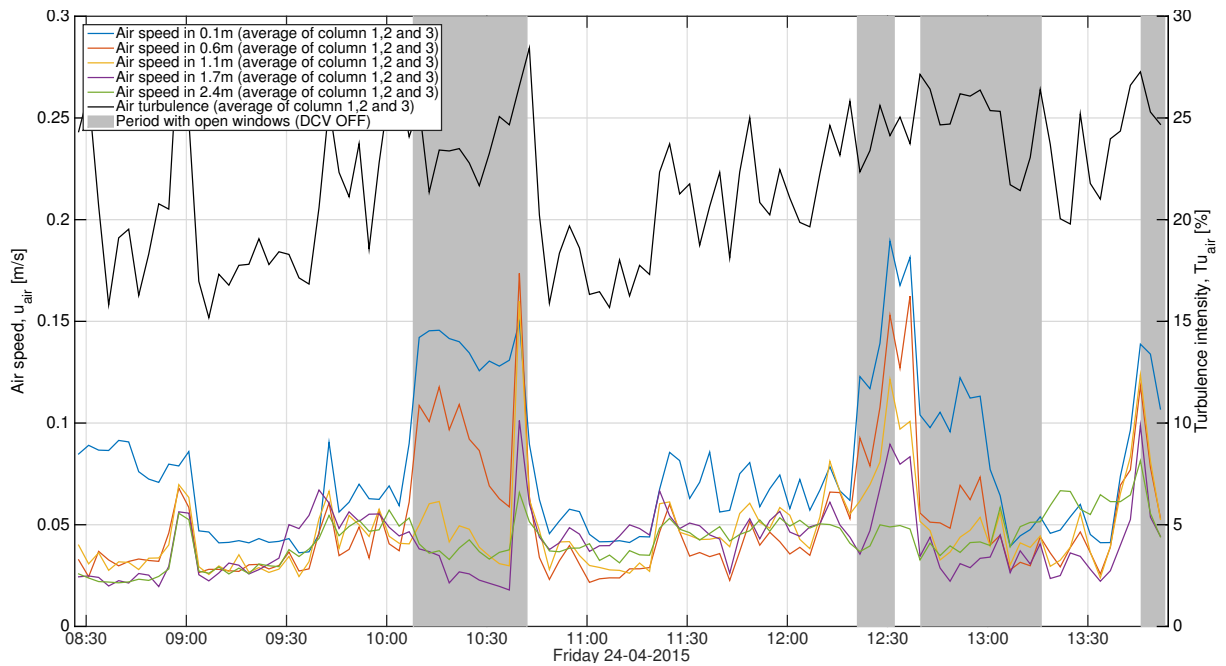


Figure 3.13: Mean air speeds in different heights and locations (left axis) and room mean turbulence intensity (right axis) in the classroom. Values are time-averaged over 3 minutes.

From the figure it is clear how the opening of windows highly affect the air velocities, however, not so much the turbulence intensity. Room mean velocity magnitude when windows are closed is as low as 0.05 m/s. The turbulence intensity is also rather low with an average of 20% during the day.

These values of turbulence intensity are more valid than those in the pilot study due to the fulfilment of the > 2 Hz sampling rate.

Temperature Distribution

From figure 3.14 the temperature measurements are shown, averaged in their respective measurement height; 0.1 m, 0.6 m, 1.1 m, 1.7 m and 2.4 m above floor level. Temperatures are generally high and only below 22 °C in the first half hour of the day. In the end of the day, air temperature in head height (1.7 m) increases beyond 27 °C and 24 °C at floor level (0.1 m). These high temperatures are properly an effect on the radiators delivering full capacity (defect BMS-connected radiator valve).

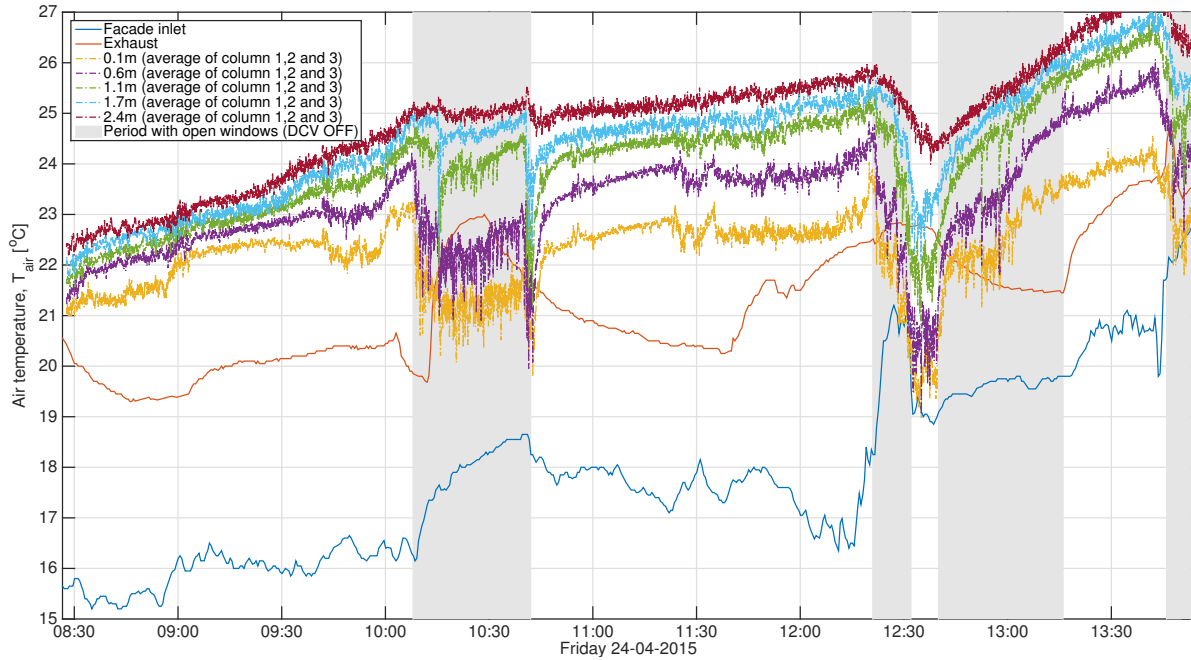


Figure 3.14: Air temperature in different heights in the classroom as well as in facade inlet and exhaust openings.

The temporal variation of the room air temperature gradient shows to be much more steady and uniform than the CO₂-concentration gradient, where variations across the room is seen. This gradient is presented in figure 3.15 in both absolute values, T_{air} and normalized in terms of the temperature effectiveness, ε_T , calculated cf. equation 1.14 on page 15.

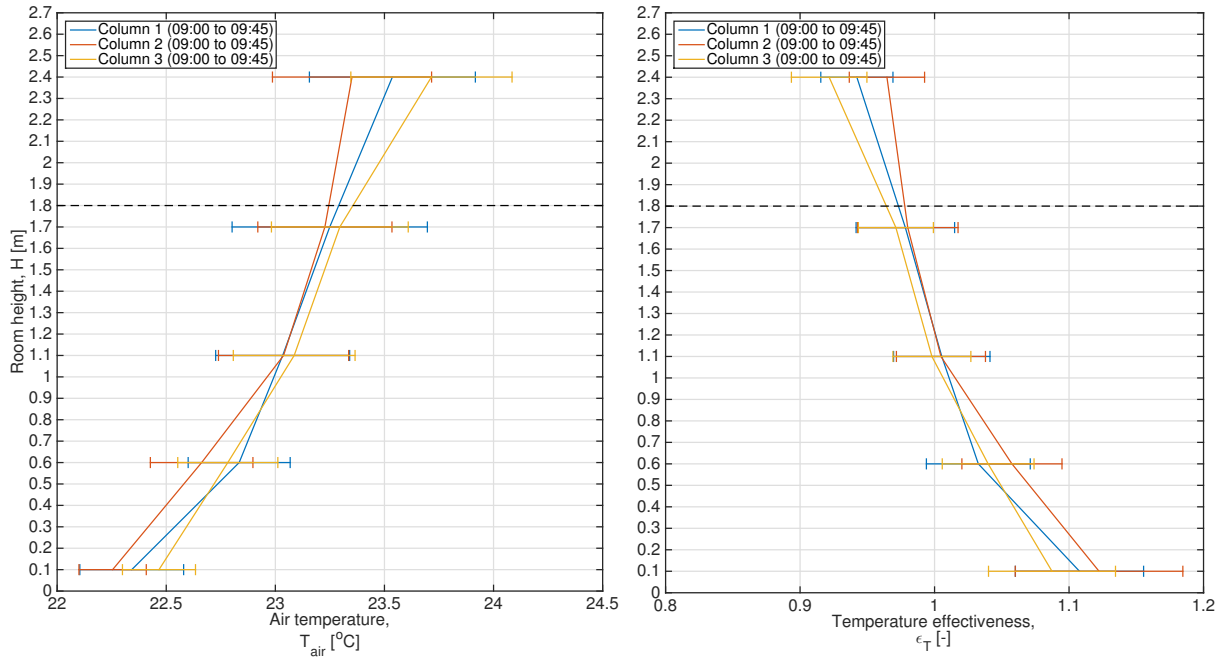


Figure 3.15: Air temperature profiles in classroom. Left: Absolute profile for three columns. Right: Temperature effectiveness for three columns. Dotted black line represent the limitation of the occupied zone.

A constant upward-positive temperature gradient is observed throughout the entire day. The gradient between head and ankles is approx. 1°C . These results are similar to what is seen from the pilot study (see figure 2.24 on page 44).

The temporal variation of the temperature effectiveness is given in figure 3.16, and show the same ventilation effectiveness as those calculated based on the CO_2 -concentrations in figure 3.12.

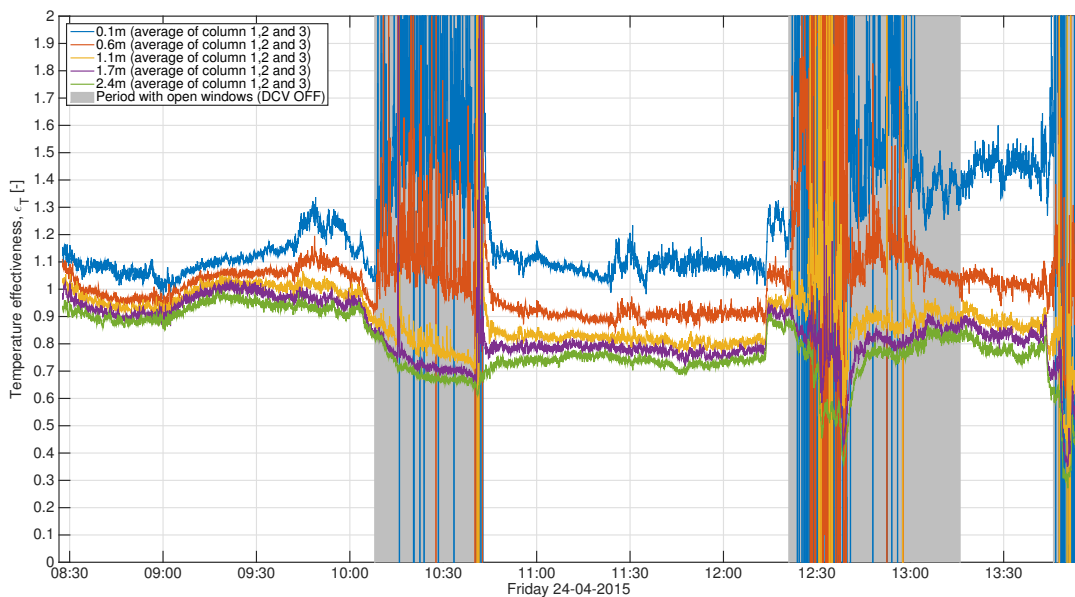


Figure 3.16: Temperature effectiveness in different heights and locations in the classroom.

Draught Distribution

Based on measurements of air speed and temperature, draught rating, DR , is calculated cf. equation (1.3) on page 10. (ISO-7730, 2006)

From figure 3.17 the draught level is given as 3 minute averaged values for the three measurement columns.

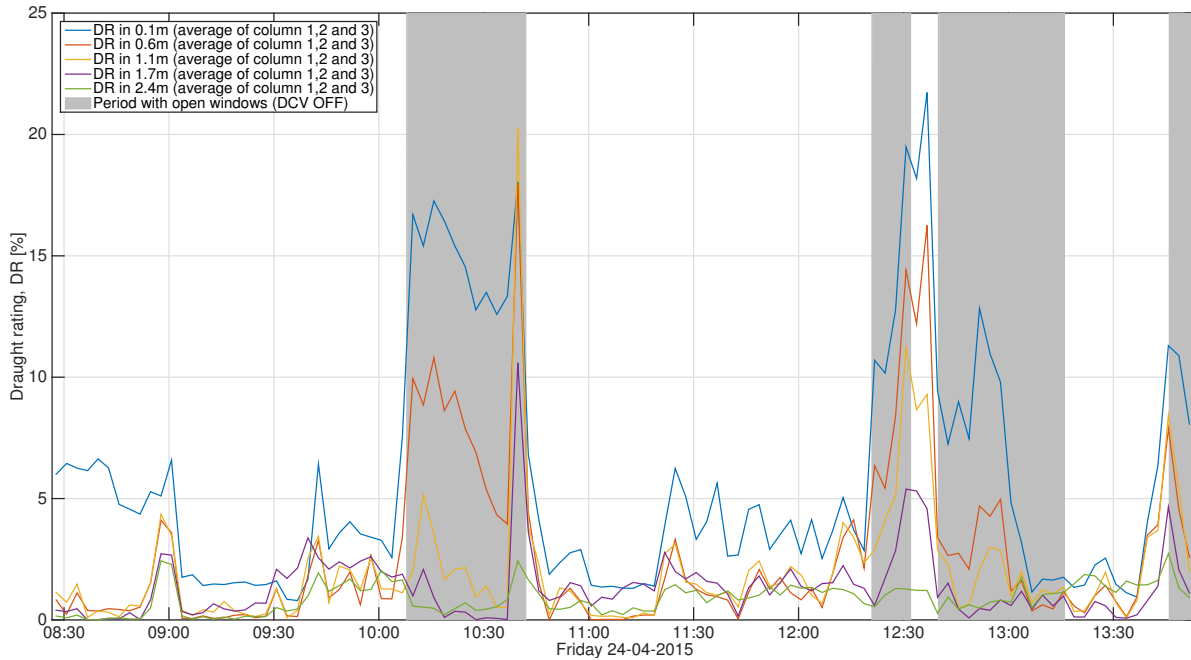


Figure 3.17: Draught rating in different heights and locations in the classroom.

As seen the mean draught level is well below 10%, indicating indoor environmental category A. Highest draught ratings are observed near the floor. Only when windows are opened is draught rating increased beyond category A.

3.7 Findings

In conclusion of the main study the following findings are highlighted.

Evaluation of the DCV system performance was successful in terms of system effectiveness and functionality and also resulting indoor environmental quality. As was also found in the pilot study, opening of the windows shuts down the ventilation system. Both pupils and teachers opened the windows several times during the tested days properly due to the malfunctioning radiator valves. However, with the DCV system being *invisible* it cannot be neglected that a psychological factor may also have played a role. Whenever windows were closed, the ventilation system was running.

Plenum works as pressure chamber. It is found that the fresh intake air is close to equally distributed across the plenum area before being pulled down through the diffuse Trolldtekt panels that make up 13% of the total suspended ceiling area. Only a slight tendency towards less fresh air with increasing distance is experienced. In general, 80-100% of the maximum plenum CO₂-concentration is obtained within the first 10% of the plenum length. As such, it is assessed that an adequate pressure chamber effect and mixing is present in the plenum. The fresh intake air is preheated to around 60-90% of the final exhaust temperature corresponding to a heat-up within the plenum of 4-5 °C.

DCV system delivers a good indoor environment. Inside the classroom itself a ventilation effectiveness between 0.8 and 1.2 is observed in periods without interference from open windows. The completely mixed air is not, however, a direct result of high air speeds as these remain low around 0.05 m/s with a turbulence intensity between 15-25%. Together with high air temperatures due to malfunctioning radiator valves ($22^{\circ}\text{C} < T_{air} < 27^{\circ}\text{C}$), draught rates below 5% is seen most of the day. In general the lowest temperatures and highest velocities and thus also draught rating, is seen at floor level. A vertical temperature gradient around 1 °C between head and ankles is observed. Had the air temperature not been artificially high due to the hot radiators, the indoor climate would be classified as environmental category A.

Part 2

Experimental and Numerical Investigations

Answering Supporting Objective 2:

To what degree does the supply opening area of a diffuse ceiling ventilation system influence the functionality and delivered indoor thermal comfort of a diffuse ceiling ventilation system?

Full-scale experimental and numerical investigations are performed to analyse the indoor environmental comfort limits in rooms using Diffuse Ceiling Ventilation. Especially the influence of the suspended ceiling design on system performance is investigated.

Chapter 4

Influence of Supply Opening Area

This initial chapter of Part 2 deals with the comfort limit assessment of DCV systems. It is done through controlled steady-state experimental investigations simulating a typical Danish classroom like the one investigated in Part 1. The reader is initially introduced to the scope of the planned investigations and later the used experimental facility and methodology applied in finding a solution to them. Following this an analysis of the experimental results are conducted. The main findings of the investigations are highlighted in the end of the chapter.

4.1 Planned Investigations

As described in the introduction, it is the goal to determine the influence of the suspended ceiling design on system performance. Focus is primarily on reviewing maximum achievable cooling capacity and ventilation rates, without causing discomfort in a controlled setup resembling a Danish Classroom. However, associated analyses of airflow patterns in both plenum and test room as well as diffuse ceiling air permeability testing are carried out in order to raise the knowledge about the DCV system in question. The following analyses are conducted:

- Cooling capacity of DCV system
- Air permeability of diffuse ceiling
- Preheating of inlet air in plenum volume
- Airflow elements and patterns

Data for the analyses is gathered through a parametric variation of the diffuse ceiling layout and boundary conditions.

Cooling Capacity of DCV System

The cooling capacity of a DCV system is calculated as given in equation 1.7 on page 12. As described in the analysis section on page 8 the cooling capacity is incorporated into a design chart for correlated values of temperature difference and ventilation rate. It is the goal to establish such correlations for different diffuse ceiling areas, A_{DC} , and to confirm whether or not they differ for diffuse ceiling configurations. For explanation of diffuse ceiling area in suspended ceiling, A_{DC} , see figure 1.2 on page 8.

It is the scope to analyse the sources of variations and make clear how they influence the cooling capacity. To do so, an analysis of the airflow patterns both above and below the suspended ceiling is necessary as well as an assessment of the sensitivity towards heat load distributions inside the ventilated room. However, it is beyond the scope of these investigations to experimentally involve variations of the heat load distribution (see chapter 5 for numerical investigation of heat load distribution).

The design chart developed through the experimental investigations is only valid for the cases, which it is based upon, i.e. a specific room geometry, heat load distribution, diffuse ceiling area and configuration, room height etc.

Air Permeability of Diffuse Ceiling

Permeability in fluid mechanics is a measure of the ability of a porous material to allow fluids to pass through it. It is expected that the suspended diffuse ceiling will supply air through both the porous panel material itself and through installation cracks, arising from the mechanical assembling of the suspended ceiling. This *crack-flow* is unwanted in terms of air distribution inside the occupied zone as the air velocity is expected to increase causing local micro-jets. The crack-flow depends upon the applied type of jointing of the panels (see section 4.2 for details about the applied assembling method of test facility).

Air permeability is not only interesting in terms of air distribution through the panels but also in terms of energy consumption for air transport. As such, the permeability express the correlation between developed pressure loss across the ceiling, $\Delta p_{ceiling}$, at a given ventilation rate, q_v .

It is a goal to test the air permeability of different DCV ceilings and to develop a correlation between diffuse ceiling area and permeability. Furthermore, it is a goal to assess the level of crack-flows.

Plenum Effects

The plenum is a distinct part of a DCV system and works as a pressure chamber distributing air across the entire suspended ceiling. It is a goal to establish correlations between preheating and pressure chamber effects in the plenum for different DCV ceiling areas.

Airflow Pattern

Distribution of the ventilation air is of great importance, both in terms of system efficiency and the indoor environmental quality of the occupied zone. Investigation of the airflow patterns does not rely on the comfort limited cases alone, which are used in determining maximum cooling capacity, as the majority of all operating hours is expected to remain outside those limiting situations. However, it remains outside the scope of these experiments to expand the investigated cases beyond those necessary for determining maximum cooling capacity.

4.2 Hotbox as Test Facility

The experimental setup used for simulating a classroom with DCV is located in a climate chamber at Aalborg University, Denmark. Inside this climate chamber a hotbox is used as the experimental setup. In figure 4.1 a cross sectional view of the hotbox is shown. In order to somewhat compare results from these investigations to the results from Part 1 the experimental setup used has a very good similarity with the DCV system in the real classroom investigated previously. To further create comparability of results various parameters are sought duplicated to a reasonable extend; e.g. the heat load in the experimental setup is directly scaled from what was observed in the classroom.

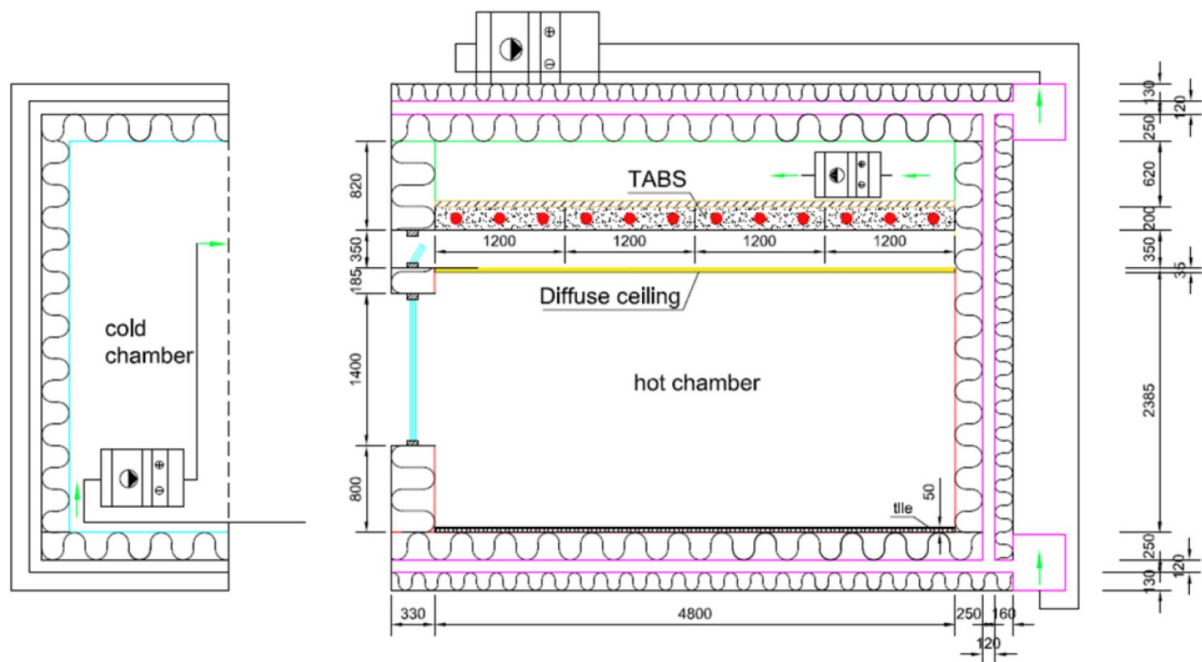


Figure 4.1: Cross sectional view of hotbox used for DCV experiments. All lengths in millimeter. Figure from: (Zhang, C. and Yu (2014)).

In figure 4.1 it can be seen how the hotbox is divided into four overall parts, a cold chamber simulating outdoor conditions (left), a hot chamber simulating indoor conditions (right), a second floor above the hot chamber (green zone above TABS) and a guarded zone (purple zone around hot chamber). Between the hot and cold chambers a window section with a damper inlet above the windows is installed, the wall including window has a U-value of $0.71 \text{ W}/(\text{m}^2\text{K})$ (Zhang, C. et al., 2014). The inlet damper is directly connected to the plenum above the suspended ceiling with no mechanical preconditioning of intake air, resembling the fresh air intake layout of the case site used in Part 1.

The experimental investigations are primarily focused on the climate in the hot chamber of the setup, as it is the DCV system and its effect on the comfort conditions in the test room which are of interest.

Cold Chamber

In the cold chamber a water-to-air cooling/heating coil conditions the "outdoor" air to a desired temperature, T_{out} , in the range $-8\text{ }^{\circ}\text{C}$ to $+35\text{ }^{\circ}\text{C}$. A fan ensures mixing of the air such that a uniform temperature distribution is reached both in the cold chamber in front of the facade window and in the fresh air inlet damper above the windows, where the inlet air temperature at the facade, T_{facade} , is measured using continuously logging thermocouples.

Hot Chamber

The hot chamber is designed to represent a two-story building; one story above and one below the concrete slabs (see figure 4.1). The geometrical dimensions of the test room below the slabs are given in table 4.1. In figure 4.2 a floor plan of the hot chamber can be seen.

Table 4.1: Geometrical dimensions of experimental test room inside hot chamber and of classroom examined in Part 1. The size ratio is calculated as experimental parameter divided by classroom parameter.

	Dimension	Experimental Test Room	Classroom in Solbjergskolen	Size Ratio [–]
Test Room	Length [m]	4.8	9.1	53 %
	Width [m]	3.3	6.3	53 %
	Height [m]	2.4	2.7	88 %
	Area [m ²]	15.8	56.7	28 %
	Volume [m ³]	37.8	154.1	25 %
Plenum	Height [m]	0.350	0.185	189 %
	Volume [m ³]	5.544	10.481	53 %
Plenum/Room	Volume Ratio [–]	15 %	7 %	214 %

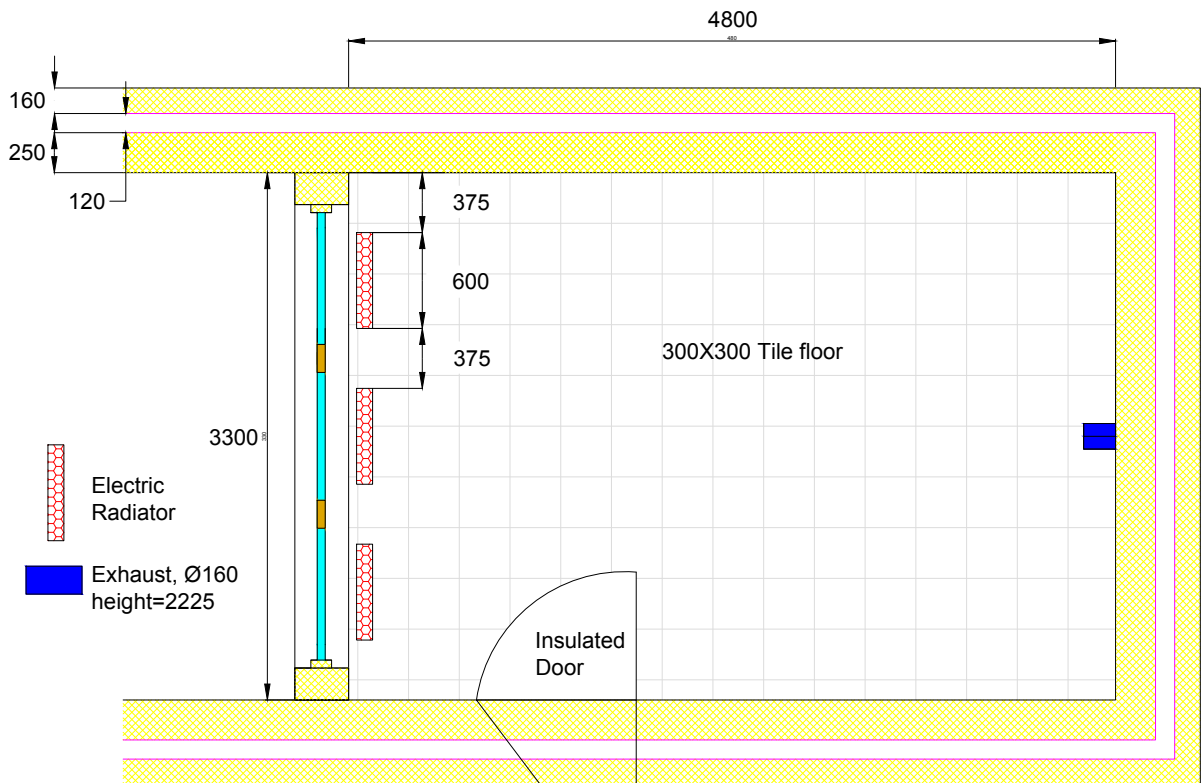


Figure 4.2: Floor plan of hot chamber in the experimental setup. All lengths in millimeter.

The diffuse ceiling in the test room is suspended on a metal frame and consists of 35 mm "ultrafine" Trolldtekt acoustic ceiling panels. Trolldtekt panels are made of cement paste and wood shavings mixed together (see figure 4.3), also known as cement-bonded wood wool panels. This type of ceiling panel have a very low heat conductivity of $\lambda_{trolldtekt} = 0.085 \frac{W}{mK}$.



Figure 4.3: Trolldtekt acoustic ceiling panels used as the diffuse ceiling in the test room. (Trolldtekt, 2015).

Between the suspended ceiling and the slabs a 350 mm high plenum is established in which the

4. Influence of Supply Opening Area

"outdoor" air is sucked in. Although the slabs installed in the setup are TABS (Thermally Activated Building Systems) these remain inactive during the experiments, hence functioning as traditional concrete slabs.

The ceiling panels installed in the experimental setup are all diffuse allowing for up to 100 % diffusive ceiling panel layout. When desired to lower the diffuser area, A_{DC} , in the suspended ceiling this is done from the room side using a vapour barrier. Apart from the diffusive characteristics of the ceiling panels themselves, the mounting of the ceiling panels also allow for small air gaps between panels as these are hung in a metal-track-system using screws. Ceiling panels are mounted with 4-6 screws per panel in thin metal plates suspended from window to back wall of the hot chamber. Because of the non-overlapping layout of the panels it is unavoidable that small air cracks between panels occur. The mounting of the panels can be seen from figure 4.4.

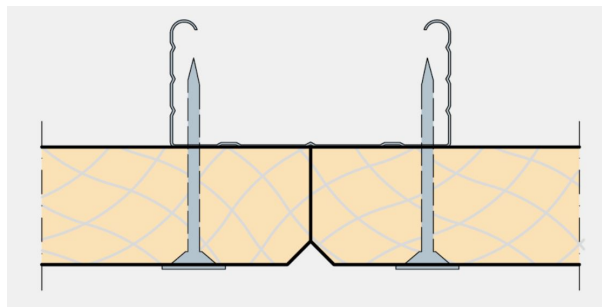


Figure 4.4: Non-overlapping mounting system of diffusive Trolldtekt ceiling panels Trolldtekt (2015).

To simulate a typical building thermal mass has been added to the room by fitting the floor with 50 mm concrete tiles to increase the thermal mass of the construction. This is necessary as the walls have a low thermal mass consisting of polystyrene and plywood.

Ventilation exhaust in the test room is mounted 80 mm below the diffuse ceiling in the wall opposite the window (see figure 4.2 and 4.7), similar to the exhaust layout of the real classroom investigated in Part 1. Similar to the classroom the mechanical air transport is done using a suction fan connected to the room exhaust channel.

Guarded Zone

To guard the whole experimental setup from external thermal influence a construction enclosing both the hot chamber and the cold chamber is installed. This guarding from the surroundings consists of 250 mm insulation, 120 mm air and finally 130-160 mm insulation. The air temperature of the 120 mm air gap between the two layers of insulation, T_{guard} , is controlled and continuously monitored throughout the experiments using thermocouples thus minimizing transmission losses. The guarded zone is seen in the cross-sectional view of the hotbox in figure 4.1.

Thermal Manikins

In order to simulate occupancy in the experimental setup eight thermal manikins are constructed cf. EN-14240 (2004), each corresponding to one pupil, hereby maintaining the same pupil density as in the classroom in Solbjergskolen (0.5 pupil/m^2).

The thermal manikins used are hollow, 1.0 m high, $\text{Ø}0.3 \text{ m}$, metal barrels with an electric fan-assisted heater hanging in the middle of it as shown in figure 4.5. The manikin construction, resulting heat release and plume characteristics have been examined prior to the main experiments to account for the effects on the indoor environment. The result may be seen in Appendix B.



Figure 4.5: Left: Picture of the heating element inside the thermal manikin used as heat load simulator in experimental setup. Right: Picture of all eight manikins used in the setup.

The heat release of each manikin during the experiments is determined by observations from the classroom made during the field investigation in Part 1 combined with table values from DS-474 (1995). Observed data of metabolic rate, height and weight of the students is used to calculate the total heat release of each manikin. To simulate a heat release close to the ones observed in the classroom in the field investigation the heat release of each manikin must be 80.0 W . A detailed calculation of heat release can be found in Appendix B.

The total heat release of all eight thermal manikins is hereby 640 W equal to a heat load of 40.4 W/m^2 floor. This heat release is kept constant throughout the experiments. The manikins are placed in couples around four symmetrical points throughout the test room as shown in figure 4.6.

4. Influence of Supply Opening Area

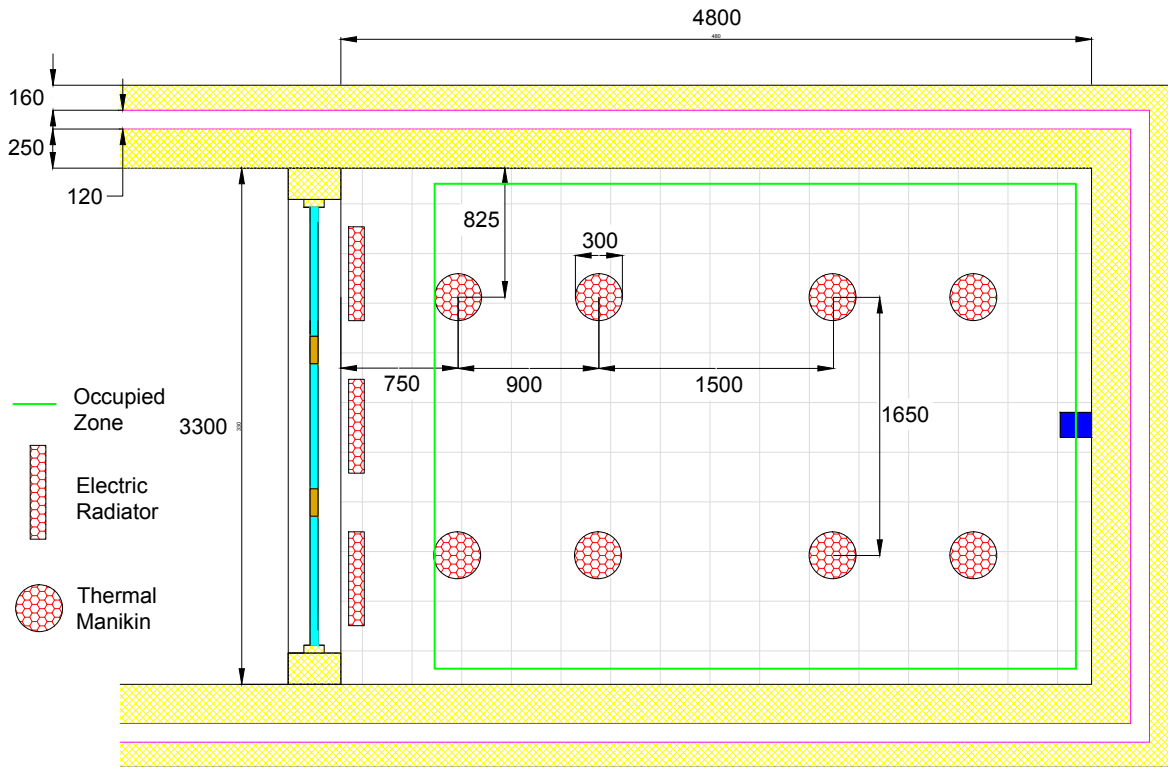


Figure 4.6: Placement of thermal manikins in the experimental setup. All lengths in millimeter.

From figure 4.7 below, pictures from the hot chamber test room is presented showing the location of thermal manikins, exhaust duct, measurement columns etc.



Figure 4.7: Pictures from inside the testroom of the hot chamber.

Other Heat Sources

As it was observed that the pupils in the real classroom only rarely used any electrical equipment, an experimental setup without computers is chosen. However, three electrical radiators below the windows are used to ensure sufficient heating capacity to maintain desired temperature setpoints (see figure 4.2). A detailed description of how this necessary heating is calculated can be found in section 4.3. It is chosen to supply the room with additional heat from the electrical radiators rather than increasing the heat load from the thermal manikins as it is desired to maintain the correct heat release from the manikins in order to simulate as realistic conditions as possible.



Figure 4.8: Electrical radiator used for adjusting heat release.

Apart from the manikins and radiators, the experimental setup features no additional heat sources. There is no artificial light installed in the setup and solar gains are also omitted.

4.3 Test Procedure and Instrumentation

To perform the planned investigations of the DCV system in the Hotbox, the following methodology is applied. It describes in detail the approach and necessary equipment in obtaining the required knowledge using the facilities of the Hotbox.

Overall Methodology

The main parameter of interest is the diffuse ceiling configuration and knowledge about how it influences the functionality and perceived thermal environment in a room supplied with DCV. The analyses are made from a set of combined experiments, which rely on parameter variations of the outer boundary conditions influencing the system;

- Diffuse ceiling area, A_{DC}
- Outdoor air temperature, T_{out}
- Ventilation rate, q_v

The investigation will simulate the indoor environment in a typical Danish classroom like the ones in Solbjergskolen, the school investigated in Part 1, when subjected to a mechanical exhaust driven DCV system. It is executed by running a series of experiments, each series with a different diffuse ceiling area, A_{DC} , and thus a different permeability of the suspended ceiling. Within each of the series of experiments the DCV system is operated at different simulated outdoor conditions in terms of different outdoor air temperatures, T_{out} , in the cold chamber (see drawing of experimental setup in figure 4.1 on page 69) and thus changing the resulting air temperature difference, ΔT , between room outlet air in the exhaust duct and inlet air at the facade.

$$\Delta T = T_{exhaust} - T_{facade} \tag{4.1}$$

where:

ΔT = air temperature difference between air inlet and outlet [°C]

$T_{exhaust}$ = air temperature in exhaust opening [°C]

T_{facade} = air temperature in facade opening [°C]

For each different simulated outdoor temperature, T_{out} , the ventilation rate, q_v , is continuously increased from a preliminary guessed value until an exceeding of the specified indoor environmental quality parameters happens at a maximum ventilation rate, $q_{v,max}$, thus defining the cooling capacity. The guessed starting value of ventilation rate is based on the previous experiment, however, never lower than the minimum value, $q_{v,min}$. The evaluation parameters are outlined below in a later section. The span between the airflow limits $q_{v,min}$ to $q_{v,max}$ make up the comfort range at any given temperature difference between inlet and outlet, ΔT .

In order to make the investigations of different outdoor conditions and overall thermal comfort comparable, the indoor room operative temperature, T_{room} , in the hot chamber is kept constant securing steady test conditions. This is outlined further below.

Air Permeability of Diffuse Ceiling

The measurement of air permeability is described in EN-13829 (2001) and this procedure is used in determining the resulting permeability of the combined suspended ceiling. It is investigated by initially measuring the properties of a single diffuse panel and subsequently the entire mounted ceiling, making it possible to conclude on the influence of installation cracks.

The air permeability testing of a single panel is performed using a pressure box where it is assured that no unwanted airflow along the sides of the panel occur. Varying the ventilation rate through the Trolldtekt panel a manometer (Furness FCO510 precision micromanometer) is used for measurements of pressure difference on each side of the panel. Data is compared to those of Zhang, C. and Yu (2014) and Trolldtekt (N.A.).

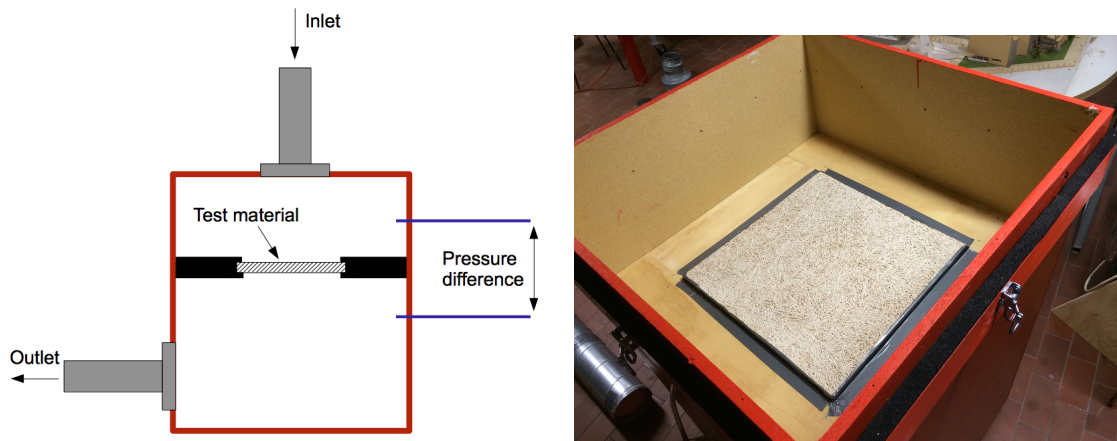


Figure 4.9: Pressure box setup for testing of air permeability of a single diffuse panel.

The air permeability of the entire suspended ceiling is measured for each experiment. It is done by measuring the pressure drop across the ceiling, $\Delta p_{ceiling}$, that arises due to the forced ventilation rate, q_v , and the air temperature, T_{air} . Because the uniformity of the air pressure in the plenum is unknown and probably varying across the length of the plenum, it is measured in three different distances from the air intake as described further below on page 84 and seen from figure 4.13.

Steady Test Conditions

Achieving the same room operative temperature, T_{room} , in all experiments is a fundamental premise for comparing the steady-state measured IEQ and concluding on any correlation between ventilation rate, q_v , and temperature difference, ΔT . To do so, adjustments of the internal heat loads are necessary to compensate for the increased/decreased heat loss. This is done by increasing the heat release from the radiators, Φ_{rad} , as function of the increased heat loss mainly through ventilation. "Human" heat release from the thermal manikins, $\Phi_{manikin}$, is kept constant

4. Influence of Supply Opening Area

throughout all experiments simulating a non-varying activity level. A simple heat balance of the hot chamber is used to roughly determine the necessary heat release.

$$\Phi_{trans} + \Phi_{vent} = \Phi_{manikin} + \Phi_{rad} \quad (4.2)$$

The heat balance is simplified further as the air temperature of the guarded zone, T_{guard} , surrounding the hot chamber and the second floor above the TABS, $T_{2ndfloor}$, is kept constant (regulated by a PI-controller) simulating adiabatic interfaces reducing the transmission losses to what is transmitted through the facade wall and windows.

$$T_{room} = T_{guard} = T_{2ndfloor} \quad (4.3)$$

Thus, the necessary heat adjustment is roughly calculated as

$$\Phi_{rad}(q_v, \Delta T) = (H_{facade} + q_v \cdot \rho \cdot c_p) \Delta T - \Phi_{manikin} \quad (4.4)$$

where:

- Φ_{trans} = heat loss by transmission [W]
- Φ_{vent} = heat loss by ventilation [W]
- $\Phi_{manikin}$ = heat load from thermal manikins (640 W) [W]
- Φ_{rad} = heat load from electric radiators [W]
- T_{room} = room operative temperature [°C]
- T_{guard} = air temperature in guarded zone around hot chamber [°C]
- $T_{2ndfloor}$ = air temperature in 2nd floor above plenum [°C]
- ΔT = air temperature difference between air inlet and outlet [°C]
- H_{facade} = specific heat transmission coefficient for facade [W/K]
- q_v = ventilation rate [m³/s]
- ρ = air density ($\approx 1.2 \text{ kg/m}^3$) [kg/m³]
- c_p = specific heat capacity of air ($\approx 1005 \text{ J/(kgK)}$) [J/(kgK)]

As the calculated heat release is a rough initial estimate for each experiment, manual adjustment might be necessary.

As mentioned above, achieving steady-state (constant room operative temperature, T_{room}) is a fundamental premise for comparability in the experiments. However, true steady-state conditions

rarely happen and only in a limited time period. Often the thermal environment is in a non-steady-state, which may be categorized as either: temperature cycles, temperature drifts or ramps, and transients cf. ISO-7730 (2006). If temperature comply with the following limitations, ISO-7730 (2006) regards the thermal environment as steady-state:

Temperature cycles: Defined as the variation of temperature with a given amplitude or frequency often due to temperature control. Peak-to-peak variations must be less than 1.0°C to be considered steady-state.

Temperature drifts or ramps: Defined as a passive monotonic (drifts) or active monotonic (ramps), steady, non-cyclic change in temperature of an enclosed space. Rate of change of temperature must be less than 2.0°C/h to be considered steady-state.

Temperature transients: Defined as a sudden change of temperature due to step-changes in the thermal environment e.g. temperature, humidity, activity or clothing. Transients are felt instantaneously and cannot be accepted.

To bring down the overall uncertainty and increase the validity of the experiments, the definition of steady-state in the experiments is further tightened in terms of acceptable temperature cycles to a maximum of 0.4°C ($\pm 0.2^{\circ}\text{C}$). The wanted room operative temperature is determined based on a thermal environmental category B. For a classroom with 0.5persons/m^2 and an activity level of 1.2 met and clothing factor of 1.0 clo, the optimum operative room temperature, T_{room} , equals 22°C cf. ISO-7730 (2006). As such, less than 10% of the pupils should be dissatisfied with the thermal state of their body as a whole when keeping the room operative temperature at 22°C during the experiments. The overall steady-state test condition for all the experiments thus becomes:

$$T_{room} = 22^{\circ}\text{C} \pm 0.2^{\circ}\text{C} \tag{4.5}$$

Eventhough the temperature is steady, the airflow is not necessarily. This could be the case both due to naturally occurring turbulence and possible flow pattern fluctuations inside the test room resulting from e.g. disturbances from the chiller in the cold chamber or plume variations above the thermal manikins due to the unsteady nature of such plumes. As with the temperature, the air velocity may vary in cycles, which could strongly influence the local discomfort evaluation and make it non-steady-state. From figure 4.10, measured air velocity in a 25 minute temperature steady-state period is plotted with different integration times (2s, 30s and 180s) but same sample rate (5 Hz) to illustrate the variations and spot any low-frequent oscillations, which might indicate only quasi-steady-state conditions.

4. Influence of Supply Opening Area

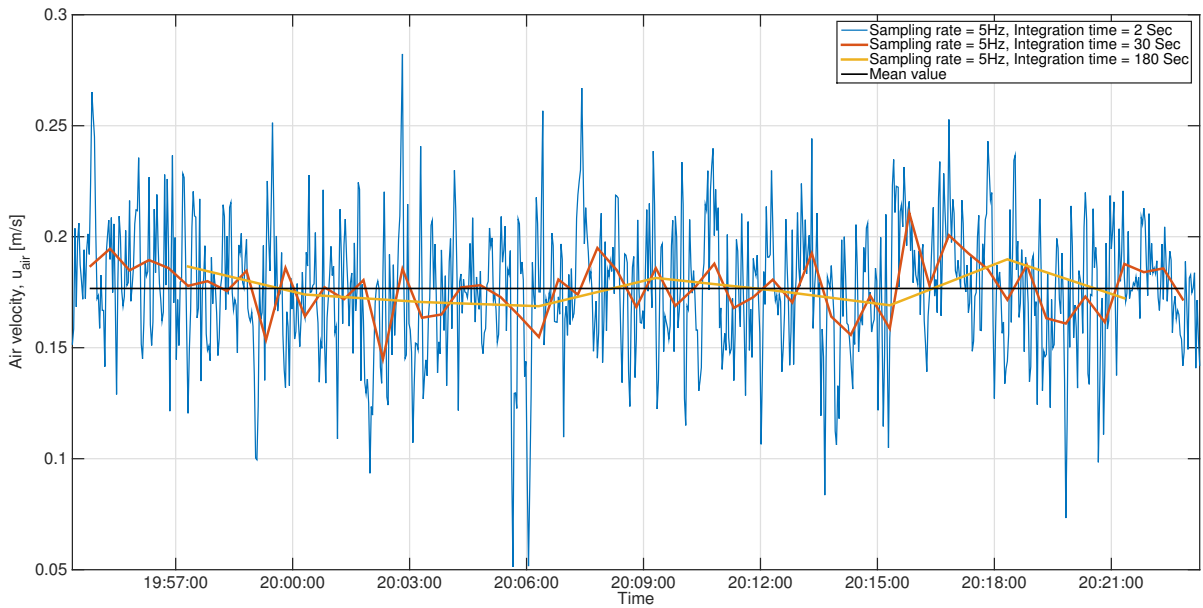


Figure 4.10: Example of measured air velocities in occupied zone during temperature steady conditions. The plot shows the velocity measurements integrated over different time intervals.

As seen from the figure, no major periodical oscillations are present, only a small 12-minute oscillation is observed when integration over 180 s and what seems to be turbulence makes the measurements fluctuate around its mean value.

Based on the requirements for overall steady-state of the operative temperature (see equation 4.5 above) and the steadiness of the air velocity, a sampling period of minimum 15 minutes in which the measured values are averaged into a single value per sensor per experiment is chosen. Hereby the 12-minute oscillation observed in figure 4.10 is accounted for and the 3-minute recommendation in SBi-130 (1983) and DS-474 (1995) taken into account.

Acceptable Indoor Environmental Quality

The DCV system is limited in the same way as all other ventilation systems; a minimum ventilation rate, $q_{v,min}$, is necessary to secure the minimum allowed IAQ according to legislation and a maximum ventilation rate, $q_{v,max}$, limits the thermal comfort at any given temperature difference, ΔT .

For schools and educational rooms Danish Building Regulations state that a minimum of 5 l/s/person and 0.35 l/s/m²_{floor} has to be supplied at all occupied hours (BR10, 2010). Thus, with the experimental room being 15.84 m² and a total of 8 simulated persons the lower limitation, $q_{v,min}$, equals 45.5 l/s. This corresponds to an Air Change Rate, ACR , of approximately 4.3 h⁻¹.

As mentioned above, the ventilation rate, q_v , is increased from an initial guess of acceptable ventilation rate (not below $q_{v,min}$) until an exceeding of the indoor environmental quality parameters has occurred. These parameters are defined in accordance with the specified categories of thermal environment in ISO-7730 (2006), which are reproduced in table 1.1 on page 10.

The local discomfort parameters (draught rating, vertical air temperature difference, warm or cold floor, and radiant asymmetry) are used as evaluative criteria for defining the maximum allowed ventilation rate, $q_{v,max}$, at a given temperature difference, ΔT . Whenever one of the local discomfort criteria are exceeded, $q_{v,max}$ is obtained as local discomfort is present. However, the criteria must be satisfied only within the occupied zone of the hot chamber. The formulation of acceptable exceeding of IEQ from EN-15251 (2007) has been adopted:

"The building meets the criteria of a specific category if the rooms representing 95 % of building volume meet the criteria of the selected category."

In this case "building" should be understood as the hot chamber and as such, the exceeding of a local discomfort criterion is obtained when the exceeding occurs in more than 5 % of the Occupied Zone, OZ , volume. 5 % of the OZ volume corresponds to measurements of 2 sensors, meaning that the comfort limit has been found if 2 steady sensor readings (8.3 % of all readings) indicate e.g. a draught rate above 20 %, which is the criteria for thermal environmental category B.

Parameter Variations of Boundary Conditions

Because the maximum ventilation rate, $q_{v,max}$, at which thermal comfort is compromised is unknown, a large number of experiments are executed to obtain the necessary information. These experiments are composed of parameter variations of the 3 variables; A_{DC} , T_{out} and q_v as described above.

The diffuse ceiling area may be given in terms of A_{DC}^+ , a dimensionless expression of the diffuse ceiling area, when normalized with the entire ceiling area.

As described above, three different variations of the diffuse ceiling area is investigated;

$$A_{DC}^+ = 1.00, 0.50 \text{ and } 0.18 \tag{4.6}$$

Their geometrical layout is illustrated in figure 4.11 below. As it is beyond the scope of these investigations to experimentally investigate how the distribution of the diffuse panels across the ceiling influence the result, all A_{DC}^+ variations utilize a uniformly distributed layout.

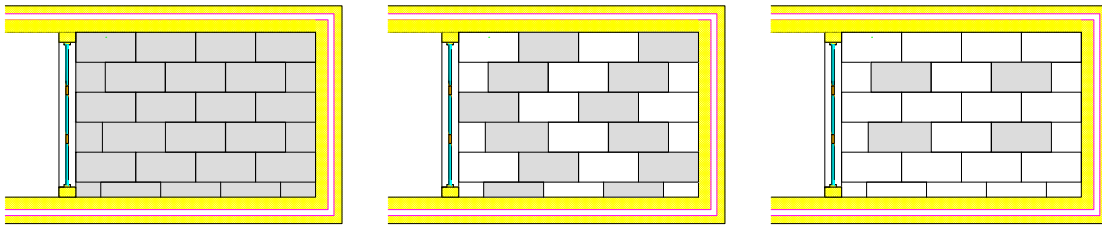


Figure 4.11: Three diffuse ceiling layouts; 100%, 50% and 18% diffuser area (grey).

Changing of diffuse ceiling area is in practice carried out by fitting a vapour barrier to the diffuse ceiling panels on the room side of the suspended ceiling (see figure 4.12).



Figure 4.12: Reduced diffuse ceiling area by fitting a vapour barrier on room side of ceiling panels.

The outdoor air temperature, T_{out} , in the cold zone is varied in five steps;

$$T_{out} = +12^{\circ}\text{C}, +7^{\circ}\text{C}, +2^{\circ}\text{C}, -3^{\circ}\text{C} \text{ and } -8^{\circ}\text{C} \quad (4.7)$$

According to equation 4.1 the temperature difference, ΔT , between exhaust air, $T_{exhaust}$, and inlet air, T_{facade} , hereby becomes:

$$\Delta T = +10^{\circ}\text{C}, +15^{\circ}\text{C}, +20^{\circ}\text{C}, +25^{\circ}\text{C} \text{ and } +30^{\circ}\text{C} \quad (4.8)$$

However, the exact outdoor air temperature depends upon the hotbox control system.

At each combination of A_{DC}^+ and T_{out} , q_v is increased using a trial-and-error methodology from an initial guess until discomfort is detected at $q_{v,max}$. The ventilation rate is handled as the normalized parameter, ACR (air change rate).

$$ACR = \frac{q_v}{V_{room}} \cdot 3600 \quad (4.9)$$

where:

T_{out}	= outdoor air temperature (cold zone) [$^{\circ}\text{C}$]
ΔT	= air temperature difference between air inlet and outlet [$^{\circ}\text{C}$]
$T_{exhaust}$	= air temperature in exhaust opening [$^{\circ}\text{C}$]
T_{facade}	= air temperature in facade opening [$^{\circ}\text{C}$]
ACR	= air change rate (air changes per hour) [h^{-1}]
q_v	= ventilation rate [m^3/s]
V_{room}	= room air volume [m^3]

Measurements of Boundary Conditions and System Functionality Parameters

Parameters related to the DCV system functionality and various boundary conditions are monitored to get a detailed description of how the system operates under given conditions. These are in particular the ones related to the plenum of the DCV.

Ventilation rate, q_v , is measured using an orifice plate in combination with a manometer (Furness FCO510 precision micromanometer), attached to the exhaust driven ventilation system. The fan is connected to the exhaust of the room, so the ventilation is suction based as it was in the real class room tested in Part 1. The exhausted air is blown into the cold chamber of the experimental setup. Ventilation rate may be assessed with a combined instrument accuracy of

4. Influence of Supply Opening Area

$\pm 5\%$. In addition, temperature variations throughout the pressure tubes between orifice and manometer cause measurement uncertainties, which are difficult to assess.

Outdoor air temperature, T_{out} , which is the air temperature of the cold zone, is measured using thick type K thermocouples in three points along a vertical line to review the uniformity of the air. It is measured with a combined instrument accuracy of $\pm 0.1^\circ\text{C}$.

Inlet facade air temperature, T_{facade} , which is the temperature of the air taken in through the inlet dampers in the facade into the plenum, is measured using thick type K thermocouples in three points along a horizontal line to review the uniformity of intake air. It is measured with a combined instrument accuracy of $\pm 0.1^\circ\text{C}$.

Plenum air temperature, T_{plenum} , is measured using thick type K thermocouples in nine points, each in the middle of the plenum gap between slabs and ceiling panels as illustrated in figure 4.13 and 4.14. The location of the measurement points are the same as the measurement points for surface temperature, underneath the diffuse ceiling panels, inside the hot chamber. It is measured with a combined instrument accuracy of $\pm 0.1^\circ\text{C}$.

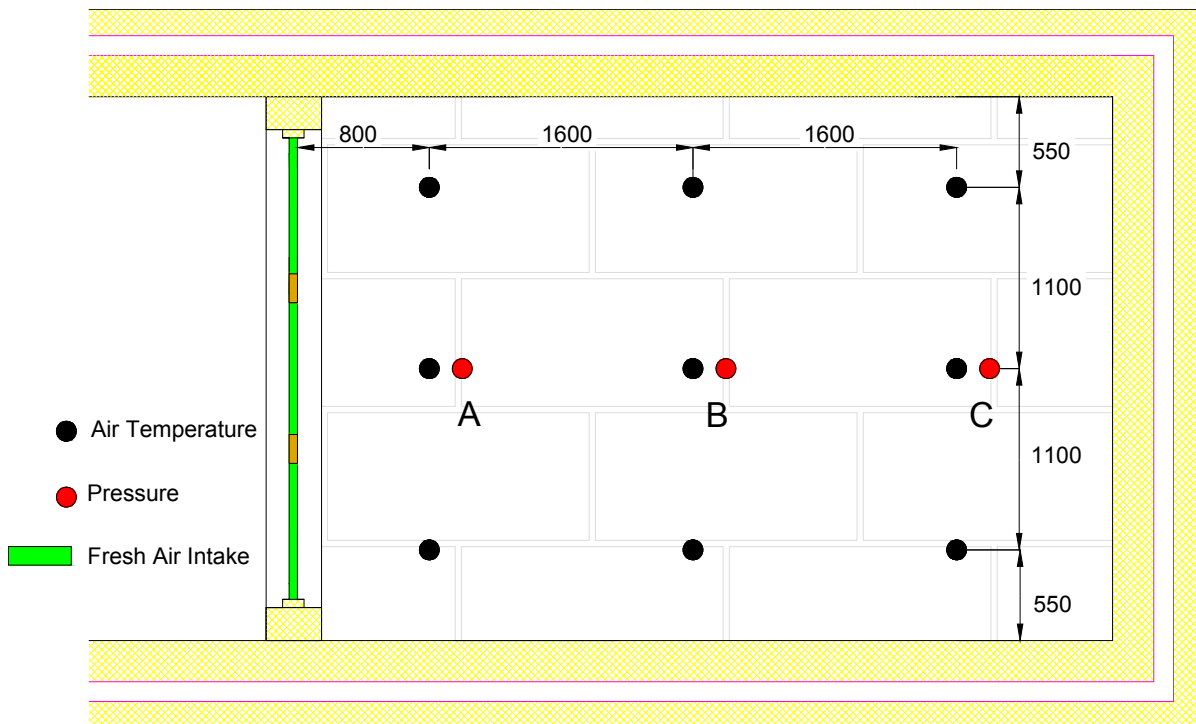


Figure 4.13: Top view of measurement points in the plenum. Pressure measuring points A, B and C used in pressure difference calculations. All lengths in millimeter.



Figure 4.14: Left: Picture of thermocouples and pressure tubes located in plenum. Right: Picture of exhaust duct with thermocouples located in duct.

Exhaust air temperature, $T_{exhaust}$, from the room is measured in the centre of the exhaust duct with two thick type K thermocouples placed 30 mm apart. The thermocouples are seen from the right picture in figure 4.14. It is measured with a combined instrument accuracy of $\pm 0.1^\circ\text{C}$.

Pressure difference, Δp , between room and plenum is measured in three different distances (A,B and C) from the intake damper perpendicularly into the plenum (see red marks on figure 4.13) using a Furness FCO510 precision micromanometer. For all the pressure difference (Δp_A , Δp_B , Δp_C) measurements in the same spot in the centre of the test room is used as reference value. Thus values of pressure difference are not logged continuously but evaluated as spot-measurements when steady-state has occurred. Pressure difference is measured with an instrument accuracy of $\pm 0.1\%$ of reading.

Measurements of Thermal Comfort in Occupied Zone

The measuring parameters for the assessment of thermal comfort are in general similar to those parameters described in Part 1. However, in these experiments it is essential to measure the extreme occurring parameters in order to assess the earliest exceeding of discomfort criteria. To do this, the occupied zone and local critical regions of airflow are initially defined;

The occupied zone, OZ , as defined in DS-474 (1995) and adopted in these experiments, is defined as a volume starting 0.6 m from external walls, 0.1 m from internal walls and spanning from floor to 1.8 meters height. Although the occupied zone is primarily used for stationary activity, and therefore could be limited to a height of 1.3 m, it has been chosen to use the full-height occupied zone to get a more comprehensive understanding of the airflow and velocity distribution in rooms with DCV.

Local critical regions within the occupied zone are determined based on smoke visualization for each series of experiments (each ceiling configuration). These regions are of interest as it is the first locations in which discomfort occurs, and therefore marks the upper limit of thermal comfort

in the OZ. Practically smoke is introduced to the fresh inlet air which will offer a qualitative measure of maximum air velocity in the occupied zone as the smoke enters the room through the diffuse ceiling.

The thermal comfort parameters in the critical regions of the occupied zone are measured using measurement columns with sensors for air velocity and air temperature (see figure 4.15 for the construction of the columns).

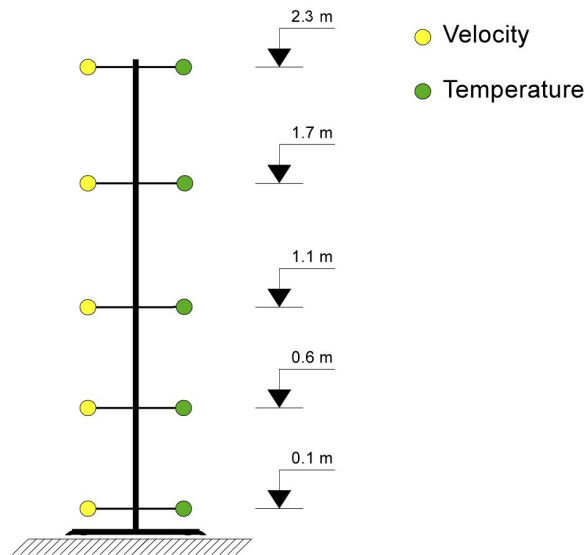


Figure 4.15: Measurement columns used in the experimental setup for velocity and temperature measurements in five different heights.

Air temperature, T_{air} , and speed, u_{air} , is measured using Dantec hot-sphere anemometers with build-in thermistors. Calibration and use of the thermistor for air temperature measurements is investigated separately and documented in Kristensen, M. H. et al. (2015). Air temperatures are used to evaluate vertical temperature gradient between head and ankles, $\Delta T_{head/ankles}$, and Draught Rating, DR . Air speeds are used to evaluate maximum air speed, $u_{air,max}$, Draught Rating, DR , Turbulence Intensity, I_{turb} , and average air speed, $\overline{u_{air}}$ - all within the occupied zone. Air speed is measured with an instrument accuracy of $\pm 5\%$ and air temperature with $0.1-1.8^\circ\text{C}$ depending on air speed $\pm 0.1^\circ\text{C}$.

Operative Temperature, T_{room} , is measured by two identical globe-sensors with thick type K thermocouples inside. The sensors are placed in a representative manner for each level of ceiling diffusivity and the two globe temperatures are averaged into a room mean operative temperature. Using a globe around the thermocouple allows the measured temperature to be the correct weighing average of air temperature and mean radiant temperature. In figure 4.16 one of the globes are seen located on a column. Operative temperature is used to evaluate the PMV and hereby the PPD-indexes. It is measured with a combined instrument accuracy of $\pm 0.1^\circ\text{C}$.



Figure 4.16: Dantec draught probe (shield pulled up) for measurements of air temperature and speed and operative temperature sensor (globe).

Surface temperatures, T_{surf} , are measured using thin type K thermocouples, attached to the surface using HCG (highly conductive grease). T_{surf} is measured in one point (wall centre) for internal walls. For the external/facade wall it is measured in three points on the windows and in two points below and above the windows. For the floor surface temperature four thermocouples are evenly distributed over the floor. As the ceiling temperature (on room side) is very interesting for the DCV-analyses 9 thermocouples are placed in a uniform grid to account for local deviations. The placement of all surface temperature measurement points can be seen on figure 4.17. Surface temperatures are used to evaluate radiant asymmetry, cold/warm surface problems and vertical temperature difference from floor to ceiling. It is measured with a combined instrument accuracy of $\pm 0.1^\circ\text{C}$.

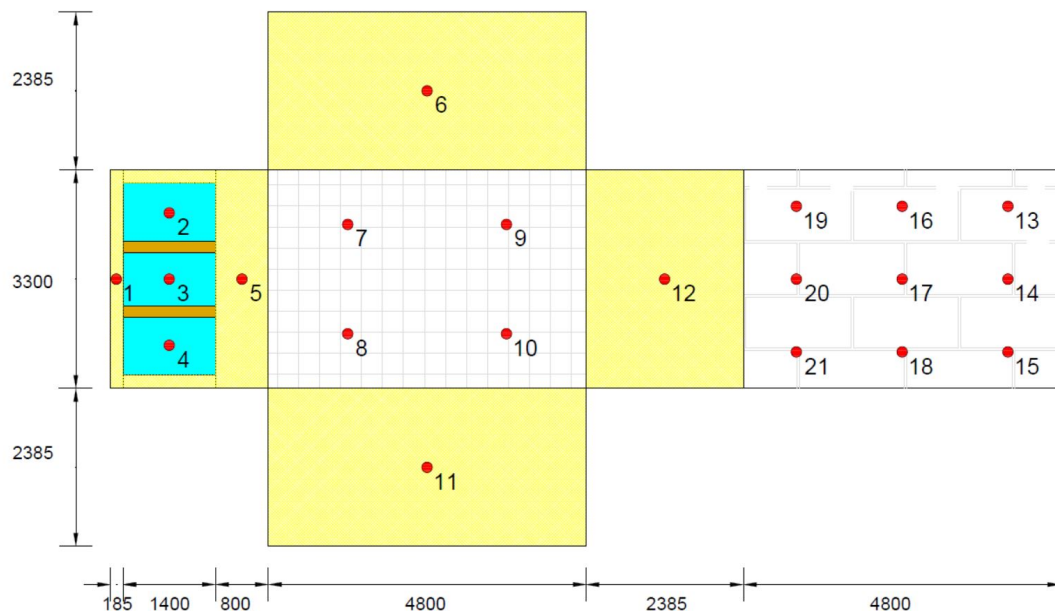


Figure 4.17: Measurement points for surface temperature in the experimental setup. Gray marks floor and ceiling. Blue marks windows. Brown marks internal walls.

4.4 Measurement Results

The following section presents measurement results obtained from the three series of experiments with different diffuser area (degrees of diffuse ceiling) and attained cooling capacity.

Location of Measurement Columns

For each different ceiling layout, A_{DC}^+ , airflows are expected to vary significantly, especially close to the suspended ceiling. As described in Section 4.3 about the methodology applied, it is important to determine local critical regions of the occupied zone where the highest air velocities are present in order to be able to observe the earliest occurrence of thermal discomfort and thus securing the validity of any conclusions on comfort limited cooling capacity. These regions was attempted found by injecting smoke to the cold chamber and in doing so it was the goal to reveal high velocity streamlines and critical regions of the airflow in the test room. However, the method proved ineffectual as the smoke was effectively diluted showing nothing but a vague all-pervading fog. In conclusion of these smoke visualisations, no high-risk regions was found.

Instead, a trial-and-error methodology was attempted where the measurement columns was placed at different locations in the test room based on educated guesses. From figure 4.18 the rejected and actual chosen locations of the measurement columns are shown.

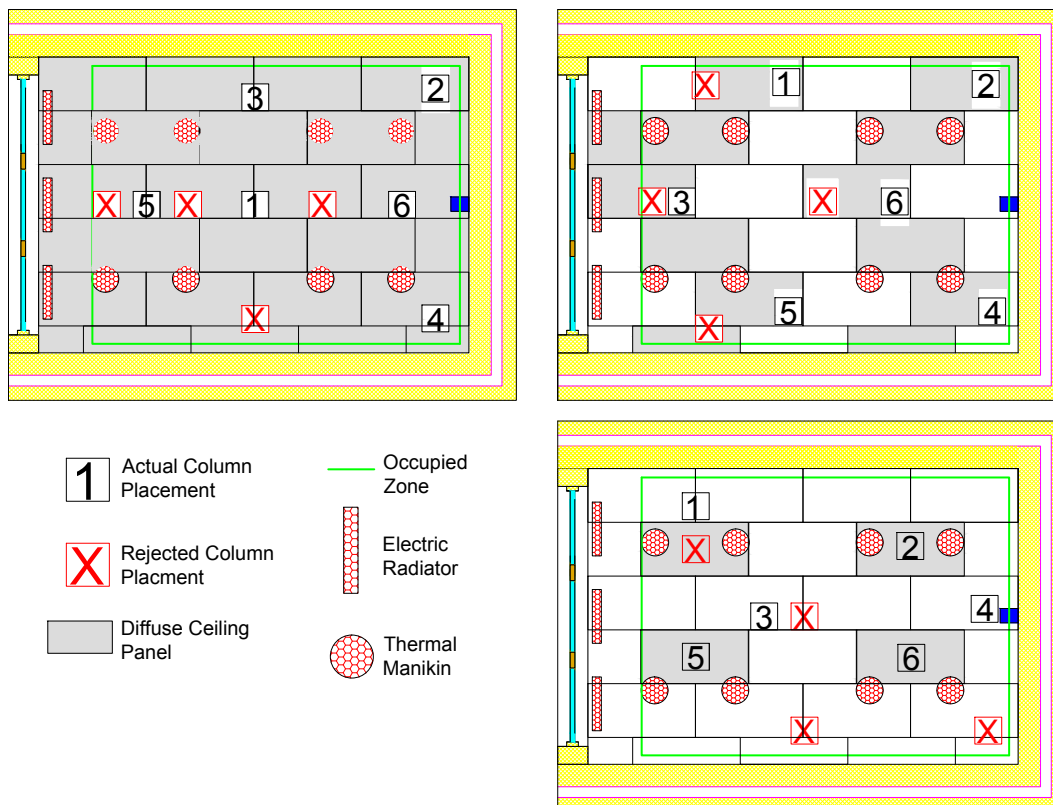


Figure 4.18: Placement of measurement columns 1-6 for for the three different ceiling layouts. From left to right: 100 %, 50 % and 18 % diffuse ceiling area.

The columns are in generally placed as far from the thermal manikins as possible as this is where the critical regions in terms of comfort will be. The hot, uprising, plume above the thermal manikins prevents cold air from the diffusive ceiling in dropping down above the manikins hence it is expected that cold intake air will be pulled down in areas where no heat sources are present.

In the two cases with reduced ceiling area (50 % and 18 %), the fresh inlet air can only enter the room through a limited number of diffuse panels above the manikins. As the ceiling inlet area is reduced the velocity of the inlet air increases for identical ventilation rates, compared to the 100 % diffuse ceiling layout, making it more interesting to measure right below the diffuse panels, despite that it is close to the manikins.

Measured Data

A total of 70 experiments have been performed in the search for the comfort limiting combinations, each with different combinations of diffuse ceiling area, A_{DC} , outdoor air temperature, T_{out} , and ventilation rate, q_v .

From table 4.2, 4.3 and 4.4 below, essential data and boundary conditions from the 70 experiments is grouped and presented based on the diffuse ceiling layout in question, either $A_{DC}^+ = 100\%$, 50 % or 18 %. Data from these tables are used in the following analyses.

4. Influence of Supply Opening Area

Table 4.2: Experimental data with 100% diffuse ceiling area.

Experiment number	A_{DC}^+ [-]	ΔT [°C]	ACR [h ⁻¹]	DR [-]	Δp_{A-D} [Pa]	Δp_{B-D} [Pa]	Δp_{C-D} [Pa]
1	1.00	10.31	12.89	<20 %	0.44	0.55	0.45
2	1.00	9.95	13.78	<20 %	0.47	0.50	0.51
3	1.00	9.82	14.81	<20 %	0.45	0.53	0.56
4	1.00	11.21	14.83	<20 %	0.45	0.52	0.54
5	1.00	10.94	15.72	<20 %	0.42	0.56	0.58
6	1.00	11.08	16.73	>20 %	0.46	0.58	0.58
7	1.00	15.21	4.11	<20 %	0.20	0.22	0.21
8	1.00	15.47	6.07	<20 %	No Data	No Data	No Data
9	1.00	15.78	8.10	<20 %	No Data	No Data	No Data
10	1.00	15.88	8.55	<20 %	No Data	No Data	No Data
11	1.00	15.87	9.00	<20 %	No Data	No Data	No Data
12	1.00	15.86	9.80	<20 %	No Data	No Data	No Data
13	1.00	16.00	10.69	<20 %	0.40	0.46	0.43
14	1.00	15.86	11.46	>20 %	0.44	0.52	0.46
15	1.00	16.35	12.10	<20 %	0.46	0.55	0.50
16	1.00	19.86	4.14	<20 %	No Data	No Data	No Data
17	1.00	20.06	6.11	<20 %	No Data	No Data	No Data
18	1.00	20.21	7.09	<20 %	0.32	0.37	0.31
19	1.00	20.30	7.54	<20 %	No Data	No Data	No Data
20	1.00	19.99	9.08	<20 %	0.42	0.49	0.42
21	1.00	19.92	9.99	<20 %	0.44	0.50	0.45
22	1.00	19.93	10.48	>20 %	0.44	0.50	0.46
23	1.00	24.90	4.29	<20 %	No Data	No Data	No Data
24	1.00	25.15	6.21	<20 %	No Data	No Data	No Data
25	1.00	24.88	5.29	<20 %	0.25	0.30	0.28
26	1.00	25.10	7.25	<20 %	No Data	No Data	No Data
27	1.00	24.73	8.08	<20 %	0.42	0.47	0.46
28	1.00	25.31	8.67	<20 %	0.41	0.50	0.44
29	1.00	24.71	9.06	>20 %	No Data	No Data	No Data
30	1.00	24.88	9.14	<20 %	0.44	0.51	0.43
31	1.00	24.64	10.02	<20 %	0.46	0.54	0.46
32	1.00	24.49	10.48	<20 %	No Data	No Data	No Data
33	1.00	24.34	10.50	<20 %	0.46	0.57	0.48
34	1.00	29.15	7.01	<20 %	0.37	0.45	0.37
35	1.00	28.99	7.56	<20 %	0.41	0.48	0.41
36	1.00	28.71	8.10	>20 %	0.43	0.50	0.42

Table 4.3: Experimental data with 18% diffuse ceiling area.

Experiment number	A_{DC}^+ [-]	ΔT [°C]	ACR [h ⁻¹]	DR [-]	Δp_{A-D} [Pa]	Δp_{B-D} [Pa]	Δp_{C-D} [Pa]
37	0.18	10.96	11.96	<20 %	2.23	2.30	2.36
38	0.18	10.77	11.96	>20 %	2.09	2.18	2.22
39	0.18	10.82	11.01	<20 %	1.93	1.98	2.05
40	0.18	15.45	9.09	<20 %	1.39	1.48	1.51
41	0.18	15.66	10.07	>20 %	1.62	1.65	1.67
42	0.18	20.06	6.86	<20 %	1.03	1.06	1.05
43	0.18	20.11	8.17	<20 %	1.29	1.30	1.28
44	0.18	20.26	8.84	<20 %	1.38	1.41	1.32
45	0.18	20.36	9.70	<20 %	1.54	1.56	1.52
46	0.18	20.45	9.99	<20 %	1.59	1.63	1.63
47	0.18	20.55	10.55	>20 %	1.70	1.74	1.76
48	0.18	25.07	9.03	<20 %	1.44	1.49	1.43
49	0.18	24.84	9.87	<20 %	1.59	1.68	1.68
50	0.18	24.71	10.43	<20 %	1.69	1.73	1.73
51	0.18	24.44	11.20	>20 %	1.83	1.90	1.90
52	0.18	29.32	8.11	<20 %	1.24	1.28	1.24
53	0.18	29.05	9.00	<20 %	1.39	1.44	1.42
54	0.18	28.72	9.75	<20 %	1.50	1.58	1.55
55	0.18	28.37	10.48	>20 %	1.62	1.71	1.69

Table 4.4: Experimental data with 50% diffuse ceiling area.

Experiment number	A_{DC}^+ [-]	ΔT [°C]	ACR [h ⁻¹]	DR [-]	Δp_{A-D} [Pa]	Δp_{B-D} [Pa]	Δp_{C-D} [Pa]
56	0.50	28.52	10.53	<20 %	0.66	0.77	0.74
57	0.50	28.61	10.51	<20 %	0.68	0.77	0.74
58	0.50	28.97	9.72	<20 %	0.62	0.70	0.69
59	0.50	29.63	8.01	<20 %	0.51	0.61	0.58
60	0.50	29.98	6.89	>20 %	0.43	0.52	0.5
61	0.50	29.96	5.80	<20 %	0.40	0.45	0.42
62	0.50	25.40	7.04	>20 %	0.46	0.53	0.50
63	0.50	25.36	6.56	<20 %	0.43	0.50	0.47
64	0.50	20.86	9.86	<20 %	0.51	0.62	0.62
65	0.50	20.91	10.49	>20 %	0.59	0.68	0.68
66	0.50	16.90	11.25	>20 %	0.58	0.65	0.66
67	0.50	17.00	10.53	<20 %	0.54	0.63	0.64
68	0.50	12.23	14.32	<20 %	0.70	0.83	0.92
69	0.50	12.13	15.10	>20 %	0.74	0.87	0.99
70	0.50	20.78	9.86	<20 %	0.59	0.68	0.68

Stability of Test Conditions

For the assessment of the comparability and of the 70 experiments, figure 4.19 shows measured values of averaged room operative temperature, T_{room} , in the measurement period of each experiment, in terms of box plots. The dotted green line represent the $\pm 0.2^\circ\text{C}$ acceptable variation of the mean value while the red dotted line represent the $\pm 0.5^\circ\text{C}$ acceptable variation of any measured value in the averaging period for it to be assumed steady-state.

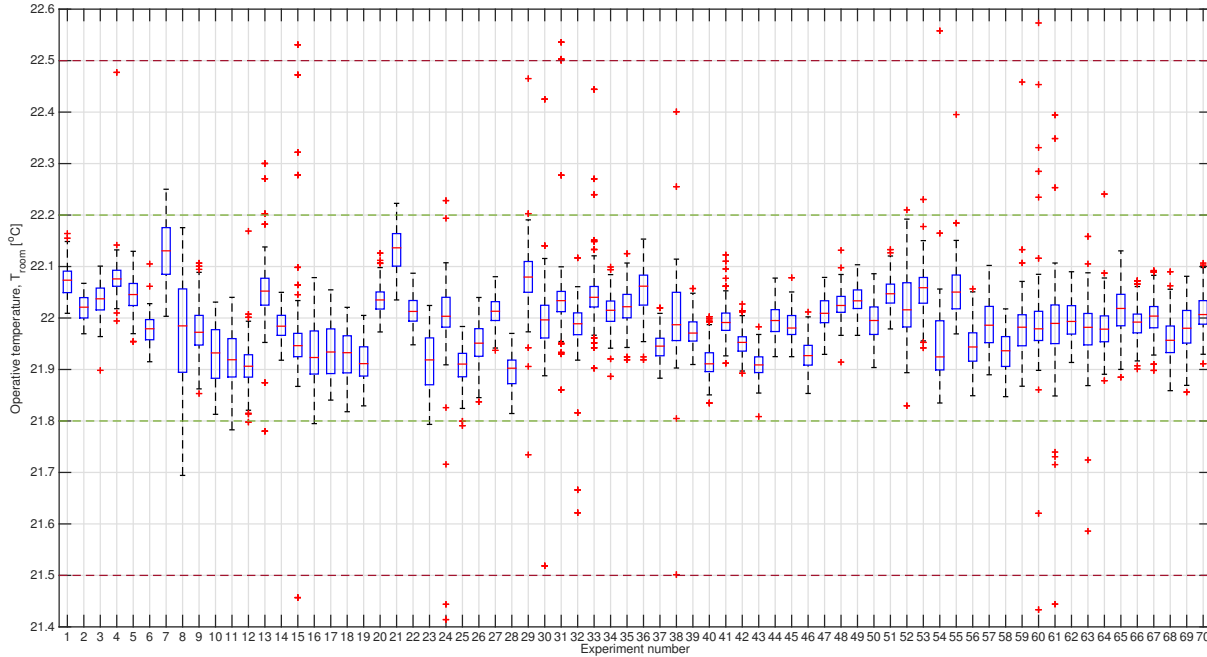


Figure 4.19: Statistical representation of measured room operative average temperatures. On each box, the central mark is the median (red), the edges of the box (blue) are the 25th and 75th percentiles and the whiskers extend to the most extreme data points not considered outliers ($\pm 3\sigma$). Outliers are plotted individually (red "+" marks).

For each of the 70 boxplots in figure 4.19, at least 50% of the measured room operative temperatures (blue boxes) are located within a variational span (temperature cycles) of $22.0^\circ\text{C} \pm 0.2^\circ\text{C}$. Only in a few experiments (experiment number 7, 8, 11, 16, 21 and 23) does either the upper or lower whisker extend beyond the $\pm 0.2^\circ\text{C}$ limit, which is seen as a neglectable error in the overall picture as the variance remains low. Measured outliers are represented by red "+" marks and are a result of measurement noise in the laboratory. As they in number only represent values more than three standard deviations from the mean (0.13th and 99.87th percentiles), they are deemed insignificant. As such, the experimental measurements are regarded valid in terms of room operative temperature steadiness and comparability, which is essential in securing the reliability and validity of any further analysis and conclusions.

4.5 Analysis of Thermal Comfort Limited Cooling Capacity

The determination of maximum cooling capacity of the DCV system while upholding thermal comfort is evaluated based on 5 successive combinations of temperature difference, ΔT , and air change rate, ACR , for each of the 3 diffuse ceiling layouts, A_{DC}^+ . Each of the 5 combinations represents the comfort limit situation in environmental category B before exceeding the discomfort criteria's changing the category to C. From table 4.5 these 5 combinations in category B as well as the 5 earliest detected combinations in category C is shown for each of the different ceiling layouts. Together the 10 points form an uncertainty band in which discomfort occurs for each ceiling layout.

Table 4.5: Experimental data used for defining comfort limited cooling capacity.

Experiment number	A_{DC}^+ [-]	ΔT [°C]	ACR [h ⁻¹]	Category [B or C]	DR [-]
5	1.00	10.94	15.72	B	<20 %
6	1.00	11.08	16.73	C	>20 %
13	1.00	16.00	10.69	B	<20 %
14	1.00	15.86	11.46	C	>20 %
21	1.00	19.92	9.99	B	<20 %
22	1.00	19.93	10.48	C	>20 %
28	1.00	24.73	8.67	B	<20 %
29	1.00	24.71	9.06	C	>20 %
35	1.00	28.99	7.56	B	<20 %
36	1.00	28.71	8.10	C	>20 %
68	0.50	12.23	14.32	B	<20 %
69	0.50	12.13	15.10	C	>20 %
67	0.50	17.00	10.53	B	<20 %
66	0.50	16.90	11.25	C	>20 %
64	0.50	20.86	9.86	B	<20 %
65	0.50	20.91	10.49	C	>20 %
63	0.50	25.36	6.56	B	<20 %
62	0.50	25.40	7.04	C	>20 %
61	0.50	29.96	5.80	B	<20 %
60	0.50	29.98	6.89	C	>20 %
39	0.18	10.82	11.01	B	<20 %
38	0.18	10.77	11.96	C	>20 %
40	0.18	15.45	9.09	B	<20 %
41	0.18	15.66	10.07	C	>20 %
46	0.18	20.45	9.99	B	<20 %
47	0.18	20.55	10.55	C	>20 %
50	0.18	24.71	10.43	B	<20 %
51	0.18	24.44	11.20	C	>20 %
54	0.18	28.72	9.75	B	<20 %
55	0.18	28.37	10.48	C	>20 %

Thermal Comfort at Maximum Cooling Capacity

As seen from table 4.5, the criterion that define critical local discomfort and thus the comfort limitation is draught rating, DR , in all cases. As mentioned previously at least 2 out of the 24 sensors in the occupied zone, equal to 5%, has to exceed the discomfort criterion's to define environmental category C, which is used as the limiting parameter.

From figure 4.20 draught rating in the 10 delimiting cases within each of the 3 experimental series is given as the percentage of DR readings that fall within the intervals $[DR < 10\%]$, $[10\% \leq DR < 20\%]$, $[20\% \leq DR < 30\%]$ or $[30\% \leq DR]$, respectively. The sum of readings is 100%. For the experimental conditions to be within environmental category B, maximum 5% of DR readings must fall within the intervals $[20\% \leq DR < 30\%]$ (blue) and $[30\% \leq DR]$ (red).

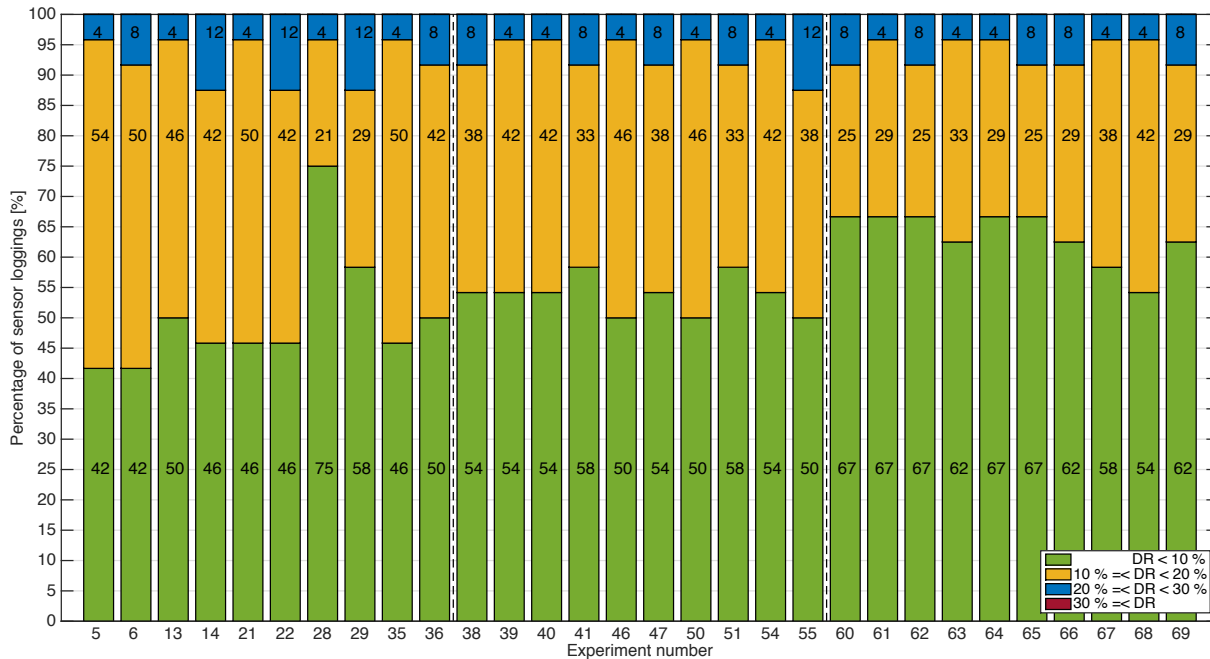


Figure 4.20: Draught rating readings in occupied zone in delimiting cases. Experiment number 5 to 26 represent cases with 100% diffuse ceiling, 38 to 55 represent cases with 50% diffuse ceiling and 60 to 69 cases with 18% diffuse ceiling.

In neither of the 30 delimiting experiments does local discomfort occur due to vertical air temperature differences, warm or cold floors or radiant asymmetry. In general, these three parameters are within the limits of environmental category A, cf. ISO-7730 (2006) (see table 1.1 on page 10) for all 70 experiments.

The developed air temperature gradients inside the test room is shown in figure 4.21 for the three different ceiling layouts. Experiment number 22, 65 and 47 has been chosen for comparison as they represent cases with the same cooling capacity ($\Delta T \approx 20^\circ\text{C}$ and $ACR \approx 10.5\text{h}^{-1}$, see table 4.5 and figure 4.22). All three experiments represent cases where the environmental category has changed from B to C due to an exceeding of the draught rating criterion.

In all three scenarios the vertical air temperature gradient inside the occupied zone is smaller than 2°C without much variation. This indicates a high degree of mixing inside the test room. However, large fluctuations are seen in the uppermost measurement point 2.3 m above floor level,

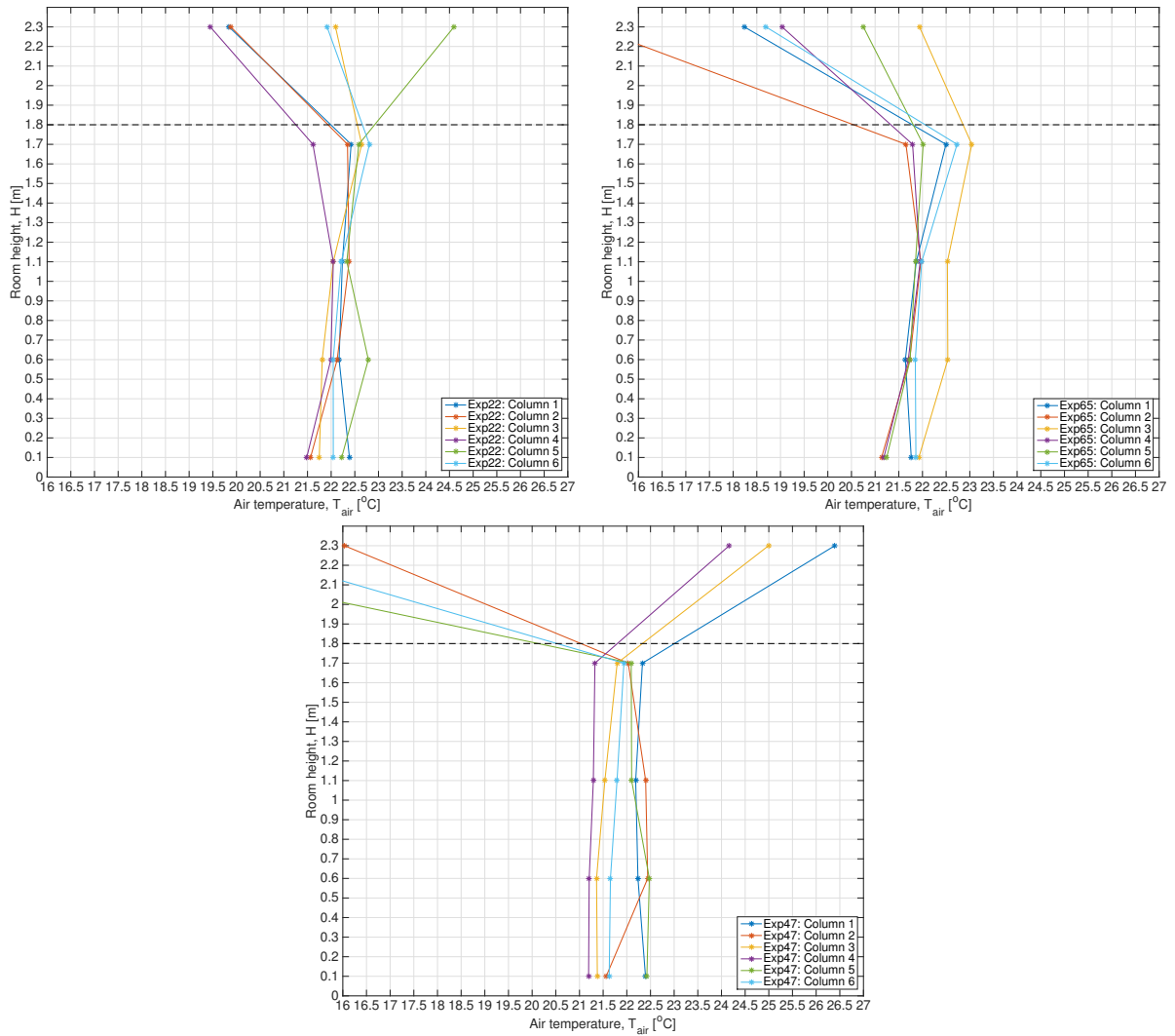


Figure 4.21: Vertical air temperature gradients for six columns in three different ceiling layout configurations (first plot = Exp. nbr. 22 [100 %], second plot = Exp. nbr. 65 [50 %] and third plot = Exp. nbr. 47 [18 %]). Dotted black line mark the delimitation of the occupied zone. Column locations are given in figure 4.18.

which is ascribed to the ceiling layout and location of columns; some are located underneath diffuse panels and others under sealed panels. This is clear when looking at the third figure showing the 18% case, where measurement column 1, 3 and 4 are placed underneath sealed panels cf. figure 4.18. For these three columns the 2.3m measurement points are clearly higher than the three others (column 2,5 and 6), which are directly exposed to the cold inlet air. In the 100% case (first figure) the differences are much smaller, which is ascribed to the less limited convection resulting in a better mixing underneath the suspended ceiling. However, column 6 differs from the rest by a higher temperature, which again could be a consequence of its location near the radiators where high-momentum thermal plumes are suspected to govern the flow regime.

Design Chart

Below, the analysed results of the comfort limited cooling capacity at different ceiling layouts is depicted in figure 4.22. The *Design Chart* express the acceptable correlation between ventilation rate and temperature difference between facade inlet and room outlet. As expected, the correlations show a decreasing tendency towards increasing ventilation rate - at least in the two cases with 100 % and 50 % diffuse ceiling area. The limits are close to a linear correlation representing a constant load, $\Delta T \cdot q_v = const.$, which means that draught in the occupied zone is independent of the ventilation rate. For the 18 % case, however, the tendency seems to be almost vertical meaning that discomfort is governed by the ventilation rate rather than the facade inlet temperature, T_{facade} , which is tested down to around -7°C (ΔT approximately 29°C).

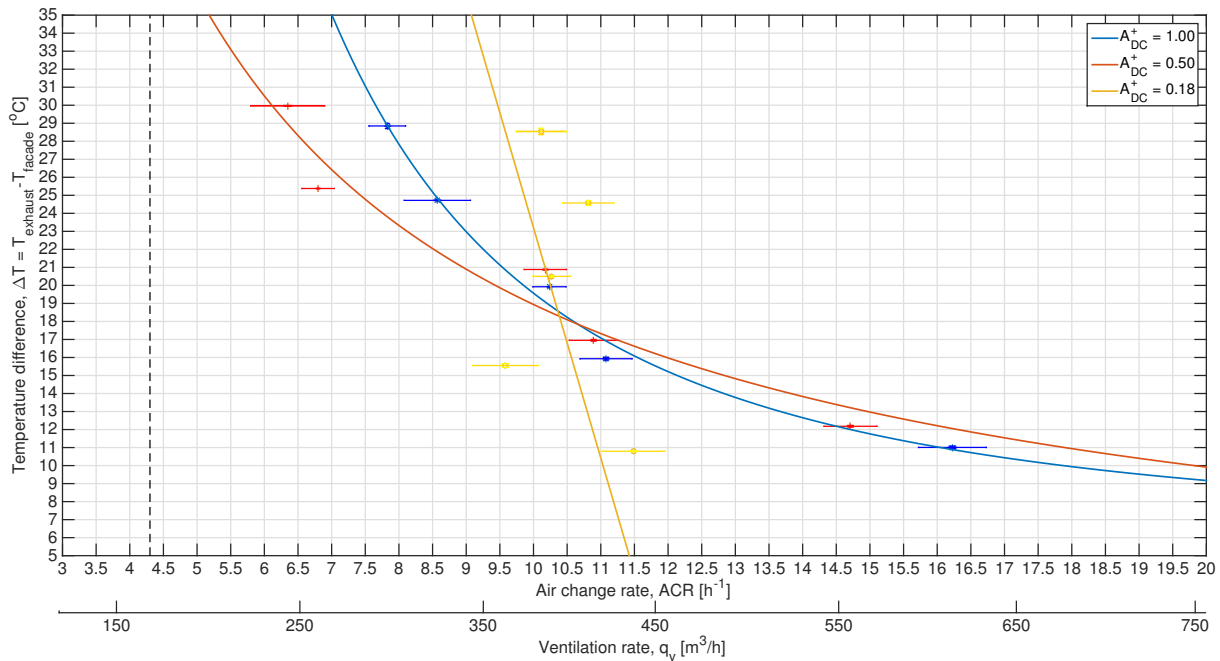


Figure 4.22: Design Chart for 100%, 50% and 18% diffuse ceiling area, respectively, when maximum 5% of the occupied zone is allowed to exceed a draught rating of 20%.

Maximum cooling capacity of the DCV system, Φ_{cool} , may be expressed as the heat energy removed by ventilation as done in equation 1.7 on page 12 and illustrated in figures 4.23 and 4.24 in terms of capacity per floor area and capacity per diffuse ceiling area, respectively.

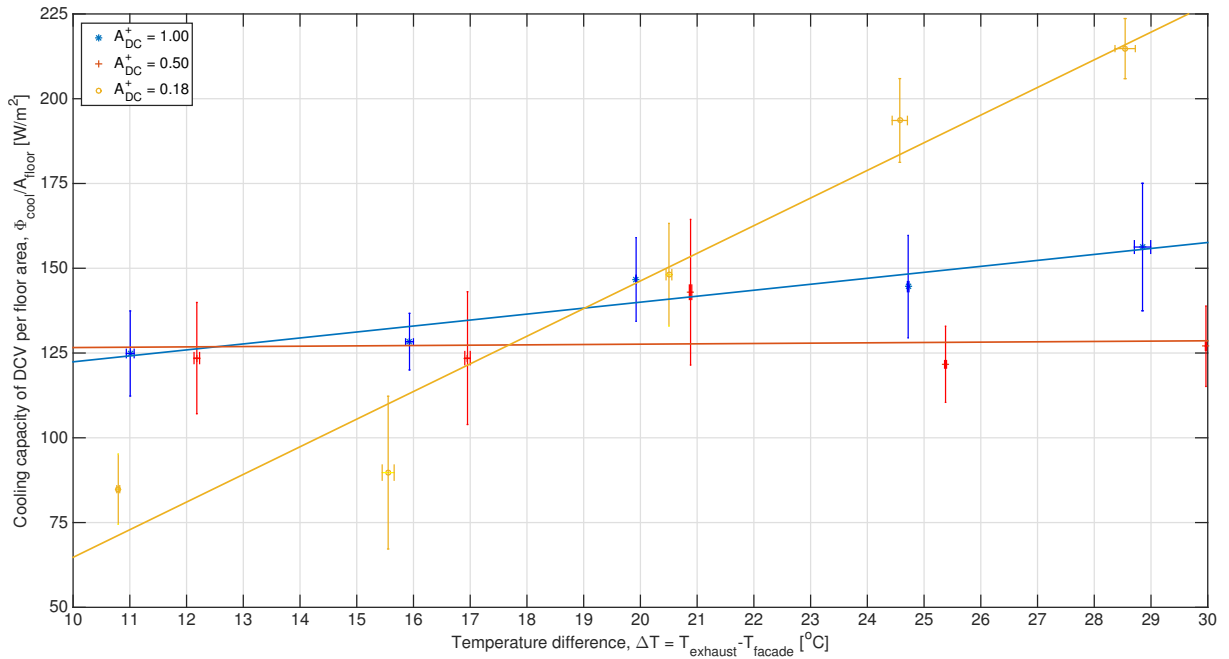


Figure 4.23: Cooling Capacity of DCV system per floor area for different ceiling layouts as function of temperature difference.

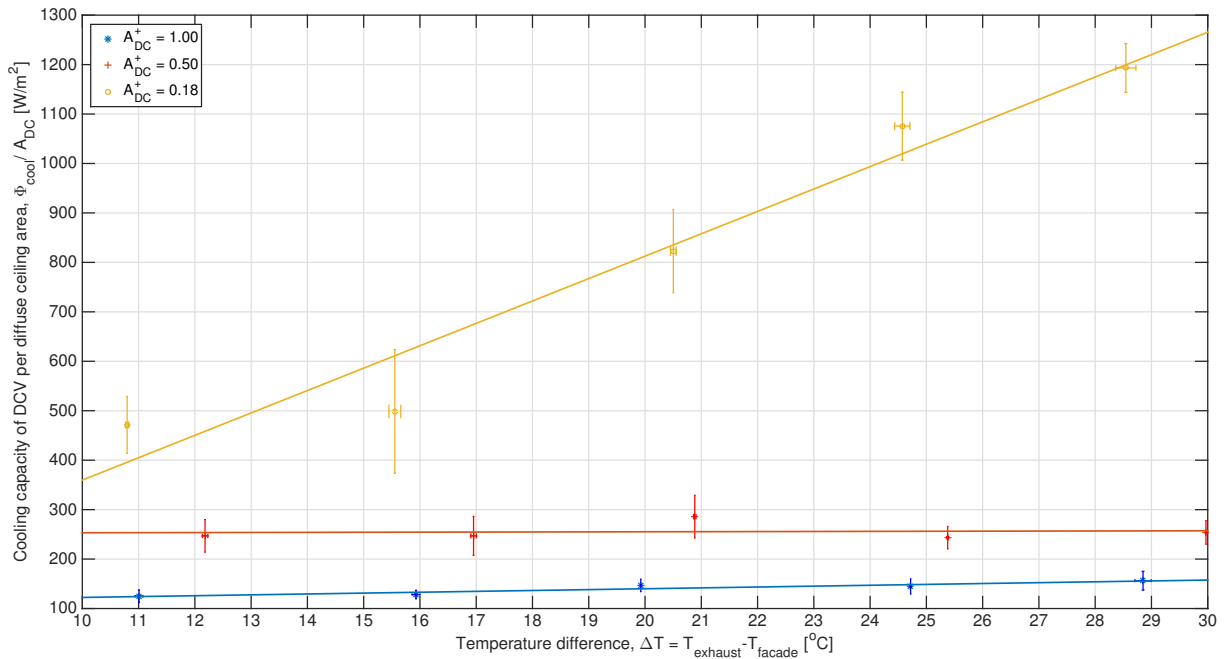


Figure 4.24: Cooling Capacity of DCV system per diffuse ceiling area for different ceiling layouts as function of temperature difference.

As seen from the figures above high cooling capacities are achievable with a DCV system. The measurements does not show unambiguous results, however, for the two cases with 100% and 50% diffuse ceiling area, capacities per floor area, Φ_{cool}/A_{floor} , of around 130-170 W/m² seems attainable in the investigated temperature range cf. figure 4.23. For the 18% case even higher

capacities are observed at high temperature differences. The different results may be partly due to the ceiling layout of the three scenarios, or in fact, the location of the heat sources underneath the ceiling panels, which gets more centrally located underneath the diffuse panels as the diffuse panel area, A_{DC}^+ , is decreased towards 18 % where the thermal manikins are located right underneath the four diffuse panels (see figure 4.18). Hereby, the hot uprising plume and the cold inlet air is directly mixed and a good cooling efficiency is attained. The picture would maybe look different had the heat sources been placed differently inside the test room. This conclusion is supported by looking at figure 4.24. Here it is seen how the capacity per diffuse ceiling area, Φ_{cool}/A_{DC} , remains constant for the two cases with 100 % and 50 % diffuse ceiling area indicating that an increased cooling power of the inlet air does not effeciently integrate with the room air excess heat. Instead, the cold inlet air is forced around the high-momentum heat plumes and pushed down in low-momentum areas. As the diffuse ceiling area is lowered, so is the seperation of cold and warm air streams and a higher cooling efficiency is attained.

4.6 Analysis of Air Permeability and Plenum Effects

The following section presents the measurement results from the three series of experiments with different degrees of diffuse ceiling in terms of the emerged pressure drop across the diffuse ceiling and developed airflow patterns inside the test room.

Air pressure difference across the ceiling, $\Delta p_{ceiling}$, is measured in three distances from the facade intake damper; 800 mm, 2400 mm and 4000 mm as shown in figure 4.13 on page 84.

Permeability of "Trolldtekt" Panels

The applied Trolldtekt ceiling panels ("ultra-fine" structured) is described in Section 4.2 on page 70. The developed pressure loss across the panels at varying airflow rates has been tested in a pressure box setup (see figure 4.9) and also by others.

From figure 4.25 correlated measurements of developed pressure difference, Δp , across a single panel of area A at vaying airflow rates, q , are shown. Values from Zhang, C. and Yu (2014), Trolldtekt (N.A.) and the authers own measurements (Kristensen & Jensen, 2015) are plotted from which a 2nd order polynomial curve fitted correlation has been derived (see equation 4.10). If disregarding Trolldstekt's own data points, a $R^2 = 0.999$ value is achieved.

$$\Delta p_{trolldtekt} = 1.95 \cdot 10^{-5} \cdot \left(\frac{q}{A}\right)^2 + 1.58 \cdot 10^{-2} \cdot \left(\frac{q}{A}\right) + 6.12 \cdot 10^{-3} \quad (4.10)$$

where:

$\Delta p_{trolldtekt}$ = pressure difference across Trolldtekt panel [Pa]

q = airflow rate [m^3/s]

A = panel area [m^2]

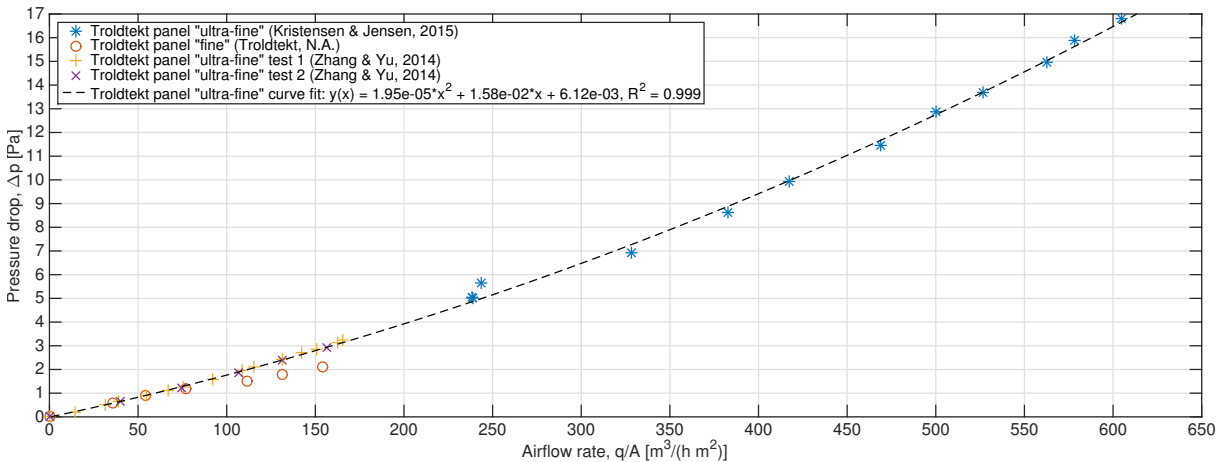


Figure 4.25: Air permeability test of "ultra-fine" structured Trolldtekt ceiling panels.

Permeability of Diffuse Ceiling Setup

As the suspended ceiling construction consists of many panels assembled on a mounting system, crack-flow (short circuit through jointings) is inevitable. The assembling principle may be seen from figure 4.4 on page 72. Due to this crack-flow the air permeability of the suspended ceiling should be higher than that of a single diffuse Trolldtekt panel.

From figure 4.26 the developed pressure difference across the suspended ceiling for the three different cases is seen (100 %, 50 % and 18 % diffuse ceiling panels in suspended ceiling). The pressure drop is plotted as function of the forced airflow through the diffuse panels alone, A_{DC} . Moreover, the Trolldtekt permeability relationship (equation 4.10) is given to render visible the influence of crack-flows (crack-flow is identified as the difference between measured values and equation 4.10). E.g. at a pressure difference of 1.5 Pa the 18 % diffuse ceiling will supply $120 \text{ m}^3/(\text{hm}^2)$ diffuse ceiling with only $85 \text{ m}^3/(\text{hm}^2)$ though the panels. As such, $35 \text{ m}^3/(\text{hm}^2)$ or approximately 30 % may be categorised as crack-flow.

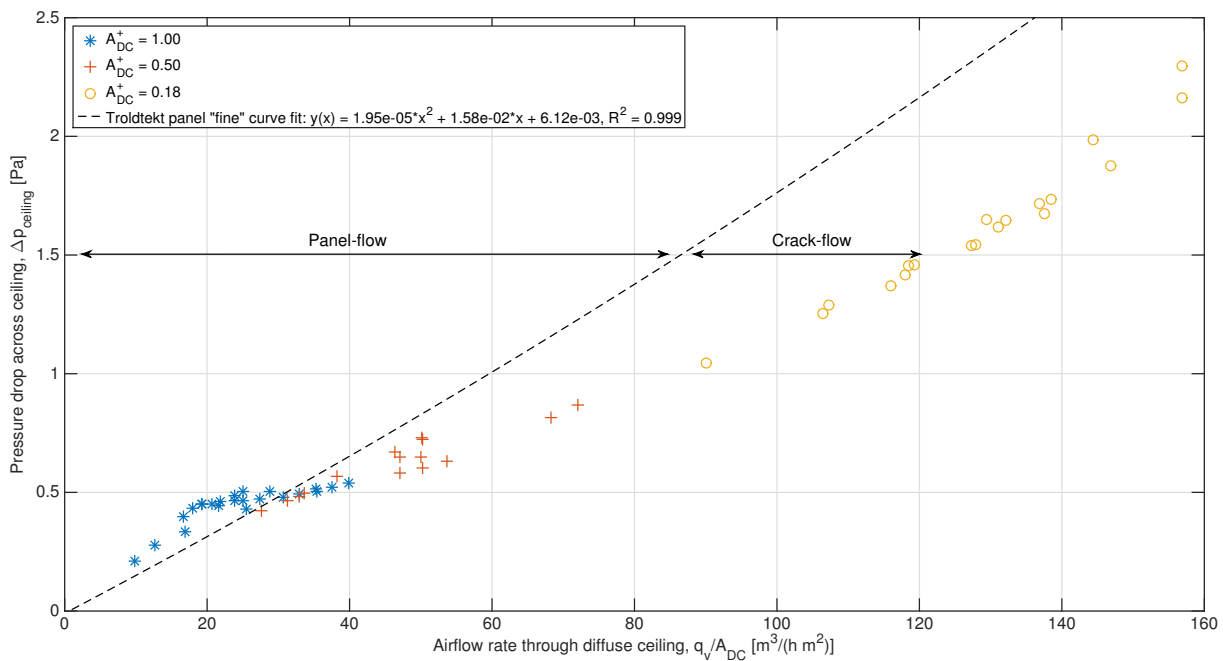


Figure 4.26: Air permeability for different degrees of diffuse ceiling area. Permeability is divided into panel-flow and crack-flow.

The pressure results are, however, questionable as high measurement uncertainty are found in measuring pressure difference in the setup (pressure tubes run through different climate zones and large temperature differences from one experiment to another influence the pressure reading).

Plenum Pressure Chamber and Preheating Effects

In figure 4.27 measured pressure drop across the suspended ceiling is given as function of distance from the facade intake with vertical errorbars indicating the standard deviation of contained values in all the measurements.

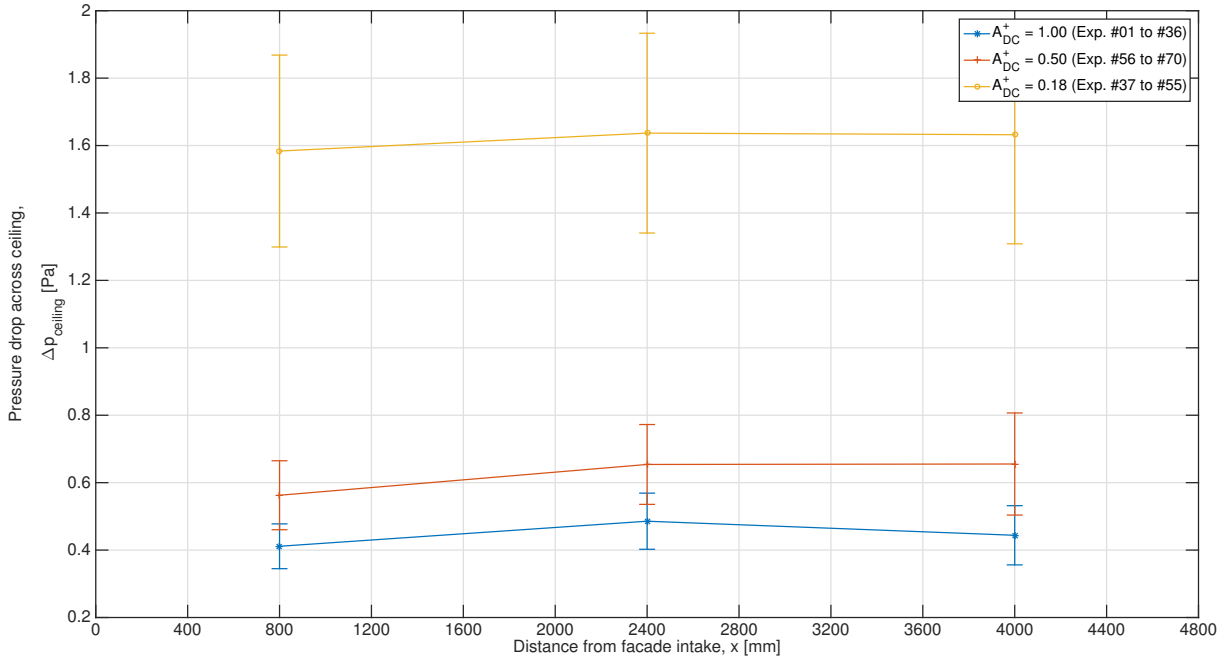


Figure 4.27: Pressure drop as function of distance from facade intake.

From figure 4.27 several conclusion should be drawn.

Pressure drop show a strong negative and significant correlation with diffuse ceiling area with the smallest diffuser area (18 % case) causing the highest pressure differences, as expected (Appendix B.5);

$$\rho_s (A_{DC}, \Delta p_{ceiling}) = -0.88$$

Within the same diffuse ceiling layouts, no significant pressure variation across the plenum volume is present in the three measurement points, indicating a developed pressure chamber effect.

Pressure difference is strongly correlated with Reynolds number for the 100 % case (Appendix B.5). No significant correlation is found for the 50 % and 18 % cases.

$$\rho_s (Re, \Delta p_{ceiling}) = +0.74 \text{ (100 \% diffuse ceiling)}$$

From figure 4.28 the plenum air temperature profile is plotted in both absolute values, T_{plenum} , and normalized values, T_{plenum}^* , according to equation 1.11 on page 14. It shows averaged air temperatures in four distances from the facade.

4. Influence of Supply Opening Area

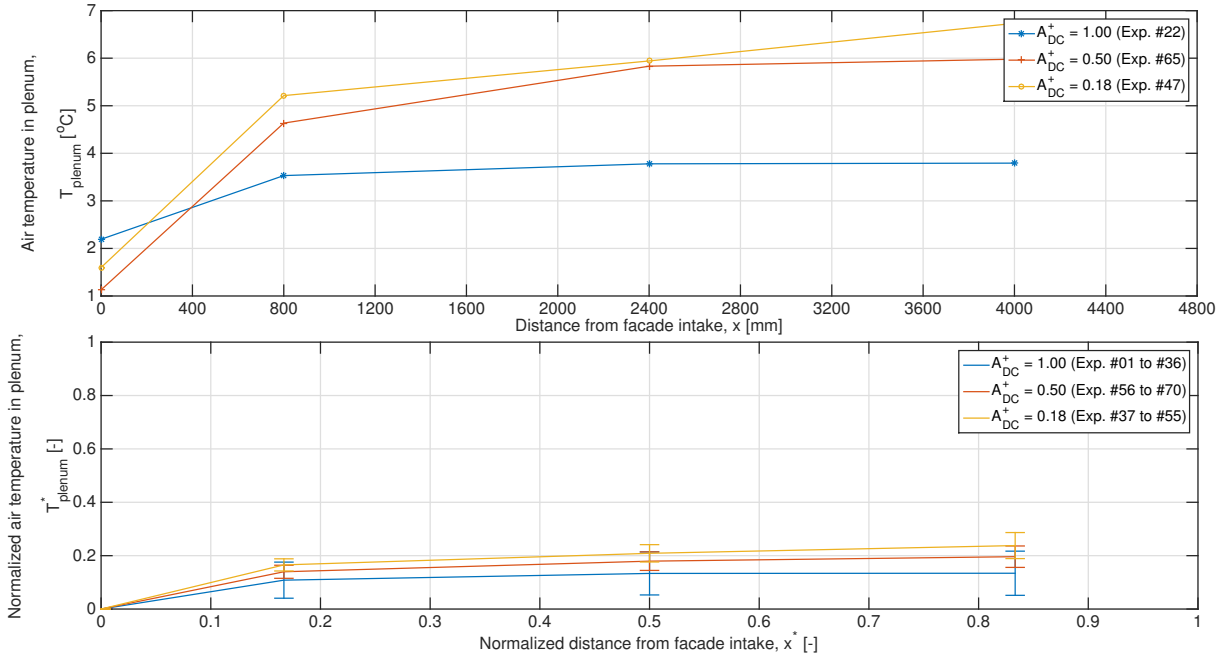


Figure 4.28: Top: Absolute air temperature profile in plenum for three selected experiments. Bottom: Normalized air temperature profile in plenum for the different ceiling layouts comprising all executed experiments.

The following conclusion may be drawn from the temperature profiles.

Diffuse ceiling layout (supply opening area) does not influence the profile tendency; plenum air temperature is unilaterally increased from a minimum at the facade intake until it reaches maximum at the farthest end at 4000 mm from the facade in all three cases.

70-80 % of the plenum heat-up takes place within the first 800 mm corresponding to around 15 % of plenum length.

In none of the investigated cases did plenum air temperature increase beyond 30 % of the total heat-up from initial intake at the facade to final exhaust temperature.

The supply opening area does influence the absolute plenum temperature even when the amount of room heating is approximately the same (maximum 10 % variation in supplied radiator heat, $\Phi_{radiator}$, from 1580 W to 1770 W). In the 100 % diffuse ceiling case plenum air is heated by around 1.6 °C while the 50 % and 18 % cases trigger a heat-up of 4.8 °C and 5.1 °C, respectively. This picture is confirmed in figure 4.29 showing a moderate negative correlation between normalized plenum mean air temperature, $T_{plenum,avg}^*$, and diffuse ceiling area. The plenum temperature has been normalized based on equation 1.11 on page 14 thus showing the amount of heating that the intake temperature at the facade, T_{facade} , undergoes in the plenum in relation to the final exhaust temperature, $T_{exhasut}$. Please note that the normalized temperature is calculated based on an average of the entire plenum air, measured by 9 thermocouples. This also counts for the facade and exhaust temperatures with 3 and 2 thermocouples respectively.

$$\rho_s \left(A, T_{plenum}^* \right) = -0.56$$

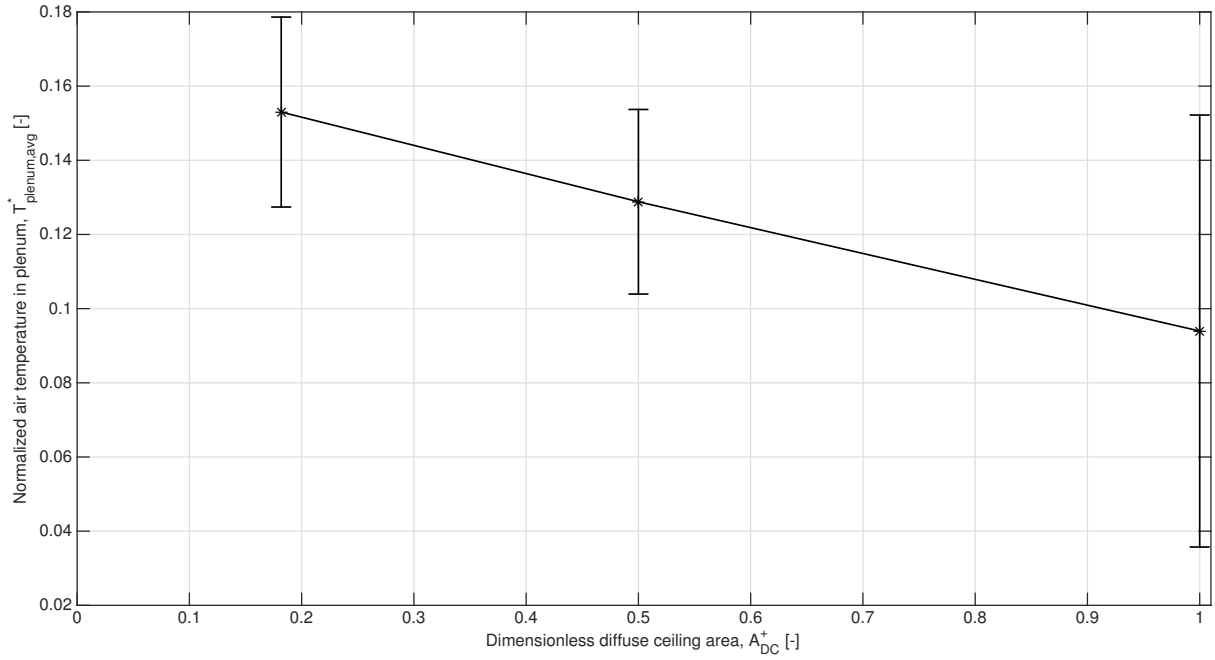


Figure 4.29: Normalized plenum air temperature as function of normalized diffuse ceiling area.

Errorbars in figure 4.29 show the standard deviation around the mean value of plenum temperature in each diffuse ceiling case.

Plenum air temperature also show a moderate to strong correlation with Reynolds number, depending on the supply opening area in question (Appendix B.5);

$$\rho_s \left(Re, T_{plenum}^* \right) = -0.73 \text{ (average of 18 \% , 50 \% and 100 \%)}$$

A strong, almost perfect, correlation with Archimedes number is present in the 100 % diffuse ceiling case alone;

$$\rho_s \left(Ar, T_{plenum}^* \right) = +0.91 \text{ (100 \% diffuse ceiling)}$$

From figure 4.30 the preheating capabilities of the three ceiling layouts are presented for all 70 experiments as function of Reynolds number (see equation 1.15 on page 15) in the upper scatter and as function of Archimedes number (see equation 1.16 on page 16) in the lower scatter.

4. Influence of Supply Opening Area

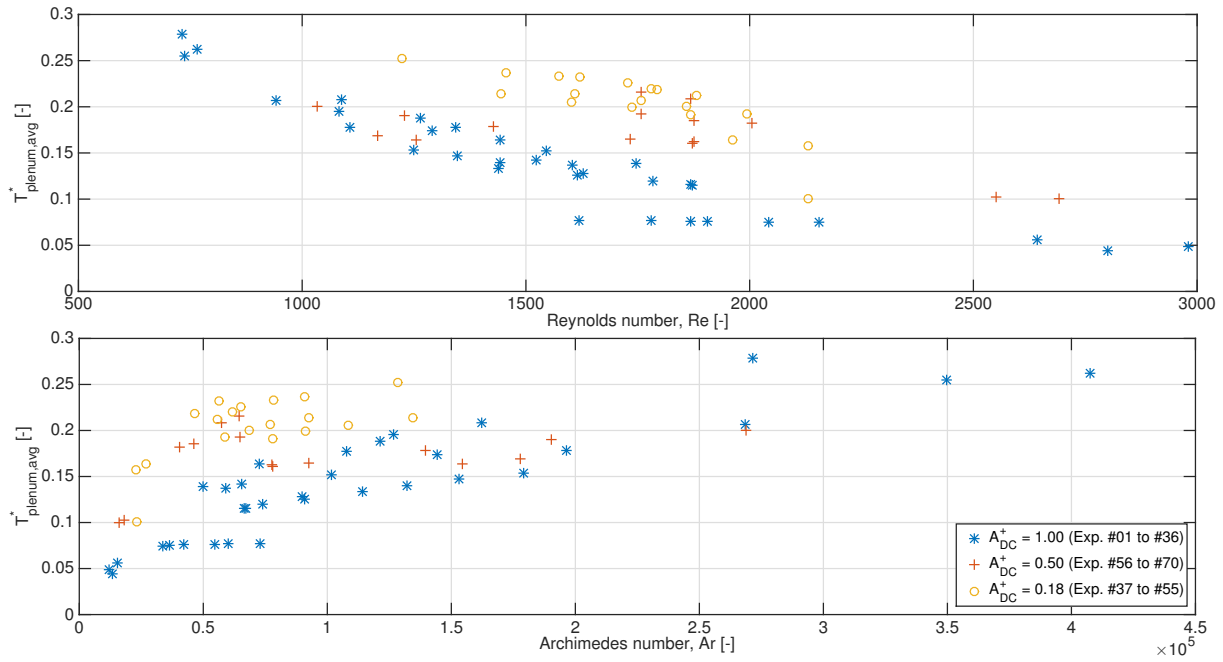


Figure 4.30: Normalized plenum mean air temperature as function of Reynolds number and Archimedes number.

Figure 4.30 show a negative correlation in terms of the preheating that takes place within the plenum with increasing Reynolds number. Each diffuse ceiling layout give rise to different correlations with the 100% diffuse ceiling case resulting in an almost perfect correlation that may be expressed by a power regression.

4.7 Analysis of Airflow Elements and Patterns

The three different ceiling layouts are compared in terms of the developed airflow patterns. For this the heat release and dimensionless numbers (Re and Ar) are used in characterising the flow field in the following subsections.

Airflow Elements

The heat sources (radiators and manikins) generate buoyancy driven flow due to natural convection around their bodies interfering with the forced convection driven inlet and outlet airflow of the ventilation system. From table 4.6 the size of these convection flows are estimated illustrating the strength ratio between the forced (DCV system) and natural (heat sources) convection flows. Airflow in terms of cold downdraft from the windows is neglected.

Table 4.6: Momentum flows generated by different sources.

Source		Momentum flow I_z [mN]
Heat sources	Radiator	107.9
	Manikin	128.0
	Combined (sum)	235.9
DCV	18 %, 5 h ⁻¹	1.1
	18 %, 10 h ⁻¹	4.6
	18 %, 15 h ⁻¹	10.3
	50 %, 5 h ⁻¹	0.4
	50 %, 10 h ⁻¹	1.7
	50 %, 15 h ⁻¹	3.8
	100 %, 5 h ⁻¹	0.2
	100 %, 10 h ⁻¹	0.8
	100 %, 15 h ⁻¹	1.9

As seen from table 4.6, the heat sources generate buoyancy driven momentum that is approximately 23 times higher than the inertia driven flow supplied by even the most "powerful" DCV configuration with 18% diffuse ceiling at 15 h⁻¹. This clearly shows the strength ratio between the flow dominating forces. Calculation of the different momentum forces is outlined below.

Inlet driven flow: Momentum flow supplied by the DCV system is defined as the time rate of change of the downward momentum embedded in the inlet jet through the diffuse ceiling (z-direction) cf. equation 4.11 and illustrated by figure 4.31. Body forces are neglected.

4. Influence of Supply Opening Area

$$I_0 = \frac{dP_0}{dt} = \frac{d(m_0 \cdot u_0)}{dt} \approx q_v \cdot \rho_0 \cdot \frac{q_v}{A_0} \quad (4.11)$$

where:

- I_0 = supply momentum flow of diffuser (momentum flow of DCV, I_{DCV}) [N]
- P_0 = supply momentum of diffuser (momentum of DCV, P_{DCV}) [Ns]
- t = time [s]
- m_0 = mass of supplied air [kg]
- u_0 = supply air speed (air speed through diffuse ceiling, u_{DC}) [m/s]
- q_v = ventilation rate [m^3/s]
- ρ_0 = supply air density ($\approx 1.2 \text{ kg/m}^3$) [kg/m^3]
- A_0 = area of diffuser (diffuse ceiling area, A_{DC}) [m^2]

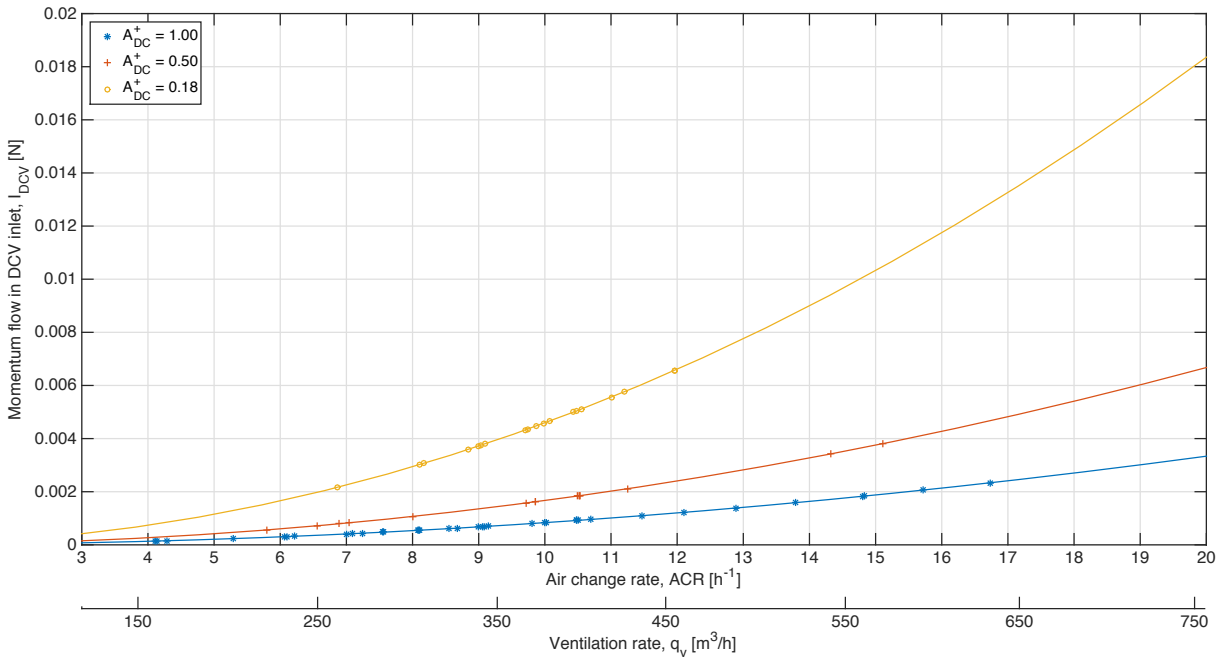


Figure 4.31: Embedded momentum flow in DCV inlets as function of ventilation rate.

Heat source driven flow (manikins): The thermal plumes and contained momentum flow generated by the used manikins, presented in table 4.6, has been experimentally investigated and documented in Appendix B.1.

Heat source driven flow (radiators): The generated upward momentum flow (z -direction) of the radiators may be calculated using equation 4.11 where the upward natural convected airflow may be calculated using the empirical correlation in equation 4.12 (Stampe, O. B. et al., 2006) by assuming the radiators to be linear heat sources.

$$q_z \approx 0.014 \cdot \left(\frac{\Phi_{rad}}{x_{rad}} \right)^{0.33} \cdot (z + z_p) \cdot x_{rad} \cdot C \quad (4.12)$$

where:

q_z	= upward airflow generated by radiator in height z [m^3/s]
Φ_{rad}	= convective heat release from radiator [W]
z	= height [m]
z_p	= distance from heating wire to radiator top opening [m]
x_{rad}	= width of radiator [m]
C	= reduction coefficient for presence of Coanda effect (≈ 0.5) [-]

Exhaust driven flow: The flow close to a return opening is a potential flow, acting like a *sink*. The velocity, u_x , generated by the exhaust flow, $q_{exhaust}$, at a distance, $x_{exhaust}$, from the exhaust opening may be modelled as the flowrate pulled through a spherical surface at a given distance, see equation 4.13 (Nielsen, P. V., 1995).

$$u_x = \frac{q_{exhaust}}{A_{exhaust} + 4\pi x_{exhaust}^2} \quad (4.13)$$

where:

u_x	= air speed at distance x from exhaust opening [m/s]
$q_{exhaust}$	= ventilation rate, q_v [m^3/s]
$A_{exhaust}$	= area of exhaust opening [m^2]
x	= distance from exhaust opening [m]

Based on this correlation exhaust driven velocity, u_x , is in figure 4.32 plotted as function of distance, $x_{exhaust}$, for four different flowrates representing the conducted experiments. It is immediately clear how the exhaust hood influences the room airflows in only a small radius from the opening. At a distance of 25 cm from the exhaust opening, velocities have fallen below 0.2 m/s for airflow rates up to 600 m^3/h and below 0.05 m/s at a distance of 50 cm.

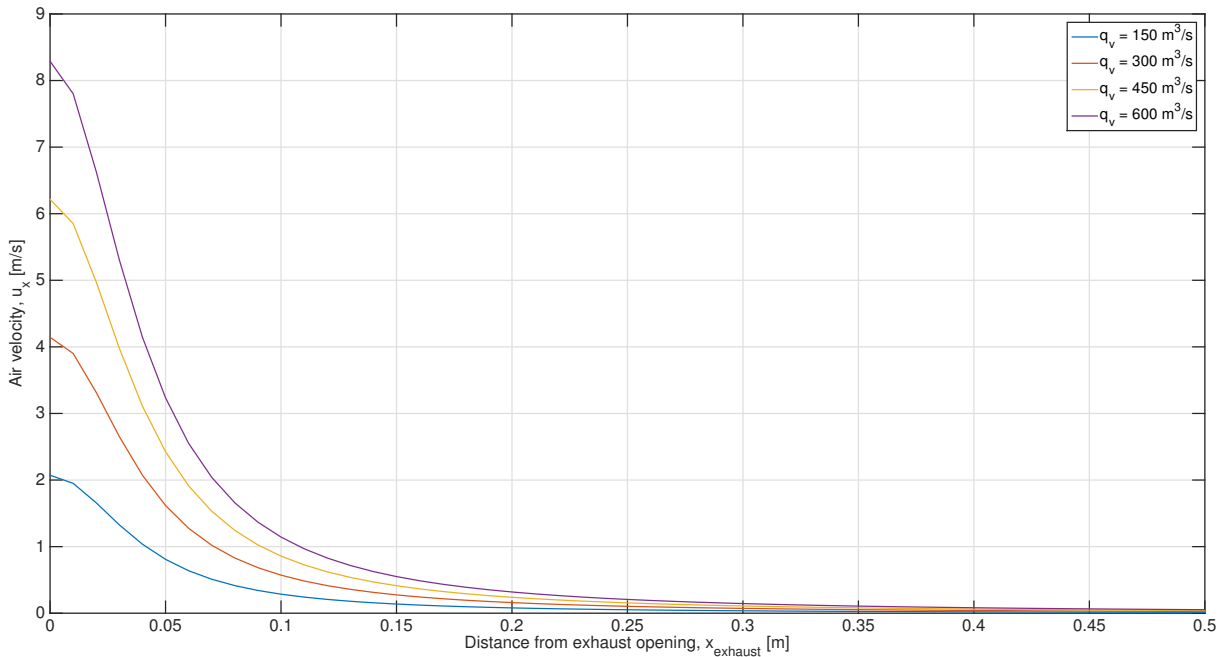


Figure 4.32: Exhaust driven velocity as function of distance for four different airflow rates.

Location of Maximum Air Speeds in Occupied Zone

In figure 4.18 on page 88 the location of measurement columns are shown. On the assumption that maximum air velocity, u_{max} , arise in the chosen measurement locations, the emerged flow field is in the following analysed.

From figure 4.33 and 4.34 the observed location of the highest measured air speeds in the occupied zone, $u_{max,OZ}$, is seen. The locations are plotted together with heat sources and the exhaust hood to underline their influence. From the plane-sectional view (figure 4.33) it is worth noticing how maximum air speeds arise far from any heat sources, as expected. However, as mass balance require the entire airflow to pass the exhaust opening, it is expected to observe the highest values near the exhaust hood, which is also the case.

Looking at the cross-sectional view it is confirmed that airflows are more dispersed in the 100% and 50% diffuse ceiling cases as maximum air speeds arise down in the occupied zone and even at floor level as well as up above the occupied zone, while they only arise near the ceiling in the 18% case. Not in a single case does maximum air speeds occur in between the manikins or even close to them. This observation supports the hypothesis that heat sources dominate the airflow patterns in rooms with DCV.

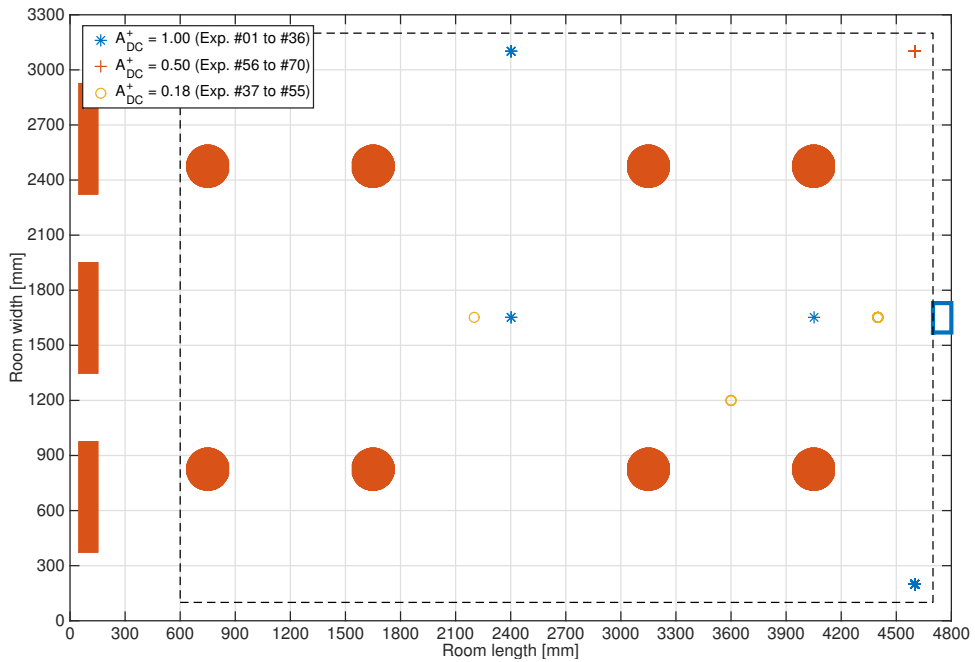


Figure 4.33: Plane-sectional view (Length vs. Width) of test room showing location of maximum air speeds. Red objects illustrate heat sources (radiators and manikins). Blue object illustrate the exhaust hood. Black dotted line represent the occupied zone.

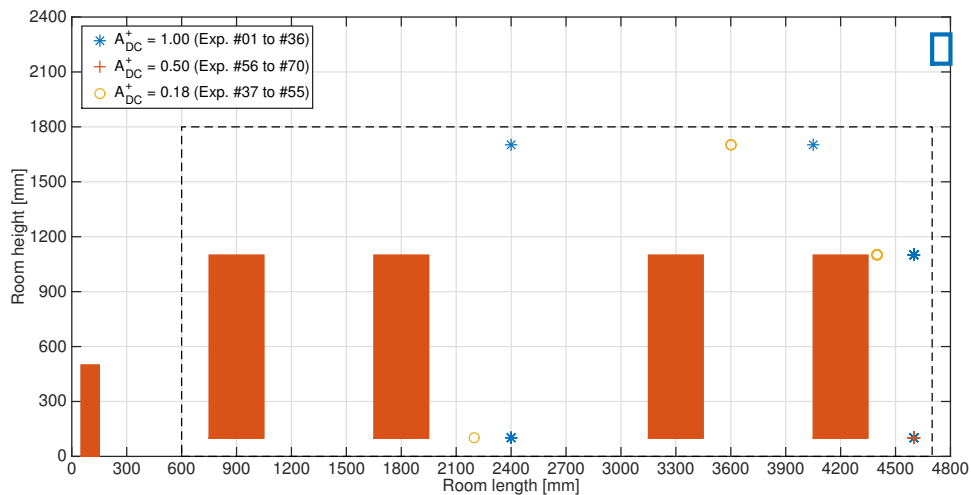


Figure 4.34: Cross-sectional view (Length vs. Height) of test room showing location of maximum air speeds. Red objects illustrate heat sources (radiators and manikins). Blue object illustrate the exhaust hood. Black dotted line represent the occupied zone.

Air Speed Distribution

In figure 4.35 on page 111 absolute air speed, u_{air} , and normalized air speed, u_{air}^* (equation 1.8 on page 13), for experiment number 22, 65 and 47 is shown. These three cases share the same cooling capacity ($\Delta T \approx 20^\circ\text{C}$ and $ACR \approx 10.5 \text{ h}^{-1}$, see table 4.2, 4.3 and 4.4 and figure 4.22).

From figure 4.35 it should be observed that while the absolute air speed gradient does not change noticeably with decreasing diffuser area, the inlet normalized values does. In the 100 % case (first row of plots) air speeds increase up to 40 times the ceiling inlet speed, while in the 18 % case (third row of plots) they only increase by a factor 5 in the occupied zone. This clearly proves how the diffuse ceiling area does not influence airflows and thus thermal comfort in the occupied zone.

In all three ceiling cases it is column 4, which measures the highest air speeds. In case of 100 % and 50 % diffuse ceiling, column 4 is located in the lower right corner of the room (see figure 4.18), while it is located right in front of the exhaust in case of 18 % diffuse ceiling.

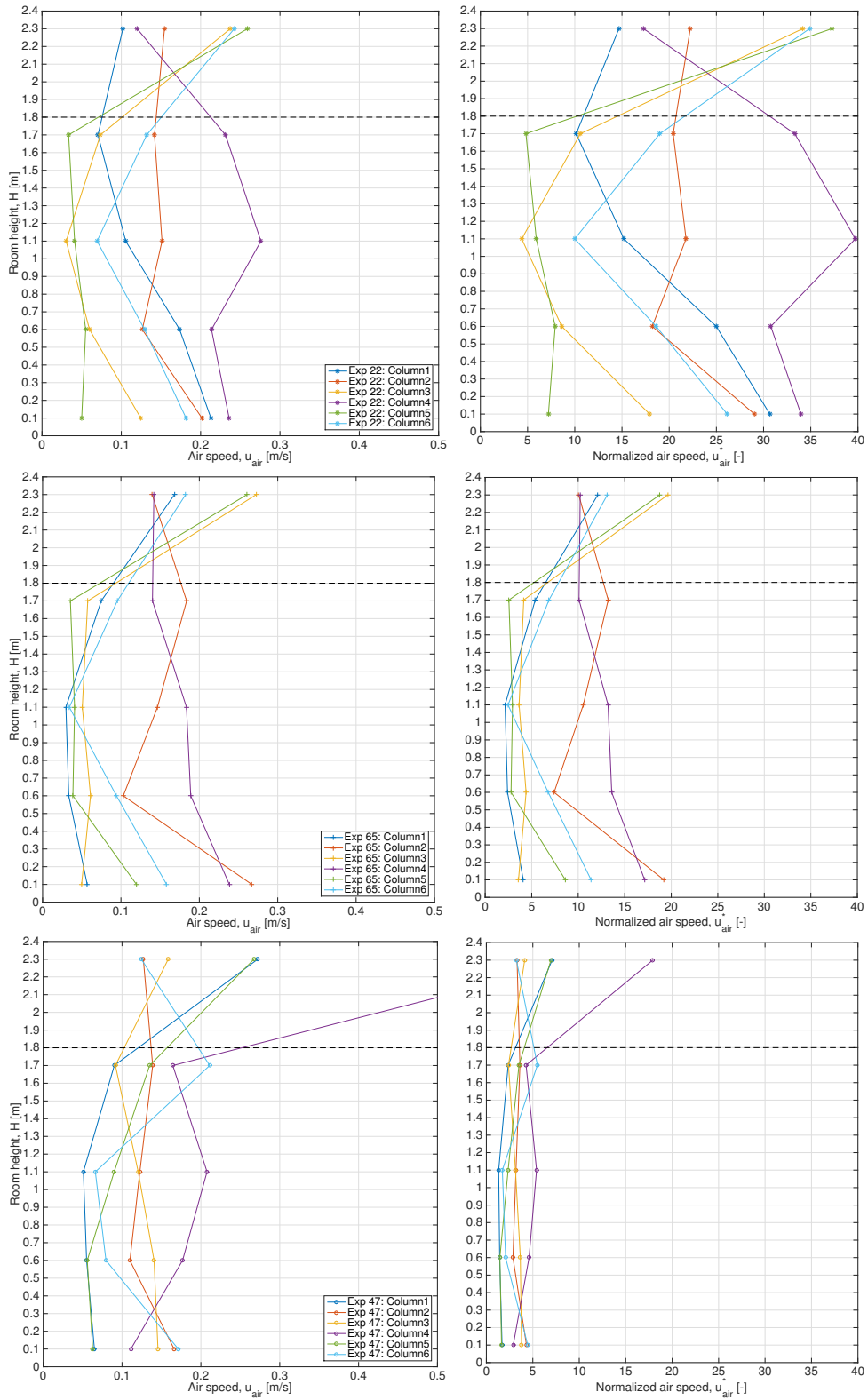


Figure 4.35: Absolute and normalized air speed gradients for six columns in three different ceiling layout configurations (first row = Exp. 22 [100 %], second row = Exp. 65 [50 %] and third row = Exp. 47 [18 %]). Dotted black line mark the delimitation of the occupied zone. Column locations are given in figure 4.18.

Supply Opening Area Dependence

To test the hypothesis that the supply opening area has a significant influence on room airflow patterns, a correlation of the important flow parameters is conducted. Figure 4.36 show a graphical representation of the data with the y-axis being comprised by normalized room maximum air speeds, u_{max}^* , (normalized for the ventilation rate, q_v , hereby making it possible to compare measured air speeds disregarding the present airflow rate), and the x-axis representing the dimensionless supply opening area, A_{DC}^+ . Data is plotted in five series - one for each temperature difference, ΔT . Vertical errorbars indicate the standard deviation around the mean of observed values. As such, the errorbars indicate variation that is not represented in the figure and thus not measured in the experiments.

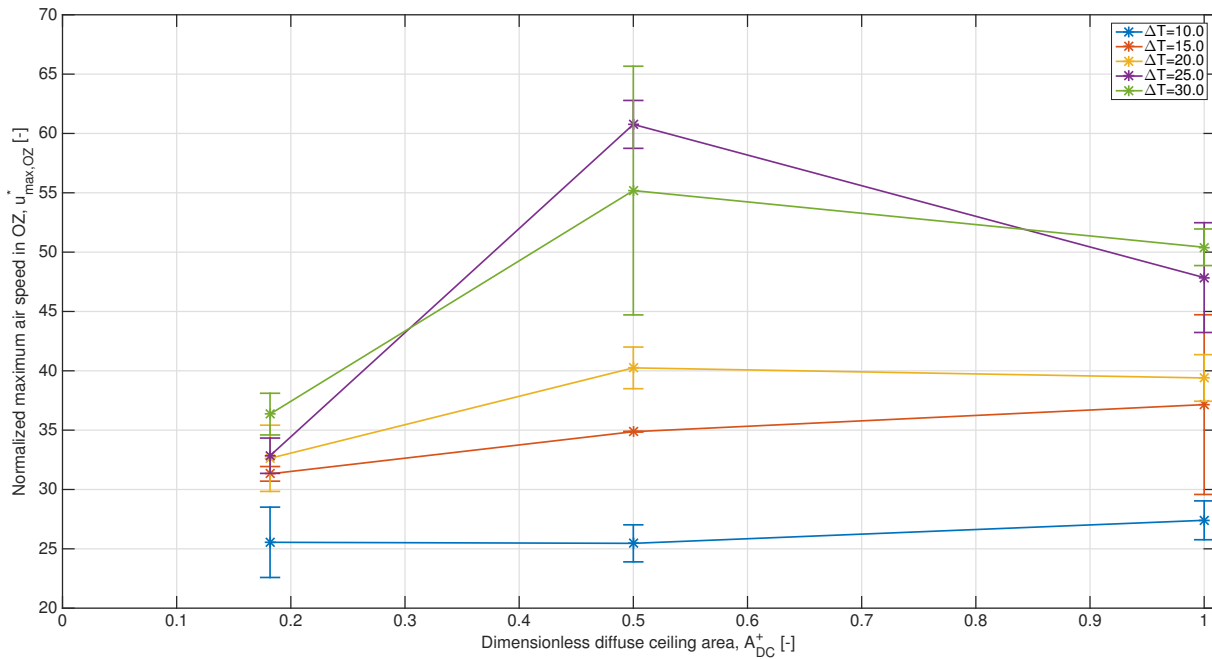


Figure 4.36: Normalized maximum air speed in occupied zone vs. dimensionless diffuse ceiling area.

From figure 4.36 a slightly increasing correlation is observed between normalized room air speeds and supply opening area, however, the correlation changes as the temperature difference is increased:

The physical interpretation of the correlation is that room air speeds does not increase - at least not significantly - with increasing supply opening area. In combination with increased temperature difference (heat release), however, a slight increment is observed, which is most significant in the 50% case.

As mentioned above, figure 4.36 express variation, in terms of the errorbars, that is not accounted for. It may be deduced that the variation, correlation error/residual e , is caused by other parameters than, A_{DC}^+ , u_{max} , q_v , ΔT . This could be the layout of the supply opening area in relation to the heat source distribution in the room. By using Spearman correlation coefficients method it shows that it is not just to perform any reliable regression on the data due to poor correlations.

Reynolds Number Dependence

In the following the developed airflows are analysed in terms of their inherent turbulence level. This is done by correlating normalized maximum air speed in the occupied zone, $u_{max,OZ}^*$, with Reynolds number, Re , representing the relationship between momentum forces and viscous forces in the flow field (equation 1.15 on page 15). The correlation is shown in figure 4.37 for the three different ceiling layouts. The characteristic length is given in terms of the square root of the ceiling area, $A_{ceiling}$. Reference velocity in Reynolds number has been chosen as the artificial supply air speed, u_{ref} , through the entire ceiling area, caused by the ventilation rate, q_v . Hereby Reynolds number express the dimensionless variation of ventilation rate alone.

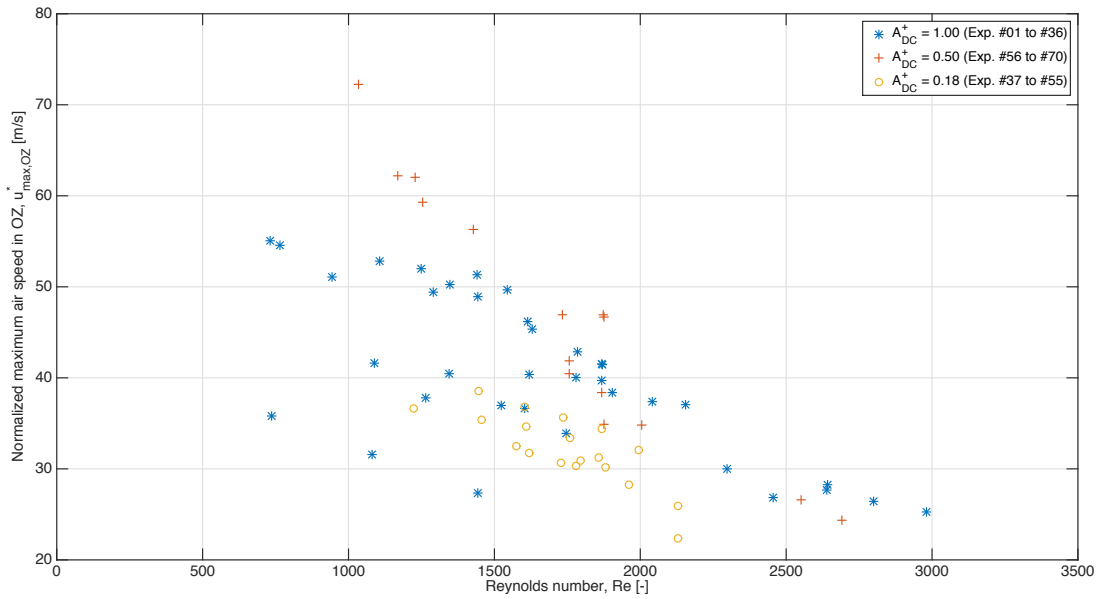


Figure 4.37: Dimensionless maximum air speed in occupied zone (y-axis) vs. Reynolds number (x-axis).

Spearman's correlation coefficient, ρ_s , is for the entire data set is strong with negative direction;

$$\rho_s \left(Re, u_{max,OZ}^* \right) = -0.79$$

For the 50% case, the correlation is almost perfect with $\rho_s = -0.95$, both correlations are statistically significant (see Appendix B.5). Regression analysis favours a power series model in the form $y = a \cdot x^b$.

The physical interpretation of the correlation is, that increasing Reynolds number - and thus ventilation rate - cause room airflows to be more dominated by inlet momentum forces of the DCV system until a critical condition, where the flow field becomes fully developed turbulent and thus Reynolds number independent. However, as no critical condition has arisen in the investigated range, the flow is indeed Reynolds number dependent and thus also described by other variables not taken into account in the present analysis.

Moreover, even though the ceiling layouts cause three different correlations, they are not significantly different which is why the hypothesis that room airflows are significantly influenced by the supply opening area cannot be confirmed from this analysis.

Archimedes Number Dependence

As mentioned in the beginning of this thesis non-isothermal airflows should be characterized by Archimedes number, Ar , representing the relationship between gravitational forces (buoyancy) and inertial forces. This correlation is plotted in figure 4.38 showing normalized maximum air speed in the occupied zone as function of the Archimedes number (equation 1.16 on page 16). As with the Reynolds number, the square root of the floor area is used as characteristic length and a fictive supply air speed described by the ventilation rate as reference velocity.

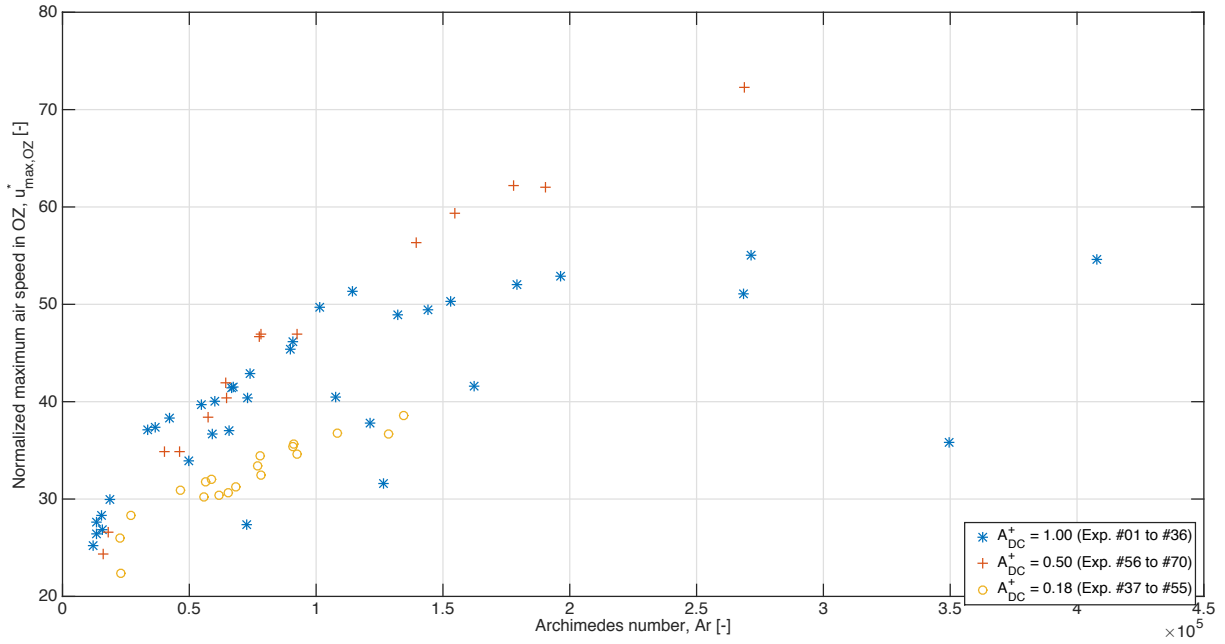


Figure 4.38: Normalized maximum air speed in occupied zone (y-axis) vs. Archimedes number (x-axis).

Note that the applied Archimedes number is a function with two predictor variables:

$$Ar = f(\Delta T, q_v) \tag{4.14}$$

From figure 4.38 it is seen how normalized maximum air speed values in the occupied zone, $u_{max,OZ}^*$, is influenced by Archimedes number and thus the relationship between thermal forces and inertial forces. The correlation is very strong with the 50 % case showing the strongest - almost perfect - correlation;

$$\rho_s \left(Ar, u_{max,OZ}^* \right) = +0.90 \text{ (average of 18 \%, 50 \% and 100 \%)}$$

$$\rho_s \left(Ar, u_{max,OZ}^* \right) = +0.99 \text{ (50 \%)}$$

Regression analysis favours a power model regression of the data correlation as is the case with the Reynolds number correlation.

The physical interpretation is; as buoyancy forces become increasingly dominant (increasing Ar), room airflows are increased likewise, however, the slope or *acceleration* decreases until a critical condition, from where any further increment in Archimedes number has no practical influence on the flow field. This critical condition is expected to evolve at high Archimedes numbers, however the range is not covered by the experimental data.

Three distinct correlations are observed for the three diffuse ceiling layouts. The smallest supply opening area, the 18% case, show a tendency towards becoming Archimedes number independent as the first of the three configurations opposite the 50% data, which correlates much steeper. This means that any heat source influence on the flow field is larger for large supply opening areas (becomes Archimedes number independent later).

Heat Load Dependence

As seen from the Reynolds number and Archimedes number analyses, the flow field is a function of both DCV inlet momentum force and buoyancy forces originating from the heat loads. From figure 4.39 the direct correlation between air speeds in the occupied zone, $u_{max,OZ}$, and heat release in terms of the embedded cooling power in the ventilation, Φ_{cool} , is depicted.

Variation of heat release is exclusively cause by radiator adjustment.

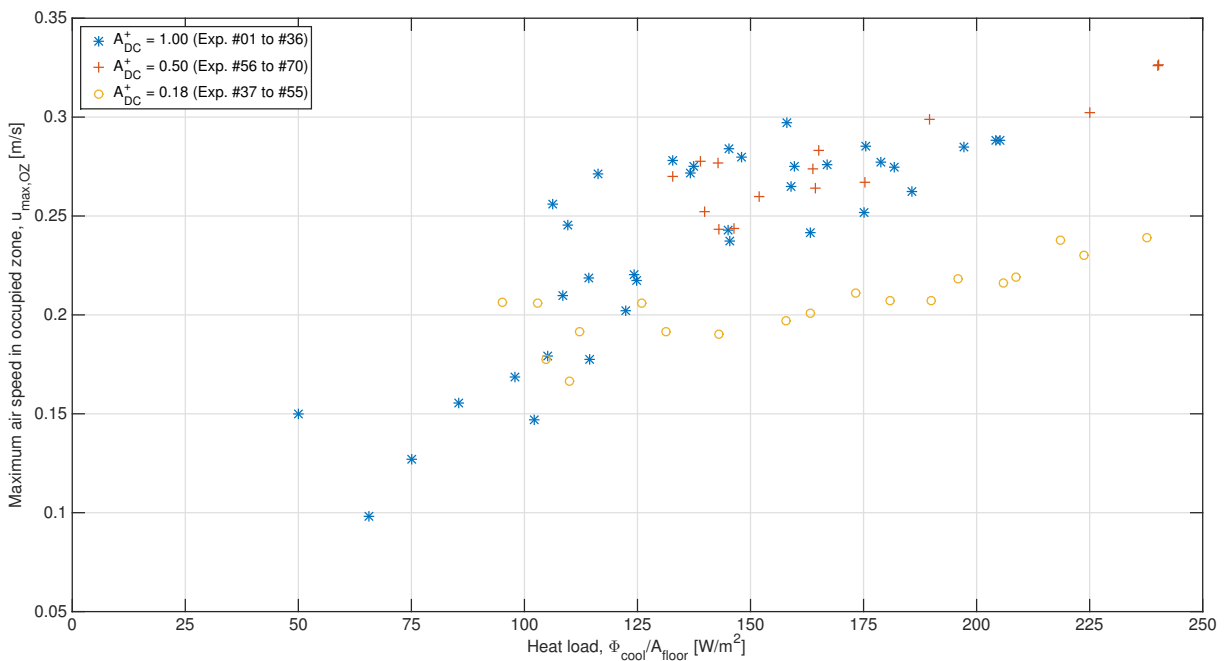


Figure 4.39: Maximum air speed in occupied zone (y-axis) vs. heat release (x-axis).

The scatter show, in average, a strong correlation ($\rho_s = +0.76$), dependent upon the ceiling layout in question (see Appendix B.5).

The physical interpretation of the correlation is that air movement is increased with increasing heat release. Even though one might expect the 18% case to be less influenced by the varying heat release of the radiator it is actually the strongest correlated of the three cases.

Ventilation Efficiency

Neither air CO₂-concentration or other contaminants are measured in the setup, which could have been used for the assessment of mass-convection, however, as the contaminant sources (manikins) are important heat sources, some information about the ventilation effectiveness may be obtained through the analysis of the temperature effectiveness, ϵ_T , as defined in equation 1.13 on page 15.

From figure 4.40 the temperature effectiveness is plotted for the three ceiling configurations. Horizontal errorbars define the standard deviation of the effectiveness in a given measurement height for each of the three series. The topmost measurement point in 2.385 m above floor level is the surface temperature of the suspended ceiling, however, as inlet air is pulled through the ceiling the air temperature at that location is considered the same.

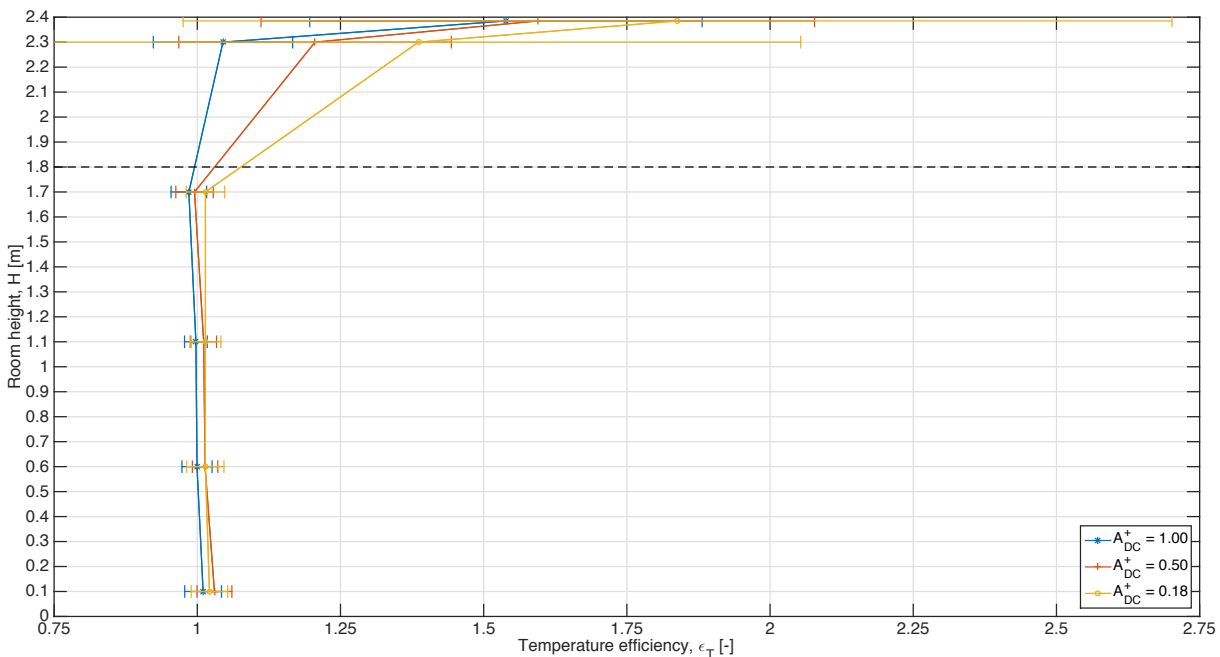


Figure 4.40: Temperature effectiveness gradient. Horizontal errorbars define the standard deviation of all effectivenesses in the given measurement height. Dotted black line mark the delimitation of the occupied zone.

It is from figure 4.40 seen how the temperature effectiveness is almost uninfluenced by the diffuse ceiling area inside the occupied zone. With an effectiveness around 1.0 the ventilation principle resembles that of mixing ventilation. However, above the occupied zone the three DCV systems differ with the 18% case causing highest effectiveness and also the largest effectiveness deviation due to the relatively few opening areas.

4.8 Findings

In conclusion of the experimental investigations in the Hotbox the following findings are highlighted.

Three different ceiling configurations has been studied as diffusers in an experimental setup resembling a classroom; 100 %, 50 % and 18 % diffuse ceiling area using cement-bonded wood wool ceiling panels made by Trolldtekt A/S. In all three cases the supply opening areas (diffuse areas) are uniformly distributed across the ceiling.

A design chart has been established for each of the three ceiling configurations (see figure 4.22 on page 96) showing maximum acceptable combinations of ventilation rate and temperature difference between exhaust and inlet. This way the design charts express a successful evaluation of the DCV systems in terms of the thermal comfort limited cooling capacity when a retention of environmental category B cf. ISO-7730 (2006) is desired in the occupied zone.

Draught rating ($DR > 20\%$) showed to be the limiting discomfort parameter in all cases. High draught rates are triggered by high air velocities, which occur far from the room heat sources.

The examined diffuse ceiling areas significantly influence the acceptable cooling capacity of DCV systems. In case of 100 % and 50 % diffuse ceiling area, capacities around $130\text{-}170\text{ W/m}_{\text{floor}}^2$ seems attainable, however, when lowering the diffuse ceiling area to 18 % even higher capacities around $200\text{ W/m}_{\text{floor}}^2$ are observed at high temperature differences ($\Delta T > 25^\circ\text{C}$). With the experimental setup available it was not possible to test the cooling capacity at temperature differences above approximately 30°C . The reason why the 18 % case seems beneficial is suspected be due to the location of the opening areas directly above the manikins, decelerating any increased momentum.

The ventilation principle in the occupied zone resemble that of mixing ventilation with well-defined effectiveness of 1.0 ± 0.1 , independent on the supply opening area. This is found based on analysis of the temperature effectiveness. Only above the occupied zone is it more temperature effective to have a small diffuser area.

Room airflow pattern is influenced by both inertial forces and buoyancy forces in combination. Airflows are observed to be in a transitional phase, not yet fully developed. The flow field may be described by both Reynolds number, Re , and Archimedes number, Ar . The correlations are strong and dependent upon the supply opening area. In continuation hereof it is found that all airflows in rooms with DCV which satisfy category B in ISO-7730 (2006) are dependent of both Re and Ar with the applied heat source distribution.

Chapter 5

Robustness of DCV System Design by Numerical Analysis

This chapter of the thesis partly answers Supporting Objective 2 (see page 6) as analyses of DCV system robustness is numerically investigated using Computational Fluid Dynamics (CFD). It is desired to perform a robustness analyses for DCV systems to establish, which parts of DCV systems are most influential on performance. Especially the design of supply opening area and heat source distribution is in focus. Initially a CFD model used for the simulations is validated using experimental results from chapter 4 and subsequently the desired investigations are conducted to fulfil the overall objective.

5.1 Planned Investigations

The results, in terms of indoor environmental quality and system functionality, obtained through the laboratory experimentation and documented in chapter 4 is tested for its robustness or uncertainty towards changes in the DCV system design and stochastically changing parameters (heat load location etc.) using computational fluid dynamics (CFD) for parametric analysis. The use of CFD for the robustness analysis makes it possible to conduct a wide array of investigations with considerable lesser effort both in terms of time and resources compared to laboratory experiments.

Benchmarking/Validation

An essential part of performing the robustness analysis is to set up and validate a reliable CFD model that may be used for the predictions. The model is validated and calibrated using the experimental result obtained in chapter 4. This discipline within CFD is known as benchmarking. Without a valid model and a reliable benchmark score, the robustness analysis cannot be performed.

Test procedure

As CFD simulations entails very few restraints on geometry and boundary condition variations a limitation of desired analysis must initially be made. The robustness analysis is subdivided into two main categories; Usage and System design. Usage refers to the dynamic parameters of a DCV system design which are here limited to alterations in placement of type of heat sources in the room. System design refers to the fixed geometry parameters of a DCV system, which once chosen in the design phase will not be subject to change. An overall table summarizing the variations of the DCV robustness analysis is seen on page 122.

Usage. The robustness analysis of room usage is limited to varying heat source distribution. These variations are expected to change the general flow pattern in the room as the fluid motion in the occupied zone is buoyancy driven. In figure 5.1 the heat source distributions analysed are shown. The heat source distribution of the experimental setup and three additional distributions for point heat sources will be investigated along with their influence on comfort. Heat source distribution is investigated for all configurations of diffuse ceiling inlet, as presented in table 5.1 below.

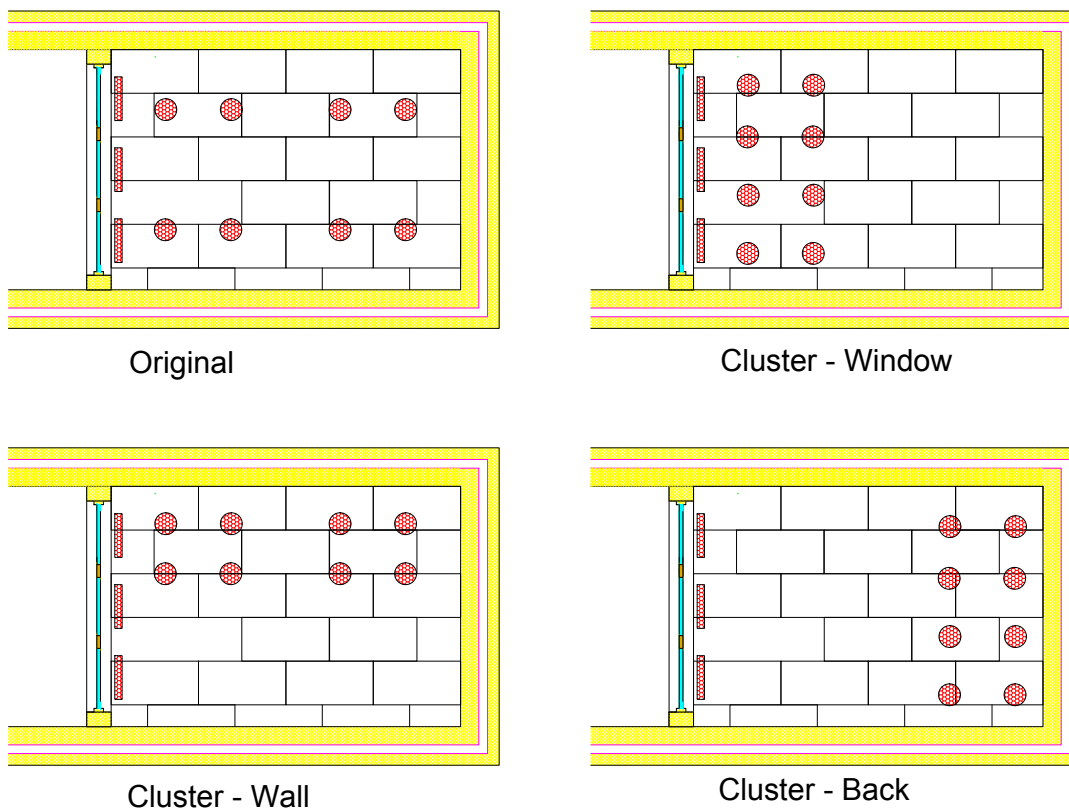


Figure 5.1: Variations of heat source distribution.

System design. Robustness analyses of system design is limited to investigations of alternative placement of diffuse ceiling panels in the suspended ceiling for 50 % and 18 % diffuse ceiling inlet.

It is desirable to see how dislocation of ceiling inlets in the suspended ceiling will affect the comfort limits and general room airflow pattern. In figures 5.2 and 5.3 the original and two different configurations of ceiling inlet distribution is seen for 50 % and 18 % respectively.

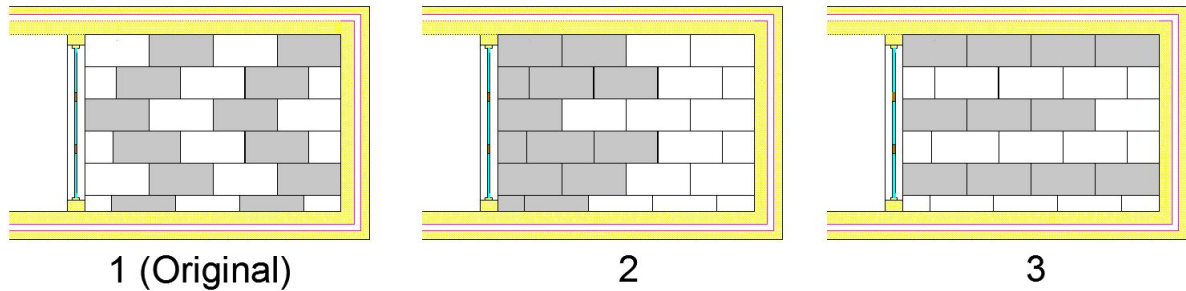


Figure 5.2: Variations of diffuse ceiling inlet distributions for 50 % diffuse ceiling.

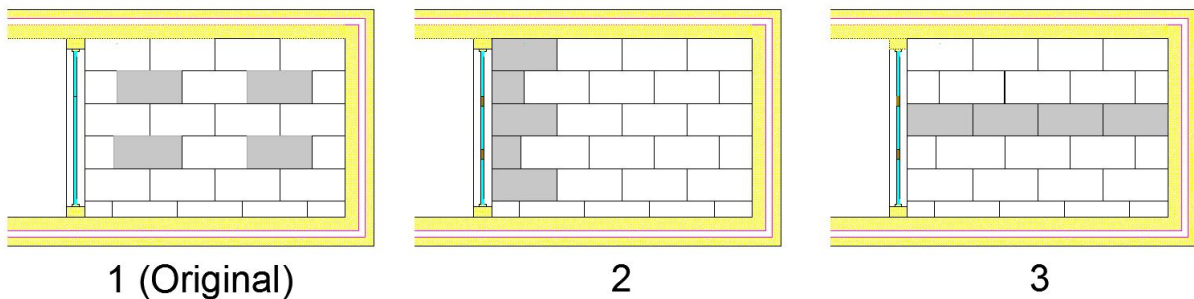


Figure 5.3: Variations of diffuse ceiling inlet distributions for 18 % diffuse ceiling.

Having described the analysis which will be conducted in order to review the robustness of DCV systems these are summarized below in table 5.1. The proposed robustness analysis will offer valuable insights in terms of which diffuse ceiling area is best suited for the intended room usage while quantifying to which degree the different variations in system design affect the airflow pattern and comfort.

Table 5.1: Overview of Robustness Analysis parametric variations.

Analysis #	Heat Source	Diffuse Layout 100 %	Diffuse Layout 50 %	Diffuse Layout 18 %
1	Original	X	-	-
2	Original	-	1	-
3	Original	-	2	-
4	Original	-	3	-
5	Original	-	-	1
6	Original	-	-	2
7	Original	-	-	3
8	Cluster Window	X	-	-
9	Cluster Window	-	1	-
10	Cluster Window	-	2	-
11	Cluster Window	-	3	-
12	Cluster Window	-	-	1
13	Cluster Window	-	-	2
14	Cluster Window	-	-	3
15	Cluster Wall	X	-	-
16	Cluster Wall	-	1	-
17	Cluster Wall	-	2	-
18	Cluster Wall	-	3	-
19	Cluster Wall	-	-	1
20	Cluster Wall	-	-	2
21	Cluster Wall	-	-	3
22	Cluster Back	X	-	-
23	Cluster Back	-	1	-
24	Cluster Back	-	2	-
25	Cluster Back	-	3	-
26	Cluster Back	-	-	1
27	Cluster Back	-	-	2
28	Cluster Back	-	-	3

5.2 Setup of CFD model

The main work load of CFD simulations is compiling a geometry model and subsequently selecting the most appropriate physical models to represent the fluid properties and behaviour of the expected flow pattern. This section of the thesis covers these disciplines.

A best practice approach to CFD in ventilated buildings is applied using existing knowledge and experience within the field of CFD.

Fundamental concept of Computational Fluid Dynamics

CFD is a numerical method used to solve various fluid dynamics problems in a wide array of scientific fields. In this thesis CFD is used to predict flow patterns, pressure distribution and heat distribution in a ventilated room similar to the experimental room investigated in chapter 4.

The fundamental idea behind CFD is to subdivide a domain into a large number of cells and through iterative numerical solution of discretized fundamental flow equation solve the flow equations for the entire domain. For a full understanding of the remainder of this chapter a basic understanding of CFD is recommended, such basic understanding can be acquired from Nielsen, P. V. et al. (2007) and Oberkampf, W. L. and Trucano (2002) which offers practical application guides for CFD in ventilated buildings.

In order to compute a CFD model which gives correct results, solved based on the correct physical models and from solution of correct flow equations, there is a number of areas within CFD which must always be carefully addressed to ensure results with as low uncertainty as possible and preferably no, or at least a minimum of, error. These areas are dealt with on the following pages within a number of different subcategories which are all vital for the overall reliability of the CFD model.

Software

Model geometry, meshing of CFD domain and assigning material properties are done using *ANSYS ICEM CFD 15.0* while *ANSYS FLUENT 15.0* is used as the CFD solver. In the solver (Fluent) physical models, boundary conditions, convergence criteria, flow equations and discretization schemes are selected.

Error and Uncertainty definition of CFD

In assessing whether a CFD model is of high-quality it is practical to distinguish between errors and uncertainties, and hence the definitions below are adopted to give a better understanding of what produces faults in CFD and which of these faults may be avoided.

- **"Error:** A recognizable deficiency in a CFD model that is *not caused by lack of knowledge*. Causes of errors, defined in this way, are:
 - Numerical errors; roundoff -, iterative convergence - and discretization errors.
 - Coding errors; mistakes or 'bugs' in the software.
 - User errors; human errors through incorrect use of the software.
- **Uncertainty:** A potential deficiency in a CFD model that is *caused by lack of knowledge*. The main sources of uncertainty are:
 - Input uncertainty; inaccuracies due to limited information or approximate representation of geometry, boundary conditions, material properties etc.
 - Physical model uncertainty; discrepancies between real flows and CFD due to inadequate representation of physical or chemical processes (e.g. turbulence, combustion) or due to simplifying assumptions in the modelling process (e.g. incompressible flow, steady flow)."

(Versteeg, H. K. and Malalasekera, 2007)

The following sections are based on best practice advise from Nielsen, P. V. et al. (2007), Oberkampf, W. L. and Trucano (2002) and Casey, M. and Wintergerste (2000) on CFD in building ventilation. Methodology of CFD, especially in terms of numerical solution schemes, discretization of equations and modelling of geometries is based on Versteeg, H. K. and Malalasekera (2007).

Model Geometry

The geometry used in the CFD model is duplicated from the experimental room presented in chapter 4. Although an exact geometric replica of the experimental room is desirable a number of simplifications are made in the model, and for some parameters of the experimental room it is not possible to create these properties in CFD e.g. for the internal plywood walls these are in reality not a perfectly smooth surface, and neither do they have a uniform surface roughness. However one of the two mentioned compromises must be chosen. In figure 5.4 the geometry of the CFD model is seen with all bounding surfaces.

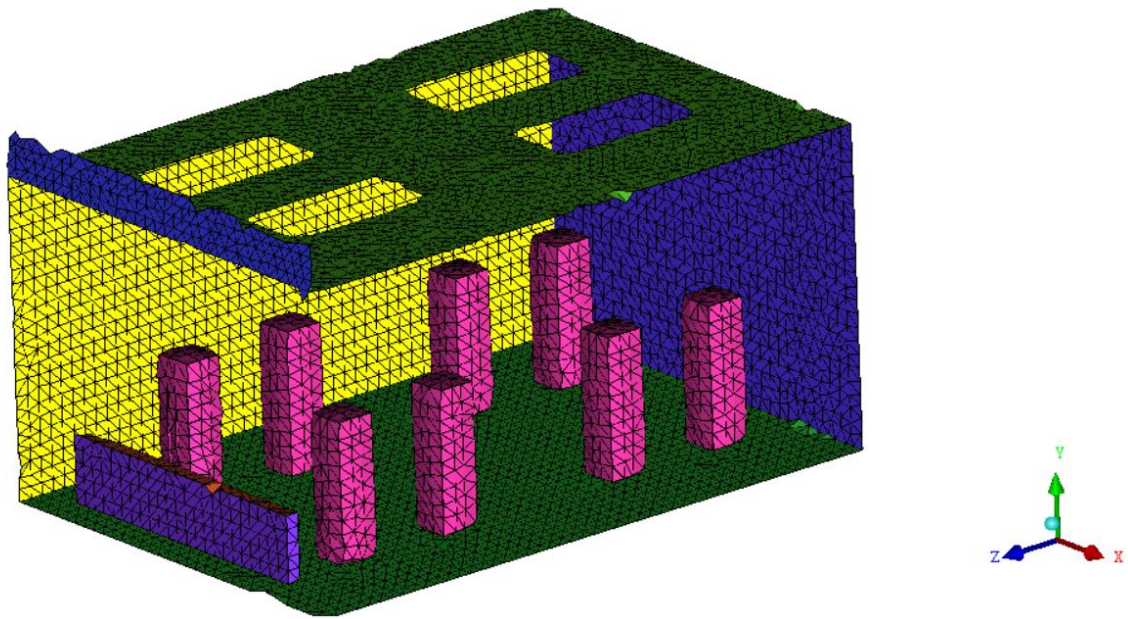


Figure 5.4: Geometry of CFD model with thermal manikins and 18 % diffuse ceiling.

Discrepancies between the CFD model and experimental setup (Hotbox) cause some uncertainty in results as reality and model representation cannot be identical. E.g. when describing surfaces of materials in CFD these surfaces are composed of straight faces or simple curves, which does not fully correspond to what is manufactured for typical building materials. Below some of the most important simplifications of the CFD model and the reasoning for these are highlighted:

Thermal manikins are simulated as rectangular boxes instead of cylinders. The total surface area of either geometry is kept identical. This assumption is made to simplify the meshing and convergence process so the entire domain may be meshed accurately using hexahedral (hex) cells, i.e. cubes. Software restrictions do, however, make it necessary to use both tetrahedral (tet) and hex-cells.

Plenum is an essential part of the model and as such, the suspended ceiling of the experimental room is defined as an internal wall with four openings similar to the 18% diffuse ceiling experiment. However simulating openings (with no pressure resistance) in the ceiling instead of ceiling panels, as in the experimental setup, allow the air to fall unobstructed into the test room. Due to the low pressure loss across the ceiling panels (0-2.4 Pa 4.3 on page 91) this

assumption is chosen over simulating interior fans, and the results of the assumption is assessed when validating the CFD-model in section 5.3 on page 131.

Ventilation inlet of the model is the facade dampers above the windows, as depicted in figure 5.4. Using this configuration the CFD-model can remain a single-zone model which limits complexity compared to a multi-zone model.

Meshing

Having defined the domain in which a solution of the governing equations of fluid flow (continuity, momentum, energy and equations of state) is desired this domain must be divided into a large number of sub-domains aka. *cells*. This procedure is known as meshing.

The size of the cells is vital for achieving accurate results as cells must be small enough to represent the changes (gradients of flow variables) occurring in the domain, e.g. heat release from a manikin. However, computational time of a CFD model increase with the number of cells, as all equations must be solved for each individual cell and it is therefore desirable to reach a compromise where the mesh is fine enough to represent the changes in flow, but not unnecessarily fine as this can increase the computational time manifold. It should be noted that especially the generation of prism layers can quite quickly increase the cell count by a factor of 10. A rule of thumb is that cell size must be smallest in regions where gradients of flow variables are largest, while bigger cell sizes can be accepted in regions with smaller gradients.

In this CFD model high density prism layers are created normal to all bounding surfaces to reduce turbulence modelling errors in the boundary layer. A cut-out of the prism layers created in this mesh can be seen on figure 5.5. Additionally it can be seen how the mesh changes from fine small tet-cells (Volume = 9 cm^3) near the thermal manikin (yellow) to the less dense hex-core mesh (Volume 1000 cm^3) in the free fluid field.

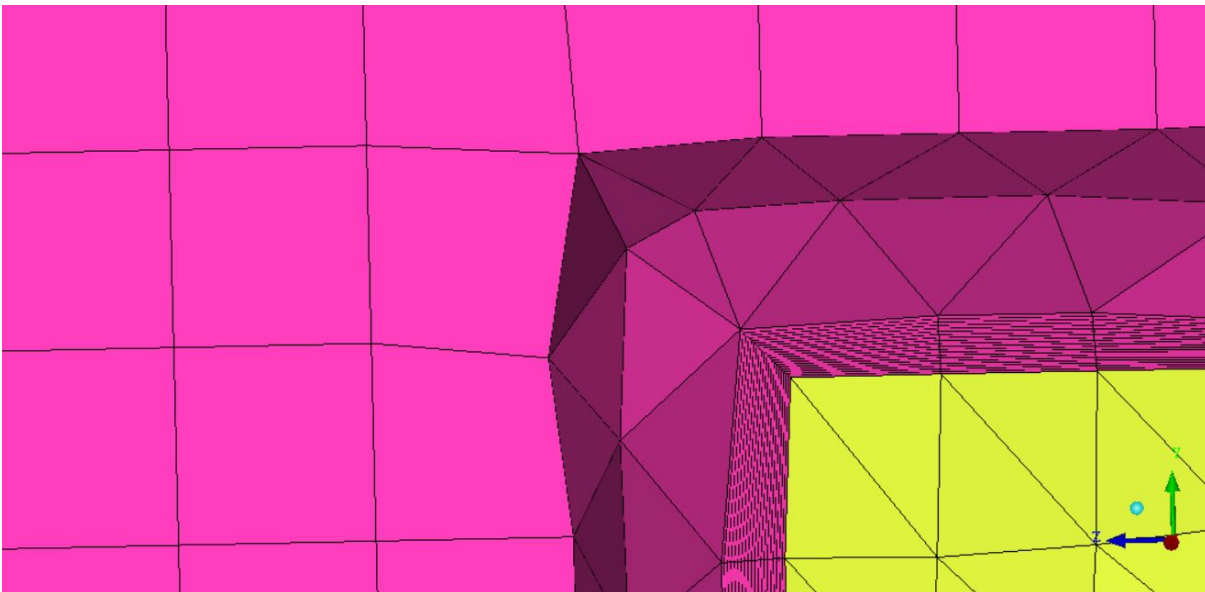


Figure 5.5: Mesh prism-layer around thermal manikin necessary to account for boundary layer

Although the boundary layer represents a very small fraction of the total fluid volume, it is extremely important in order to compute e.g. heat transfer from solid to fluid. Recommendation from Nielsen, P. V. et al. (2007) is that the inner 0.02 m of the fluid domain adjacent to the walls contains at least 20 uniformly distributed cells to accurately simulate viscous boundary layers, this recommendation is adopted in the CFD model in this report. This high density mesh is, however, not needed throughout the entire domain, and in an effort to save computational time larger cells sizes are accepted in some parts of the domain. For CFD simulations in ventilated rooms with room heights of approximately 3 m a 0.10 m vertical grid spacing and 0.30 m horizontal grid spacing can be used in unobstructed regions of the domain (Nielsen, P. V. et al., 2007).

In this CFD model the maximum allowed cell length in any direction is 0.10 m. A cross-sectional view of the computed mesh in the CFD-model can be seen in figure 5.6 where the transition from prism-layers and tet-mesh near surfaces convert into hex-mesh in the unobstructed regions of the test room modelled.

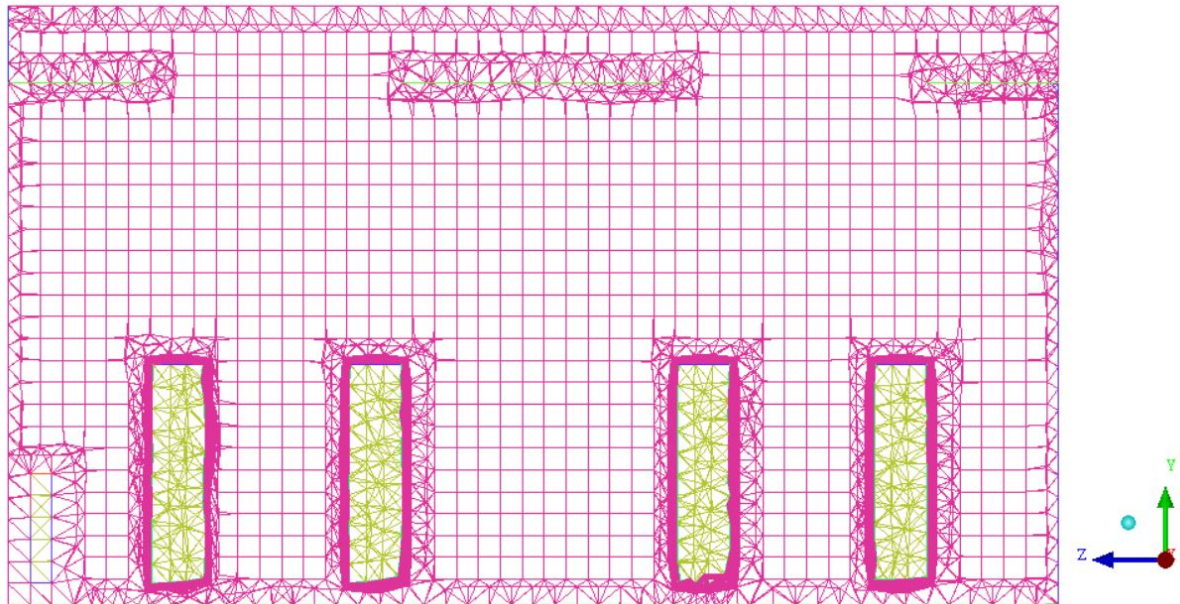


Figure 5.6: Cross-sectional view of mesh showing tet-boundary cells and hex-core mesh. Openings in diffuse ceiling are seen as continued hex-core mesh between plenum and test-room.

Apart from appropriate cell size selection it must also be ensured that the cell quality in the mesh is overall good, otherwise a numerical error is introduced. Cells should not be distorted, deformed or degenerated. The numerical error introduced by hex-cells is lower than that of tet-cells but computational limitations made it necessary to use both hex and tet cells. A number of quality parameters are used in assessing the overall quality of the mesh and these, along with their target values, are presented below.

Target values are adopted from Nielsen, P. V. et al. (2007), Oberkampf, W. L. and Trucano (2002), ANSYS (2013).

- Expansion ratio < 2
- Aspect ratio < 50
- Skewness < 0.6
- Cell boundaries must be aligned with dominating flow directions in the domain

All the above defined limits are general guidelines, which the majority of the cells should fulfil.

In table 5.2 all the relevant mesh and quality quantities for the mesh used in this CFD model is tabulated. As it is necessary to utilize tet-cells it is not possible to align all cell boundaries with dominating flow directions, and the regions of tet-cells must be examined to see if they give physical meaningful results.

Table 5.2: Mesh quality data.

Quality parameter	Cells within limit
Expansion ratio, < 9.0	97.8 %
Aspect ratio < 50	99.2 %
Skewness < 0.6	85.2 %

Note from the table above that it was not possible to extract mesh quality data for an expansion ratio from 0-2.0, and therefore the quality data tabulated covers expansion ratios from 0-9.0 instead. The percentage of cells with aspect ratio less than 50 is satisfying and judged on the other quality parameters it is assumed that the cells with expansion ratio less than 9.0 is clustered in the lower interval close to zero, but the precise number of cells below 2.0 is not known. For the overall skewness of the cells the skewed elements are mainly in the tet-cells between prism-layers and hex-core of the fluid region, and whether this causes problems in the solution must be investigated in the validation of results. Normally a subdivision of the highly skewed cells into smaller cells will improve the mesh, but as the upper limit of cells for the software is reached this operation is not possible.

Physical Models and CFD Solver

If converged results are not reached by use of the appropriate physical models these results can not be regarded as accurate, and in most cases small changes in model setup will cause unrealistic physical behaviour in the fluid properties.

Fluid density modelling. As seen in the experimental results in chapter 4 on page 67 the flow in the test room is dominated by the heat sources in the room, i.e. the flow is buoyancy driven. Combined with that fact that the heat transfer in the room is dominated by natural convection, due to the low velocities, an incompressible ideal-gas assumption or the Boussinesq approximation can be applied to compute fluid density. As the boundary conditions for the heat sources are computed as heat-flux on a surface this causes high temperatures in some cells and therefore an incompressible ideal-gas assumption is preferred over Boussinesq.

Turbulence modelling. The $k-\omega$ -model combined with Shear Stress Transport (SST) and low Re-correction is chosen. This models predicts more correct shear stresses than the more commonly used $k-\epsilon$ -model and furthermore the low-Re correction for near wall treatment smooths the calculations process for turbulence in cells near boundaries (boundary-layer) where flow velocity is almost zero. Standard wall functions are applied near walls to ensure a more correct flow and heat transfer regime in the boundary layer, where flow and solid interact. This turbulence model is also suggested for use by Nielsen, P. V. et al. (2007) for fluid problems similar to the one presented here.

Radiation modelling. A Surface-to-surface (S2S) radiation model calculating radiation in an enclosure of gray-diffuse surfaces is used in the computation. This model is chosen as it offers the highest accuracy of the available radiation models in *Fluent*. Normally the S2S-model is very expensive in computational time, but as the number of faces in this model is relatively modest and a lot of surfaces can not "see" each other the computational times is limited significantly. Radiation exchange is based on view-factors between surfaces in the enclosure and the energy flux leaving either surface. As temperatures of all surfaces are known from the experimental investigation an accurate radiation model is achieved. The S2S-model does not account for scattering, absorption or emission.

Discretization scheme. The MUSCL scheme (Monotonic Upstream-Centered Scheme for Conservation Laws) is used for all flow equations. Hereby discretization errors in the solution are avoided due to the third-order accurate nature of the scheme. This scheme is chosen as it is well suited for complex three-dimensional flows ANSYS (2013). Discretization error is a major source of error in CFD, it originates from the algebraic expressions of the general flow equations. This error decreases when the order of the applied discretization scheme increases, so at least second-order accurate discretization schemes should be applied for the final solution. The computational time is, however, higher for the high-order schemes so in this model the solution uses first-order schemes in the initial iterating process of the solution. When residual values are stationary the order of the discretization schemes are increased. To further limit the error produced by the solver a 64-bit solution is applied as this decreases the roundoff error by allowing more digits in the solution.

Solution algorithm. A pressure-based segregated solver is used to calculate the pressure flow field in the entire domain, as this is best suited for natural convection problems in closed domains for incompressible fluids. Additionally the pressure based solver makes it possible to simulate a floating operating pressure which corrects for the temperature and density variations of the fluid. This solution-scheme for pressure field is known as SIMPLE (Semi-Implicit Method for Pressure Linked Equations) solves the pressure field based on the continuity equation and equation of state. (ANSYS, 2013)

Boundary Conditions - BC

Ventilation inlet of the room duplicates the intake damper from the experimental setup. This boundary type prescribes inlet velocity and inlet temperature equally distributed over the entire inlet area. Air direction is 1-dimensional, normal to the surface. This causes uncertainty in CFD results as it is seen from the experimental results in chapter 4.4 on page 88 that the inlet temperature is not uniformly distributed, and hereby neither is the inlet velocities.

Ventilation outlet is simulated as a pressure outlet and is prescribed a target mass-flow rate and temperature equal to the measured quantity from the experiment being simulated. Using the pressure outlet BC it is ensured that the sum of the mass balance is equal to zero as desired. The CFD-model has no unwanted permeability or infiltration, and airflow into or out of the domain can only happen in inlet and outlet.

Walls, floors and ceiling are all assigned a constant temperature equal to the measured surface temperature of the experiment that is simulated. However for the facade wall a heat flux boundary condition is prescribed using the U-value ($0.71 \text{ W/m}^2\text{K}$) and measure temperature difference between cold-zone and operative room temperature.

Heat sources are defined as walls prescribed with a constant surface temperature and a thickness. The temperature BC is converted into a heat-flux by the software, and temperatures prescribed are chosen to duplicate the plume-profile investigated in appendix B. A material thickness of minimum 5.0 cm must be used as this eases the heat source simulation in the software (ANSYS, 2013).

Grid Independence Study

The purpose of the grid independence study is to ensure that the mesh is so dense that it does not affect the solution of flow-variables in the final solution. The study is performed by creating an initial coarse mesh and refining it until the solution of flow variables does no longer vary with changes in mesh density, i.e. until the solution is independent of mesh size.

In the CFD solver used in this thesis, the Academic version of Ansys Fluent 15.0, there is an upper limit of 512,000 cells in the solver and this logically sets an upper boundary for mesh-density. As the computational time for a 500,000 cell mesh is not very expensive with the applied hardware, a mesh with 490,000 cells is used for simulations. This cell count corresponds to a medium quality mesh when compared to the recommendations in (Nielsen, P. V. et al., 2007).

5.3 Validation

Having considered key-elements in producing a good CFD model this must be validated against reference data before the model can be used for robustness analysis. All three ceiling panel layouts has been made to asses a wide range of scenarios, but time considerations has limited this analysis to mainly focus on a model where the ceiling area is 18% diffuse and identical to the experiments performed in chapter 4. The validation process is initially made for a single experiment (exp 41) from which the boundary conditions are adopted, these boundary conditions are tabulated below.

Table 5.3: Boundary conditions for experiment number 41 used for validation of CFD model.

Boundary Conditions	Value
A_{DC}^+	0.18 -
ACR	10.1 h ⁻¹
ΔT	12.9 °C
Φ_{rad}	980 W

Convergence

Before utilizing the results of the simulation it must be ensured that the solution is converged, i.e. all flow equations are solved correctly. It is important to notice that a converged solution is not necessary accurate. Accuracy also strongly depends on the assumptions and models of the CFD, which are accounted for in section 5.2 of this chapter. Convergence is typically, and also in this thesis, evaluated on two levels; conservativeness and residual values.

Conservativeness is a fundamental criteria for a numerical solution to be physically realistic and governs the compliance with the conservation laws of physic. Conservativeness as a convergence criteria is here that e.g. energy conservation and mass-flow balance is correct. These balances are important to ensure that the transport of matter and energy are in equilibrium. The sum of heat-flux for all surfaces in the model must be zero, as a steady-state solution similar to the experimental results is desired. Mass balance is equally important as this accounts for the correct amount of mass transported into and out off the model, avoiding false sources or sinks in the domain. The physical balance of the simulation result can be seen from table 5.4 where the calculated deficits of each flow equations are tabulated.

Table 5.4: Deficits of flow equations for convergence assessment.

Physical Balance Rate	Relative size of deficit
Mass Flow Rate	$-1.38 \cdot 10^{-6}$ kg/s 0.001 %
Total Heat Transfer Rate	-20.6 W 0.320 %
Radiation Heat Transfer Rate	-4.1 W 0.080 %

From the size of the mass imbalance in table 5.4 and knowledge from literature, it is concluded that the imbalance is caused by round off error and does not represent a actual physical

phenomenon (Nielsen, P. V. et al., 2007). The relative size of the total heat transfer deficit and the radiation heat transfer deficit is included in table 5.4. Both these deficits are acceptably small to conclude that the overall energy balance is ensured.

Residual values are used to monitor how well the flow equations are solved. It is important that residual values are small as this reflects the size of changes between iterations. Residual values should be in the order of 10^{-3} for all flow equations, except the energy equation where the residual should be closer to 10^{-6} (ANSYS, 2013). In figure 5.7 the residual values for the converged solution analysed in this section can be seen. Apart from having a proper magnitude it is crucial that the residual values are steady and does no longer change for each iteration. In order to ensure that the residual values are steady the under-relaxation factor must be 1.0 to ensure the iterative solution is not bounded.

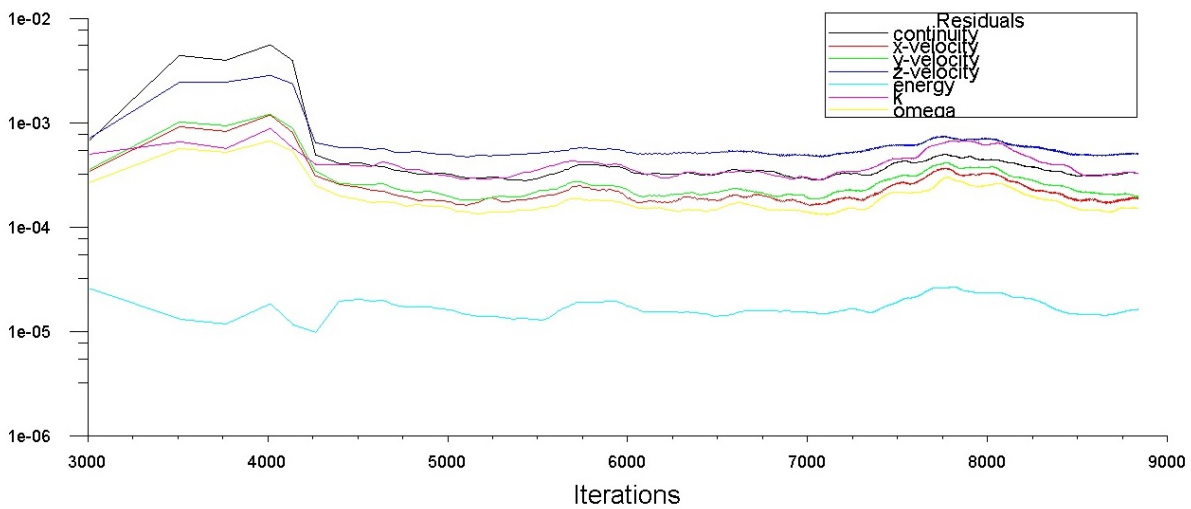


Figure 5.7: Plotted residual values for flow equations.

As mentioned about *convergence* above it is necessary to evaluate the convergence of the solution before analysing the data in detail. The stability and magnitude of residual values can be seen in figure 5.7 and these are, based on the argumentation in the previous section, acceptable. Hereby analysis of specific results of the CFD simulation can commence.

Agreement with Experimental Results

As mentioned previously the validity of computed results is assessed based on their agreement with experimental results. Benchmarking of computed and measured results are made for 20 points in the model similar to 20 measurements points from the experimental data set of the given experiment. These 20 reference points represent 4 measurement columns in the experimental setup and is selected to ensure validation in most of the domain. In table 5.5 the measured and computed results are compared and absolute and relative error for each point is calculated. Consistency of results is compared for air temperature and velocity. As proposed in Nielsen, P. V. et al. (2007) and (Oberkampf, W. L. and Trucano, 2002) the relative difference in results should be below 10 % to have satisfactory and usable results. Notice that in order to compare measured velocities to computed ones, the measured air speed must be converted into velocity by using the turbulence intensity as described in Kristensen, M. H. et al. (2015).

The mean and maximum values of the relative errors in the bottom of table 5.5 are calculated for the absolute positive values of the errors, see equation 5.1 and 5.2. The standard deviation (σ) is calculated with respect to sign, e.g. values of error can assume a negative value.

$$E_{abs} = \phi_{meas} - \phi_{CFD} \quad (5.1)$$

$$E_{rel} = \frac{\phi_{meas} - \phi_{CFD}}{\phi_{meas}} \quad (5.2)$$

where:

- E_{abs} = absolute error of CFD prediction [$^{\circ}\text{C}$ or m/s]
- E_{rel} = relative error of CFD prediction [-]
- ϕ_{meas} = measured variable (either temperature or velocity) [$^{\circ}\text{C}$ or m/s]
- ϕ_{CFD} = simulated variable (either temperature or velocity) [$^{\circ}\text{C}$ or m/s]

Table 5.5: Comparison of simulated and measured values of air temperature and velocity.

	Height	Temperature		Velocity	
		E _{abs}	E _{rel}	E _{abs}	E _{rel}
Column 3	0.1 m	-1.39 °C	-7%	-0.06 m/s	-35%
	0.6 m	-1.48 °C	-7%	0.06 m/s	97%
	1.1 m	-1.67 °C	-8%	0.05 m/s	69%
	1.7 m	-0.88 °C	-4%	0.05 m/s	149%
	2.3 m	1.60 °C	7%	-0.02 m/s	-15%
Column 4	0.1 m	-1.03 °C	-5%	-0.01 m/s	-11%
	0.6 m	-0.89 °C	-4%	0.06 m/s	57%
	1.1 m	-0.56 °C	-3%	0.14 m/s	299%
	1.7 m	-0.27 °C	-1%	0.04 m/s	50%
	2.3 m	1.47 °C	6%	0.46 m/s	275%
Column 5	0.1 m	-1.22 °C	-5%	-0.13 m/s	-70%
	0.6 m	-0.66 °C	-3%	-0.20 m/s	-80%
	1.1 m	-1.06 °C	-5%	-0.30 m/s	-78%
	1.7 m	-1.21 °C	-6%	-0.27 m/s	-70%
	2.3 m	-9.15 °C	-74%	0.00 m/s	-1%
Column 6	0.1 m	-0.84 °C	-4%	0.00 m/s	-1%
	0.6 m	-0.42 °C	-2%	0.00 m/s	-1%
	1.1 m	-0.30 °C	-1%	0.00 m/s	6%
	1.7 m	-2.08 °C	-10%	0.05 m/s	41%
	2.3 m	-6.33 °C	-43%	0.01 m/s	9%
Outlet	2.3 m	-0.07 °C	0%	-0.22 m/s	-24%
	Min	-9.15 °C	–	-0.30 m/s	–
	μ	-1.35 °C	-8%	-0.01 m/s	32%
	Max	1.60 °C	74%	0.46 m/s	299%
	σ	2.34 °C	18 %	0.16 m/s	103%

As seen in table 5.5 the air temperature results are within the 10 % limit of accuracy for 19 of 21 reference points. The average value and standard deviation for the temperatures is $-8\% \pm 18\%$.

Oppositely the velocity measurements are far from the acceptable limit of accuracy, as only 5 of 21 points have errors less than 10 %. The magnitude of relative error for the velocities are in general very high, and the average relative error is $32\% \pm 103\%$.

The results presented in table 5.5 are the best results achieved from simulations based on a total of 16 geometries and approximately 50 different solution set-ups, where discretization schemes, physical models, fluid properties, boundary conditions and initial solutions are varied in order to produce the most correct results.

Based on these results the CFD-model generated is not suited for performing the desired robustness analysis as the results are not reliable.

To analyse the error distribution of the computed results a bell curve is made for both absolute temperature error (figure 5.8) and velocity error (figure 5.9). The computed results (red curves) are shown for a standard deviation of 3σ and plotted with an ideal bell curve, computed from 2000 randomly generated values. As seen the temperature distribution fits the ideal bell curve better than the velocity error curve. It can also be seen how the most frequent velocity error is in the range of 0.15-0.20 m/s which are very large errors when considering the typical air velocities in a ventilated building. The most frequent error of temperature is close to 1.25°C which is not as critical for the results as the velocity error. This analysis further documents how attention should be focused on solving the velocity field of the domain in a more appropriate manner.

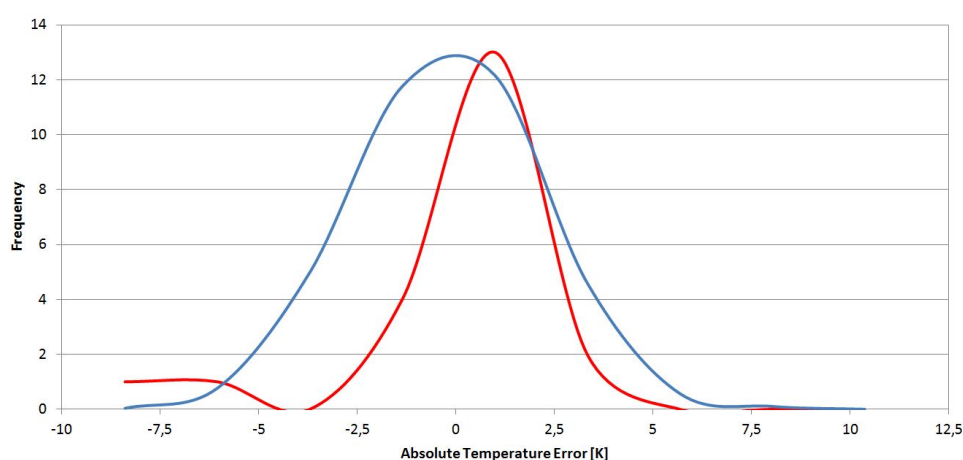


Figure 5.8: Normal distribution of absolute temperature error for computed results (red curve). Blue curve represents ideal normal distribution with 3σ .

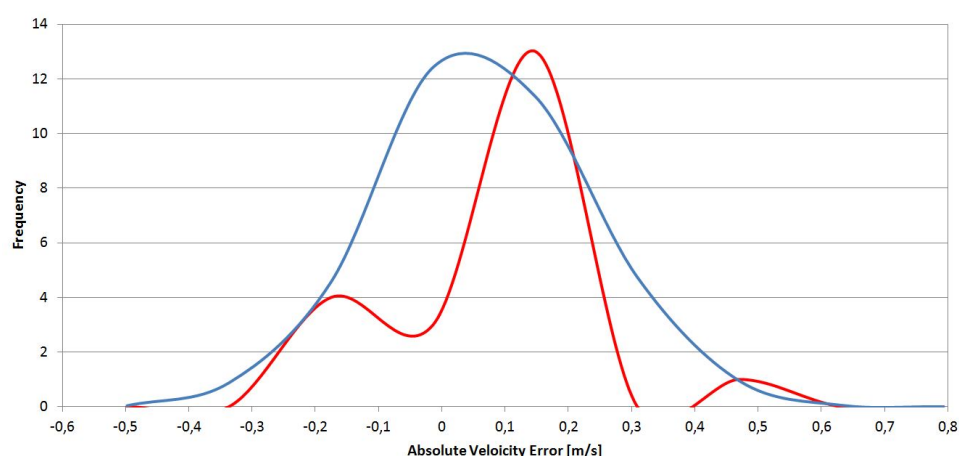


Figure 5.9: Normal distribution of absolute velocity error for computed results (red curve). Blue curve represents ideal normal distribution with 3σ .

Airflow Pattern and Temperature Distribution

Although the computed velocities are not correct, it is still worth analysing the results to see where the CFD model produces incorrect results. In the following pages several contour plots are analysed to assess the overall flow pattern of the simulated test room. In figure 5.10 and 5.11 the air temperatures for selected cross sections of the test room can be seen.

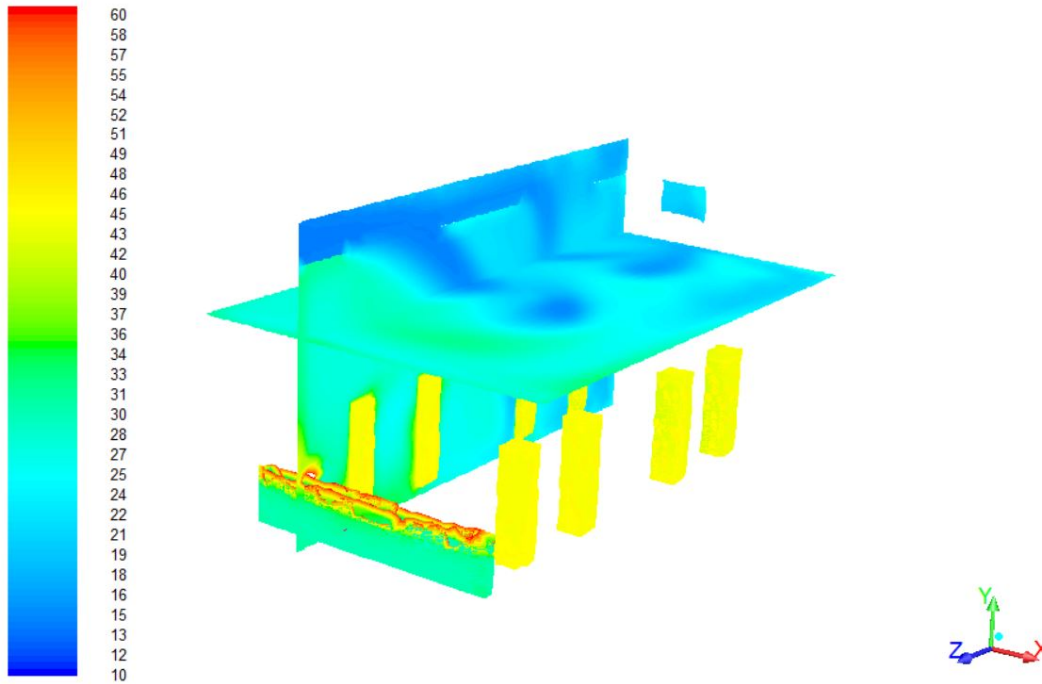


Figure 5.10: Computed air temperatures for selected cross sections. Scale is in degree celsius.

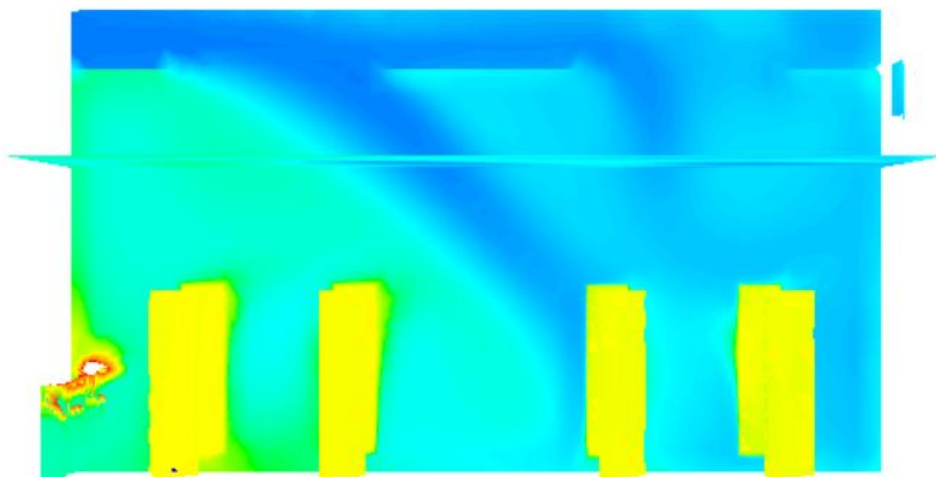


Figure 5.11: Computed air temperatures for selected cross sections. Scale is in degree celsius.

It is clear to see how the cold jet from the plenum plunges into the test room through the diffuse ceiling panels as expected. The thermal plumes generated by the manikins and the radiator pushes the inlet jet to areas where there are no heat sources (see the four cold areas in figure 5.10). This displacement of the inlet jet, which without the heat sources would fall vertically, is also what was observed in the experimental setup in Part 2. It can furthermore be seen how the heat load from the radiator influences the entrainment length of the inlet jet, as this is pushed further into the test room closest to the radiator.

Further investigating the velocity field from figures 5.12 and 5.13 shows how the computed solution, like the measured results (see lower left corner of figure 4.35 on page 111), have highest velocities in the region above the occupied zone and near the floor. From figure 5.12 it can be seen how the thermal plumes from the manikins push the cold inlet air away and hereby creates higher velocities e.g. down along the internal walls.

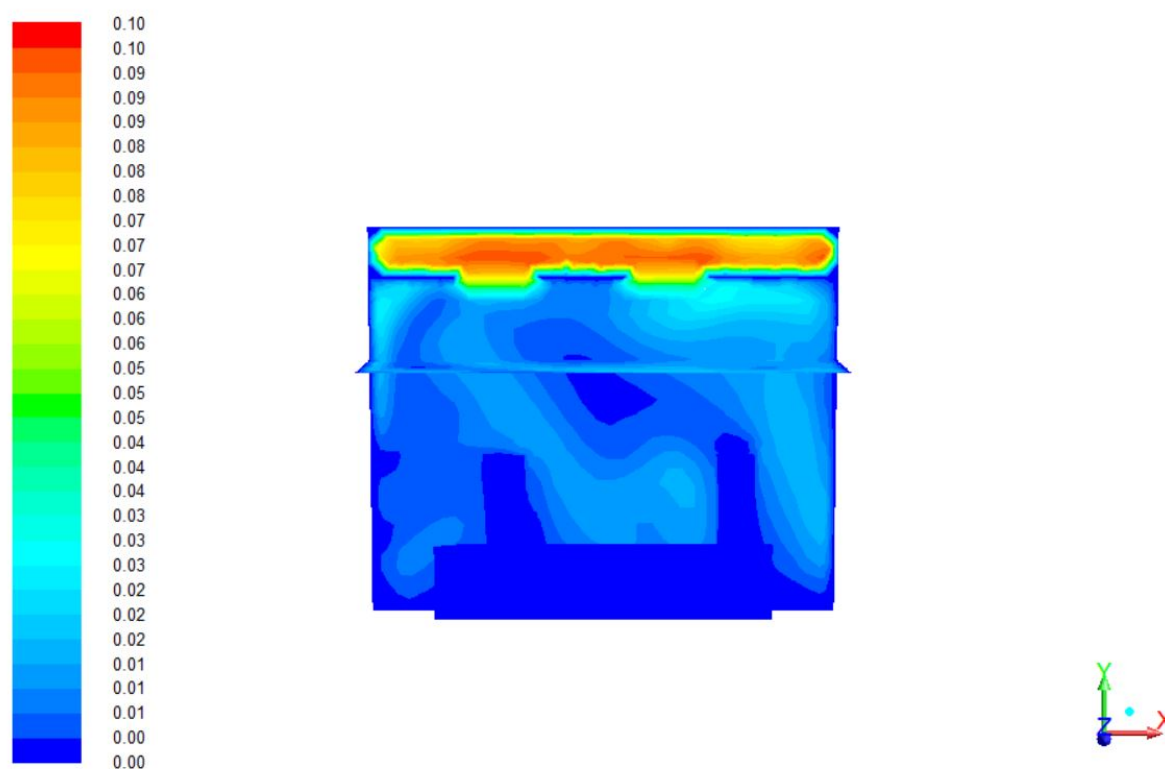


Figure 5.12: Computed air velocity for cross section through and over manikins. Scale in meters per second.

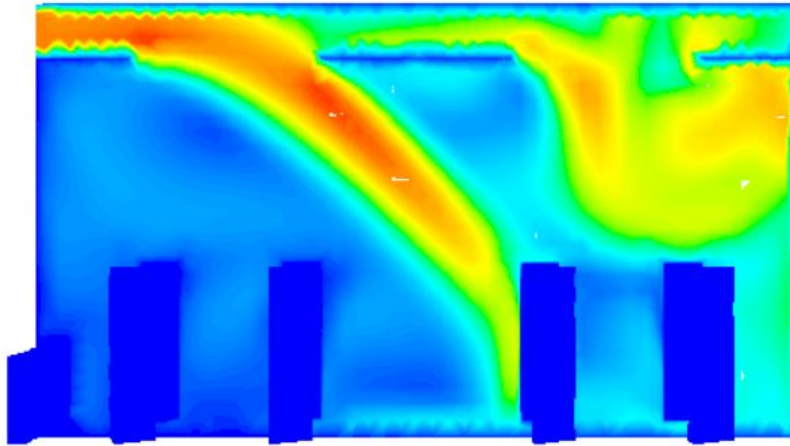


Figure 5.13: Computed air velocity for cross section with inlet (left top corner) and outlet (right wall). Scale in meters per second.

The observed airflow pattern where the heat sources dominates the heat flow in the room is to some extent present in the computed solution as well. Temperatures and velocities are in general in alignment with the measured results, but the velocity field is computed with too low velocities. It seems problematic for the CFD model to compute velocities very close to zero, as so many cells have a velocity of zero.

Evaluation of Thermal Plumes

As the heat sources dominate the flow pattern it is especially interesting to see if the simulated plumes above the thermal manikins are consistent with measured results. Comparison of volumetric flow and momentum flow generated by the plumes show how this exceed the similar quantities of the inlet air, hence the plumes should still remain intact for the airflow rate ($ACR = 10.1 \text{ h}^{-1}$) in the simulated solution. Do note that the measured values used for comparison are generated in a test-room with no ventilation and therefore it is not expected that these are fully identical.

Looking at figure 5.10 it can be seen how an expected increase in air temperature is evident above the thermal manikins. Excess air temperature and velocity in the plume above each of the 8 manikins is evaluated and compared with experimental measurements (see Appendix B) in table 5.6. The table show both absolute and relative error calculated in accordance with equation 5.1 and 5.2. The results are evaluated in a single point 0.7 m above the manikins and represent the center of the plume.

Table 5.6: Comparison of thermal plume data for simulated and measured results. All results evaluated 0.7 m above manikins.

Manikin number	Excess Temperature		Velocity	
	E_{abs}	E_{rel}	E_{abs}	E_{rel}
1	1.89 °C	208%	-0.018 m/s	-1769 %
2	-1.79 °C	-197%	0.007 m/s	-485 %
3	-0.64 °C	-70%	-0.005 m/s	-763 %
4	-0.72 °C	-79%	0.004 m/s	-529 %
5	-6.32 °C	-694%	0.019 m/s	-335 %
6	-4.08 °C	-449%	0.044 m/s	-189 %
7	2.15 °C	236%	-0.018 m/s	-1845 %
8	5.37 °C	590%	-0.021 m/s	-1068 %
$\mu \pm \sigma$	$-0.52 \text{ °C} \pm 3.26 \text{ °C}$	$-57 \% \pm 358 \%$	$0.001 \text{ m/s} \pm 0.020 \text{ m/s}$	$-1068 \% \pm 786 \%$

The differences tabulated in table 5.6 clearly show how the simulation of the thermal plumes is erroneous. Simulated excess air temperature inside the thermal plume is generally underestimated with approximately $57\% \pm 358\%$ ($\mu \pm \sigma$) cf. actual measured values. In addition, air velocity is wrong with more than 1000 % in average with a standard deviation of almost 800 %. As such, the thermal plumes are not simulated in a sufficiently valid way contributing to the overall rejection of the model as a valid prediction of future outcome. Looking at the cross-sections of temperature (figure 5.11) and velocity (figure 5.13) it is seen how the plumes are not clearly visible. In the region furthest from the inlet (right end of figures) it is seen how air movement is not caused by the thermal plumes, but rather the inlet jet from above. This conflicts with the hypothesis that the airflow pattern should be governed by natural convecting heat loads rather than forced ventilation from the DCV system.

Geometry adaptation

As the CFD model analysed in the section above produce inapplicable results a number of geometry adaptations are performed to produce an applicable model. As the mesh quality, physical models, boundary conditions and convergence are judged satisfactory the focus is turned on creating a geometry which better corresponds to the experimental setup. The assumptions made about diffuse ceiling inlet modelling is of interest to the improvement. The use of a holes instead of ceiling panels for inlets in the suspended ceiling produce too little resistance. However, efforts to model the openings as porous surfaces with a variable pressure drop calculated from mass flow through the panels proved unsuccessful and results with the original geometry are more correct. Modelling of the diffuse ceiling panels as fans with a constant pressure increase independent of mass flow also give results which are less correct than modelling openings in the suspended ceiling.

Efforts to create a multi-zone CFD model capable of handling non-isothermal bidirectional flow through the diffuse ceiling was unsuccessful. It is, however, expected that separating the fluid domain into a test-room domain and a plenum domain could more accurately compute the fluid motion seen in the performed experiments, this theory is backed by results from Iqbal, A. et al. (2013). It is however important that fluid flow through the diffuse ceiling is bidirectional as heat from the test-room must be allowed to disperse into the plenum and mix. The importance of this mixing is supported by the findings from Part 1.

That the plenum is important in simulations of DCV-systems is confirmed by modelling efforts where the plenum is neglected, and the diffuse ceiling panels are used as one-way ventilation inlets, i.e. backflow is not possible. This geometry was tested for CFD-models simulating both 100 % and 18 % diffuse ceiling inlet, as depicted below in figure 5.14.

The simulation errors in the reference-points for the models without plenum are a least 3 times higher than the error for models where plenum is simulated. Apart from the larger error in the reference points, it is also observed that the thermal plumes above the manikins are even smaller compared to simulations with plenum. Hence this dominating factor for the fluid motion in the room is simulated more incorrectly, which is also a reason that this modelling technique is not recommended for simulating DCV systems.

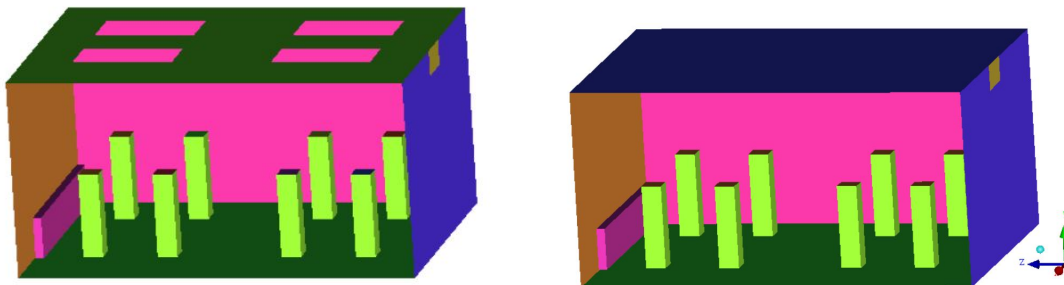


Figure 5.14: Geometry of alternative ventilation inlet modelling without plenum. Left: 18 % diffuse ceiling inlet. Right: 100 % diffuse ceiling inlet.

5.4 Findings

The computed results of the compiled CFD model are not reliable and cannot be validated. Although a best practice method was applied concerning CFD simulations in ventilated buildings and a converged solution is ensured in terms of conservativeness and steady residual values of appropriate size, the computed result proved invalid and failed the benchmarking against experimental results.

The expected two main sources of inaccuracy is the modelling of diffuse ceiling panels and the modelling of internal heat sources. In the created single zone model an accurate representation of pressure resistance through the diffuse ceiling panel is not achieved, which leads to uncertainty in the erroneous results.

Additionally the thermal plumes generated above the manikins show to be modelled in an incomplete way. The plumes are too cold (approximately 60 % in average) resulting in much too little momentum flow embedded in the plumes (air velocities approximately 1000 % lower than measured in average).

For future CFD modelling of DCV systems attention should be focused on correct modelling of heat sources as these are vital in the overall validation of such predictions. A different Boundary condition approach could prove beneficial as fixed heat-flux from surfaces generate too high surface temperatures compared to measured results.

The Robustness analysis is not performed due to the invalid results produced by the CFD model.

Part 3

Recapitulation

A discussion and final conclusion that serve to sum up on the project work and findings, put them into perspective and to account for the fulfilment of the Thesis Statement and Supporting Objectives.

Chapter 6

Discussion

Throughout this discussion the applied methodology and results of the research is reflected upon to clarify the choices made and the validity of the result found.

6.1 Field Study Investigations

Research Relevance

In the field study investigations of Solbjergskolen in Part 1, a currently operating DCV system with cement-bonded wood wool ceiling panels (approximately 15% of ceiling is diffuse/permeable) is assessed in terms of both system functionality and indoor environmental quality. As described in the Literature Study (page 3), only a few other publications seem to have documented similar systems before; Jacobs, P. et al. (2008) and Jacobs, P. and Knoll (2009) and Hviid, C. A. and Terkildsen (2012). Yet, only Hviid, C. A. and Terkildsen (2012) have reported reliable result obtained through thorough analysis of both ventilation effectiveness and indoor environmental impact, however the influence of the pressure chamber (plenum) is not investigated in Hviid, C. A. and Terkildsen (2012) and as such, conclusions about the pressure chamber remains unsupported in literature so far. The only study that have previously reported an evaluation of a DCV system with cement-bonded wood wool ceiling panels is Hviid, C. A. and Terkildsen (2012). This is interesting as such products are widely applied in Danish buildings due to the excellent sound absorption properties, which help to reduce noise and create good acoustics. Hereby, the field study investigation documents a scenario not previously investigated and thus contribute to the approval of DCV systems in general.

Validity of Research Design

The construct validity of the methodology applied (field experiments) is high as the measurements are carried out during true operating conditions in their natural setting. As such, the measurement results reflect what actually happened and how the system performed during the test period. However, as the field experiment is an isolated stand-alone investigation the findings are to some extent only valid for that scenario (sampling validity is low). The initial measurement programme were to be executed for at least three whole school days in both the pilot study and in the main study to create a strong empirical foundation for drawing conclusions that would cover as many stochastically varying phenomena as possible. However, due to practical problems with

the BMS system and hot and bright sunny measurement days, the analyses of the measurement data were reduced to only include measurements from a single day (two days in total, one for the pilot study and one for the main study). This limitation clearly lowers the sampling validity of the findings resulting in less general and predictive validity. This means that it is debatable whether the findings represent the general case or not.

This issue is to some extent dealt with by giving results as dimensionless values and normalizing them for system specific parameters whenever possible (inlet air temperature and CO₂-concentration as well as geometrical dimensions) and thus several of the conclusion will find a broader and more general application. To further increase the knowledge of DCV systems in general during true operating conditions, investigations of systems with other diffuse ceiling panels/tiles needs to be performed. Moreover, assessments should be executed during capacity critical conditions e.g. cold winter days.

The assessment of ventilation effectiveness is carried out based on measurements of air CO₂-concentration. As CO₂-concentration is used as evaluating parameter, and generated by occupants, local peak concentrations inside the test room can occur and must be taken into consideration. Alternatively, effectiveness measurements can be performed using a tracer-gas, which otherwise is not present in the environment. This way any interference is ruled out. However, this methodology was not possible.

Reliability of Measurement Execution

To not artificially reduce instrument reliability and accuracy, all sensors applied are individually calibrated before measurements. In general, measured values are only recorded by one sensor except in critical boundary points where two sensors are utilized to increase reliability. This is the case for measurements of facade inlet and exhaust duct parameters. When two sensors are utilized, their values are averaged. In analyses where measurement points are averaged in space and time, errorbars are given indicating the standard deviation of the varying parameter. This approach is executed when e.g. showing distance-averaged temperature and CO₂-concentration from the facade and when measurement columns are averaged across the room floor. All together measurement reliability is deemed high.

Findings

Results from the field study at Solbjergskolen is generally in good agreement with what is found by Hviid, C. A. and Terkildsen (2012) and in other controlled laboratory experiments. Virtually no risk of draught is observed due to strong preheating of the inlet air inside the plenum and only a low-varying and, generally, uniform temperature and air distribution is detected. However, as the pupils were very active during the measurements (going in and out of the classroom many times a day), it cannot be entirely neglected that they significantly contribute to the perfect air mixing that was observed. For the first time, measurements inside the pressure chamber (on top of diffuse panels) are performed in a building with DCV systems, contributing to the knowledge base of DCV functionality. They show how room air penetrates the suspended ceiling and mixes with fresh air raising the plenum air temperature and CO₂-concentration. This supports the hypothesis that room air distribution is mainly governed by heat loads and thus Archimedes number dependent, which, to some extent disagree with finding by Petersen, S. et al. (2014)

claiming that location, size and strength of heat loads define the airflow pattern, but also that neither vertical air velocity profile, temperature distribution nor ventilation effectiveness can be described by Archimedes number.

The study also reveals that the school has troubles controlling the system satisfactory. The opening of windows efficiently closes the exhaust VAV-damper regulating the airflow resulting in deactivated ventilation. Even though the control of the system has nothing to do with the effectiveness and performance of the DCV system when running, the continuous shifting between activation/deactivation makes it difficult to obtain all the benefits of the DCV principle. Measurements clearly show how IAQ and thermal comfort is worsened when windows are opened, nonetheless, according to the occupants, they find pleasure in actually knowing and feeling the natural ventilation from the windows compared to the 'invisible' and diffuse mechanical ventilation from the ceiling. As such, a psychological factor may influence the actual performance of DCV systems. A solution to this could be to better inform the occupant about how the system operates.

6.2 Experimental Investigations

Research Relevance

In the experimental laboratory investigations in Part 2, a correlation study methodology is applied to investigate whether or not the supply opening area (diffuse ceiling area) of a DCV system has an impact on selected system functionality and indoor environmental parameters. Such analyses serve as documentation for proper design guidelines when selecting future DCV system layouts. No previous studies of such correlations have been found in literature and as such, the research may be characterized as exploratory in nature. However, a working hypothesis is established beforehand to support the analysis; the supply opening area have a significant influence on airflow patterns in both the occupied zone and in the plenum volume.

Validity of Research Design

Construct validity relates to the suitability of the methods applied. The study is constructed around a type of parametric variation, where variations of the investigated variable - the supply opening area of inlet air - is combined with variations of outdoor air temperature (inlet air temperature) and ventilation rate thus varying cooling power. However, because the approach in finding the comfort limited combinations of temperature difference between inlet and outlet together with ventilation rate rely on a trial-and-error procedure, the overall methodology cannot be entirely categorised as parametric variation because that would require the ventilation rate to be systematically varied like the temperature and ceiling layout. This procedure does not affect the validity of the results but only the effectiveness of the experimental work. As such, the research design is overall constructed in a valid and generally accepted way.

The sampling validity, the degree to which the data quantity or coverage is vast, is in general deemed sufficient. Each of the three comfort limited cooling capacity correlations rely on 5 data points (combinations of temperature and ventilation rate). Obtaining the 5 comfort limited combinations requires no more than two experiments for each point - an upper and lower limit combination - one on each side of the borderline to define the uncertainty band

in which discomfort occurs, thus a minimum of 30 experiments is necessary for drawing a 5-point design chart for three different ceiling layouts ($3 \times 5 \times 2 = 30$). The data points cover a range of intake air temperature from -8°C to $+12^{\circ}\text{C}$. A wider range of data points would not significantly increase sampling validity, but increasing the resolution (number of points) would to some extent. Increasing the data set to e.g. 10 points would increase confidence in the correlations being able to predict future outcome or other combinations outside the range of the conducted variations. Especially results obtained in the 18 % case show less reliable correlations and would thus benefit from a larger data quantity. In terms of defining the 5 data points, the trial-and-error methodology resulted in a total of 70 experiments. The gap of 40 experiments between what is the minimum requirements (30 experiments) and what is actually carried out (70 experiments) is a result of the exploratory nature of the investigation; *we did not know where to look*. As such, the sampling validity in terms of ventilation rates examined is vast and sufficient.

Formative validity, the extend to which the results may be used to assess DCV comfort limited capacity in general applications, is a central premise for the usability of the findings. It is a prerequisite for drawing conclusions about the interconnected correlation between the different steady-state combinations, that the same level of overall thermal comfort is retained. Each combination is achieved with a room operative temperature of $22^{\circ}\text{C} \pm 0.2^{\circ}\text{C}$, time-averaged across at least 15 minutes securing also information about variations in the velocity field (see figure 4.10 on page 80). The retention of 22°C at varying cooling power is conducted by adjusting the radiator heat release. This way of simulating the various heat loads (sun radiation, heat transmission etc.) is dubious because during cooling conditions, heat will not be uniformly released from radiators creating high momentum airflows but originate from a combination of sun radiation, heat transmission and internal excess heat all influencing in different ways. The extend to which the radiators influence the airflow pattern is difficult to assess and the problem is not exhaustively addressed in the thesis, however, as the heat loads are large (from approximately $75\text{-}200 \text{ W/m}_{\text{floor}}^2$), powerful and dominating airflows are created. In order to further increase the validity of the results the heat load adjustment could in future investigations be simulated by more realistic means e.g. electric carpets in front of the window, which can better resemble the sun radiation that will cause the cooling needed situation.

Reliability of Measurement Execution

Before measurements, all stationary measurement equipment is individually calibrated and tested securing consistency and accuracy of measurements. Moreover, critical values are measured with more than one sensor to secure internal consistency reliability. This is, i.a., the case with the inlet air temperature at the facade opening, where three thermocouples (TC's) measure the variation across the opening and likewise in the exhaust duct with the use of two TC's. Where more than one sensor is used for measuring the same variable, their values are averaged. Throughout all 70 experiments, the same measurement setup is utilized except for the location of measurement columns, which are changed with the ceiling layout (three scenarios). All together values are measured consistently.

Test-retest reliability is not obtained by redoing the experiments for comparison, but by logging a steady-state sequence of measurements for at least 15 minutes in each experiment. Measurements from each periods are time-averaged into a single steady-state defined value.

The reliability of the experimental facility itself - the hotbox - is, however, questionable. In the cold chamber, fans blow air through a cooling coil to adjust the cold zone temperature (outdoor air). As these fans are located right in front of the facade inlet opening, approximately 2 meters away, they influence the air distribution across the suspended ceiling - this is confirmed from measurements. On this basis, the validity of the results is affected negatively, but as the phenomenon occurs consistently throughout all experiments, data is still comparable. In addition to this temperature cycles are observed in the cold zone due to unsteady air temperature control. An average temperature cycle of 1.30°C is observed throughout all 70 experiments with a standard deviation of 0.96°C . The average time period is approximately 12.5 minutes, which is smaller than the steady-state sampling period of at least 15 minutes.

Findings

Results are generally in good agreement with literature in cases where comparison is meaningful. The conclusion that room airflows and thus draught rating are dominated by heat loads (only the heat release itself and not the location is investigated) and may be described by Archimedes number, is supported by other publications, e.g. in the literature review by Zhang, C. et al.. Moreover, measurements of maximum air speeds show that cold inlet air is forced down in areas with no heat loads, which is also observed in a study of the displacement effects in DCV by Petersen, S. et al. (2014). A strong negative correlation (statistically significant) is also found between the development of room air speeds and Reynolds number, strongest for the 18 % diffuser area. Airflows are still in a developing phase.

The cooling capacity of DCV is found for the three investigated diffuse ceiling areas and are in general high compared to e.g. mixing ventilation. In all cases, high draught ratings showed to be the cooling limiting comfort parameter. Neither PD-indices for temperature gradients, temperature asymmetry nor warm or cold floors are even close to exceed their allowed value. And as air velocities are generally very laminar with low turbulence intensity, high cooling capacities are achievable. The supply opening area do, however, significantly influence the capacity. As the cooling capacity has not been methodically investigated before for similar setups, no meaningful comparison can be made.

6.3 Numerical Investigations

Research Relevance

An analysis of the indoor environmental quality robustness towards changes in boundary conditions and system design parameters is highly relevant. A comprehensive analysis of the influence of the various system parameters is not seen before using experimentally verified numerical predictions. Thus, the research holds great potential for producing new and more detailed correlations between system critical parameters and indoor environmental quality. Similarly to the experimental investigation this investigation is exploratory as no hypotheses is established beforehand.

Validity of Research Design

Computational Fluid Dynamics (CFD) as a numerical calculation approach is in general a valid and accepted method for studying airflow patterns in ventilated rooms and many other fluid flow related problems, thus the construct validity is ensured. Many publications of successful CFD analysis are available studying a huge range of different fluid phenomena, however, for it to be truly trusted as an accepted tool in predicting fluid motion, a reliable documentation of model construction and benchmarking needs performed. As good quality benchmarking data exist from the laboratory experiments, the methodology of using a CFD model for creating the data necessary for a comprehensive robustness analysis is in principle valid.

In terms of criterion-related validity, i.e. comparing experimentally derived test results from chapter 4 with computational outcome, the CFD model is, however, not validated. The assumptions made, especially with regards to heat load modelling and diffuse ceiling modelling, causes the CFD model to produce invalid results. This furthermore means that the intended robustness analysis of DCV system design is not carried out, as results from such an analysis will hold no scientific validity.

The validity of computed results is assessed by comparison with experimental results in 21 measurement points in the test-room (different heights on columns and in exhaust duct). Comparison points are selected to represent the entire room volume hereby representing areas with both high gradients of convective and radiation heat transfer and regions with lesser heat transfer. It is important that benchmarking data used for validation exist for a large number of points in the room to ensure an overall identical solution, and not just point-wise resemblance. For the general flow field, air temperatures and velocities are examined with a relative error in the 21 comparison points ($\mu \pm \sigma$) of $-8\% \pm 18\%$ and $32\% \pm 103\%$, respectively. Especially the computed air velocities diverge a lot from true experimental values. Further investigation of the erroneous flow field show that the source of error mainly originates from:

- Inadequate heat source modelling (manikins)
- Missing diffuse ceiling modelling

Comparison of measured and computed air temperature and velocity inside the thermal plumes above the manikins show extremely high deviations. Computed air velocities are more than 1000% smaller than measured in average above the eight manikins with a standard deviation of approximately 800%. This deviation is caused by wrong heat release modelling from the manikins (prescribed surface heat-flux).

A proper way of including the membrane that make up the permeable/diffuse ceiling panels in the CFD model is not found. As such, the entire DCV system, both plenum and classroom underneath, is treated as a single flow domain. The suspended ceiling is thus created as a horizontal wall with openings for air inlet. This results in an inadequate pressure chamber effect and also a missing diffuse inlet jet. Iqbal, A. et al. (2013) shows however, that by using multi-zone modelling and porous boundary conditions it is possible to simulate pressure resistance correctly through diffuse ceiling panels for unidirectional isothermal flow. To the authors knowledge at the time of writing, publications of successful CFD modelling of DCV systems similar to the experimental setup in this thesis has not been made.

Reliability of Computational results

Reliability of CFD results is first and foremost based on stability/convergence of the applied solver. The same result (with only a small margin of error) must be reached for every identical iteration cycle for the solution to be regarded reliable and thus valid. The ANSYS software used in this thesis (ICEM and FLUENT) is fully capable of computing reliable results for the fluid problems examined. It is important that the numerical mathematics and solution schemes available does not entail errors e.g. roundoff errors. All widely available commercial CFD programming packages are today reliable, however some products are better suited for specific subcategories of CFD, e.g. ventilation flows in buildings. The DCV system is not, however, modelled in other software's as the applied software should suffice.

Findings

The applied modelling of especially geometry and boundary conditions for internal heat sources causes inaccurate representation of measured airflow in the simulated test-room. Subsequently the results produced by the compiled CFD model failed a benchmarking test against measured results from the experimental investigation.

The importance of comprehensive and high-quality benchmarking data is essential in the validation process of simulated results from CFD models and validation of CFD models must always be performed before any valid conclusions can be drawn from such simulations.

The applied CFD software is fully capable of simulating the airflow of the investigated test room and will be adequate for future CFD simulations of similar problems.

6.4 Comparison of Field and Experimental Findings

As CFD simulations gave no valid results these are omitted from the following comparative analyses.

For comparison of results that are dependent on the diffuse ceiling area it is most fair to compare data for the 18 % diffuse ceiling area experiments and the field study (which has 15 % diffuse ceiling area).

Comfort analyses of the two studies show similar results in terms of the investigated parameters related to local discomfort, i.e. for vertical temperature gradient and draught rating, which represent temperature, speed and turbulence intensity of the rooms. It is observed that both studies provide results which fulfil category B from ISO-7730 (2006). As the operative temperature in the experiments is fixed at 22 °C a PMV/PPD comparison of thermal comfort for the body as a whole does not provide any reliable information.

The calculated temperature effectiveness in the occupied zone of both studies shows an effectiveness close to 1.0 when DCV is active. In extension to this observed similarity the vertical temperature gradient of both studies also gives similar results with a temperature difference between ankles and head of 1.0 °C.

Although an identical absolute 6 °C preheating effect is seen from facade inlet to the middle of the plenum air, the normalized preheating offers a much more representative comparison.

A significant difference in preheating can be seen between the two studies when analysing the

total heating of air from facade to exhaust. In the field study 85 % of the total air heating happens in the plenum, while the same number is only 20 % for the experimental setup. Discrepancies can partially be explained by the artificial light armatures installed in the plenum of the field study combined with the lower plenum height, which causes more of the inlet air to come into contact with these heat sources.

6.5 Future Work

DCV systems may be configured in many different ways and present research only document a small amount of possible layouts and internal correlations. As such, many correlations between various system critical parameters and indoor environmental quality and energy consumption remain uncharted. This includes the parameters:

- Plenum dimensions
- Permeable materials and geometry/construction
- Room dimensions
- Exhaust hood layout and location
- Documentation of energy savings using DCV versus more classical ventilation principles

From analyses performed in this thesis the next logical step would be to investigate the combined effect on airflow pattern from varying heat source distribution and diffuse ceiling area. This was intended in this thesis but not performed due to invalid CFD results.

Furthermore the combination of DCV with active cooling or heating in the plenum is worth exploring. Studies of DCV and TABS are currently performed at Aalborg University, and show promising results.

Chapter 7

Conclusion

The overall project conclusion presented in this chapter evaluates the fulfilment of established project goals in the Thesis Statement.

Supporting Objective 1

Based on findings of the initial pilot study and later main study of the DCV system at Solbjergskolen in both a 6th grade and 9th grade classroom, the following conclusions are drawn. The pilot study was conducted in November 2014 and the main study in April 2015 during true operating conditions meaning that measurements of system critical parameters and indoor environment was performed meanwhile actual teaching and lectures were held. As such, the conclusions reflect conditions that were present at time of investigation. It is found that:

- Plenum works as a pressure chamber distributing inlet air equally across the suspended ceiling (15 % cement-bonded wood wool diffuse ceiling panels).
- Plenum air is to a great extent mixed with room air inside the plenum before being pulled down through the suspended ceiling. Between 40-100 % of the final CO₂-concentration is obtained even before the air enters the room.
- Inlet air is preheated 4-5 °C before entering the room, corresponding to 60-90 % of the final temperature increase from facade to exhaust.
- Ventilation inside the classroom resembles mixing ventilation with effectiveness ≈ 1.0 .
- Air movement is characterized by low turbulence with intensities around 15-25 %, even when pupils move around.
- Indoor environmental quality is generally very good with DR < 5 % most of the time. Air temperature difference between head and ankles below 1 °C is normal.

Results are in good agreement with existing knowledge for those values where comparison is meaningful.

Supporting Objective 2

Based on 70 controlled laboratory experiments focusing on parametric variation of the supply opening area and its effect on thermal comfort, the following conclusions are drawn. Correlations are tested with a 5% significance level.

- Design charts are established for three different supply opening areas; 18%, 50% and 100% showing that for smaller supply openings indoor comfort is limited almost only by the ventilation rate and not the temperature of the inlet air.
- Cooling capacity of a DCV system is influenced by the supply opening area, however, no precise and unambiguous correlation is found. Result indicate that the cooling capacity is largely influenced by the layout of the supply opening area in relation to room heat loads. Cooling capacities above $130 \text{ W/m}_{\text{floor}}^2$ seems attainable for all ceiling layouts.
- Draught rating is the limiting discomfort parameter in all three ceiling layout scenarios.
- Ventilation inside the room resembles mixing ventilation with effectiveness around 1.0. The temperature effectiveness is negatively correlated with Archimedes number.
- Airflow pattern is heat load dominated and may be described by Archimedes number. However the airflow pattern is not independent of DCV inlet momentum and can therefore be described by Reynolds number as well.
- Preheating effects in the plenum volume is affected by the supply opening area through a negative correlation. Additionally, it is seen that the temperature distribution in plenum is fully developed 1 m from facade inlet.

Due to invalid computational results from the CFD model the intended robustness analysis is not performed. Future CFD simulations of DCV systems should focus especially on a correct representation of pressure chamber effect in the plenum and the modelling of diffuse ceiling panels in the suspended ceiling. It is concluded that the compiled single-zone model does not represent a correct fluid flow and further studies should focus on multi-zone modelling capable of bidirectional non-isothermal flow through the diffuse ceiling.



Part 4

References and Nomenclature

Bibliography and listed overview of symbols, figures and tables.

Bibliography

- ANSYS. *ANSYS Help Viewer - Definition of cell skewness*. Version 15.0. SAS IP, 2013.
- Artmann, N., R. Vonbank, and R. Jensen. *Temperature measurements using type K thermocouples and the Fluke Helios Plus 2287A data logger*. Technical Report 052, Indoor Environmental Engineering Research Group, Department of Civil Engineering, Aalborg University, 2008. ISSN: 1901-726X.
- Ayyub, B.M. and R. McCuen. *Probability, Statistics and Reliability for Engineers and Scientists*. CRC-Press Taylor & Francis Group, 3rd edition, 2011. ISBN 978-1-4398-0951-8.
- Bascon-A/S. *Technical Drawings of Solbjerg Skole, Window replacement etc.*, N.A. Drawings not published by Bascon.
- BR10. *Danish Building Regulations 2010*. Danish Enterprise and Construction Authority, 2010. ISBN 978-87-92518-60-6.
- Casey, M. and T. Wintergerste. *ERC OFTAC - Best Practice Guidelines, Version 1.0*. Special Interest Group on Quality and Trust - Industrial CFD. European Research Community On Flow, Turbulence And Combustion, 2000.
- Cedar Crest College. *Correlation Coefficient*, 2015. URL <http://www2.cedarcrest.edu/academic/bio/hale/biostat/session24links/corrcoeff.html>. Accessed: 05th June 2015.
- DS-474. *Code for Thermal Indoor Climate*. Dansk Standard, 1995. ICS: 91.120.40.
- DuBois, D. *A formula to estimate the approximate surface area if height and weight be known*. *Archives of Internal Medicine*, 17:863–871, 1916.
- EN-13829. *Thermal Performance of Buildings - Determination of air permeability of buildings*. European Committee for Standardization, 2001. ICS: 91.120.10.
- EN-14240. *Ventilation of Buildings - Chilled Ceilings - Testing and Rating*. European Committee for Standardization, 2004. ICS: 91.140.30.
- EN-15251. *Indoor environmental input parameters for design and assessment of energy performance of buildings addressing indoor air quality, thermal environment, lighting and acoustics*. European Committee for Standardization, 2007. ICS: 91.040.01.
- Fanger, P. O. *Thermal comfort: analysis and applications in environmental engineering*. Danish Technical Press, Copenhagen, 1st edition, 1970. ISBN 87-571-0341-0.

- Hviid, C. A. and S. Terkildsen. *Experimental study of diffuse ceiling ventilation in classroom*. Proceedings of 33rd AIVC conference, 2012.
- Hyldgaard, C. E. *Thermal Plumes Above a Person*. Dept. of Building Technology and Structural Engineering., Aalborg University, 1999.
- Iqbal, A., H. Kazimi, S. Rahimi, and A. Afshari. *Use of perforated acoustic panels as supply air diffusers in diffuse ceiling ventilation*. SBI 2013:12. Statens Byggeforskningsinstitut, 1st edition, 2013. ISBN 778-87-92739-33-9.
- ISO-7726. *Ergonomics of the Thermal Environment - Instruments for Measuring Physical Quantities*. International Organization for Standardization, 2nd edition, 1998. ICS: 13.180.
- ISO-7730. *Ergonomics of the thermal environment - Analytical determination and interpretation of thermal comfort using calculation of the PMV and PPD indices and local thermal comfort criteria*. International Organization for Standardization, 3rd edition, 2006. ICS: 13.180.
- Jacobs, P. and B. Knoll. *Diffuse ceiling ventilation for fresh classrooms*. Proceedings of 4th Symposium on Building and Ductwork Air tightness, 2009.
- Jacobs, P., E. Van Oeffelen, and B. Knoll. *Diffuse ceiling ventilation, a new concept for healthy and productive classrooms*. Proceedings of Indoor Air, 2008.
- Kristensen, M. H., J. Jensen, and R. Jensen. *Air Temperature Measurements Using Dantec Probes*. Technical Report 189, Indoor Environmental Engineering Research Group, Department of Civil Engineering, Aalborg University, May 2015. ISSN: 1901-726X.
- Nielsen, P. V. *Lecture Notes on Mixing Ventilation*. Department of Building Technology and Structural Engineering, Aalborg University, 1995. ISSN 0902-8005 U9513.
- Nielsen, P. V., F. Allard, H. Awbi, L. Davidson, and A. Schälín. *Computational Fluid Dynamics in Ventilation Design*. REHVA Guidebook nr. 10. Federation of European Heating and Air-conditioning Associations, 2007. ISBN 2-9600468-9-7.
- Oberkampf, W. L. and T. Trucano. *AIAA - Verification and Validation in Computational Fluid Dynamics*. Unlimited Release. Sandia National Laboratories, 2002.
- Petersen, S., N. Christensen, C. Heinsen, and A. Hansen. *Investigation of the displacement effect of a diffuse ceiling ventilation system*. *Energy and Building*, 85:265–274, 2014.
- SBI-130. *Måling af termisk indeklime*. Statens Byggeforskningsinstitut - Aalborg Universitet, 1983. ISBN 87-563-0483-8.
- Simone, A., J. Babiak, M. Bullo, G. Landkilde, and B. Olesen. *Operative temperature control of radiant surface heating and cooling systems*. DTU Copenhagen, 2007. Proceedings of Clima 2007 Wellbeing Indoors.
- Stampe, O. B., H. Hansen, and P. Kjerulf-Jensen. *Varme- og Klimateknik - Grundbog*. Danvak APS, 3rd edition, 2006. ISBN 87-982652-8-8.

- Troldtekt. *Troldtekt Installation instructions*, 2015. URL http://www.troldtekt.dk/~media/Files/Installation%20instructions/Troldtekt/Danish/Troldtekt_K0_K5_K5V_K11_C60_dk.pdf. Accessed: 16th Feb.
- Troldtekt. *Pressure loss data for Troldtekt ceiling panels*. Unpublished, N.A.
- Versteeg, H. K. and W. Malalasekera. *An Introduction to Computational Fluid Dynamics*. Pearson Education Limited, 2nd edition, 2007. ISBN 978-0-13-127498-3.
- Zhang, C. and T. Yu. *Experimental report - Natural Cooling and Ventilation through Diffuse Ceiling Supply and Thermally Activated Building Constructions*. Department of Civil Engineering, Aalborg University, November 2014. Part of PSO-project 345-061. Unpublished.
- Zhang, C., P. Heiselberg, and P. Nielsen. *Diffuse ceiling ventilation: A review*. Unpublished.
- Zhang, C., T. Yo, P. Heiselberg, and M. Pomianowski. *Experimental Study of an Integrated System with Diffuse Ceiling Ventilation and Thermally Activated Building Constructions*. Technical Report 182, Indoor Environmental Engineering Research Group, Department of Civil Engineering, Aalborg University, 2014. ISSN: 1901-726X.
- Zukowska, D., A. Melikov, and Z. Popiolek. *Impact of geometry of a sedentary occupant simulator on the generated thermal plume: Experimental investigation*. *HVAC&R Research*, 18(4), 2012. ISSN: 1078-9669.

Nomenclature

Abbreviations

AHU	Air Handling Unit
BMS	Building Management System
CAV	Constant Air Volume
CFD	Computational Fluid Dynamics
DC	Diffuse Ceiling
DCV	Diffuse Ceiling Ventilation
DR	Draught Rating
DV	Displacement Ventilation
HVAC	Heating, Ventilation and Air Conditioning
IAQ	Indoor Air Quality
IEQ	Indoor Environmental Quality
MV	Mixing Ventilation
OZ	Occupied Zone
PMV	Predicted Mean Vote
PPD	Predicted Percentage Dissatisfied
TABS	Thermally Activated Building Systems
TC	Thermocouple
VAV	Variable Air Volume

Symbols (greek)

α	Thermal diffusivity or significance level	m^2/s or –
β	Thermal expansion coefficient	$1/\text{K}$
δ	Uncertainty or deviation	–
Δ	Absolute difference	–
ε	Effectiveness	–
λ	Thermal heat conductivity	$\text{W}/(\text{mK})$
ν	Kinematic viscosity	m^2/s
ρ	Density or correlation coefficient	kg/m^3 or –
σ	Standard deviation	–
ϕ	Heat flux (rate of change of heat energy per unit area)	W/m^2 or –
Φ	Heat flow (time rate of change of heat energy)	J/s or W

Symbols (latin)

A	Area	m^2
ACR	Air Change Rate	h^{-1}
Ar	Archimedes number	–
BSA	Body Surface Area	m^2
C	Heat capacity	J/K
c	Concentration, e.g. CO ₂ -conc.	ppm
c_p	Specific heat capacity	J/(kgK)
d	Diameter or depth dimension	m
DR	Draught Rating	%
g	Acceleration of gravity	$9.81 m/s^2$
h	Height dimension	m
I	Momentum flow (time rate of change of momentum)	N
i	Index number	–
l	Length dimension	m
m	Mass	kg
\dot{m}	Mass flow (time rate of change of mass)	kg/s
n	Number in sequence	–
P	Momentum	Ns
p	Pressure	Pa
q	Volume flow or airflow (time rate of change of volume)	m^3/s
Q	Energy	J or kWh
R	Thermal Resistance	$(m^2K)/W$
r	Radius	m
Re	Reynolds number	–
RH	Relative Humidity	–
SFP	Specific Fan Power	kJ/m^3
T	Temperature	K or °C
t	Time	s
Tu	Turbulence Intensity	%
U	Heat transmission coefficient	$W/(m^2K)$
u	Air speed or air velocity component in x-direction	m/s
V	Volume	m^3
v	Air velocity component in y-direction	m/s
w	Air velocity component in z-direction	m/s
x	Length in x-direction	m
y	Length in y-direction	m
z	Length in z-direction	m

Subscripts and Superscripts

*	Dimensionless or Normalized
2nd floor	2nd floor (room above test room)
abs	Absolute
air	Room air
avg	Average
ceiling	Ceiling of room
comp	Computed value from CFD-simulation
cr	Critical value
DC	Diffuse Ceiling
exhaust	Exhaust opening
facade	Facade inlet
floor	Floor
guard	Guarded zone
head/ankles	Measure between head and ankle height of a human
i	Index number
inlet	Inlet flow
j	Index number
local	Local point or measurement point
manikin	Human Body Simulator / Thermal manikin
max	Maximum
meas	Measured value
min	Minimum
n	Number in sequence
o	Omnidirectional value
out	Outdoor air
outlet	Outlet flow
plenum	Plenum above diffuse ceiling
plume	Uprising plume above heat emitting object
pr	Radiant temperature asymmetry
rad	Radiator
ref	Reference
rel	Relative
room	Room or room operative temperature
surf	Surface
T	Temperature
trans	Transmission
v	Ventilation or ventilation system
vel	Velocity
wall	Wall
win	Window

List of Figures

1.1	Four different types of air distribution systems.	2
1.2	Sketch defining DCV parameters.	8
1.3	Exemplary design chart.	12
1.4	Correlation of data.	18
2.1	Location of case site: Solbjergskolen, Denmark.	26
2.2	Cross-sectional sketch of DCV system in classroom.	27
2.3	Picture of classroom facade.	27
2.4	Technical drawings of ventilation inlet and exhaust.	28
2.5	Top-view of suspended ceiling layout in 6th grade classroom.	28
2.6	Cement-bonded wood wool ceiling panels.	29
2.7	Plenum above suspended ceiling.	29
2.8	Flow diagram of BMS logic control for DCV on room level.	30
2.9	PI-diagram of BMS control connections on room level.	31
2.10	Eltek GC10 wireless transmitter attached to diffuse ceiling panel.	33
2.11	Eltek GD47 wireless transmitter located in exhaust opening.	33
2.12	Sketch of three moveable measurement columns and the attachment of sensors.	34
2.13	Sketch of the classroom divided into 9 possible column locations.	35
2.14	Location of moveable measurement column in classroom.	35
2.15	Air current tube used for visualising air distribution.	36
2.16	Presence of people during pilot study.	37
2.17	Air temperature underneath ten diffuse ceiling panels.	39
2.18	Air temperature profiles across plenum.	40
2.19	Air CO ₂ -concentration in two heights heights in the classroom.	41
2.20	Ventilation effectiveness for two heights in the classroom.	42
2.21	Mean air speeds and turbulence intensity.	42
2.22	Air temperature in different heights in the classroom.	43
2.23	Air temperature effectiveness in different heights and locations in the classroom.	44
2.24	Air temperature profiles in classroom.	44
2.25	Draught rating in different heights and locations in the classroom.	45
3.1	Top-view of suspended ceiling layout in 9th grade classroom.	48
3.2	Protecting steel frame used for outdoor air measurements.	49
3.3	Eltek GD47 wireless transmitter located above diffuse ceiling panel.	50
3.4	Outdoor air temperature and CO ₂ -concentration.	51
3.5	Presence of people and periods with open windows and doors.	52

3.6	CO ₂ -concentration above eight diffuse ceiling panels.	53
3.7	CO ₂ -concentration profiles across plenum.	54
3.8	Air temperature above eight diffuse ceiling panels.	55
3.9	Air temperature profiles across plenum.	56
3.10	Location of measurement columns (C1, C2 and C3).	57
3.11	CO ₂ -concentration in different heights and locations in the classroom.	57
3.12	Ventilation effectiveness, based on CO ₂ , in classroom	58
3.13	Mean air speeds and turbulence intensity.	59
3.14	Air temperature in different heights in the classroom.	60
3.15	Air temperature profiles in classroom.	61
3.16	Temperature effectiveness in different heights and locations in the classroom.	61
3.17	Draught rating in different heights and locations in the classroom.	62
4.1	Cross sectional view of hotbox.	69
4.2	Floor plan of hot chamber in the experimental setup.	71
4.3	Troldtekt acoustic ceiling panels.	71
4.4	Mounting system of diffusive Troldtekt ceiling panels.	72
4.5	Thermal manikins and heating elements.	73
4.6	Placement of thermal manikins in the experimental setup.	74
4.7	Pictures from inside the testroom of the hot chamber.	74
4.8	Electrical radiator used for adjusting heat release.	75
4.9	Pressure box setup for testing of air permeability.	77
4.10	Air velocities in occupied zone during temperature steady conditions.	80
4.11	Three diffuse ceiling layouts	82
4.12	Reduced diffuse ceiling area by fitting a vapour barrier on room side of ceiling panels.	82
4.13	Top view of measurement points in the plenum.	84
4.14	Pictures of plenum and exhaust duct.	85
4.15	Measurement columns.	86
4.16	Dantec and globe sensors on column.	87
4.17	Measurement points for surface temperature.	87
4.18	Placement of measurement columns for three ceiling layouts.	88
4.19	Statistical representation of measured room operative average temperatures.	92
4.20	Draught rating readings in occupied zone in delimiting cases.	94
4.21	Vertical air temperature gradients in three different ceiling layout configurations	95
4.22	Design Chart for 100%, 50% and 18% diffuse ceiling area.	96
4.23	Cooling Capacity per floor area as function of temperature difference.	97
4.24	Cooling Capacity per diffuse ceiling area as function of temperature difference.	97
4.25	Air permeability test of "ultra-fine" structured Troldtekt ceiling panels.	99
4.26	Crack-flow through suspended ceiling for different degrees of diffuse ceiling area.	100
4.27	Pressure drop as function of distance from facade intake.	101
4.28	Plenum air temperature profile for the different ceiling layouts.	102
4.29	Normalized plenum air temperature as function of normalized diffuse ceiling area.	103
4.30	Plenum heat-up as function of Re and Ar.	104
4.31	Embedded momentum flow in DCV inlets as function of ventilation rate.	106
4.32	Exhaust driven velocity as function of distance for four different airflow rates.	108

4.33	Plane-sectional view of test room showing location of maximum air speeds.	109
4.34	Cross-sectional view of test room showing location of maximum air speeds.	109
4.35	Absolute and normalized air speed gradients.	111
4.36	Normalized maximum air speed in occupied zone vs. dimensionless diffuse ceiling area.	112
4.37	Dimensionless maximum air speed in occupied zone vs. Reynolds number	113
4.38	Normalized maximum air speed in occupied zone vs. Archimedes number.	114
4.39	Maximum air speed in occupied zone vs. heat release.	115
4.40	Temperature effectiveness gradient.	116
5.1	Variations of heat source distribution.	120
5.2	Variations of diffuse ceiling inlet distributions for 50 % diffuse ceiling.	121
5.3	Variations of diffuse ceiling inlet distributions for 18 % diffuse ceiling.	121
5.4	Geometry of CFD model with thermal manikins and 18 % diffuse ceiling.	125
5.5	Mesh prism-layer around thermal manikin necessary to account for boundary layer .	126
5.6	Cross-sectional view of mesh showing tet-boundary cells and hex-core mesh.	127
5.7	Plotted residual values for flow equations.	132
5.8	Normal distribution of absolute temperature error for computed results.	135
5.9	Normal distribution of absolute velocity error for computed results.	135
5.10	Computed air temperatures for selected cross sections. Scale is in degree celsius. . .	136
5.11	Computed air temperatures for selected cross sections. Scale is in degree celsius. . .	136
5.12	Computed air velocity for cross section through and over manikins.	137
5.13	Computed air velocity for cross section with inlet and outlet.	138
5.14	Geometry of alternative ventilation inlet modelling.	140
A.1	Eltek GD10 (left) and GD47 (right) telemetry transmitters.	4
A.2	ALS F200 Precision Thermometer and Innova 1412 Photoacoustic Field Gas-Monitor. .	5
B.1	Technical drawing of thermal manikin used in experimental investigations.	10
B.2	256-point measurement grid for investigation of plume.	13
B.3	Thermographic picture of manikin construction.	14
B.4	Schlieren pictures of manikin plume.	15
B.5	Contour plot of plume air velocity generated by manikin.	16
B.6	Contour plot of air excess temperature generated in manikin plume.	16
B.7	Air speed and temperature profiles in surroundings for plume experiment.	17
B.8	Air speed and temperature variations in surroundings 1.8 m above floor.	18
B.9	Gaussian distributions of plume air speed and excess temperature.	19
B.10	Component Setup for temperature measurements.	20
B.11	Orifice plate used in experiments to determin ACR.	22
B.12	Chart for hypothesis test of the significance of a correlation.	24

List of Tables

1.1	Categories of thermal environment.	10
1.2	Strength of correlations.	18
2.1	Setup of three moveable measurement columns.	34
2.2	Location of moveable columns in classroom during the measurement period.	41
4.1	Dimensions of experimental test facility.	70
4.2	Experimental data with 100 % diffuse ceiling area.	90
4.3	Experimental data with 18 % diffuse ceiling area.	91
4.4	Experimental data with 50 % diffuse ceiling area.	91
4.5	Experimental data used for defining comfort limited cooling capacity.	93
4.6	Momentum flows generated by different sources.	105
5.1	Overview of Robustness Analysis parametric variations.	122
5.2	Mesh quality data.	128
5.3	Boundary conditions for experiment number 41 used for validation of CFD model.	131
5.4	Deficits of flow equations for convergence assessment.	131
5.5	Comparison of simulated and measured values of air temperature and velocity.	134
5.6	Comparison of thermal plume data for simulated and measured results.	139
A.1	Transmitter specification for Eltek GD10 and GD47.	4
A.2	ALS F200 Precision Thermometer specifications.	5
A.3	Innova 1412 Photoacoustic Field Gas-Monitor specifications for measuring CO ₂	5
A.4	Calibration expressions for Eltek transmitters.	6
A.5	Calibration expressions for Eltek transmitters, continued.	7
B.1	Manikin surface temperatures.	14
B.2	Geometrical data of manikin plume.	17
B.3	Integral characteristics of manikin plume.	19
B.4	Spearman rank correlation coefficients.	24

Part 5

Appendix Report

Content supporting and elaborating on the work in the thesis.

Appendix A

Field Investigations

The following appendix contains description of the Eltek data logging system and calibration used for measurements during the field study investigations at Solbjergskolen.

Individual calibration for each sensor used in the field investigations is performed in controlled setups at Department of Civil Engineering, Aalborg University.

For detailed descriptions of the remaining measurement equipment used in the field investigations see Kristensen, M. H. et al. (2015).

A.1 Temperature and CO₂ measurements

Description of Equipment

The Eltek GenII monitoring system provides wireless data logging of wide range of applications. The system used consists of Eltek telemetry transmitters and Eltek receiver/logger.

Two different Eltek telemetry transmitters is used:

- GC10 transmitter with build-in digital RH and temperature sensors
- GD47 transmitter with build-in digital RH, temperature and CO₂ sensors

The transmitters are depicted below with specifications in the table.



Figure A.1: Eltek GD10 (left) and GD47 (right) telemetry transmitters.

Table A.1: Transmitter specification for Eltek GD10 and GD47.

Transmitter	Sensors	Range	Resolution	Accuracy
GC10	RH	0% to 100%	0.1%	2%
	Temperature	-30 °C to +65 °C	0.1 °C	0.4 °C
GD47	RH	0% to 100%	0.1%	2%
	Temperature CO ₂	-30 °C to +65 °C 0 ppm to 5000 ppm	0.1 °C 3%	0.4 °C 50 ppm

Calibration

In order to ensure a uniform calibration all the sensors have been batch calibrated. This has been done in a hotbox, which is a controlled enclosure as the one used for experimental investigations

in part 2 of the thesis. The hotbox is an insulated room with controllable air temperature and ventilation rate (re-circulation within the room).

For temperature calibration, a reference temperature has been recorded using a ALS F200 Precision Thermometer with specifications listed in table A.2.

Table A.2: ALS F200 Precision Thermometer specifications.

Range	Resolution	Accuracy	Stability
-200 °C to +850 °C	0.001 °C	0.01 °C over full range	0.005 °C per year

A total of 4 calibration points for temperature have been carried out. They are: 31.06 °C, 24.82 °C, 22.81 °C and 17.26 °C. Corresponding Eltek measurements has been used to create a calibration expression for each transmitter based on linear regression. These are listed below in table A.4 and A.5.

For CO₂ calibration, a reference gas concentration has been recorded using an Innova 1412 Photoacoustic Field Gas-Monitor with specifications listed in table A.3.



Figure A.2: ALS F200 Precision Thermometer and Innova 1412 Photoacoustic Field Gas-Monitor.

Table A.3: Innova 1412 Photoacoustic Field Gas-Monitor specifications for measuring CO₂.

Range	Resolution	Accuracy	Calibration
0 ppm to 75 000 ppm	0.001 ppm	0.75 ppm over full range	October 2014 at AAU

The gas-monitor has initially been calibrated using a 0 ppm and a 1000 ppm CO₂ calibration gas in accordance with the manufacturers specifications. In order to calibrate the Eltek sensors pure CO₂ has been injected into the hotbox. A total of 3 calibration measurements of CO₂ has been done. Corresponding measurements from Eltek sensors and the Innova gas-monitor has been used for calculating the calibration expression. These are listed below in table A.4.

Table A.4: Calibration expressions for Eltek transmitters.

Serial number	Transmitter	Sensor	Calibration expression ($y=ax+b$)	
			a	b
T-8878	GC10	Temperature	1.0327	-0.7736
T-8880	GC10	Temperature	1.0546	-1.6389
T-8882	GC10	Temperature	1.0625	-1.9096
T-8883	GC10	Temperature	1.0697	-2.2161
T-8884	GC10	Temperature	1.0389	-0.9447
T-8885	GC10	Temperature	1.0545	-1.8446
T-8896	GC10	Temperature	1.0509	-1.6314
T-8897	GC10	Temperature	1.0705	-1.9151
T-9042	GC10	Temperature	1.0311	-1.2127
T-9043	GC10	Temperature	1.0625	-2.2882
T-9044	GC10	Temperature	1.0467	-1.6254
T-9046	GC10	Temperature	1.0545	-1.8446
T-9047	GC10	Temperature	1.0545	-1.4228
T-9048	GC10	Temperature	1.0632	-1.9082
T-9049	GC10	Temperature	1.0389	-1.2564
T-9050	GC10	Temperature	1.0636	-1.7411
T-9052	GC10	Temperature	1.0304	-0.8903
T-9053	GC10	Temperature	1.0411	-1.2377
T-9054	GC10	Temperature	1.0538	-1.9320
T-9055	GC10	Temperature	1.0457	-1.2635
T-9056	GC10	Temperature	1.0621	-1.9973
T-9057	GC10	Temperature	1.0705	-2.1292
T-10599	GD47	Temperature	1.0227	-0.5321
T-12092	GD47	Temperature	1.0289	-0.7588
T-13431	GD47	Temperature	1.0155	-0.4360
T-13432	GD47	Temperature	1.0145	-0.0064
T-13433	GD47	Temperature	1.0071	-0.1846
T-13438	GD47	Temperature	1.0080	-0.1775
T-13439	GD47	Temperature	1.0078	-0.1786
T-13441	GD47	Temperature	1.0133	-0.4594
T-13845	GD47	Temperature	0.9956	0.1293
T-13853	GD47	Temperature	1.0142	-0.7101
T-13856	GD47	Temperature	1.0033	-0.1489
T-13860	GD47	Temperature	1.0161	-0.8348
T-13862	GD47	Temperature	1.0093	-0.2029

Table A.5: Calibration expressions for Eltek transmitters, continued.

Serial number	Transmitter	Sensor	Calibration expression ($y=ax+b$)	
			a	b
T-13867	GD47	Temperature	1.0157	-0.5319
T-9193	GD47	Temperature	1.0449	-0.8195
T-9198	GD47	Temperature	1.0386	-1.0346
T-9199	GD47	Temperature	1.0202	-0.1705
T-9265	GD47	Temperature	1.0239	-0.8607
T-9274	GD47	Temperature	1.0500	-1.8619
T-9275	GD47	Temperature	1.0315	-0.9246
T-9297	GD47	Temperature	1.0161	-0.6475
T-9303	GD47	Temperature	1.0155	-0.7359
T-9310	GD47	Temperature	1.0553	-1.8616
T-10599	GD47	CO2	0.966	-34.292
T-12092	GD47	CO2	0.996	45.452
T-13431	GD47	CO2	0.943	-5.755
T-13432	GD47	CO2	0.994	121.668
T-13433	GD47	CO2	0.963	69.262
T-13438	GD47	CO2	0.977	-30.889
T-13439	GD47	CO2	0.936	-10.534
T-13441	GD47	CO2	0.930	-51.512
T-13845	GD47	CO2	0.924	-44.924
T-13853	GD47	CO2	0.930	-183.029
T-13856	GD47	CO2	1.001	-34.707
T-13860	GD47	CO2	0.929	-58.233
T-13862	GD47	CO2	0.964	-15.079
T-13867	GD47	CO2	0.955	6.840
T-9193	GD47	CO2	0.957	-7.908
T-9198	GD47	CO2	0.945	-42.328
T-9199	GD47	CO2	0.931	6.042
T-9265	GD47	CO2	0.933	-28.901
T-9274	GD47	CO2	0.922	18.110
T-9275	GD47	CO2	0.934	39.296
T-9297	GD47	CO2	0.992	57.285
T-9303	GD47	CO2	0.928	-39.888
T-9310	GD47	CO2	0.929	-2.783

Appendix B

Experimental Investigations

This appendix contains a detailed description of the measurement equipment used in the Hotbox measurements described in Part 2. To ensure precision in measurements and hereby being able to conduct valid analyses based on correct results, and to characterize other installations essential to the experimental setup numerous sub-analyses has been made for various components used in the investigations. Individual calibration has been performed for the vast majority of the sensors in the setup, and for those where it has been neglected the use of high precision measurement equipment has made additional calibration obsolete.

B.1 Assessment of Thermal Manikin Construction

Thermal characteristics of the barrel-constructed human body simulators (thermal manikins) are in the following investigated experimentally. The results are used in assessing the reliability of the experimental results obtained in Part 2, Section 4.4 of the thesis. Moreover, they are also used in assessing the setup of the CFD-model in Part 2, Chapter 5.

The manikin is evaluated based on two investigated parameters:

- Radiation properties of barrel surface
- Convective properties of thermal plume above manikin

Manikin Construction

The manikin is constructed based on guidelines in EN-14240 (2004). It is made of 1.0 m high $\text{Ø}300$ mm ventilation ducts as depicted in figure B.1. As recommended by the standard the outer surface of the barrel is painted black to achieve an emissivity of 0.9, which should ensure correct radiation properties.

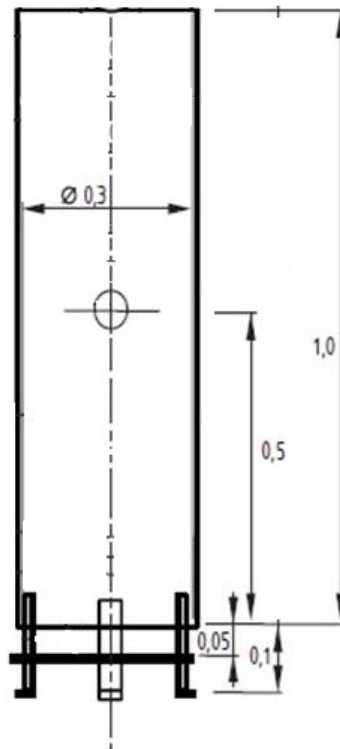


Figure B.1: Technical drawing of thermal manikin used in experimental investigations. All lengths in meter.

Some differences to what is proposed in EN-14240 (2004) has been made to the construction of the manikin. Instead of three 60 W light bulbs, a single electrical heating element of 250 W is

mounted in the middle of the barrel. The heat release of the heating element can be continuously regulated from 0-250 W for each manikin. Additionally, the holes in the top of the cylinder was not made, as these, based on experience of a third party, cause too high convective airflow out of the top of the manikin.

The barrel-construction is evaluated and compared to the results found by Zukowska, D. et al. (2012) and Hyldgaard, C. E. (1999) based on measurements above the manikin. The cited data-sources uses very detailed thermal manikins to simulate a person.

Heat Release to Simulate Children

As it is desired to duplicate the heat sources of the field investigations in Part 1 in the experimental investigations in Part 2, the heat release of each manikin must correspond to that of a elementary school pupil.

In order to simulate a heat release equal to the one from the pupils of a Danish classroom it is necessary to calculate it explicitly as the values proposed in DS-474 (1995) only apply for adults.

The observed activity level of the pupils during lessons in the field study is 1.2 MET approximately equal to 70 W/m² body surface (DS-474, 1995). Calculation of the Body Surface Area (BSA) is done using the Du Bois-formula (equation B.1) (DuBois, D., 1916) based on observed average values of height, H , and weight, W of the pupils.

$$BSA = 0.007184 \cdot W^{0.425} \cdot H^{0.725} \quad (\text{B.1})$$

With an average height and weight of approximately 150 cm and 50 kg, respectively, the BSA equals 1.43 m². The effective sensible human heat load that is released to the indoor air make up approximately 80 % of the total release, cf. Stampe, O. B. et al. (2006), which is what the thermal manikins should resemble. From these known quantities the heat release of each manikin is calculated in equation B.2.

$$\Phi_{manikin} = 70 \text{ W/m}^2 \cdot 1.43 \text{ m}^2 \cdot 80 \% \approx 80 \text{ W} \quad (\text{B.2})$$

This heat release is kept constant throughout the plume investigations and it is assured prior to measurements that the manikin has reached a steady-state heating level where surface temperatures of the barrel are constant.

Methodology and Instrumentation

The methodology applied in investigations of the surface properties and the thermal plume properties is outlined below. Similar for both investigations are that the Hotbox test facility, described in Part 2, is used without any forced ventilation.

Radiation Properties: Surface Temperature

The surface temperature of the manikin is recorded using a thermographic camera to investigate the uniformity of the heat release. Moreover, ambient conditions are measured simultaneously so relative excess temperatures can be assessed if needed.

Convection Properties: Thermal Plume

The convective performance of the thermal manikin is evaluated based on the steady-state shape of the thermal plume generated 0.7 m above the manikin (and 1.8 m above the floor) and the integral characteristics of the plume. These are; volumetric flow, momentum flow and heat flow. The shape is assessed in relation to temperature and velocity. From the equations below, the integral characteristics are defined.

$$\text{Volumetric Flow [m}^3/\text{s]} : q_z = \sum_{i=1}^n v_{z,i} \cdot \Delta A_i \quad (\text{B.3})$$

$$\text{Momentum Flow [N]} : I_z = \rho \cdot \sum_{i=1}^n v_{z,i}^2 \cdot \Delta A_i \quad (\text{B.4})$$

$$\text{Heat Flow [W]} : \Phi_z = \rho \cdot c_p \cdot \sum_{i=1}^n \Delta T_i \cdot v_{z,i} \cdot \Delta A_i \quad (\text{B.5})$$

Measurements necessary for calculating the evaluative parameters are; air temperature inside the plume, $T_{plume,i}$, air temperature of the surroundings, T_{air} .

Together they express the excess air temperature in the plume, ΔT_i , and the upwards velocity component (z-direction) inside the plume, $v_{z,i}$. These quantities are measured in a 1.5 m x 1.5 m square plane 0.7 m above the manikin. The measurements are carried out in a 16 x 16 point orthogonal grid ($x \times y$), giving a total of 256 measurement points, n (see figure B.2). They are performed using 16 Dantec 54R103 probes, equally distributed with an internal distance of 0.1 m along a line in a frame resulting in an elementary cross-sectional plume area, ΔA_i , of 0.1 m². The probes record for 5 minutes after which the frame is moved 0.1 m to its next position, $x + 1$. As documented in Kristensen, M. H. et al. (2015), and adopted in this experimental investigation, the Dantec anemometers must be placed perpendicular to the dominating flow direction, which here is upwards as no forced ventilation is utilised in the measurements.

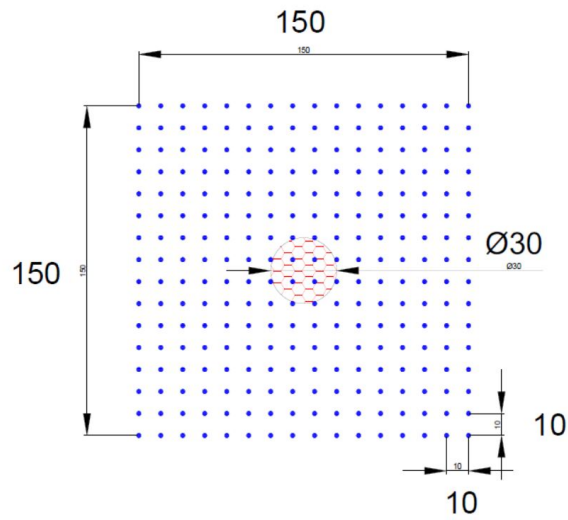


Figure B.2: 256-point measurement grid for investigation of plume 0.7 m above thermal manikin. Manikin position is sketched in the grid centre. All lengths in centimeter.

The surrounding boundary conditions are measured using a column with probes in 0.1 m, 0.6 m, 1.1 m, 1.8 m and 2.3 m above the floor. The measured surrounding air temperature, T_{air} , used in the calculations of the thermal plume is the one measured in 1.8 m above floor, equivalent to the measurement height above the manikin.

Results and Analysis

Surface Temperatures

A thermographic image of the manikin construction is seen from figure B.3 below when supplied with 80 W. Measured surface temperatures in evaluation points are given in table B.1.

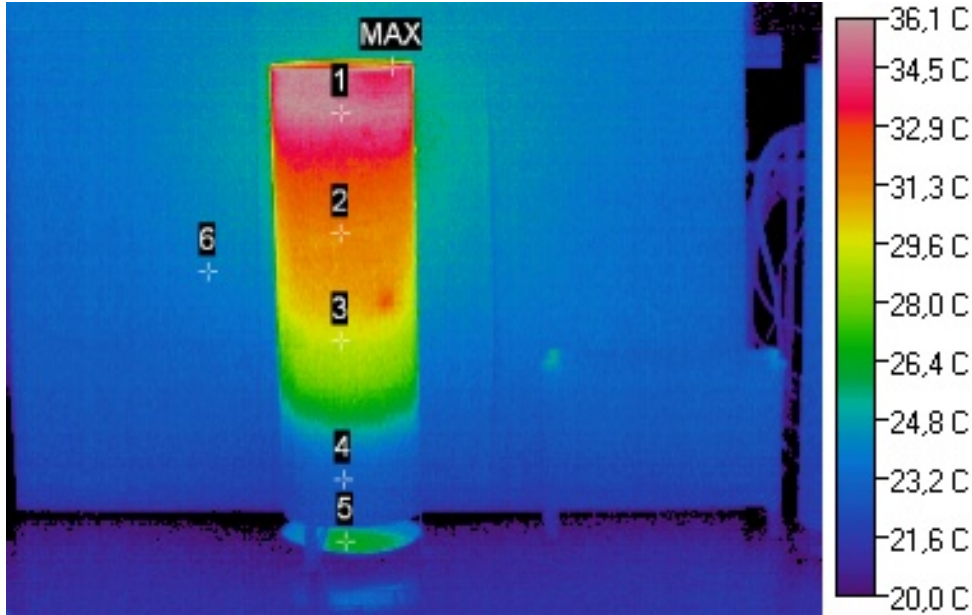


Figure B.3: Thermographic picture of manikin construction.

Table B.1: Manikin surface temperatures.

Measurement Point	Surface Temperature T_{surf} [$^{\circ}C$]
MAX	37.4
Point 1	35.5
Point 2	31.9
Point 3	29.7
Point 4	22.8
Point 5	26.8
Point 6	24.1

A maximum surface temperature of approximately $37.5^{\circ}C$ is measured on the top plate of the manikin. Generally, temperatures are highest in the top part of the manikin as illustrated in figure B.3. A temperature gradient of approximately $10^{\circ}C$ is observed between top and bottom of the manikin surface. The average body skin temperature of a human being is approximately $33.8^{\circ}C$ with most parts of the skin surface ranging between $32-34^{\circ}C$, which corresponds to the averaged surface temperature observed on the thermal manikin.

Thermal Plume

Schlieren imaging - Qualitative investigation Based on schlieren imaging of the air movement around the manikin, a very thin upward moving boundary layer is observed around the manikin, which transforms into a turbulent plume when reaching the top. The turbulence is observed in terms of flow separation and vortex shedding. Pictures of the schlieren imaging is shown in figure B.4, where surrounding air temperature is measured to be 23.8 °C. The pictures capture 550 mm x 550 mm.

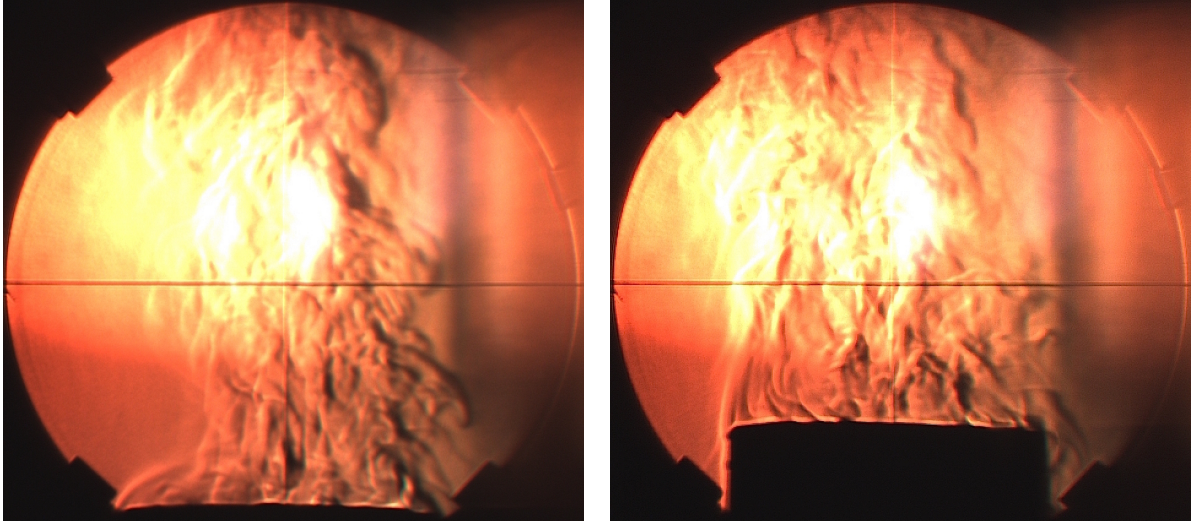


Figure B.4: Schlieren pictures of manikin plume generated from the top of thermal manikins and upwards.

From the schlieren pictures the generated uprising plume is observed to collapse or shrink to a minimum at a distance of 100 mm to 300 mm above the top plate. This distance fluctuates a lot depending on surrounding air movement.

Air and Temperature Measurements - Quantitative investigation The measured plume air speed and air excess temperature is shown in figures B.5 and B.6, illustrating the profiles when measurements are interpolated from the 16 x 16 measurement grid to a 160 x 160 grid using 4th order accurate cubic spline interpolation. Measured air velocities below 0.05 m/s are neglected and assumed 0.0 m/s due to the accuracy of the hot-sphere Dantec 54R103 anemometers.

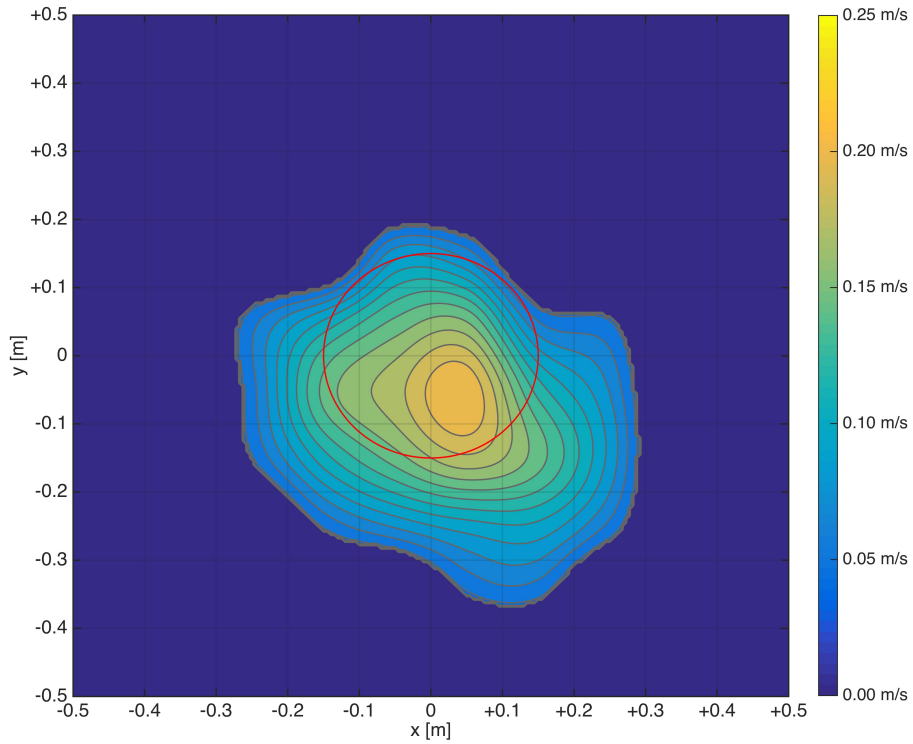


Figure B.5: Contour plot of plume air velocity generated by manikin.

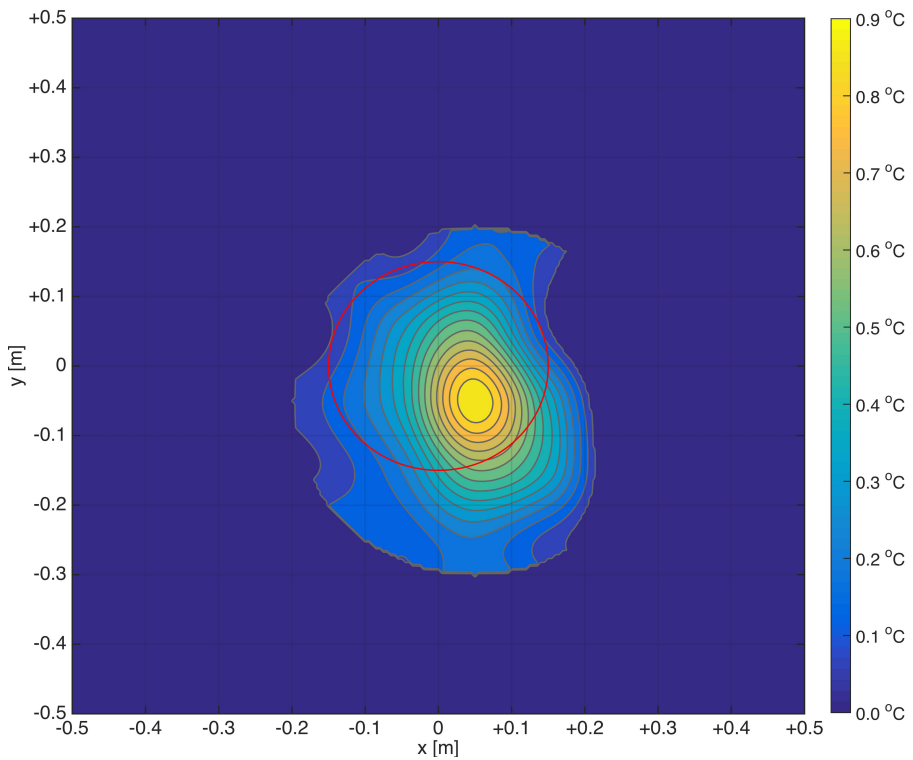


Figure B.6: Contour plot of air excess temperature generated in manikin plume.

Both the velocity and temperature excess profiles are asymmetrical and displaced from the center

of the manikin. Their position, radius and area of the profiles are shown in table B.2.

Table B.2: Geometrical data of manikin plume.

Parameter	Velocity plume	Temperature excess plume
Center, x_0	+0.04 m	+0.05 m
Center, y_0	-0.06 m	-0.05 m
Maximum radius, r_{max}	0.73 m	0.75 m
Area, A	0.33 m ²	0.25 m ²

The displaced center of the profiles in relation to the manikin center may be explained by temperature gradients present in the test room. Even very small horizontal gradient could displace the plume. From figure B.7 and B.8 the measured air velocity and temperature of the surroundings are shown for each of the 16 grid steps of 0.1 m the x-direction.

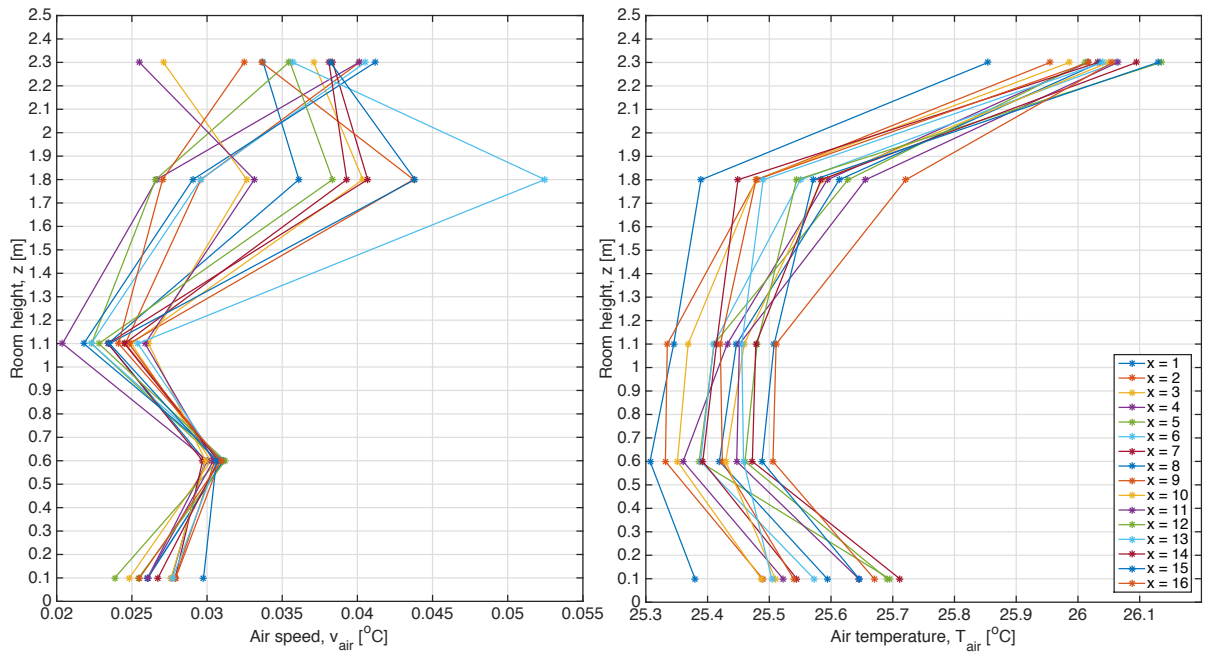


Figure B.7: Air speed (left) and air temperature (right) profiles in surroundings during plume experiment.

B. Experimental Investigations

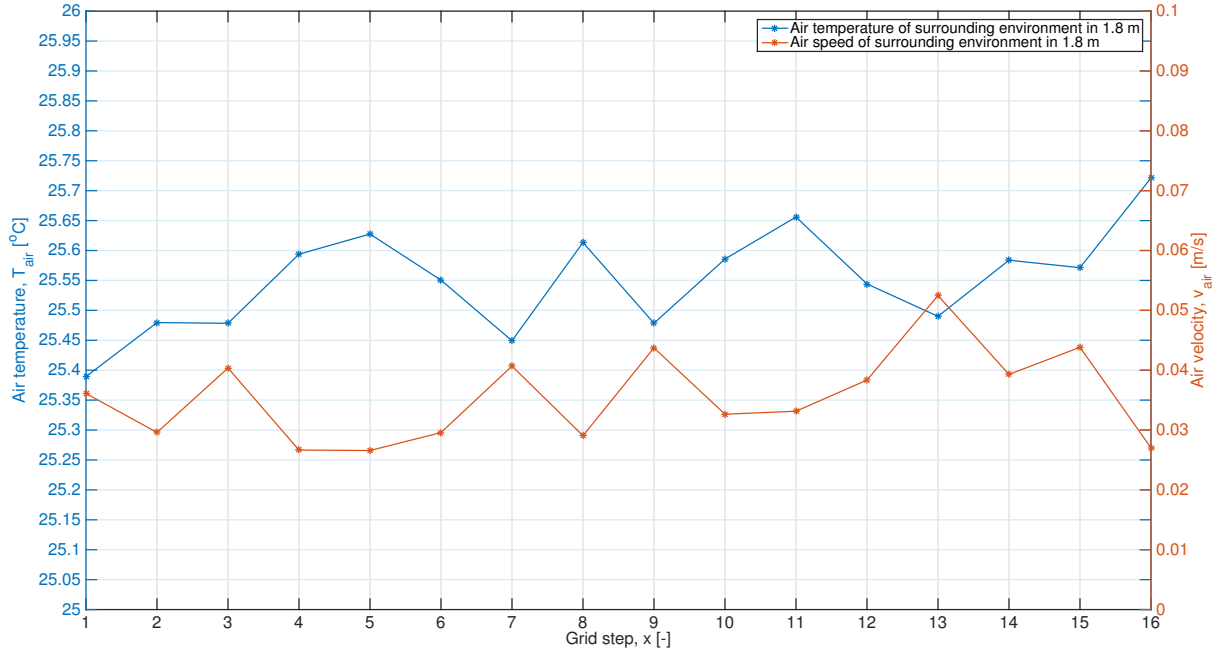


Figure B.8: Air speed and air temperature variations 1.8 m above floor in surroundings during experiment.

The figures show how especially the air temperature fluctuates during the measurement period from minimum 25.4°C to maximum 25.7°C. However, as the measured plumes represent a diameter of around 0.4 m the effective measurement points are only x-point 6-11 lowering the boundary air temperature fluctuation to 0.2°C. The measured surrounding air velocity is generally below 0.05 m/s, which is the lower limit of the sensor range.

Based on the two measured plume profiles Gaussian distributions are derived showing the measured values as function of distance from the center of the profile, r_i . A Gaussian distribution is selected based on the work in Zukowska, D. et al. (2012), where this was successful in terms of representing plume data distribution.

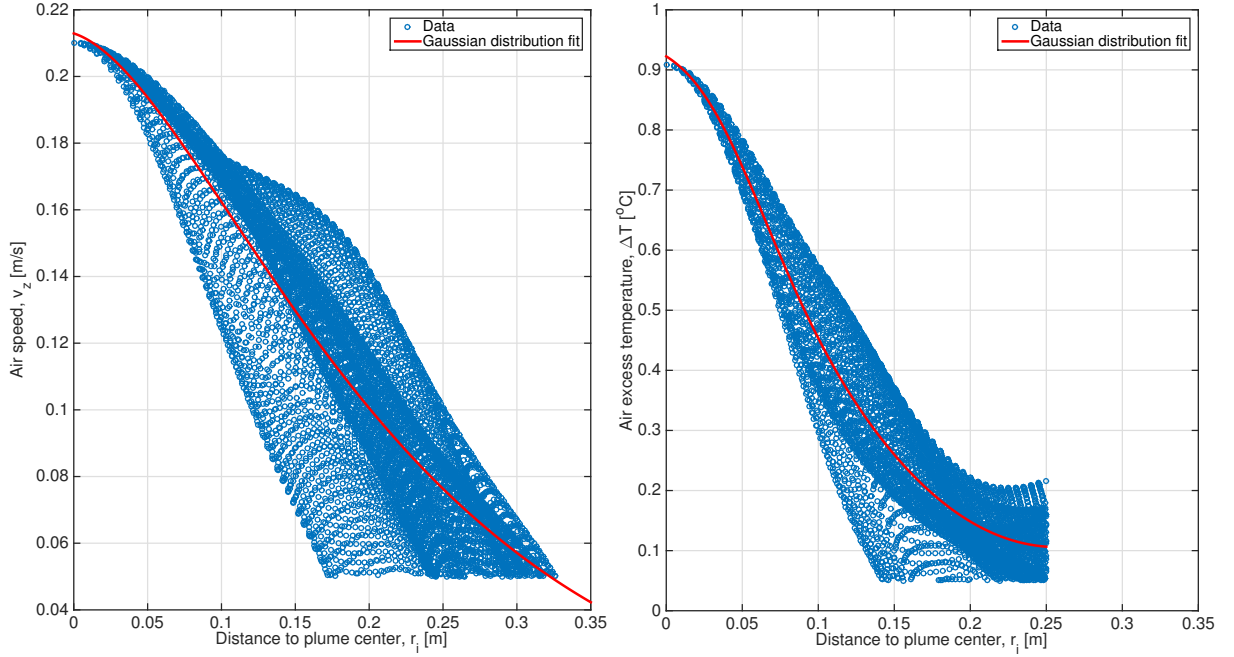


Figure B.9: Gaussian distributions of plume air speed and excess temperature.

Calculated integral characteristics of the thermal plume are given in table B.3.

Table B.3: Integral characteristics of manikin plume.

Maximum velocity, $v_{z,max}$	Maximum excess temperature, ΔT_{max}	Volumetric flow, q_z	Momentum flow, I_z	Heat flow, Φ_z
0.21 m/s	0.91 °C	0.101 m ³ /s	0.016 N	34.28 W

Conclusion

Based on measurements of surface temperature, Schlieren imaging of plume flow and measurements of plume cross-sectional profiles for both air speed and excess air temperature, the following conclusion is drawn.

The results show that the surface temperature of the human body simulator (thermal manikin) resemble that of a human being. However, a temperature gradient of approximately 10 °C is observed resulting in highest temperatures on the top plate of the barrel.

The generated plume is concentrated and remains circular with some deformation present due to fluctuating boundary conditions. The plume is described in terms of its integral characteristics and a Gaussian distribution for both air speed and excess air temperature in the plume is representative for the results. Such results are applicable in the assessment of CFD models.

B.2 Temperature Measurements Using Thermocouples

Calibration guidance, figures and equipment specifics for this section are based on Artmann, N. et al. (2008).

For all temperatures measured using thermocouples (TC) in the experiments type K thermocouples that are either thin or thick is used. Temperature is logged using a Fluke Helios Plus 2287A data logger. Ice Point Reference (IPR) is achieved using a KAYE K 170-50.

Thick TC's are used to measure air temperature in the experimental setup, whereas thin TC's are used to measure surface temperatures. All thin TC's are embedded in a thin layer of Thermo-paste to ensure there is a purely conductive heat transfer between sensor and solid.

For the temperature measurements performed in the experiments a principle layout of the entire temperature-measurement setup can be seen from figure B.10.

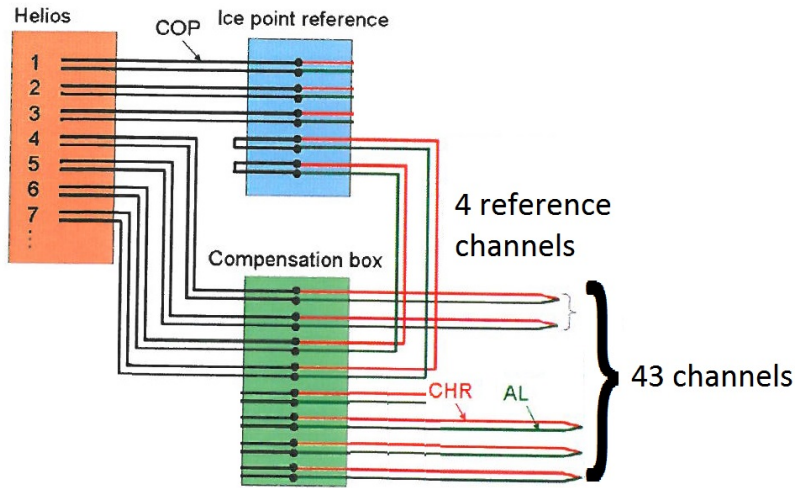


Figure B.10: Principle layout for temperature measurements using thermocouples, compensation box, ice-point reference and datalogger. Figure modified from Artmann, N. et al. (2008).

As seen from the figure above all TC's in the experimental setup are connected to the same compensation box shielded from ambient conditions. As TC's measure the temperature differences between two points it is necessary to have a known junction. The temperature of this compensation box is known by using four TC's connected to an IPR which serves as the known temperature junction for compensation box. As the setup features around 50 TC's for temperature measurements in the experimental setup it is more convenient to connect the TC's in an external compensation box rather than directly in the IPR.

The use of an IPR replaces the build-in reference junction temperature in the data-logger which is significantly less accurate than the IPR-temperature. The IPR used in this setup is capable of maintaining a temperature of 0 °C with variation less than 0.02 K.

Accuracy

The uncertainty related to the temperature measurements originate from several sources which are outlined with their individual estimated uncertainties below;

- Voltage measurements of the data logger: ± 0.075 K
- Cell temperature of the Ice Point Reference: ± 0.02 K
- Composition of the thermocouple alloys: Thick ± 0.028 K, Thin ± 0.023 K
- Temperature difference between different channels in the compensation box: ± 0.005 K

Apart from these quantifiable uncertainties the local change of the alloys at the junction also gives an uncertainty which is sought minimized by cold joining. Material of the wires and terminals of the Ice Point Reference is included in the calibration of the thick reference thermocouples.

As careful calibration was performed in accordance with the method described in (Artmann, N. et al., 2008). As the exact same equipment is used the uncertainties from the literature is assumed to be valid for the measurements performed in this thesis as well.

Uncertainty is estimated by quadrature addition for both types of thermocouple based on the uncertainties listed above. For the thick thermocouple there is calculated both a measuring and a reference uncertainty as the thick thermocouples measuring in the experiments are affected twice by the uncertainty of the composition of alloys. This is also why the composition of alloys for both thin and thick is included in the calculation of δ_{thin} in eq. B.6. The measurements of reference temperature are not affected by the difference between channels in the compensations box, as these measurements originate from the Ice Point Reference.

$$\begin{aligned}
 \delta_{thin} &= \sqrt{0.075^2 + 0.02^2 + 0.028^2 + 0.005^2 + 0.023^2} = \pm 0.086K \\
 \delta_{thick} &= \sqrt{0.075^2 + 0.02^2 + 0.028^2 + 0.005^2 + 0.028^2} = \pm 0.087K \\
 \delta_{thick,ref} &= \sqrt{0.075^2 + 0.02^2 + 0.028^2} = \pm 0.083K
 \end{aligned} \tag{B.6}$$

This estimation of uncertainty does however not include the contribution from radiation when measuring air or surface temperatures. For measurements of surface temperatures these can be shielded from radiation by use of reflective tape.

Operative Temperature using Thermocouples

To measure operative temperature in the experimental setup a configuration using globe thermometer has been adopted. The choice of globe thermometer is made on a basics of the investigations in Simone, A. et al. (2007) where it was found that for moderate thermal indoor environments where velocity is normally lower than 0.20 m/s and the difference between air- and mean radiant temperature is less than 5.0 K; a sphere of diameter 3-5 cm gave the best results compared to the temperature experienced by a person.

The same study shows that if it is possible to place the operative sensor in the centre of the room, then a spherical shape is the best choice. Hence, operative temperature is measured in the centre of the experimental room using spheres in the experiments conducted in the hot-box.

In the investigations in Simone, A. et al. (2007) the globe thermometer geometry suggested in ISO-7726 (1998) is also included, but the other layout gives better results for this specific experimental setup.

Structurally a thick thermocouple is placed in the centre of a table tennis ball with a diameter of 3.0 cm. The ball is painted grey to ensure correct representation of short-wave radiation, as it is concluded in Simone, A. et al. (2007) that black sensors overestimates and white underestimates the short-wave radiation. For long-wave radiation the colour is not important.

B.3 Measurements of Ventilation Rate

The measurements of ventilation rate are performed using two orifice plates, a fan and a micro-manometer. The ventilation fan is powered through a frequency converter to ensure the desired RPM of the fan to get a constant Air Change Rate (ACR) in the test room. The tolerance of the orifice plates are $\pm 5\%$, and combined with the manual conversion from pressure difference to flow rate this will introduce some inaccuracy in the measurements. A Furness FCO150 precision micro-manometer is used for measuring pressure difference, this has an accuracy of 0.1 % of the reading for temperatures between 0-45 °C.

With a room volume of 37.78 m³ the orifice plates selected for measurements can give from 3.7-31.7 h⁽⁻¹⁾ ACR. An example of the flow-chart from which pressure difference is converted into airflow is shown in figure B.11 for the small orifice. The digital micro-manometer measures the pressure difference across the orifice and by conversion this will give the volumetric flow rate from the test room. It is assumed that there is no additional airflow in the room, apart from what is sucked by the fan through the exhaust, i.e. no infiltration or crack flow.

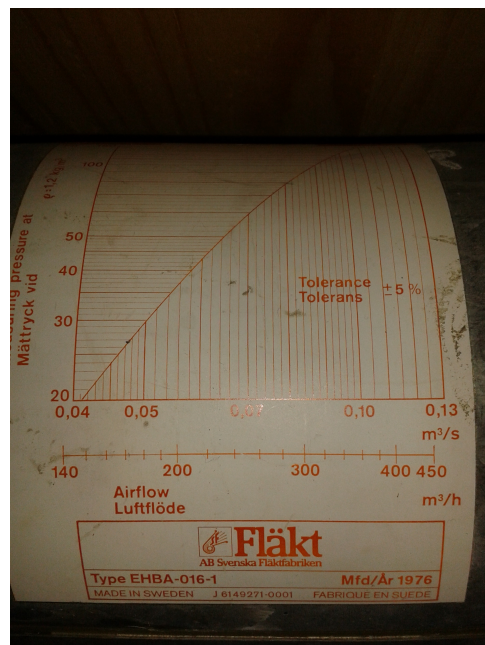


Figure B.11: Pressure-flow rate correlation for orifice plate used to determine Air Change Rate in the test room.

The values of pressure difference is read of the micromanometer when steady states is observed. Steady state is here defined as when the 20 sec time averaged value displayed on the micrometer changes less than ± 0.1 Pa over 2 minutes.

B.4 Measurements of Pressure Difference

In order to measure the pressure difference between the test room centre and 3 points in the plenum a setup with a Furness FCO510 Micromanometer is used. The tubes for measuring pressure are all the same length. The Micromanometer has an accuracy of 0.1 % of the reading for temperatures between 0-45 °C. The values of pressure difference is read of the micromanometer when steady states is observed, i.e. when the 20 sec time averaged value displayed on the micrometer changes less than ± 0.01 Pa over 2 minutes. The three points in the plenum from where pressure difference is measured can be seen from figure 4.13 on page 84.

B.5 Correlation Coefficients

Calculated values of Spearman's ranked correlation coefficients, ρ_s are given in the table. Explanation is of the correlation coefficient is given in section 1.5. Green values indicate that the correlation is statistically significant at a 5% significant level, while red values are insignificant correlations at the 5% level (see figure below). However, their actual significance level is not tested.

Table B.4: Spearman rank correlation coefficients.

Predictor variable		Criterion variable					Δp
		$u_{max,OC}$	$u_{max,OC}^*$	DR	ε_T	T_{plenum}^*	
Re	100%	+0.75	-0.63	+0.86	+0.25	-0.97	+0.74
	50%	-0.49	-0.95	-0.40	+0.74	-0.43	+0.02
	18%	+0.28	-0.79	+0.49	+0.39	-0.80	+0.43
	μ	+0.18	-0.79	+0.32	+0.46	-0.73	+0.36
Ar	100%	-0.58	+0.77	-0.74	-0.37	+0.91	-0.69
	50%	+0.68	+0.99	+0.58	-0.68	+0.23	-0.04
	18%	+0.16	+0.94	-0.13	-0.77	+0.44	-0.45
	μ	+0.08	+0.90	-0.10	-0.61	+0.53	-0.34
Φ_{cool}	100%	+0.81	+0.27	+0.63	-0.66	-0.40	+0.25
	50%	+0.63	-0.04	+0.73	-0.06	-0.05	+0.13
	18%	+0.83	+0.53	+0.51	-0.89	-0.16	+0.27
	μ	+0.76	+0.25	+0.62	-0.53	-0.21	+0.17
A_{DC}		+0.25	+0.32	-0.19	-0.54	-0.56	-0.88

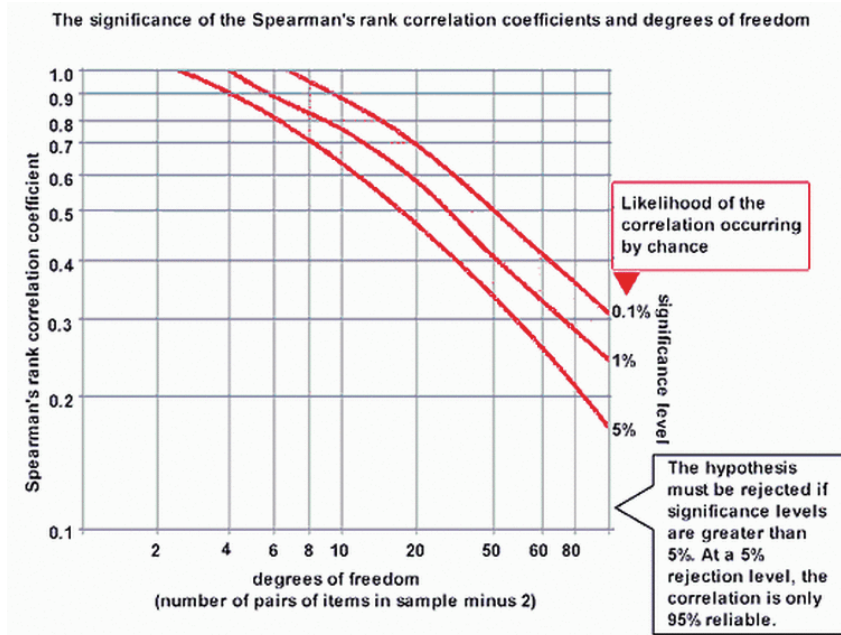


Figure B.12: Chart for hypothesis test of the significance of a correlation.